UNIVERSIDADE FEDERAL DO RIO GRANDE DO SUL

INSTITUTO DE GEOCIÊNCIAS

PROGRAMA DE PÓS-GRADUAÇÃO EM GEOCIÊNCIAS

GÊNESE E EVOLUÇÃO TECTÔNICA DO CRÁTON LUIS ALVES, SUL DO BRASIL

LEANDRO MENEZES BETIOLLO

ORIENTADOR: Prof. Dr. Everton Marques Bongiolo

Porto Alegre, 2022

UNIVERSIDADE FEDERAL DO RIO GRANDE DO SUL

INSTITUTO DE GEOCIÊNCIAS

PROGRAMA DE PÓS-GRADUAÇÃO EM GEOCIÊNCIAS

GÊNESE E EVOLUÇÃO TECTÔNICA DO CRÁTON LUIS ALVES, SUL DO BRASIL

LEANDRO MENEZES BETIOLLO

ORIENTADOR: Prof. Dr. Everton Marques Bongiolo

BANCA EXAMINADORA:

Profa. Dra. Carla Cristine Porcher – Universidade Federal do Rio Grande do Sul

Prof. Dr. Gustavo Luis Campos Pires – Universidade Federal do Rio de Janeiro

Prof. Dr. Viter Magalhães Pinto – Universidade Federal de Pelotas

Tese de Doutorado apresentada como
requisito parcial para obtenção do Título
de Doutor em Ciências.

Porto Alegre, 2022

CIP - Catalogação na Publicação

Betiollo, Leandro Menezes
GÊNESE E EVOLUÇÃO TECTÔNICA DO CRÁTON LUIS ALVES, SUL DO BRASIL / Leandro Menezes Betiollo. -- 2022.
185 f.
Orientador: Everton Marques Bongiolo.

Tese (Doutorado) -- Universidade Federal do Rio Grande do Sul, Instituto de Geociências, Programa de Pós-Graduação em Geociências, Porto Alegre, BR-RS, 2022.

1. Petrologia Metamórfica. 2. Geoquímica. 3. Aerogeofísica. 4. Formações Ferríferas Bandadas (BIF). 5. Granulito. I. Bongiolo, Everton Marques, orient. II. Título.

Elaborada pelo Sistema de Geração Automática de Ficha Catalográfica da UFRGS com os dados fornecidos pelo(a) autor(a).

Agradecimentos

Em primeiro lugar agradeço a minha esposa, que sempre me apoiou e esteve comigo ao longo dessa jornada que é um doutorado, e tantas outras jornadas e desafios a mais. Agradeço por toda a ajuda que ela sempre me deu, braçal, intelectual e afetiva.

Agradeço aos meus filhos, duas crianças lindas e maravilhosas que sempre tem um sorriso no rosto, uma brincadeira e um carinho para me apoiar, trazendo alegria e força para continuar.

Agradeço aos meus pais, por tudo que me deram desde sempre, todo o suporte e estrutura para hoje eu estar aqui finalizando uma Tese de doutorado, eles são parte disso. Agradeço ao meu irmão, por além de ser irmão também ser um grande amigo e estar junto ao longo da vida e suas encruzilhadas.

Agradeço ao meu orientador, por estar junto nos momentos difíceis, por passar tranquilidade e não desistir de me ajudar e entregar a Tese.

Agradeço ao Serviço Geológico do Brasil e ao Estado Brasileiro por financiar e fornecer todos os dados utilizados e pelo apoio institucional para a realização desta Tese. Também agradeço aos meus colegas do SGB pela ajuda nos campos, nos trabalhos de escritório e debates geológicos.

RESUMO

O Cráton Luis Alves (CLA) é um terreno granulítico de médio-grande porte Neoarqueano-Paleoproterozoico que funcionou como uma das massas de terra que deram estrutura para o desenvolvimento do Orógeno Brasiliano – Pan Africano no Neoproterozoico durante a amalgamação do supercontinente Gondwana Oeste. O CLA é composto por unidades Paleoproterozoicas e foi intrudido e recoberto parcialmente por unidades Neoproterozoicas do ciclo Brasiliano. O Complexo Granulítico de Santa Catarina (CGSC), de idade Sideriana-Riaciana, é predominante no CLA e divide-se em quatro unidades geológicas, (i) Complexo Ultramáfico Barra Velha composto por metapiroxenitos à plagioclásio, (ii) Sequência Metassedimentar Joinville composta por BIF, quartzito e granulitos pelíticos, (iii) Ortognaisses Luis Alves composto por granulitos máficos e félsicos, e (iv) Suíte Rodeio-Rio da Luz composta por granitos à piroxênio. Com levantamento aerogeofísico de alta resolução, integração de dados geológicos-estruturais e dados litogeoquímicos, foi possível definir unidades e estruturas principais, bem como blocos e setores geológicos distintos e particulares ao CLA. O levantamento aeromagnetométrico revelou uma estrutura regional de forma elipsoidal a sigmoide, com aproximadamente 70 x 50 km, delimitada por lineamentos magnéticos de 1ª ordem que correspondem a zonas de cisalhamento regionais, e com estruturas internas particulares. Essa estrutura é interpretada como um *metamorphic core complex* (MCC), o que traz implicâncias de interpretação e condicionantes geotectônicas e de geodinâmica. O estudo litogeoquímico nos BIFs, granulitos máficos e félsicos, e nos granitos à piroxênio, demonstrou os ambientes magmáticos, tectônicos e deposicionais que deram origem aos protólitos e as rochas hoje granulíticas. Os granulitos máficos e félsicos demonstraram afinidade com ambiente de arco de ilhas com fusão parcial de rochas da crosta oceânica em sua geração. Também demonstraram afinidades no campo e nos resultados litogeoquímicos, apresentando assinaturas e padrões litogeoquímicos que alinham e se complementam. Da mesma forma, os granitos à ortopiroxênio também se complementam e formam trends com os dados dos granulitos félsicos. Os BIFs do CLA são divididos em duas fácies com base em sua mineralogia: fácies óxido e silicato. O quartzo e a magnetita predominam na fácies óxido, enquanto na fácies silicato também contém ferrosilita, granada e olivina. Os dados geoquímicos expuseram que a principal fonte para ambas as fácies, silicato e óxido dos BIFs do

CLA, é a água do mar com maior influência de fontes hidrotermais de baixa T, seguida de contribuição menos importante de sedimentação continental. A fácies óxido representaria a sedimentação mais próxima das fontes hidrotermais e com fraca influência da sedimentação clástica continental, enquanto a fácies silicato representaria uma zona contrastante mais próxima do continente com sua influência. Os BIFs do CLA não têm uma associação direta e clara com apenas um dos tipos de depósito. Dependendo das fácies analisadas, podem apresentar mais características do tipo Algoma ou Superior. Essa ambigüidade de informações nos leva a inferir que os BIFs do CLA são representativos de um ambiente de transição do tipo Algoma para o tipo Superior. Após esse cenário de arco de ilhas com uma bacia adjacente, próxima a uma zona divergente e fontes hidrotermais, esses protólitos foram subductados e condicionados ao metamorfismo granulítico, formando um *large hot orogen* e um platô orogênico. Junto com este metamorfismo granulítico houve a fusão parcial dessas rochas, que acabaram por dar origem aos granitos da Suíte Rodeio-Rio da Luz. Esse cenário de colagem de grandes placas tectônicas com formação de um platô orogênico com metamorfismo granulítico e fusão parcial na sua crosta inferior, foi seguido de um evento extensional. Esse evento possibilitou a ascensão de rochas dúcteis da crosta média-inferior e a formação e exumação de um MCC, que hoje compõe grande parte do CLA, no final do Riaciano. O CLA permaneceu estável até a amalgamação do Supercontinente Gondwana Oeste.

ABSTRACT

The Luis Alves Craton (LAC) is a medium-large-sized Neoarchean-Paleoproterozoic granulitic terrain that functioned as one of the landmasses that provided structure for the development of the Brasiliano – Pan African Orogen in the Neoproterozoic during the amalgamation of the West Gondwana supercontinent. The LAC is composed of Paleoproterozoic units and was intruded and partially covered by Neoproterozoic units of the Brasiliano cycle. The Santa Catarina Granulitic Complex (SCGC), of Siderian-Rhyacian age, is predominant in the LAC and is divided into four geological units, (i) Barra Velha Ultramafic Complex composed of plagioclase-bearing metapyroxenites, (ii) Joinville Metasedimentary Sequence composed of BIF, quartzite and pelitic granulites, (iii) Ortogneisses Luis Alves composed of mafic and felsic granulites, and (iv) Rodeio-Rio da Luz Suite composed of orthopyroxene-bearing granites. With high-resolution aerogeophysical survey, integration of geological-structural data and lithogeochemical data, it was possible to define main units and structures, as well as geological blocks and sectors that are distinct and particular to the LAC. The aeromagnetometric survey revealed a regional structure of ellipsoidal to sigmoid shape, with approximately 70 x 50 km, delimited by 1st order magnetic lineaments that correspond to regional shear zones, and with particular internal structures. This structure is interpreted as a metamorphic core complex (MCC), which brings interpretation implications and geotectonic and geodynamic constraints. The lithogeochemical study in the BIFs, mafic and felsic granulites, and in the orthopyroxene-bearing granites, demonstrated the magmatic, tectonic and depositional environments that gave origin to the protoliths and the granulitic rocks today. The mafic and felsic granulites demonstrated affinity with the island arc environment with partial melting of oceanic coast rocks in their generation. They also demonstrated affinities in the field and in the lithogeochemical results, presenting signatures and lithogeochemical patterns that align and complement each other. Likewise, the orthopyroxene-bearing granites also complement each other and form trends with the felsic granulites data. LAC BIFs are divided into two facies based on their mineralogy: oxide and silicate facies. Quartz and magnetite predominate in the oxide facies, while in the silicate facies it also contains ferrosilite, garnet and olivine. The geochemical data showed that the main source for both facies, silicate and oxide of LAC BIFs, is seawater with greater influence from low-T hydrothermal vents,

followed by a less important contribution from continental sedimentation. The oxide facies would represent the sedimentation closest to the hydrothermal vents and with weak influence of the continental clastic sedimentation, while the silicate facies would represent a contrasting zone closer to the continent with its influence. LAC BIFs do not have a direct and clear association with just one of the deposit types. Depending on the analyzed facies, they may present more characteristics of the Algoma or Superior-type. This ambiguity of information leads us to infer that the LAC BIFs are representative of an environment of transition from the Algoma-type to the Superior-type. After this island arc scenario with an adjacent basin, close to a divergent zone and hydrothermal vents, these protoliths were subducted and conditioned to granulitic metamorphism, forming a large hot orogen and an orogenic plateau. Along with this granulitic metamorphism, there was a partial melting of these rocks, which eventually gave rise to the granites of the Rodeio-Rio da Luz Suite. This scenario of collage of large tectonic plates with formation of an orogenic plateau with granulitic metamorphism and partial melting in its lower crust, was followed by an extensional event. This event allowed the rise of ductile rocks from the lower-middle crust and the formation and exhumation of an MCC, which today makes up a large part of the LAC, at the end of the Rhyacian. The LAC remained stable until the amalgamation of the West Gondwana Supercontinent.

SUMÁRIO

1. Introdução

Os terrenos granulíticos têm sua origem e significado geológico estudados desde Weiss (1803) (O'Brien, 2006). Nas últimas quatro décadas, a modelagem geológica de granulitos aproveitou o conjunto de dados termodinâmicos robustos (Holland e Powell, 1985; Powell e Holanda, 1985; 1988) e avanços em técnicas analíticas. Eventos metamórficos de até 1200 °C e 6 GPa (ou até 200 km de profundidade na crosta) foram determinados, e campos petrológicos metamórficos extremos foram construídos em associação com visões geodinâmicas (Brown, 2007a,b; 2014; Stuwe, 2007; Brown e Johnson, 2019). A geração dos terrenos granulíticos foi principalmente relacionada a ambientes de arco vulcânico e continental com fontes extras de calor (Harley 1989, 1992; Bohlen 1991; Ashwal *et al*., 1992; Gerya e Meilick, 2011; Kramers *et al*., 2011; Lexa *et al*., 2011; Sajeev *et al*., 2013), e seu entendimento atual envolve: (i) a formação, evolução e consolidação de grandes orógenos quentes (Chardon *et al*., 2009; Franek *et al*., 2011; Jamieson e Beaumont, 2013; Kohn, 2014; Harley, 2016; Perchuk *et al*., 2018; Brown e Johnson, 2019; Dziggel *et al*., 2019), (ii) amalgamação de supercontinentes (Bleeker, 2003; Zhao *et al*., 2004; Brown, 2007a; Vansutre e Hari, 2010; Bradley 2011; Touret *et al*.. 2016), e (iii) os ciclos de tempo da Terra (Brown e Johnson, 2019). No entanto, mesmo com os avanços científicos proeminentes, a exumação, os caminhos P-T-t, os padrões deformacionais, os processos microestruturais e a estruturação regional desses terrenos da crosta inferior ainda são objetos de investigações crescentes (Harley, 1989, 1992; Barbosa *et al*., 2006; Taylor *et al*., 2010; Jamieson e Beaumont, 2011; Kelsey e Powell, 2011; Spalla *et al*., 2011; White e Powell, 2011; Endo *et al*., 2012; Block *et al*., 2016; Dharmapriya *et al*. , 2017; Girelli *et al*., 2018; Zhang *et al*., 2021).

O *Metamorphic Core Complex* (MCC) é uma estrutura tectônica regional encontrada em todos os continentes e amplamente conhecida no Fanerozoico (Lister e Davies, 1989; Verdel *et al*., 2007; Wang *et al*., 2012; Daoudene *et al*., 2013; Tichomirowa e Kohler, 2013; Whitney *et al*., 2013; Toraman *et al*., 2014; Cao *et al*., 2017; Wiest *et al*., 2019; Cheng *et al*., 2020; Kamaci e Altunkaynak, 2020; Österle *et al*., 2020), com raros registros no Proterozoico (Rizzotto *et al*., 2019; Tiddy *et al*., 2020) e em segmentos crustais mais antigos (James e Mortensen, 1992; Hoffmann *et al*., 2015). No Paleoproterozoico, e principalmente em terrenos Arqueanos, geralmente ocorrem estruturas *dome-and-keel* caracterizadas por tectônica vertical (Van Kranendonk *et al*., 2004; 2007; Harris *et al*., 2012; Lin e Beakhouse, 2013; Thebaud e

Rey, 2013; Gerya , 2014; Bédard, 2018; Zulauf *et al*., 2019), como nas áreas do Quadrilátero Ferrífero (QF – Quadrilátero Ferrífero) e Carajás no Brasil (Marshak *et al*., 1997; Cutts *et al*., 2019; Costa *et al*. , 2020), nos domos Monte Edgar e Yalgoo na Austrália (Sandiford *et al*., 2004; François *et al*., 2014; Clos *et al*., 2019; Roberts e Tikoff, 2021) e no *greenstone belt* de Barberton na África do Sul (Lana *et al*., 2010). Por outro lado, a formação e exumação de um MCC da crosta inferior, é considerado resultado da tectônica horizontal, intrinsecamente atribuída a regimes extensionais, muitas vezes durante estágios pós-orogênicos (Scheffer *et al*., 2016; Searle e Lamont, 2020), como aqueles registrados nos orógenos Egeu (Searle e Lamont, 2022) e Cordilheirano (Lister e Davies, 1989; Stevens *et al*., 2017). Sua formação reflete condições reológicas particulares, como aquelas associadas à profundidade e temperatura de Moho, concentração de calor e o volume e composição da fusão parcial aprisionada (Whitney *et al*., 2013; Platt *et al*., 2015; Cooper *et al*., 2017; Brun *et al*., al., 2018). Os MCCs ocorrem na litosfera continental ou oceânica (i.e., *Oceanic Core Complex - OCC*), exumando rochas profundas da crosta ou do manto, respectivamente (Hayman *et al*., 2011; Whitney *et al*., 2013; Lagabrielle *et al*., 2015; Brun *et al*. al., 2018). Os MCCs normalmente abrigam domos gnáissicos (Eskola, 1949; Allen e Chamberlain, 1989; Norlander *et al*., 2002), uma estrutura relacionada à exumação de rochas metamórficas de alto grau da crosta continental média-inferior. Na verdade, é frequentemente difícil individualizar MCCs de domos gnáissicos associados a estruturas do tipo *dome-and-keel*, porque eles compartilham padrões estruturais regionais e mecanismos geológicos de formação, sendo o diapirismo um dos mais comuns (Teyssier e Whitney, 2003; Burg *et al*., 2004; Gerya *et al*., 2004; Whitney *et al*., 2004a; Blenkinsop, 2011; Platt *et al*., 2015). Tanto os MCCs quantos os domos gnáissicos contêm migmatitos formados na fácies metamórficas anfibolito médio-alto, raramente na fácies granulito (Gerya *et al*., 2004; Barbosa *et al*., 2004; Blenkinsop, 2011; Chardon *et al*., 2011; Klepeis *et al*., 2016; Liu e Wei, 2018). Além disso, a formação do domo gnáissico pode ser a partir de vários processos geológicos (Yin, 2004), gerando um quebra-cabeça regional de terrenos individuais com suas próprias histórias evolutivas (Soula, 1982; Duncan, 1984; Guo *et al*., 2008; Denèle *et al*., 2009; Chardon *et al*., 2011; Kruckenberg e Whitney, 2011; Spalla *et al*., 2011; Baldim e Oliveira, 2016; Billerot *et al*., 2017; Walczak *et al*., 2017; Zhang *et al*., 2017).

O levantamento aeromagnetométrico provou ser uma ferramenta poderosa para revelar a compartimentação regional (Riedel *et al*., 2013; Mieth e Jokat, 2014a;

Rajaram e Anand 2014; Xiong *et al*., 2016; Golynsky *et al*., 2018), as características geológico-estruturais e suas interpretações em diferentes terrenos geológicos (Aitken e Betts, 2009; Tominaga e Sager, 2010; Blanco-Montenegro *et al*., 2011; Jordan *et al*., 2013; Anudu *et al*., 2014; Gernigon *et al*., 2015; Block *et al*., al., 2016; Hartmann *et al*., 2016; Oladunjoye *et al*., 2016; Eldosouky *et al*., 2017; Kayode *et al*., 2017; Chopin *et al*., 2019). Este tipo de levantamento proporciona o reconhecimento de grandes estruturas (Dossing *et al*., 2010; Dufréchou, 2017; Maacha *et al*., 2017; Catalan *et al*., 2018; Domingos *et al*., 2020; Tiddy *et al*., 2020), delimitando unidades geológicas individuais (Mieth e Jokat, 2014b; Oladunjoye *et al*., 2016; Kumar *et al*., 2018; Launay *et al*., 2018), blocos de associações geológicas (Aitken *et al*., 2014; Araujo *et al*. , 2019), e características superficiais escondidas por florestas (Rosa *et al*., 2014; Rosa *et al*., 2016; Scandolara *et al*., 2017; Costa *et al*., 2020), gelo (Goodge e Finn, 2010; Jordan *et al*., 2013), ou cobertura de bacias sedimentares (Betts *et al*., 2003; Murthy e Babu, 2006; Ogunmola *et al*., 2016; Minelli *et al*., 2018). A aerogamaespectrometria também contribui para o mapeamento geológico regional, sendo seus principais usos o (i) detalhamento de elementos regionais previamente reconhecidos por aeromagnetometria, e (ii) mapeamento de plutons magmáticos e limites de bacias sedimentares (Hartmann *et al*., 2016; Maacha *et al*., 2017; Araújo *et al*., 2019; Costa *et al*., 2020; Domingos *et al*., 2020).

As *Banded Iron Formation* (BIF) são um tipo de rocha presente em todos os continentes que se desenvolveram fortemente na Era Neoarqueana – Paleoproterozoica e está ligada a condições ambientais intrínsecas a essa Era, como o Grande Evento de Oxidação (GOE), com ligação entre geobiologia, sistemas hidrotermais, nível do mar e deposição, além de certa configuração tectônica para seu pleno desenvolvimento (Trendall, 2002; Bekker *et al*., 2010; Konhauser *et al*., 2017). A combinação das condições tectônicas e ambientais cria bacias com sistemas sedimentares e físico-químicos que irão refletir na mineralogia e formar as diferentes fácies de BIFs (James, 1954). O desenvolvimento de BIFs e sua distribuição podem estar relacionados com o ciclo dos supercontinentes, sendo mais uma ferramenta para revelar a evolução das placas tectônicas (Bekker *et al*., 2010).

James (1954) foi quem definiu as fácies dos BIFs baseado na mineralogia formada a partir de precipitados químicos, e as dividiu em quatro fácies: óxido, silicato, carbonato e sulfeto. No entanto, originalmente a fácies sulfeto consistia de um folhelho carbonáceo pirítico e não um sedimento químico, e portanto atualmente não é mais

considerada uma fácies de BIF (Bekker *et al*., 2010). Todas as fácies possuem a presença de quartzo, sendo que adicionalmente a fácies óxido é composta por magnetita e/ou hematita, a fácies carbonática por siderita e/ou anquerita, enquanto a fácies silicato é mais complexa e dependendo do grau de metamorfismo pode ser composta por cummingtonita, grunerita, granada, piroxênio e faialita (Klein, 2005; Bekker *et al*., 2010; Lan *et al*., 2019).

Gross (1980, 1983) foi quem lançou as primeiras caracterizações e interpretações dos ambientes deposicionais e tectônicos que formaram os BIFs e associou as diferentes fácies a esses ambientes. Com isso ele também cunhou os nomes dos principais depósitos reconhecidos mundialmente, os tipos Algoma e Superior. Os depósitos do tipo Algoma, principalmente arqueanos, têm geralmente volumes menores e são estreitos, associados a rochas vulcânicas e grauvacas em *greenstone belts*. Os depósitos do tipo Superior, principalmente paleoproterozoicos, são maiores e mais espessos, associados a extensas plataformas continentais e intercalados com arenitos, carbonatos e folhelhos.

BIFs são rochas que normalmente contêm mais de 15% de Fe, com micro- a macro-bandamento formado por intercalação de magnetita e/ou hematita e quartzo. Sua mineralogia original no momento da deposição é inferida como um gel de Fe-silicato de composição do tipo greenalita, um Fe-oxihidróxido inicial, Fe-óxidos amorfos, ferri-hidrita [$Fe(OH)_3$] e hidromagnetita [$Fe_3(OH)_8$] (Klein, 2005; Bekker *et al*., 2010; Konhauser *et al*., 2017; Aftabi *et al*., 2021). Esses géis precipitados foram posteriormente transformados por diagênese e metamorfismo nos principais minerais de ferro que hoje são reconhecidos nestas rochas, a magnetita e a hematita.

Os principais depósitos de BIFs, como os de Carajás (Justo *et al*., 2020; Klein e Ladeira 2002; Tavares *et al*., 2018), Hamersley (Haugaard *et al*., 2016; Trendall *et al*., 2004; Warchola *et al*., 2018), Transvaal (Bau e Dulski 1996; Franchi e Mapeo 2019; Pickard, 2003; Smith e Beukes, 2016) e do Quadrilátero Ferrífero (Araújo e Lobato, 2019; Spier *et al*., 2007; Soares *et al*., 2017) no Brasil, passaram por metamorfismo de no máximo fácies anfibolito. BIFs que passaram por metamorfismo em fácies granulito ao redor do mundo são raros e ocorrem em volume limitado, como no oeste da Groenlândia (Friend *et al*., 2008; Nutman *et al*., 2002; Papineau *et al*., 2010), no Maciço Cristalino Voronezh (Fonarev *et al*. ., 2006), no Terreno Granulítico do Sul (Dutta *et al*., 2022; Reddy and Sashidhar, 1989; Yellappa *et al*., 2016), no Cráton Dharwar (Mukhopadhyay, 2020), no Cráton Kaapvaal (Horváth *et al*., 2014), no Cráton

do Norte da China (Han *et al*., 2014; Lan *et al*., 2014; 2019; Li *et al*., 2019; Zheng *et al*., 2017), no Cráton Yangtze (Cen *et al*., 2012), Cráton do Congo (Ganno *et al*., al., 2017; Moudioh *et al*., 2020; Teutsong *et al*., 2017) e, a partir desta tese, no Cráton Luis Alves. Como as bacias sedimentares associadas ocorrem segmentadas e deformadas e, a mineralogia e textura das rochas sendo extremamente modificadas, o reconhecimento do contexto das BIF em terrenos granulíticos pode ser muito difícil, com exceção da fácies óxido bandada (Klein, 2005).

O Cráton Luis Alves – CLA (Kaul, 1979; 1980) é uma pequena peça no quebra-cabeça mundial de ca. 35 pedaços de crosta Arqueano-Paleoproterozoica exposta (Bleeker, 2003), e é considerado um importante núcleo de crescimento crustal sideriano bem documentado na América do Sul (Brito Neves, 2011). Sua principal unidade é o Complexo Granulítico de Santa Catarina – CGSC (Hartmann, 1979), que é composto por rochas metaultramáficas, metamáficas, gnaisses TTGs, metagranitos, quartzitos e BIFs, todos metamorfoseados em fácies granulito em arranjo estrutural complexo e com presença de ferrosilita (com exceção do quartzito) marcando o metamorfismo de alto grau (Basei, 1998; Betiollo *et al*., 2018; Passarelli *et al*., 2018).

No CLA, Fornari (1998) considerou BIFs de fácies óxido com estrutura maciça e compostos por 100% de magnetita como magnetititos provenientes de um contexto de complexo ígneo estratiforme cumulático associado as rochas ultramáficas. No entanto, as relações de campo com as rochas hospedeiras, bem como a descoberta de BIFs de fácies silicato próximos a essas rochas maciças a magnetita, apontam para interpretação dessas rochas como BIFs enriquecidos em magnetita por processo metamórfico. É importante mencionar que, de acordo com estudos prévios (Angerer *et al*., 2013; Duuring *et al*., 2020; Egglseder *et al*., 2016; Morrisey *et al*., 2016; Stanton, 2006; Zheng *et al*., 2017), a formação de depósitos de minério de ferro de alto teor está correlacionada com hidrotermalismo, deformação, metamorfismo e processos de segregação e concentração mineral. Além do trabalho de Fornari (1998), o único trabalho adicional desenvolvido nos BIFs do CLA é o de Barbosa (1940). Este útimo autor faz uma abordagem exploratória na qual calcula uma reserva estimada em 2 milhões de toneladas, e também constata que essas reservas de ferro possuem alto teor de P, tornando-as de baixa qualidade e impróprias para exportação.

A união dos dados geológico-estruturais regionais, petrografia e levantamento aerogeofísico de alta resolução obtidos nessa tese permitiu a reinterpretação regional do arcabouço geológico-tectônico, dos processos de formação e do significado

regional do CLA no sul do Brasil. A integração de dados incluiu informações já publicadas na literatura e os últimos avanços no campo da petrologia metamórfica, ciclo de supercontinentes e processos geodinâmicos. A presença de BIFs metamorfoseados em fácies granulito no CLA nos dá um caminho de pesquisa para revelar informações sobre a antiga bacia sedimentar do Cráton Luis Alves, quais eram as configurações tectônicas antes e durante o metamorfismo granulítico, e finalmente como o cráton evoluiu. Utilizando novos dados de campo, associados à petrografia e à geoquímica dos elementos maiores, traços e ETR+Y (REE+Y = REY) dos BIFs pretendemos desvendar essas características do CLA. Este trabalho também contribui para a caracterização e registro de rochas raras, que são os BIFs em fácies granulito com presença de ortopiroxênio, granada e olivina, pois até o presente momento, não há estudos dessa natureza no CLA.

2. Objetivos

Esta Tese tem como objetivo geral aprofundar o conhecimento sobre o Cráton Luis Alves, um segmento crustal granulítico Neoarqueno-Paleoproterozoico de médio-grande porte representante da crosta média-inferior e dos processos geodinâmicos que ali ocorrem, com uma história antiga e complexa ainda pouco estudada e que merece aprofundamento.

Para aprofundar nesse conhecimento geral cito como objetivos específicos:

Integração e reavaliação de dados geológicos e aerogeofísicos para interpretação e mapeamento do arcabouço geológico-estrutural, definindo unidades e estruturas principais, bem como blocos e setores geológicos distintos e particulares ao CLA.

Estudo petrográfico e litogeoquímico petrogenético nos BIFs e ortognaisses. O estudo litogeoquímico nos granulitos máficos e félsicos irão fornecer dados sobre o ambiente tectônico que esse magmatismo Neoarqueano se desenvolveu, gerando os protólitos dos ortognaisses que hoje encontramos no CLA.

A ocorrência de BIFs no CLA possibilita o estudo e a reconstituição da bacia que existiu adjacente ao ambiente tectônico e magmático formador desses protólitos dos ortognaisses, bem como das outras rochas que foram geradas nessa bacia, como os metassedimentos e granulitos pelíticos.

A integração desses dados geológico-estruturais, aerogeofísicos e litogeoquímicos possibilitará a reconstituição dos ambientes tectônicos, magmáticos e deposicionais do CLA, seus processos e resultados, antes, durante e depois do metamorfismo granulítico de idade Riaciana.

3. Conceitos aplicados à petrologia metamórfica

3.1. Avanços da petrologia metamórfica nas últimas décadas

Nos últimos 40 anos o estudo de rochas metamórficas evoluiu significativamente devido ao avanço tecnológico. Com o aparecimento de novos instrumentos analíticos, a possibilidade de análises *in situ* nos materiais geológicos e o aumento do poder de processamento de dados por parte dos computadores fez com que se ampliasse a extensão P-T dos ambientes metamórficos (Harley, 1998; Brown, 2009, 2014). Novas interpretações, classificações, delimitação de fácies metamórficos e pontos de abordagem científica surgiram, e a petrologia metamórfica contribuiu significativamente no entendimento geral da geotectônica e particularmente da litosfera (Bleeker, 2003; Stüwe, 2007; Brown, 2007).

Uma mudança importante que ocorreu nos últimos 20 anos foi a comprovação da extensão das condições de P e T que o metamorfismo é capaz de alcançar, chegando a pressões de 6 GPa, temperaturas de 1200°C, e profundidades de 200 km (Harley, 1998; Chopin, 2003; Brown, 2009). Com base nos últimos estudos (Stüwe, 2007; Brown, 2007, 2014) novos gráficos para a classificação das rochas metamórficas foram ampliados e elaborados, tanto com base em visões petrológicas quanto geodinâmicas (Figs. 1 e 2).

Segundo Brown (2007, 2009), os cinturões metamórficos são classificados em três tipos e consequentemente também em três fácies (Fig. 1):

- alta razão d*T*/d*P* = baixa P / alta T; Fácies G-UHTM (granulito de ultra-alta temperatura de metamorfismo);

- razão intermediária d*T*/d*P* = similar ao metamorfismo Barroviano; Fácies E-HPGM (eclogito média temperatura - metamorfismo granulítico de alta pressão);

- baixa razão d*T*/d*P* = alta P / baixa T; HPM-UHPM (alta pressão – ultra-alta pressão de metamorfismo).

Baseado em condições geotermais (Figs. 1B e 2B), Stüwe (2007) propôs uma nova abordagem para as condições P-T de metamorfismo, comparando se condições termais dos picos metamórficos são mais frios ou mais quentes que a geoterma continental normal. Isso nos mostra campos que são formados por diferentes processos tectônicos, diferente de campos composicionais formados pelo equilíbrio das assembleias minerais que nos mostra diferentes condições tectônicas. O autor

mostra uma abordagem geodinâmica e que leva em conta a participação da litosfera nos processos metamórficos.

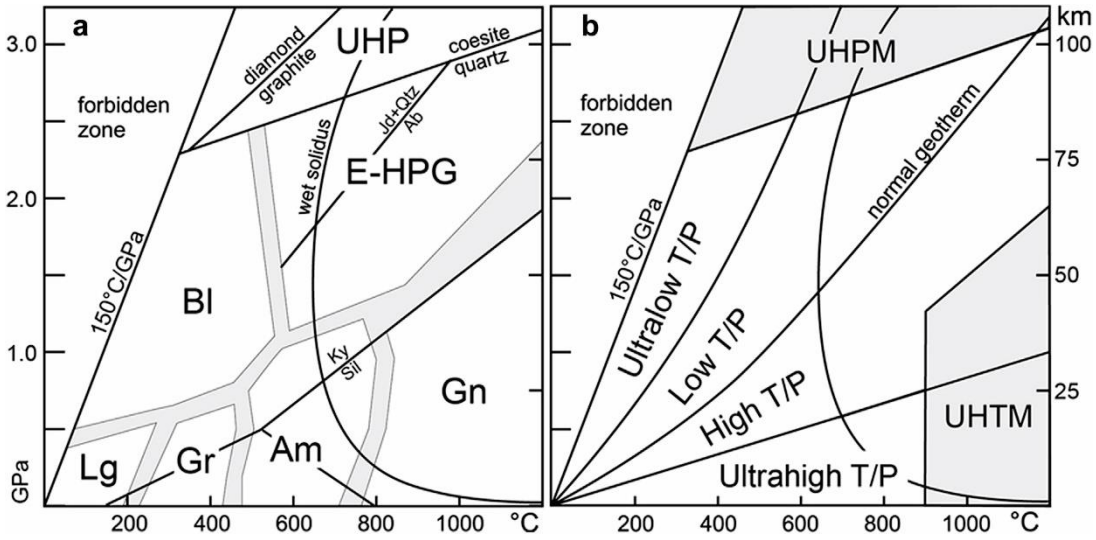

Figura 1: A) Visão petrológica de classificação com as principais fácies metamóricas; B) visão geodinâmica de classificação, modificado de Stüwe (2007). Legenda: Lg, metamorfismo de baixo grau, incluindo a fácies zeólita; Gr, fácies xisto verde; Am, fácies anfibolito; Gn, fácies granulito; e, UHT, metamorfismo de ultra-alta temperatura, incluída na fácies granulito sob condições de T> 900°C. As fácies de alta- a ultra-alta pressão são: Bl, fácies xisto azul; E-HPG, fácies eclogito-granulito de alta pressão; UHP, metamorfismo de ultra-alta pressão. Figura segundo Brown (2014).

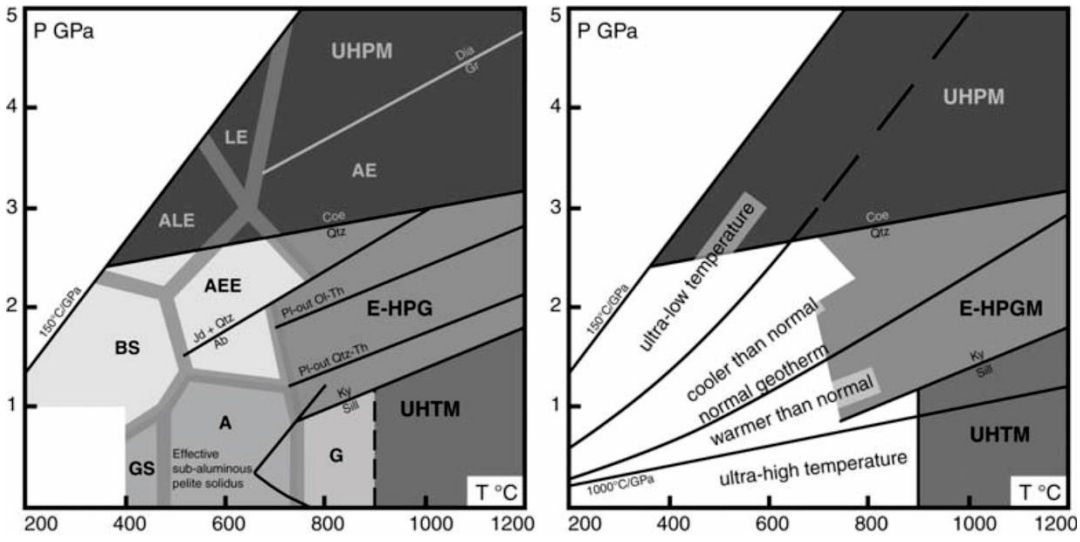

Figura 2: Gráficos com classificação mais detalhada das fácies metamórficas e com pressões que chegam a 5 GPa. A) visão petrológica; B) visão geodinâmica de

classificação, modificado de Stüwe (2007). Legenda: BS, fácies xisto azul; AEE, fácies eclogito anfibólio-epidoto; ALE, fácies eclogito lawsonita anfibólio; LE, fácies eclogito lawsonita; AE, fácies eclogito anfibólio; UHPM, metamorfismo de ultra-alta pressão; GS, fácies xisto verde; A, fácies anfibolito; E-HPG, metamorfismo granulito de alta pressão eclogito de média temperatura; G, fácies granulito, enquanto UHTM é a parte metamórfica de ultra-alta temperatura das fácies granulito. Figura segundo Brown (2007, 2009).

A partir dessas novas abordagens foi possível construir novas correlações entre tipo de metamorfismo, temperatura, pressão, gradiente geotermal e idade dos eventos metamórficos, principalmente dos eventos de metamorfismo extremo. Brown (2014) usando uma série de dados próprios e de outros disponíveis na literatura elaborou gráficos que distinguem bem os tipos de metamorfismo conforme as idades, gradientes geotermais, temperaturas e pressões (Figs. 3, 4, 5 e 6).

Na Figura 3 observa-se que nestes gráficos a temperatura de metamorfismo se manteve de certa forma uniforme, ocorrendo sob condições de média-alta temperatura até o início do Paleozoico, quando há uma queda na temperatura do metamorfismo e um aumento nas pressões. Na Figura 4 observa-se que no mesmo intervalo de tempo houve um incremento da pressão à partir do Neoproterozoico, com o surgimento do metamorfismo UHP – ultra-alta pressão.

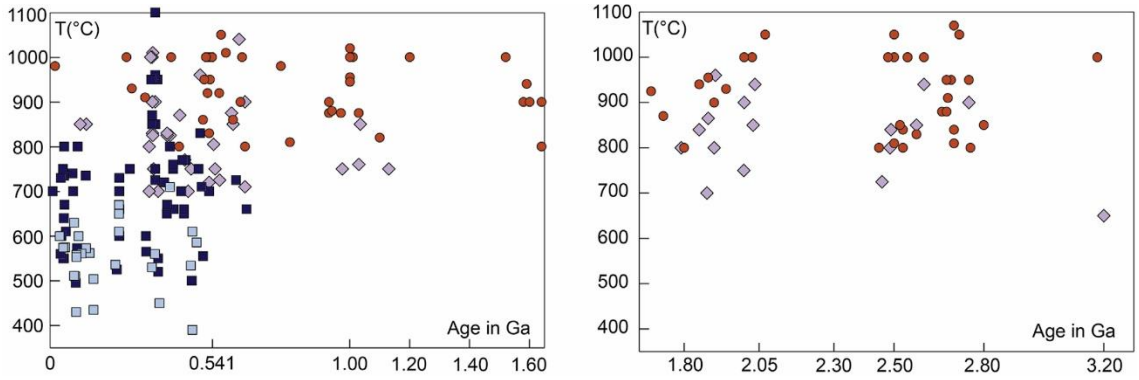

Figura 3: Pico metamórfico de temperatura *vs*. idade dos três tipos de cinturões metamórficos. Legenda: metamorfismo granulítico de ultra-alta temperatura (G-UHT, bolas laranjas); metamorfismo eclogito-granulito de alta pressão (E-HPG e diamantes roxos claros); metamorfismo de alta pressão (HP), composto por lawsonita xistos

azuis e eclogitos (quadrados azuis pálidos); metamorfismo de ultra-alta pressão (UHP) eclogitos de ultra-alta pressão (quadrados azuis escuros). Figura segundo Brown (2014).

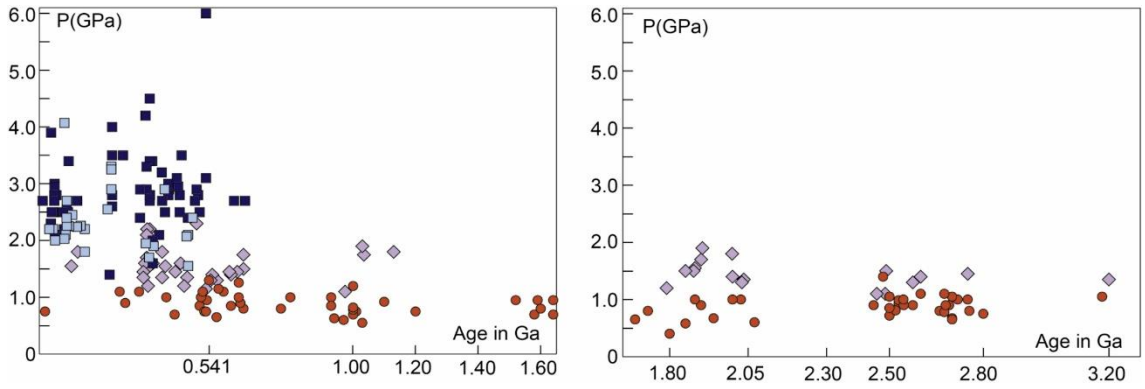

Figura 4: Pico metamórfico de pressão *vs*. idade dos três tipos de cinturões metamórficos. Legenda: metamorfismo granulítico de ultra-alta temperatura (G-UHT, bolas laranjas); metamorfismo eclogito-granulito de alta pressão (E-HPG e diamantes roxos claros); metamorfismo de alta pressão (HP), composto por lawsonita xistos azuis e eclogitos (quadrados azuis pálidos); metamorfismo de ultra-alta pressão (UHP) eclogitos de ultra-alta pressão (quadrados azuis escuros). Figura segundo Brown (2014).

Na Figura 5 observa-se o gradiente geotermal ao longo do tempo geológico para os diferentes tipos de metamorfismo e é visível a ocorrência do metamorfismo UHP somente à partir do Neoproterozoico, com gradientes que não ultrapassam os 400°C/GPa, como também vê-se que o gradiente geotermal para os outros dois tipos de metamorfismo manteve-se praticamente o mesmo ao longo do tempo.

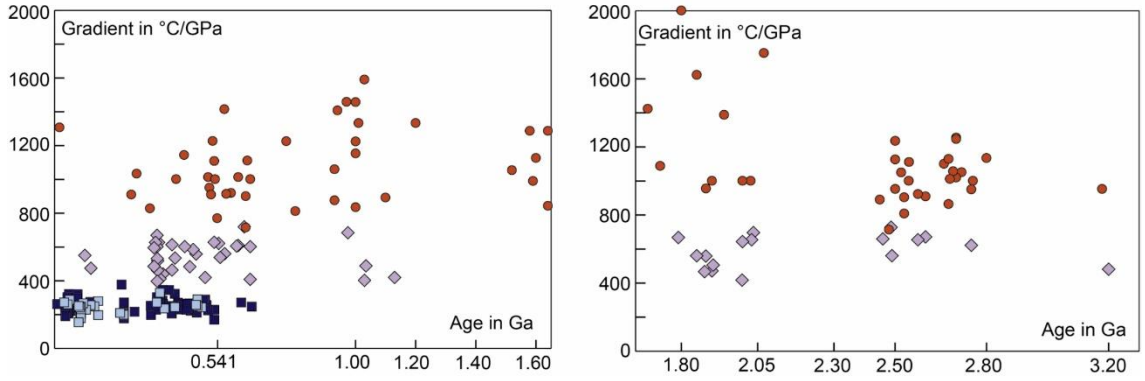

Figura 5: Gradiente termal aparente *vs*. idade dos três tipos de cinturões metamórficos. Legenda: metamorfismo granulítico de ultra-alta temperatura (G-UHT, bolas laranjas); metamorfismo eclogito-granulito de alta pressão (E-HPG e diamantes roxos claros); metamorfismo de alta pressão (HP), composto por lawsonite xistos azuis e eclogitos (quadrados azuis pálidos); metamorfismo de ultra-alta pressão (UHP) eclogitos de ultra-alta pressão (quadrados azuis escuros). Figura segundo Brown (2014).

Na Figura 6 observa-se que os diferentes tipos de metamorfismo plotam ao longo do gradiente geotermal esperado. Por exemplo, o metamorfismo UHP não ultrapassa os 350°C/GPa, como também o metamorfismo UHT mantém seu gradiente geotermal acima de 750°C/GPa. Isto implica que cada tipo de metamorfismo tem um cenário tectônico associado como também as fácies metamórficas refletem bem as características de cada gradiente geotermal.

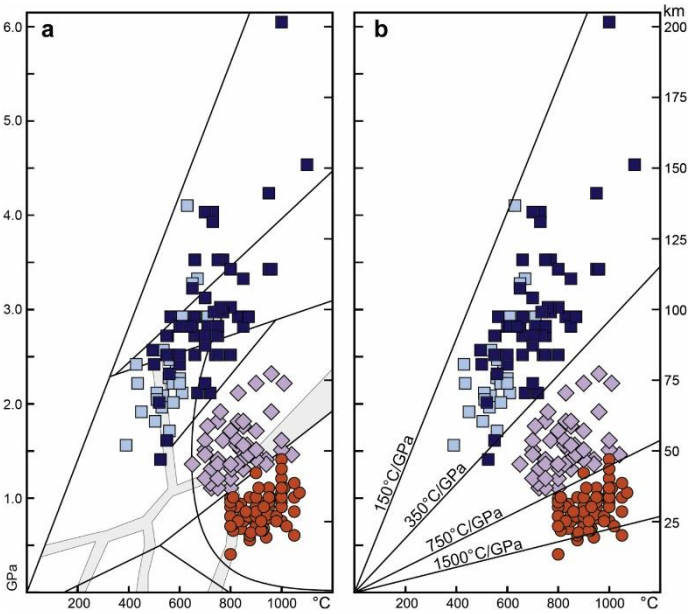

Figura 6: Pico metamórfico segundo as condições P-T para os três tipos de cinturões metamórficos no gráfico P-T ampliado para 6 GPa. A) gráfico P-T na visão petrológica; B) gráfico P-T na visão geodinâmica. Legenda: metamorfismo granulítico de ultra-alta temperatura (G-UHT, bolas laranjas); metamorfismo eclogito-granulito de alta pressão (E-HPG e diamantes roxos claros); metamorfismo de alta pressão (HP), composto por lawsonita xistos azuis e eclogitos (quadrados azuis pálidos); metamorfismo de ultra-

alta pressão (UHP) eclogitos de ultra-alta pressão (quadrados azuis escuros). Figura segundo Brown (2014).

Na Figura 7 são plotados os tipos de metamorfismo no gráfico P-T separados em três idades (>850 Ma, 850 – 485 Ma e <485 Ma), juntamente com as curvas dos gradientes geotermais. Nele é possível observar o declínio do metamorfismo UHT a partir do Criogeniano e o aumento do metamorfismo UHP à partir do Ordoviciano.

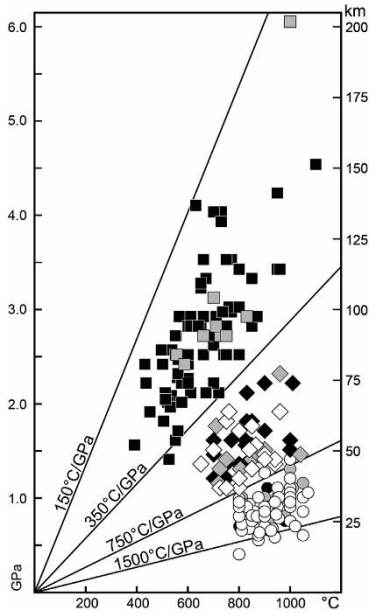

Figura 7: Tipos de cinturões metamórficos plotados por idade *vs*. os gradientes termais, onde bolas brancas são cinturões onde as condições de pico P-T são >850 Ma, símbolos cinza estão entre 850 – 485 Ma e símbolos pretos <485 Ma. Condições G-UHT são círculos, E-HPG são diamantes, e HP-UHP são quadrados. Figura segundo Brown (2014).

Com a definição dos parâmetros citados acima foi a correlação entre eventos extremos de metamorfismo, de ultra-alta temperatura (UHT) ou ultra-alta pressão (UHP), com o ciclo de formação dos supercrátons e supercontinentes, conforme disposto na Figura 8, com claras correspondências entre os eventos metamórficos extremos e o amalgamento da litosfera continental (Bleeker, 2003; Brown, 2009). Além disso, Brown (2007, 2009) também correlaciona esses eventos e padrões com a mudança do regime de tectônica de placas, argumentando que com o aparecimento

da dualidade de regimes termais e cinturões metamórficos emparelhados (Miyashiro, 1961) desde o Neoarqueano, o que significa uma mudança na geodinâmica da Terra e marca o início da tectônica de placas. No Neoarqueano houve a formação dos supercrátons (Bleeker, 2003) com a passagem de um momento estagnado para o Regime de Placas Tectônicas do Proterozoico, caracterizado por um gradiente geotermal médio a alto com ocorrência dos metamorfismos dos tipos G-UHTM e E-HPGM. No Neoproterozoico, com o adelgaçamento da crosta oceânica e o espessamento da litosfera, houve uma transição para ambientes termais mais frios e com isso o aparecimento do metamorfismo tipo UHP, dando início ao Regime de Placas Tectônicas Moderno, que além de ter um gradiente geotermal mais frio também se caracteriza pela subducção profunda da crosta continental dentro do manto em profundidades que podem chegar a 300 km.

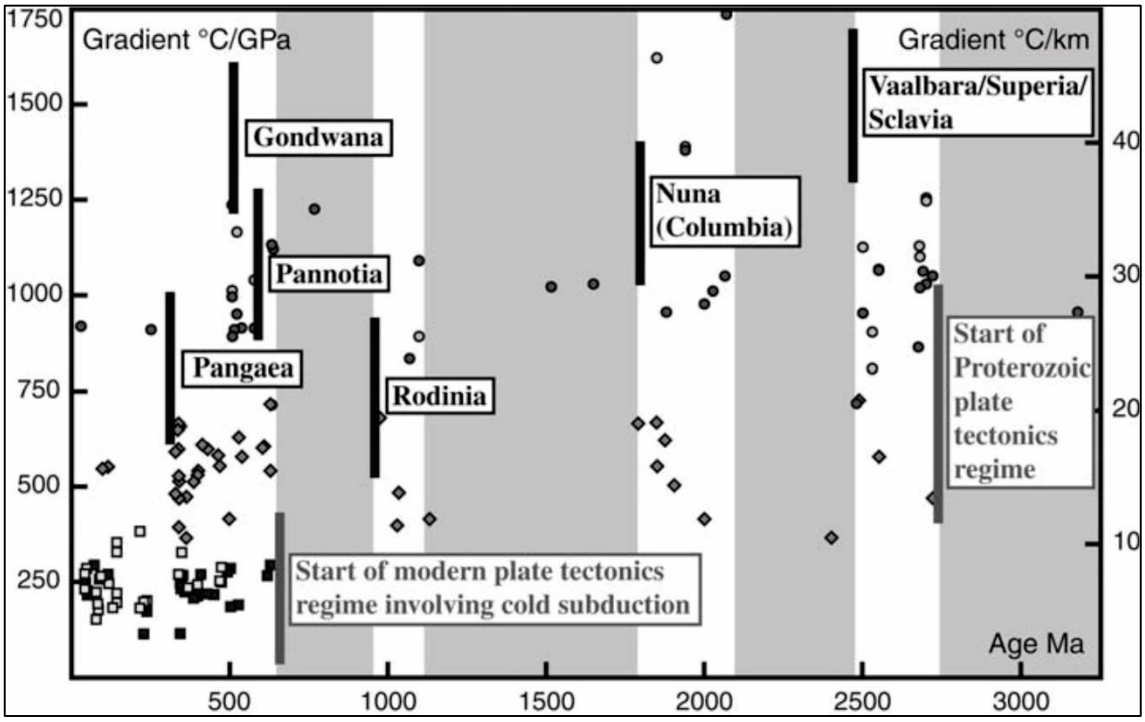

Figura 8: Gráfico do gradiente termal aparente *vs*. idade do pico metamórfico para os três tipos de metamorfismo extremo, fazendo correlação com a formação dos supercrátons (Vaalbara, Superia e Sclavia) e supercontinentes (Nuna /Columbia), Rodínia, Pannotia, Gondwana e Pangea), e também com o início do regime de placas tectônicas do Proterozoico e do regime moderno de placas tectônicas em relação aos gradientes termais dos três principais tipo de cinturão metamórfico. Legenda: G-UHT

são círculos, E-HPG são diamantes, e HP-UHP são quadrados. Figura segundo Brown (2009).

3.2 Geração e preservação de granulitos

A geração e preservação de granulitos é um tema debatido já há algumas décadas (Harley, 1989; Bohlen ,1991; White e Powell, 2002; Winter, 2014), tanto com enfoque tectônico quanto petrológico. Quais os ambientes de formação de granulitos? Quais os processos físico-químicos de formação? Quais tipos de ambientes geram calor e/ou pressão suficientes? Ocorre fusão parcial na geração de granulitos? Como as assembleias de alto grau se preservam e a rocha é exumada?

Os ambientes reconhecidos para formação dos granulitos são variados, ocorrendo em margens continentais ativas, rifts, hot spots, regiões de crosta espessada, associados a extensos batólitos e outros. Ernst (1976; *in* Winter, 2014) fez uma correlação esquemática da ocorrência das fácies metamórficas com o ambiente tectônico de arco de ilhas (Fig. 9). Neste esquema é possível visualizar que granulitos são rochas de base da crosta que ocorrem próximo a fontes extras de calor, como câmaras magmáticas. Saindo do nível crustal aquecido dos granulitos, em níveis mais rasos da crosta começam a ocorrer os anfibolitos e no mesmo nível de crosta, porém sem fontes de calor, a tendência é ocorrer eclogitos. No entanto a natureza é muito mais complexa e variada e muitos fatores influenciam no fluxo termal e consequentemente na formação das rochas metamórficas, como a taxa de subducção, idade da crosta subductada, subducção de porções de *Large Igneous Provinces* (LIPs) ou da cordilheira mesoceânica.

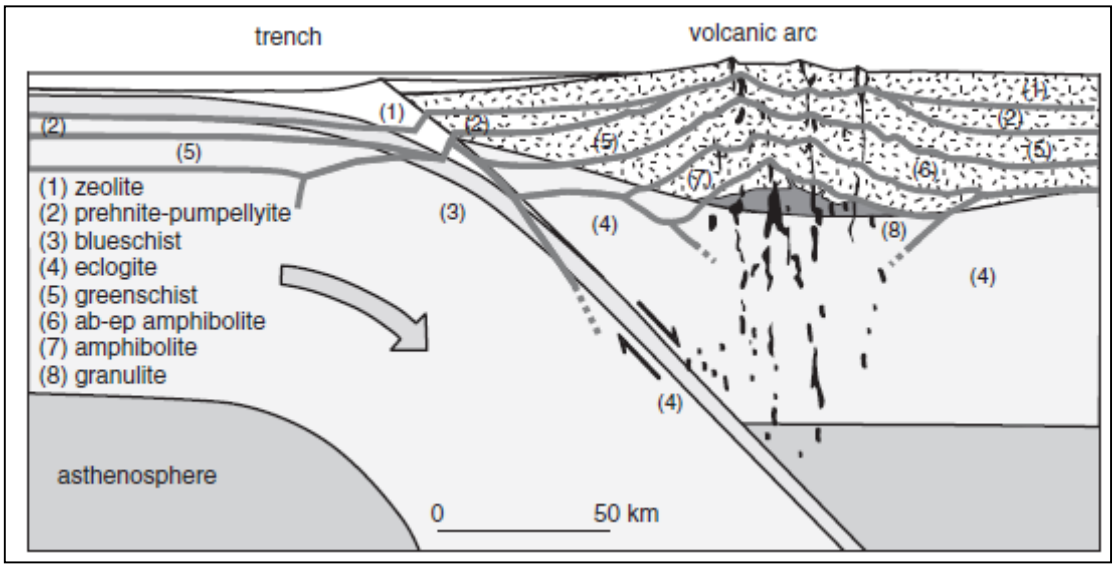

Figura 9: Seção esquemática ao longo de um arco de ilhas mostrando os diferentes setores onde ocorrem as fácies metamórficas. Winter (2014) modificado de Ernst (1976).

Para o estudo e compreensão da formação de granulitos utilizam-se análises geotermobarométricas que caracterizam o ciclo metamórfico das mesmas, que fica registrado como uma trajetória pressão-temperatura-tempo – P-T-t da rocha. As trajetórias podem ser horárias ou anti-horárias, sendo que a característica de diferenciação entre elas é que a horária atinge o P máximo antes do T máximo e a anti-horária atinge o T máximo antes do P máximo (Harley, 1989; Bohlen ,1991; Winter, 20) (Fig. 10).

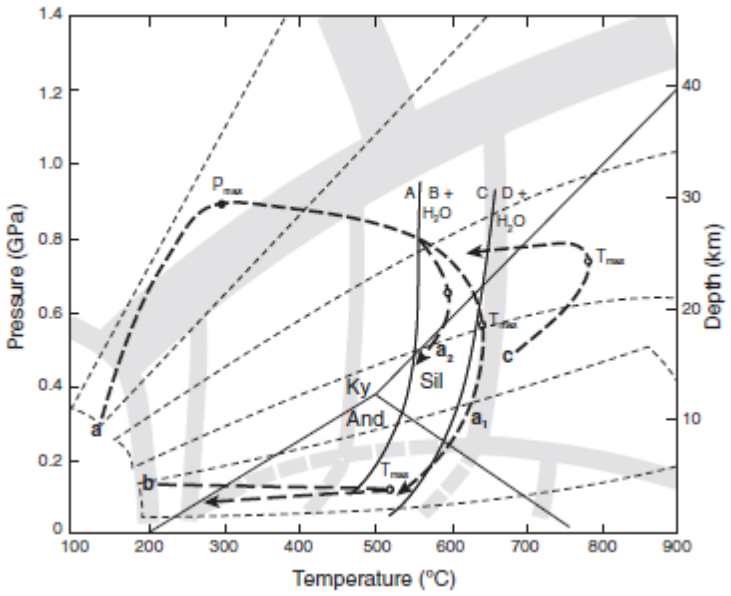

Figura 10: Seção esquemática de trajetórias P-T-t mostrando em A) trajetória horária, comum em ambiente de espessamento crustal, finalizando com descompressão isotermal; B) magmatismo raso, comum em metamorfismo de contato; e c) trajetória anti-horária, alguns tipos de granulitos, comum em ambiente com aporte extra de calor, finalizando com resfriamento isobárico. Winter (2014).

Além da trajetória metamórfica como um todo, se horária ou anti-horária, a etapa final da mesma, quando ocorre a exumação das rochas, é caracterizada por apresentar dois caminhos principais. Elas podem finalizar com resfriamento isobárico ou descompressão isotermal, ou ainda um meio termo entre estes dois processos (Figs. 10 e 11). Esta parte final da trajetória P-T-t nos fornece pistas sobe o ambiente tectônico de formação, se houve ou não aporte de calor, por exemplo com intrusões de magma, ou se as rochas residiram por algum tempo na crosta média, entre outros (Harley, 1989; Bohlen ,1991; Winter, 2014).

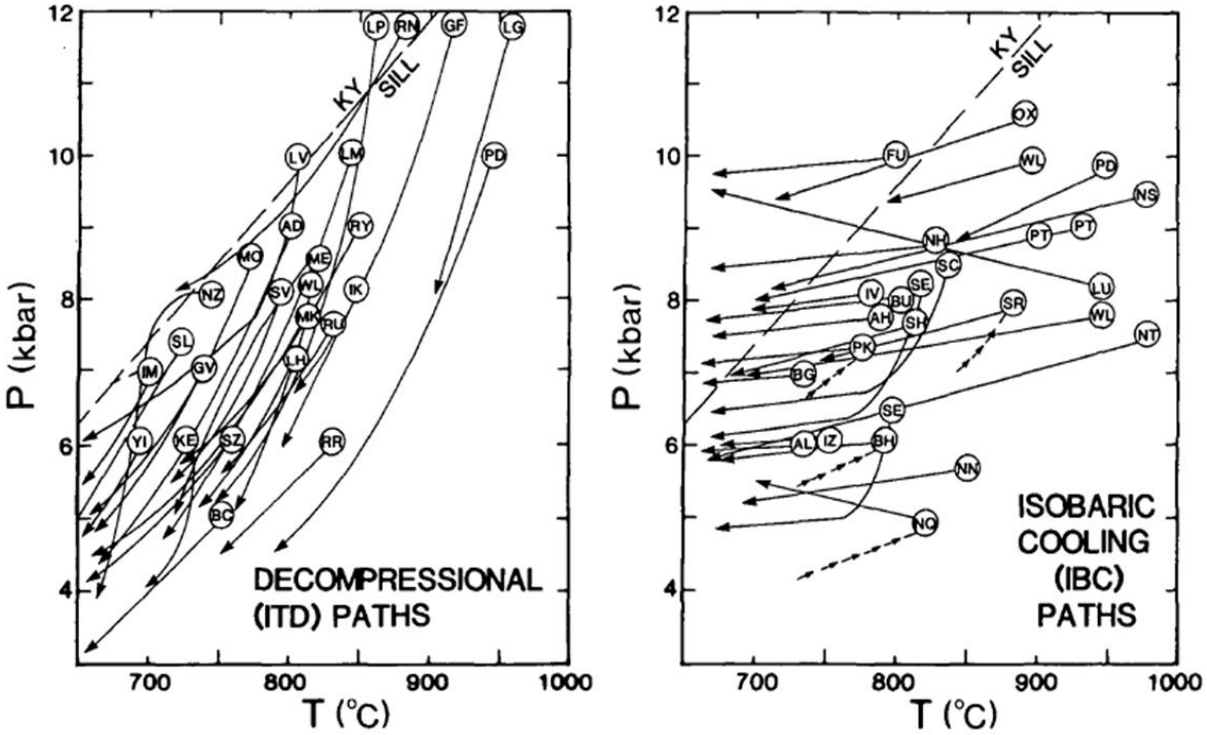

Figura 11: Exemplos de trajetórias de terrenos granulíticos com descompressão isotermal (esquerda) e resfriamento isobárico (direita). Extraído de Harley (1989).

As duas trajetórias P-T, horária e anti-horária, podem ocorrer em mais de um ambiente tectônico, e ambas as trajetórias podem ter a etapa final, após o pico térmico máximo, terminando com resfriamento isobárico na exumação. Já a descompressão isotermal mostrou-se um pouco mais característica de locais com grande aporte de calor ou correlacionado a ambientes extensionais (Harley, 1989; Bohlen ,1991; Winter, 2014).

As estimativas P-T são baseadas nas assembleias minerais em equilíbrio e nas reações entre as mesmas, resultando em texturas indicativas das trajetórias das reações (Harley, 1989; Winter, 2014). No entanto muitas vezes somente as reações de um último evento metamórfico ou do segmento retrógrado da trajetória ficam registradas nas rochas.

Mas além dos ambientes tectônicos propícios e das trajetórias percorridas para a formação dos granulitos, como se preservam as assembleias de alta temperatura sem sofrerem alterações e retrometamorfismo para fácies de grau mais baixo durante a exumação? E como que essas rochas não fundem em temperaturas tão elevadas?

Uma característica dos granulitos é serem formados dominantemente por minerais anidros, sendo o mineral ferro-magnesiano característico o piroxênio (Harley, 1989; Winter, 2014). Hornblenda e biotita são minerais menos abundantes e quando presentes representam o início da fácies granulito, pois em temperaturas mais elevadas há a quebra destes minerais por desidratação (Harley, 1989; Bohlen, 1991; White e Powell, 2002; Winter, 2014).

Neste ponto há a ligação da geração de migmatitos e granulitos. Ambas rochas ocorrem sob as mesmas condições de pressão e temperatura, no entanto o migmatito é uma rocha rica em fluidos e minerais hidratados, e associada a processos de fusão parcial, características opostas às do granulito. A quebra dos minerais hidratados gera a fusão parcial, o leucossoma, o que caracteriza o migmatito (Winter, 2014). Este líquido que gera o leucossoma pode ser retirado ou não do local de sua geração (i.e., *partial* ou *batch melting*), caso permaneça gerará um migmatito, caso retirado o restito gerará um granulito, que é como um resíduo formado pelos minerais resistatos e desidratados (Winter, 2014).

A migração do líquido que gera o leucossoma também é importante para a preservação do granulito porque a sua presença pode desestabilizar as assembleias minerais anidras de alta temperatura, causando retrometamorfismo ao longo da exumação da rocha (White e Powell, 2002; Winter, 2014). A composição original da rocha, o volume de leucossoma retirado, o número de vezes de retirada do leucossoma e as condições P-T dessas perdas de fusão parcial também irão influenciar na preservação ou não das assembleias minerais granulíticas (White e Powell, 2002). Essa perda de fusão parcial pode acontecer desde pequenas quantidades até centenas de milhares de quilômetros cúbicos de fusão, estes algumas vezes formando corpos graníticos co-genéticos com os granulitos e deixando este último depletado em certos elementos químicos (Guernina e Sawyer, 2003; Dostal *et al*., 2006).

3.3 Complexo de Núcleo Metamórfico (*Metamorphic Core Complex*)

Os Complexos de Núcleo Metamórfico (CNM), conhecidos por *Metamorphic Core Complex* (MCC) na língua inglesa, foram formalmente reconhecidos na década de 1980 (Davis; 1983; Coney and Harms, 1984) na Cordilheira Norte Americana no oeste dos Estados Unidos (Fig. 12). O mapa da figura abaixo (Whitney *et al*., 2013)

nos dá uma ideia da distribuição dos principais MCCs Fanerozoicos do mundo, Eon geológico em que eles ocorrem mais e são melhor reconhecidos, sendo relativamente raras as ocorrências Proterozoicas e Arqueanas (James e Mortensen, 1992; Tiddy *et al*., 2020).

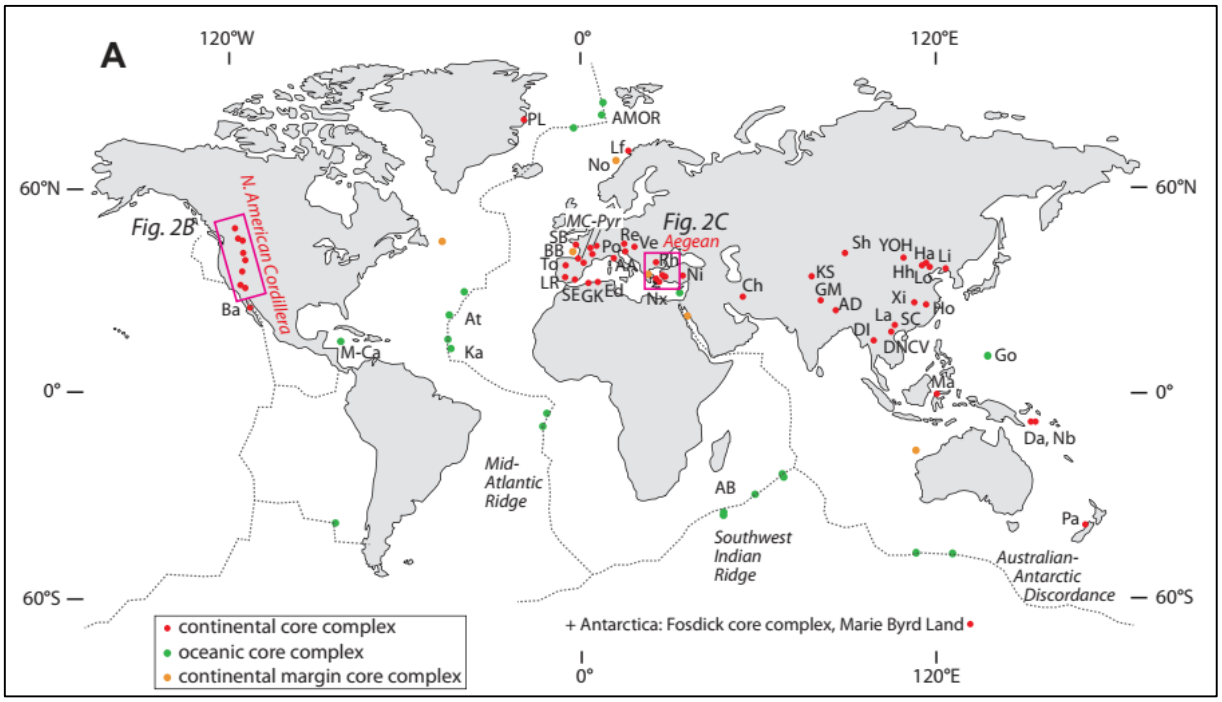

Fig. 12: Mapa mundial das ocorrências Fanerozoicas de Complexos de Núcleo Metamórfico (MCC) (*continental core complex* no mapa), Complexo de Núcleo Oceânico (*oceanic core complex*) e Complexo de Margem Continental (*continental margin core complex*), segundo Whitney *et al*., (2013).

Os MCCs são definidos como uma estrutura geológica dômica ou arqueada composta de rochas deformadas ductilmente sob médio a alto grau metamórfico e incluindo intrusões associadas, subjacentes a uma zona de cisalhamento normal dúctil-rúptil de alta deformação (*dátachment zone*) que experimentou dezenas de quilômetros de deslocamento em resposta à extensão litosférica (Whitney *et al*., 2013). Devido a essa estrutura dômica são muitas vezes confundidos com domos gnáissicos, estes que na verdade podem ter origem por diferentes processos que não o formador de MCC (Yin, 2004; Whitney *et al*., 2004).

Pode-se dizer que os MCCs têm três elementos principais (Platt *et al*., 2015): (i) um núcleo de rocha metamórfica, geralmente com 10 km ou mais de diâmetro, afetado por deformação dúctil e recristalização metamórfica associada, e derivado da crosta média ou inferior; (ii) núcleo metamórfico coberto por uma descontinuidade tectônica sub-horizontal com mergulho regional suave, comumente referido como uma *détachment zone*, compreendendo uma superfície de falha rúptil discreta, com metros a dezenas de metros de rochas cataclásticas em sua *footwall*, subjacente por sua vez a uma zona milonítica a ultramilonítica, que podem ter centenas a milhares de metros de espessura, graduando-se para baixo no núcleo metamórfico principal; (iii) a *détachment zone* é recoberta por rochas da *hanging-wall* que não são metamorfoseadas, ou são de grau metamórfico significativamente inferior ao núcleo metamórfico, onde normalmente ocorre uma série de falhas normais.

A Figura 13 (Brun *et al*., 2018) representa o modelo esquemático dos componentes e estruturação de um MCC. Nele observa-se em ambiente extensional a quebra e abertura da *hanging-wall* com o arqueamento da crosta média-inferior na *footwall*, estes separados pela *détachment zone*, com rochas de alto-grau formando o MCC. Na Figura 13C são mostrados os detalhes dos diferentes pontos, tipos e graus de deformação.

Outra característica dos MCCs e representado esquematicamente na Figura 14 é sua assimetria na distribuição das unidades geológicas e litotipos internos, diferenciando-se assim da simetria presente em diápiros (Burg *et al*., 2004). Esta assimetria, por exemplo, é muito bem representada no MCC de Naxos, na Grécia (Cao *et al*., 2017).

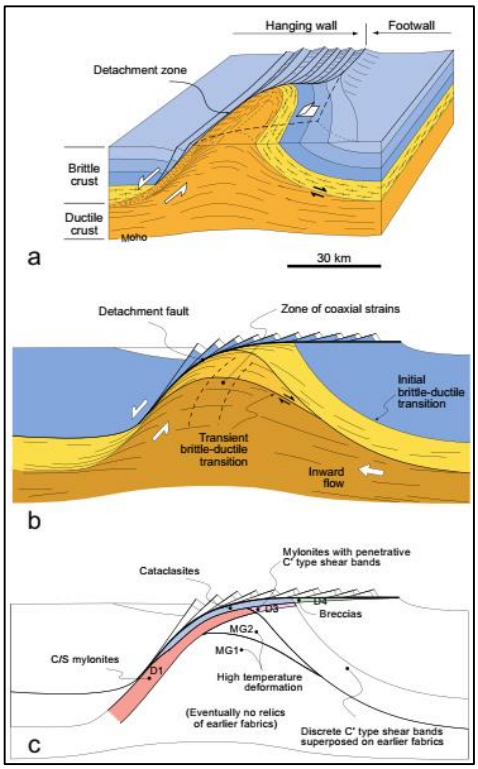

Figura 13: Estrutura de um MCC. A) visão 3D. B) seção esquemática. C) seção esquemática mostrando os diferentes pontos, tipos e graus de deformação (Brun *et al*., 2018).

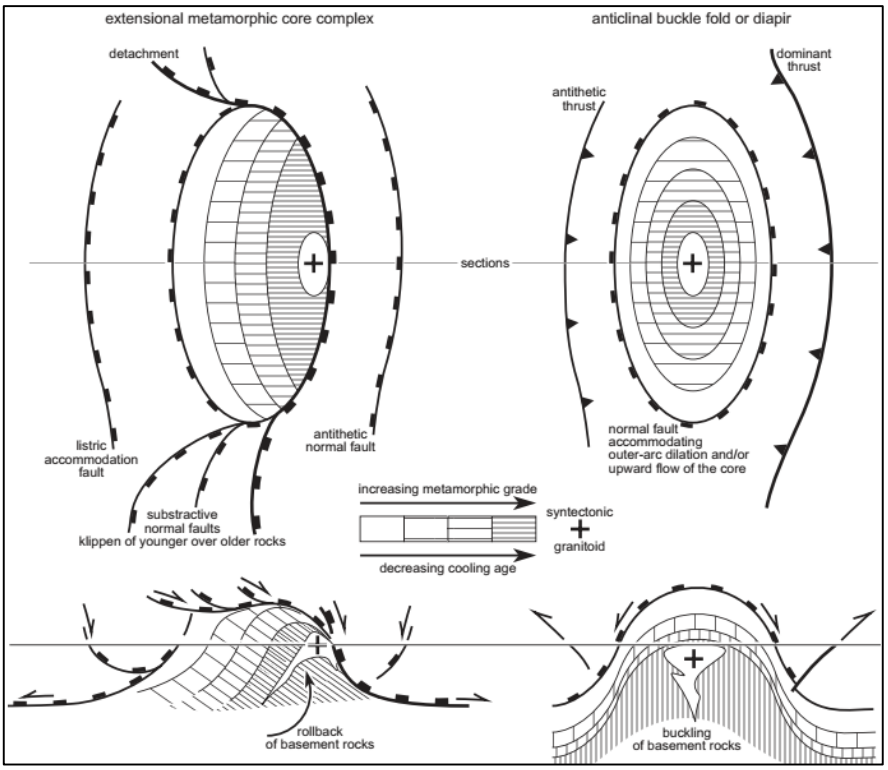

Figura 14: Desenho esquemático em planta e em seção mostrando as diferenças entre um MCC (à esquerda) de ambiente extensional e uma intrusão diapírica (à

direita). Extraído de Burg *et al*. (2004). Ambos processos formam estruturas dômicas, no entanto o MCC apresenta uma assimetria na distribuição dos litotipos enquanto nos diápiros essa distribuição é simétrica.

A identificação de MCCs e zonas *détachment* associadas como produtos de extensão continental de grande magnitude mudou consideravelmente a compreensão da deformação da litosfera (Brun *et al*., 2018), pois registram processos termomecânicos da extensão da litosfera e a compreensão da exumação dessas rochas dúcteis da crosta média e inferior sob falhas normais de baixo ângulo, bem como a dinâmica das falhas, é relevante para o entendimento da evolução crustal e sismogênese da litosfera em extensão (Whitney *et al*., 2013). Os MCCs são estruturas comuns na extensão de orógenos, como também ao longo das zonas divergentes das cadeias mesoceânicas. A descoberta de rochas do manto oceânico exumadas em zonas mesoceânicas de expansão lenta e ultra-lenta nos oceanos Atlântico e Índico em associação com falhas *détachment* de baixo ângulo levaram ao conceito de Complexos de Núcleo Oceânico (*oceanic core complex, OCCs*) por analogia aos *Metamorphic Core Complex* (Brun *et al*., 2018; Whitney *et al*., 2013). Além disso ocorre um terceiro tipo de exumação de rochas mantélicas por extensão na litosfera continental de menor ocorrência, chamado de Complexo de Margem Passiva por Brun *et al*. (2018) ou Complexo de Núcleo de Margem Continental por Whitney *et al*. (2013). Os processos de extensão da litosfera que levam à exumação de rochas dúcteis profundas, tanto da crosta inferior quanto do manto, são classificados em três categorias de estruturas extensionais. Essas distinções vêm de diferenças em termos geológicos: localização no limite de placas ou intra-placas, litosfera continental *vs*. oceânica, natureza crustal *vs*. mantélica das rochas exumadas e padrão de deformação que acomoda a exumação e sua estrutura resultante (Fig. 15).

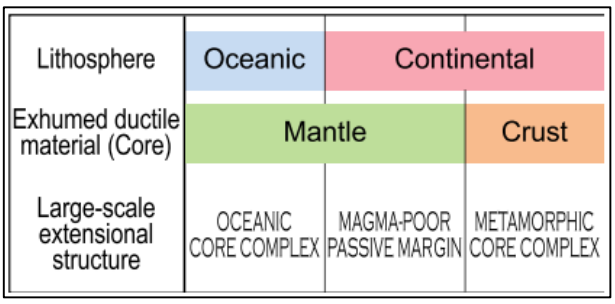

Figura 15: Tabela mostrando as diferenças entre Complexo de Núcleo Metamórfico (*metamorphic core complex*), Complexo de Núcleo Oceânico (*oceanic core complex*) e o terceiro tipo chamado de Complexo de Margem Passiva (segundo Brun *et al*., 2018) ou Complexo de Núcleo de Margem Continental (segundo Whitney *et al*., 2013).

Para uma visualização das condicionantes envolvidas nos processos em crosta continental e oceânica, nas Figuras 16 e 17 abaixo as seções esquemáticas realçam os principais elementos dos *metamorphic core complex* e *oceanic core complex* (Whitney *et al*., 2013). Na Figura 5A está representado um MCC desenvolvido em uma região intraplaca de crosta continental, o qual exuma crosta continental média a inferior na *footwall*, com desenvolvimento de várias falhas normais na *hanging-wall* e influência de água meteórica como fluido. A Figura 16B representa um OCC, desenvolvido em crosta oceânica e exumando manto oceânico, onde há influência da cordilheira mesoceânica mudando o ângulo dos falhamentos, e o fluido principal é a água do mar. Na figura 6 a seção esquemática de quatro complexos de núcleos reais, dois formados no continente (MCCs) e dois no oceano (OCCs).

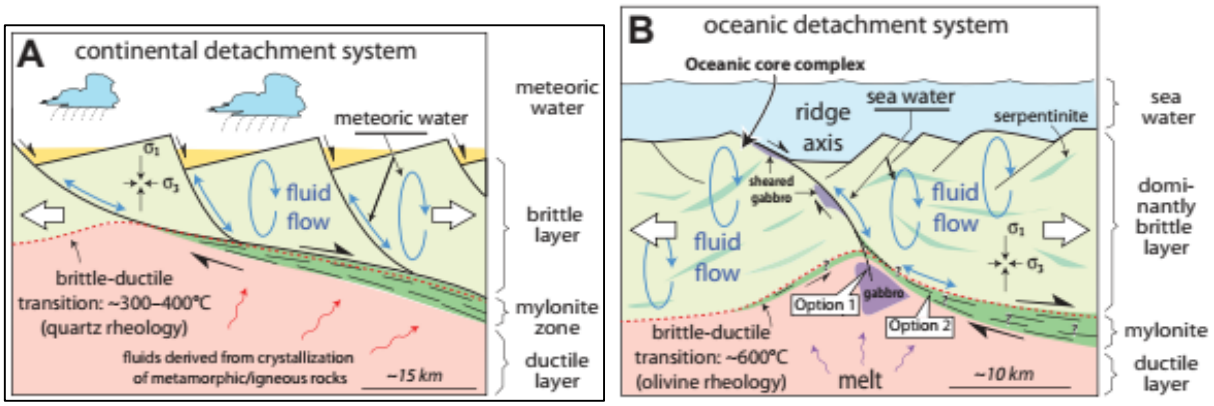

Figura16: Seção esquemática de complexos de núcleo mostrando as diferenças na arquitetura, rochas e fluidos envolvidos. A) Complexo de Núcleo Metamórfico. B) Complexo de Núcleo Oceânico. Extraído de Whitney *et al*. (2013).

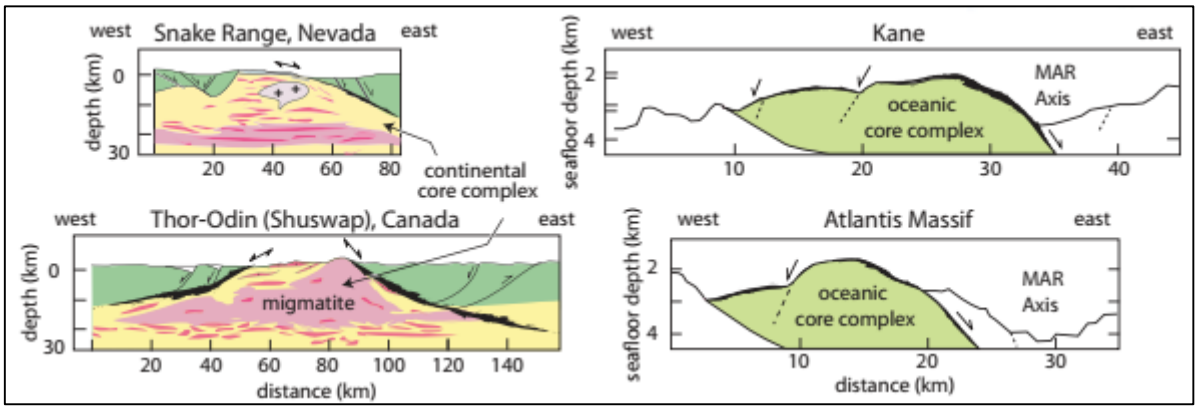

Figura 17: Seção esquemática de exemplos de complexos de núcleo reais e estudados. À direita dois MCCs e à esquerda dois OCCs. Extraído de Whitney *et al*. (2013).

Para entender a formação e geometria desses MCCs e OCCs, modelos análogos e numéricos começaram a ser feitos. Na construção desses modelos, e tendo por base os exemplos reais, percebeu-se que a presença de material de baixa viscosidade, representando rochas dúcteis e aquecidas, é um elemento importante para a formação de um MCC. Na Figura 18 exemplos de modelos análogos, onde fica evidenciado que quando há presença de material dúctil de baixa viscosidade e a crosta superior quebra, esse material tende a subir e exumar (Brun *et al*., 2018).

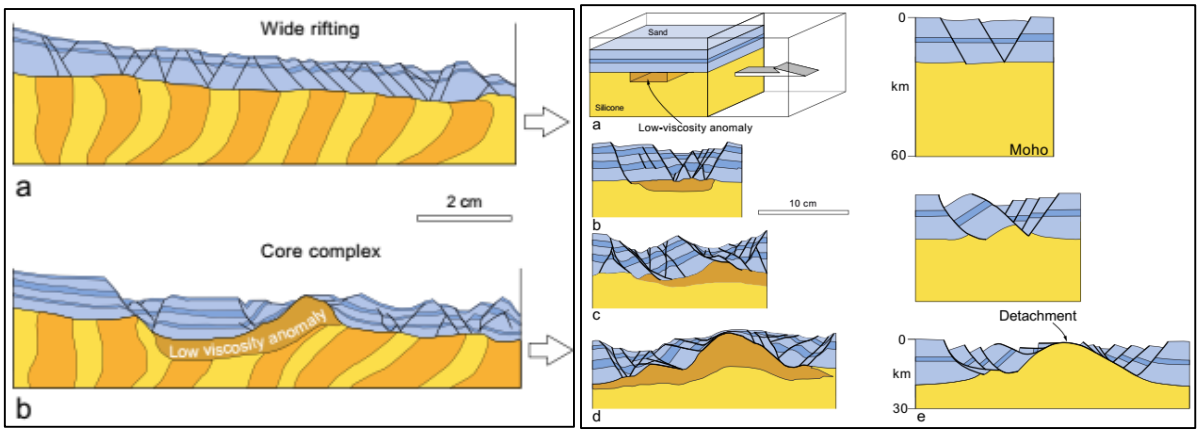

Figura 18: Modelos análogos mostrando a diferença de quando há ou não material de baixa viscosidade em um processo extensional. Na direita, A) modelo sem material de baixa viscosidade, crosta superior quebra com o desenvolvimento de várias falhas normais, mas não há arqueamento da crosta média-inferior; B) modelo com material de baixa viscosidade, mostrando que ao quebrar a crosta superior, o material dúctil

viscoso da crosta média-inferior tende a arquear e subir. Na esquerda, a e b representam o desenvolvimento de um MCC com o passar do tempo (Brun *et al*., 2018).

Na Figura 19 também são apresentados modelos análogos, onde o grau de aquecimento da crosta e a posição dos fluidos de fusão parcial na crosta influenciam no tipo de processo de exumação e formação dos MCCs (Whitney *et al*., 2013).

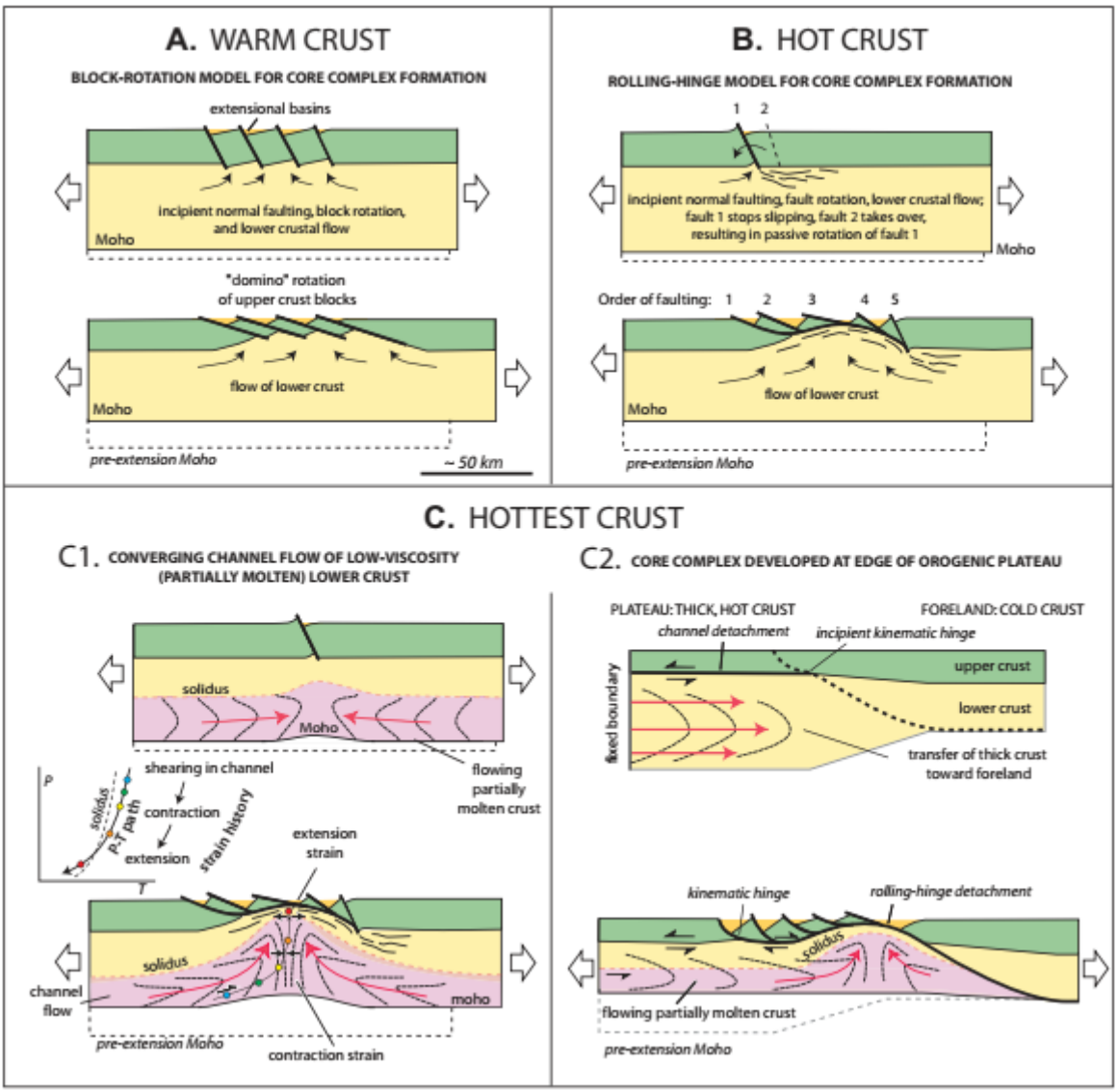

Figura 19: Modelo análogo de formação de MCCs. A) com crosta continental aquecida. B) crosta continental quente. C) crosta continental muito quente, onde dependendo da posição da fusão parcial na crosta a geometria do MCC pode ser

diferente. Observar a elevação da linha de Moho em todos os modelos de formação de MCC. Extraído de Whitney *et al*. (2013).

Com crosta aquecida domina o processo de rotação de blocos, enquanto que com crosta quente predomina o processo da charneira-rolante (*rolling-hinge*). Já com a crosta muito aquecida dois processos podem ocorrer a depender da espessura da crosta e da posição da fusão parcial na mesma. No meio da placa com espessura constante tende a operar o processo de fluxo por canal, se for na borda de um platô orogênico onde há variação da espessura crustal o processo de charneira-rolante irá predominar, formando uma raíz do MCC mais assimétrica (Whitney *et al*., 2013). Observar que em todos os modelos a linha de Moho também soergue e opera no arqueamento dessas rochas da crosta média-inferior.

Modelos numéricos para a compreensão da geodinâmica dos MCCs também foram desenvolvidos, onde é possível medir e controlar certas variáveis como as taxas de strain e cisalhamento. Brun *et al*., (2018) apresenta um modelo no qual vai demonstrando a formação e evolução de um MCC com o passar do tempo e extensão continuada. Na figura 20A estes autores demonstram a geometria e as condições do experimento, representando a crosta média-inferior em contato com o manto e com uma anomalia de viscosidade granítica. Nas Figuras 20B a 20E é mostrado o modelamento dos MCC com a evolução da extensão, as taxas de deformação e cisalhamento e a formação do MCC com sua geometria dômica. No primeiro estágio (Fig. 20B) há o adelgaçamento e quebra da crosta superior rúptil com falhamentos, o que faz com que os líquidos na base da crosta que tem menor densidade e viscosidade comecem a ascender através crosta. Nas Figuras 20C a 20E o que se observa é a consolidação e ampliação do MCC com o aumento da extensão.

Outro modelo numérico (Fig. 21) que leva em consideração um ambiente tectônico mais específico é apresentado por Whitney *et al*. (2013). Esse modelo é construído simulando duas situações em uma borda de platô orogênico onde começa a ocorrer uma extensão por um período de 12 Ma. Na primeira situação não há ascensão de fusão parcial, pelas próprias características de um fluido mais denso e viscoso que tende a fluir mais lateralmente, e o desenvolvimento de um domo com fluxo vertical é moderado. Na segunda simulação a fusão parcial é menos densa e menos viscosa, tendendo a um fluxo mais vertical e ascendendo pela crosta, tendo o pleno desenvolvimento de um domo, além de a deformação geral na base da crosta ser mais intensa com a presença de líquidos de baixas densidade e viscosidade.

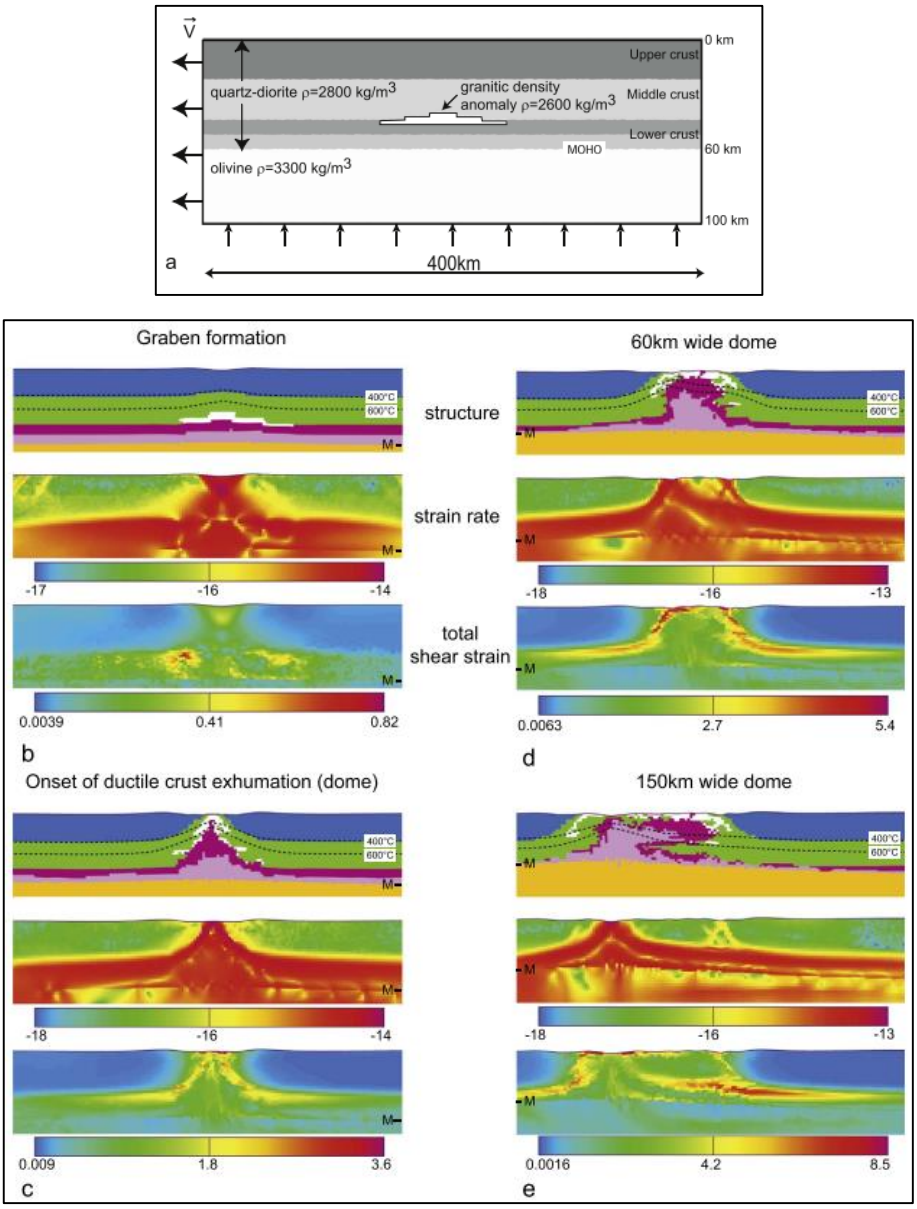

Figura 20: Modelagem numérica de desenvolvimento de um MCC em escala litosférica. A) Geometria do modelo e condições dos limites de velocidade. B a D) Seções de modelos com extensão cada vez maior. Cada painel apresenta a estrutura do modelo e as isotermas de 400 °C e 600 °C (seção superior), a taxa de deformação (seção intermediária) e taxa de deformação total por cisalhamento (seção inferior). Extraído de Brun *et al*. (2018).

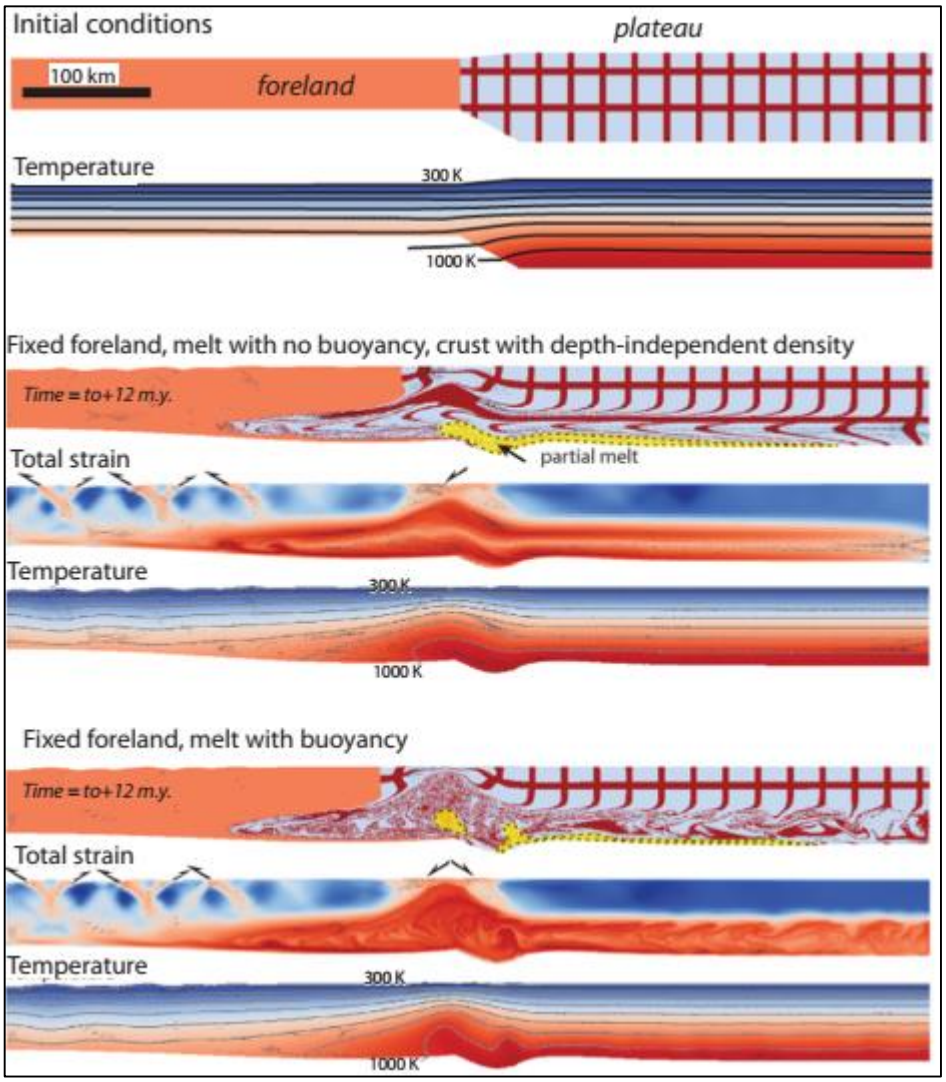

Figura 21: Modelos Ellipsis bidimensionais de desenvolvimento de um MCC na borda de um platô orogênico. Painel superior: Condições iniciais; Moho do platô T = 790 °C e Moho *foreland* T = 560 °C. Painel do meio: experimento com a densidade independente da profundidade na crosta, mesmo na região de fusão parcial. Após 12 Ma, a crosta inferior do platô fluiu 150 km lateralmente para a crosta da *foreland* e continua fluindo a uma velocidade de 1 cm/ano. A crosta superior da *foreland* se espessa por falhas. Acima da rampa do platô forma-se um domo, mas na superfície a exumação é moderada. Painel inferior: Experimento com fusão parcial flutuante (2366 kg m^{-3}). O fluxo lateral da crosta inferior do platô é menor (120 km), e um domo se forma plenamente, exumando as rochas da crosta inferior para a superfície. Extraído de Whitney *et al*. (2013).

Para sintetizar as etapas de desenvolvimento de um MCC, Brun *et al*. (2018) elaborou o croqui da Figura 22 baseado no modelo numérico apresentado na Figura 20. Os autores individualizam as etapas de desenvolvimento do MCC em duas principais, início e amplificação, mas podemos considerar um estágio intermediário entre o primeiro arqueamento da crosta média-inferior e o seu pleno desenvolvimento. No início do processo ocorre a quebra da crosta rúptil por falhamentos e o arqueamento inicial da crosta inferior, até o dado momento quando começa a operar a zona *détachment*. A partir desse momento o MCC se estabelece com exumação das rochas da crosta média-inferior, passando para a etapa de amplificação, que é o crescimento do MCC.

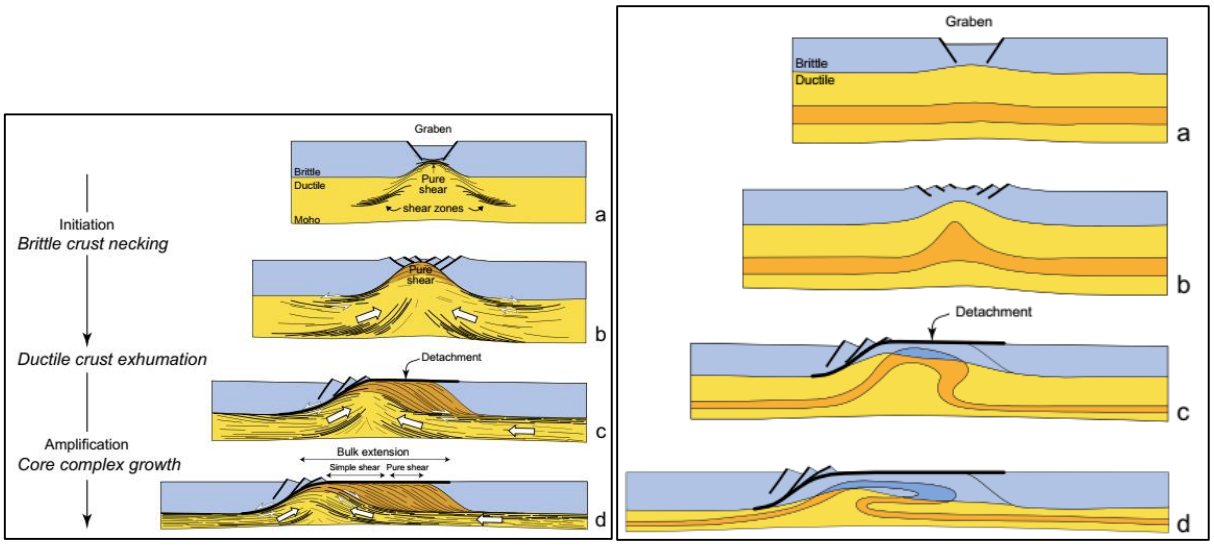

Figura 22: Síntese do desenvolvimento de um MCC baseado no modelo numérico da Figura 20. A) e B) estágio inicial, com a quebra da crosta superior e arqueamento inicial da crosta média-inferior. C) estágio intermediário, exumação da crosta dúctil e início do desenvolvimento da zona *détachment*; D) estágio final, amplificação e crescimento do MCC com aumento da zona *détachment* e de dobramentos. Extraído de Brun *et al*. (2018).

Estudado nas últimas 4 décadas, hoje se tem conhecimento sobre os processos e os condicionantes formadores dos MCCs, como também no que isso implica ao reconhecer essa estrutura regional no terreno em que se estiver estudando. A ocorrência de um MCC implica numa certa geodinâmica da litosfera com variáveis

fundamentais, entre elas a presença de fusão parcial de baixas densidade e viscosidade, em conjunto com uma tectônica extensional operando.

4. Materiais e Métodos

Três projetos de mapeamento geológico realizados pelo Serviço Geológico do Brasil (SGB – CPRM) na última década (Iglesias *et al*., 2011; Betiollo *et al*., 2018; Iglesias *et al*., 2021) levantaram um conjunto robusto de dados geológicos (escalas 1:250.000 e 1:50.000) usados nesta Tese. O conjunto de dados consiste em mais de 1.000 afloramentos descritos e a produção de cerca de 500 lâminas petrográficas, que foram todas integradas e reavaliadas aqui para a compreensão regional do Complexo Granulítico de Santa Catarina – CGSC e do Cráton Luis Alves – CLA. Dados geológicos e estruturais regionais obtidos durante o trabalho de campo identificaram os principais litotipos e estruturas condicionantes ao longo do CLA. Dados estruturais (ou seja, principalmente foliações e bandamentos gnáissicos) obtidos em campo também foram usados para validar os lineamentos aerogeofísicos regionais reconhecidos.

O levantamento aerogeofísico (CPRM, 2011) utilizado nesta Tese abrangeu mais de 140.000 km² de linhas aeromagnéticas e aerogamaespectrométricas de alta resolução sobre o escudo Paraná-Santa Catarina. As linhas de voo têm perfil a uma elevação de 100 m e foram orientadas N-S com espaçamento de 500 m, enquanto as linhas de amarração são E-W e foram espaçadas em 10.000 m. Os dados foram adquiridos e processados pela Lasa Prospecções S.A. (Rio de Janeiro), utilizando rotinas do *software* Oasis Montaj, que incluem correção de paralaxe, remoção de campo de referência geomagnética internacional, correção diurna, nivelamento, entre outras. Mais informações sobre o levantamento aerogeofísico, processamento de dados e banco de dados aerogeofísico estão disponíveis no site da SGB – CPRM (https://rigeo.cprm.gov.br/handle/doc/11241).

Mapas aeromagnetométricos foram selecionados para avaliar e interpretar estruturas regionais na área de estudo (por exemplo, Nabighian *et al*., 2005; Hinze *et al*., 2013). A primeira derivada vertical (nas cores cinza e RGB) e a Amplitude do Sinal Analítico (ASA) foram usadas para mapear a geometria e as estruturas internas de corpos geológicos e unidades geotectônicas e para identificar estruturas magnéticas profundas (por exemplo, Reeves, 2005). Dados de raios gama compostos por canais K (%), eU (ppm) e eTh (ppm), foram representados em contagem gama total e mapas ternários (por exemplo, IAEA, 2003). Dados radiométricos foram utilizados para mapear as bordas dos corpos e as propriedades internas das unidades geotectônicas, refletindo a diversidade dos litotipos. Finalmente, dados magnéticos e

gamaespectrométricos reconhecidos por análises aerogeofísicas foram investigados em campo para aumentar a confiança de nossas interpretações.

As amostras de rocha para litogeoquímica (n= 85) foram reduzidas para tamanho de grão <200 mesh em um moinho de disco de ágata após o esmagamento. As análises foram realizadas nos Laboratórios SGS GEOSOL por fusão de metaborato de lítio e leitura por ICP-AES para elementos principais e ICP-MS para REE, e digestão multi-ácido e leitura por ICP-MS para outros oligoelementos. Procedimentos analíticos detalhados estão disponíveis em https://www.sgsgeosol.com.br/.

Nos resultados analíticos do REE, no caso dos BIFs, o Y foi adicionado conforme metodologia de Bau e Dulski (1996), configurando um padrão REY (REE+Y) com o Y inserido entre o Dy e o Ho de acordo com o raio iônico. Os dados REY foram normalizados para PAAS (*Post-Archean Australian Shale*; Taylor e Mclennan, 1985) e as anomalias de Ce*, Eu* e outras, também normalizadas para PAAS e identificadas por "sn" (*shale-normalized*), foram calculadas segundo Bau e Dulski (1996) e Bolhar *et al*. (2004).

5. Contexto Geológico

O Cráton Luis Alves – CLA (Kaul, 1980) no sul do Brasil (Fig. 23) atuou como uma das massas de terra que deram suporte para o desenvolvimento da orogenia Neoproterozoica Brasiliano – Pan-Africana durante a colagem do Gondwana Ocidental (Basei *et al*., 1998; 2009; Heilbron, 2008; Brito Neves, 2011; Passarelli *et al*., 2018; Bruno *et al*., 2018). O CLA (Fig. 24) é composto pelo Complexo Granulítico de Santa Catarina – CGSC (Hartmann *et al*., 1979; Fig. 24), que apresenta uma história evolutiva do Neoarqueano ao Orosiriano (Basei *et al*., 1998; 2009; Hartmann *et al*., 2000; Heller *et al*., 2021) através da geração de TTG (2,68 e 2,5 Ga), BIF e outras rochas com protólitos sedimentares, seguido por dois eventos metamórficos granulíticos de alto grau (2,35 e 2,18 Ga), e terminando com metamorfismo retrógrado de fácies anfibolito em ca. 2,0 Ga.

Outras unidades geológicas dentro da área cratônica são de idade Neoproterozoicas, correlacionadas com o ciclo Brasiliano, incluindo os granitoides da Suíte Serra do Mar e as bacias sedimentares de Campo Alegre, Guaratubinha e Corupá. O CLA é circundado por quatro unidades geotectônicas e parcialmente recoberto pela Bacia Paleozoica do Paraná. Três dessas unidades foram geradas durante a orogenia Neoproterozoica, a saber: Faixa Norte do Cinturão Dom Feliciano, Cinturão Ribeira Meridional e Bloco Paranaguá. A quarta unidade geotectônica ao redor do CLA é a Microplaca Curitiba, parte do Cinturão Ribeira Meridional, que contém remanescentes Arqueano-Paleoproterozoicos fortemente migmatizados durante a orogenia Brasiliano – Pan-Africana (Basei *et al*., 2009).

Os trabalhos geológicos de cunho regional indicam que as rochas metamórficas do CLA sofreram, no Neoarqueano - Paleoproterozoico, pelo menos duas fases de metamorfismo regional na fácies granulito e uma na fácies anfibolito, além de retrometamorfismo na fácies xistos verdes, em zonas de cisalhamento estreitas e em zonas de falhas, tendo atingido estabilidade tectônica no Paleoproterozoico em torno de 1,8 Ga (Hartmann; Silva; Orlandi Filho, 1979; Kaul; Teixeira, 1982; Mantovani *et al*., 1987; Hartmann, 1988; Basei *et al*, 1998; Hartmann *et al*., 2000).

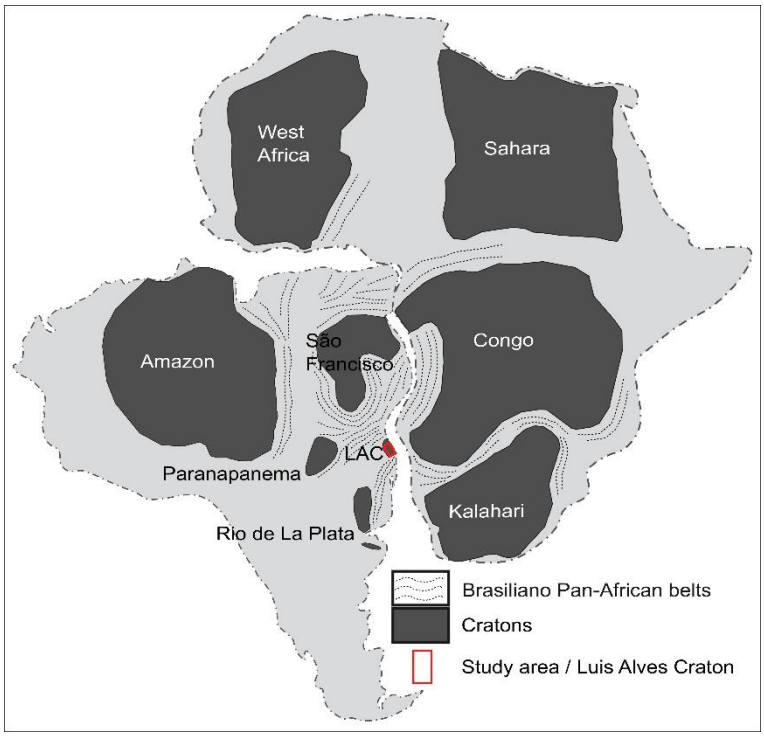

Figura 23: Mapa esquemático do Gondwana Oeste mostrando a área de estudo (modificado de Heilbron *et al*., 2004; Passarelli *et al*., 2018; De Toni *et al*., 2020).

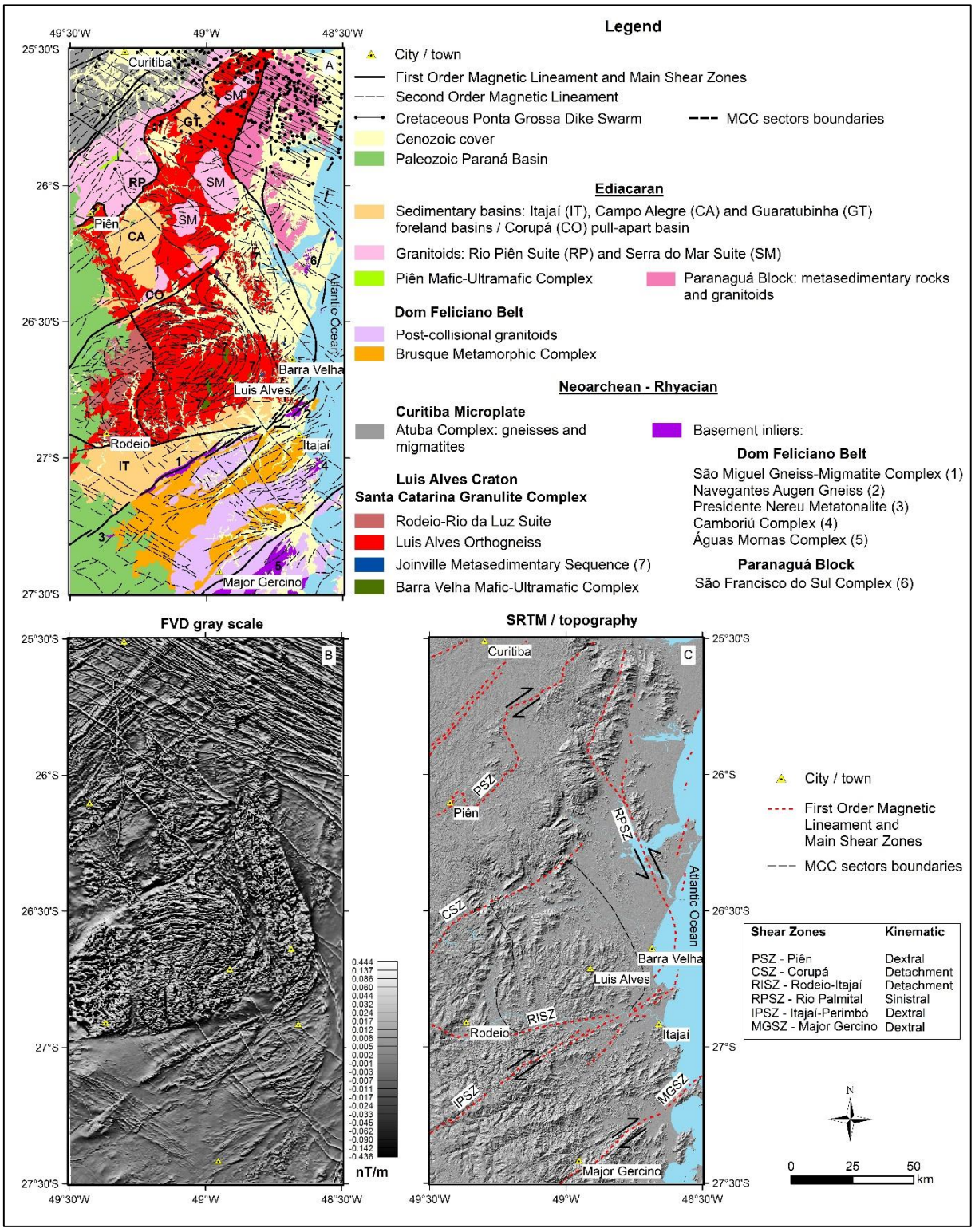

Figura 24: Mapa geológico e imagens aerogeofísica e de sensor de satélite. A) Mapa geológico simplificado da área de estudo e blocos tectônicos adjacentes (modificado de Iglesias *et al*., 2011; Betiollo *et al*., 2018; Bruno *et al*., 2018; Passarelli *et al*., 2018). B) Imagem da Primeira Derivada Vertical (FVD) em tons de cinza que destaca a estrutura elipsoidal do MCC na porção central, e os lineamentos magnéticos de primeira e segunda ordem, revelando estruturas regionais e diferentes terrenos

magnéticos. As principais zonas de cisalhamento coincidem com lineamentos magnéticos de 1ª ordem. C) Imagem topográfica SRTM (*Shuttle Radar Topography Mission*) mostrando que o MCC não é uma feição de superfície e não possui correspondência na topografia. Os lineamentos magnéticos de primeira ordem e as principais zonas de cisalhamento que limitam a área do MCC também são mostrados para referência.

Artigo 1

Gmail **Leandro Betiollo <le.vermelho@gmail.com>**

Confirming submission to Journal of Geodynamics

1 mensagem

Journal of Geodynamics <em@editorialmanager.com> 20 de maio de 2022 às 14:55
Responder a: Journal of Geodynamics <support@elsevier.com>
Para: LEANDRO MENEZES BETIOLLO <le.vermelho@gmail.com>

This is an automated message.

Aerogeophysical and geological data highlights a Siderian–Rhyacian granulite Metamorphic Core Complex in the Luis Alves Craton (Southern Brazil)

Dear Sr BETIOLLO,

We have received the above referenced manuscript you submitted to Journal of Geodynamics.

To track the status of your manuscript, please log in as an author at https://www.editorialmanager.com/geod/, and navigate to the "Submissions Being Processed" folder.

Thank you for submitting your work to this journal.

Kind regards,
Journal of Geodynamics

More information and support

You will find information relevant for you as an author on Elsevier's Author Hub: https://www.elsevier.com/authors

FAQ: How can I reset a forgotten password?
https://service.elsevier.com/app/answers/detail/a_id/28452/supporthub/publishing/
For further assistance, please visit our customer service site: https://service.elsevier.com/app/home/supporthub/publishing/
Here you can search for solutions on a range of topics, find answers to frequently asked questions, and learn more about Editorial Manager via interactive tutorials. You can also talk 24/7 to our customer support team by phone and 24/7 by live chat and email

#AU_GEOD#

To ensure this email reaches the intended recipient, please do not delete the above code

---

In compliance with data protection regulations, you may request that we remove your personal registration details at any time. (Use the following URL: https://www.editorialmanager.com/geod/login.asp?a=r). Please contact the publication office if you have any questions.

Aerogeophysical and geological data highlights a Siderianï Rhyacian granulite Metamorphic Core Complex in the Luis Alves Craton (Southern Brazil)

Leandro Menezes Betiollo[1,2*], Everton Marques Bongiolo[2], Jairo Francisco Savian[2], Carlos Moacyr da Fontoura Iglesias[1]

[1]Gerência de Geologia e Recursos Minerais, Serviço Geológico do Brasil (SGB ï CPRM), Rua Banco da Província 105, 90840-030, Porto Alegre, Rio Grande do Sul, Brazil

[2]Programa de Pós-graduação em Geociências, Universidade Federal do Rio Grande do Sul, Avenida Bento Gonçalves 9500, 91500-000, Porto Alegre, Rio Grande do Sul, Brazil

*corresponding author: leandro.betiollo@cprm.gov.br

Abstract

Cratonic granulite terranes record geological processes considered important sources to understand the primordial Earth's evolution. In the last decades, granulite geological modeling took advantage of thermodynamic datasets provided by advancing analytical techniques in association with new geodynamic views. The Luis Alves Craton (LAC) is considered a fragment of a mid- to large-scale granulitic terrane including Archean-Paleoproterozoic rocks within the worldwide supercratons puzzle. Previous studies developed in the LAC focused mostly on petrological and geochronological data, and its role in the Neoproterozoic Gondwana Supercontinent assembly. However, even with the prominent scientific advances, little is known about the tectonic settings that took place during and after granulite formation. In this contribution, we use regional geological-structural mapping, petrography, and a high-resolution aerogeophysical survey to determine the geological-tectonic framework, processes of formation and exhumation, and the regional significance of the LAC in the light of metamorphic petrology, supercontinent cycles, and Paleoproterozoic geodynamic processes. Although the Southern LAC domain has characteristics of gneissic dome, diapir and dome-and-keel structures, we propose it represents a rare, partially preserved Siderian-Rhyacian granulite Metamorphic Core Complex (MCC), a structure commonly seen and largely known in the Phanerozoic. The Luis Alves Craton MCC is limited by first-order magnetic lineaments, mostly corresponding to shear zones, and locally to structures interpreted as paleo-detachment zones associated with the development of

sedimentary basins. The MCC is subdivided into three sectors with their own geological, magnetic and gamma-ray characteristics. The occurrence of granulite facies MCC has important implications for the Siderian-Rhyacian geodynamics since they are mostly found within Phanerozoic terranes. The LAC is characterized as a G-UHTM metamorphic belt with thermobaric ratios between 750 – 1500 °C/GPa, implying the development of a large hot orogen followed by a post-orogenic extension and exhumation of the MCC, that may take place during the Rhyacian-Orosirian transition under retrograde amphibolite facies metamorphism associated with shear zones and detachments activations. The LAC had an oblivious tectonic history to the main Paleoproterozoic collisional events, representing: (i) the amalgamation and fragmentation of an older continental segment, or (ii) one of the first collisional events of the Columbia supercontinent which was already exhuming by the end of the Rhyacian, while the remaining Columbia supercontinent blocks were still colliding until the end of the Orosirian.

Keywords: aeromagnetometry, aerogammaspectrometry, metamorphic core complex, supercontinent cycle, large hot orogen, gneiss dome.

1. Introduction

Granulite terranes have their origin and geological meaning studied since Weiss (1803) (O'Brien, 2006). In the last four decades, granulite geological modeling took advantage of robust thermodynamic datasets (Holland and Powell, 1985; Powell and Holland, 1985; 1988), and advances in analytical techniques. Metamorphic events under up to 1200 °C and 6 GPa (or up to 200 km crustal depth) were determined, and these extreme metamorphic petrological fields were built in association with geodynamic views (Brown, 2007a,b; 2014; Stuwe, 2007; Brown and Johnson, 2019). Granulite terrane generation was mainly related to volcanic and continental arc environments with extra heat sources (Harley 1989, 1992; Bohlen 1991; Ashwal et al., 1992; Gerya and Meilick, 2011; Kramers et al., 2011; Lexa et al., 2011; Sajeev et al., 2013), and their present understanding involve: (i) the formation, evolution and consolidation of large hot orogens (Chardon et al., 2009; Franek et al., 2011; Jamieson and Beaumont, 2013; Kohn, 2014; Harley, 2016; Perchuk et al., 2018; Brown and Johnson, 2019; Dziggel et al., 2019), (ii) supercontinent amalgamation (Bleeker, 2003; Zhao et al., 2004; Brown, 2007a; Vansutre and Hari, 2010; Bradley 2011; Touret et al.. 2016), and (iii) Earth time's cycles (Brown and Johnson, 2019). However, even with

the prominent scientific advances, exhumation, P-T-t paths, deformational patterns, microstructural processes, and the regional structuration of these lower crust terranes, are still subjects of increasing investigations (Harley, 1989, 1992; Barbosa et al., 2006; Taylor et al., 2010; Jamieson and Beaumont, 2011; Kelsey and Powell, 2011; Spalla et al., 2011; White and Powell, 2011; Endo et al., 2012; Block et al., 2016; Dharmapriya et al., 2017; Girelli et al., 2018; Zhang et al., 2021).

Metamorphic Core Complex (MCC) is a regional tectonic structure found on all continents and largely known in the Phanerozoic (Lister and Davies, 1989; Verdel et al., 2007; Wang et al., 2012; Daoudene et al., 2013; Tichomirowa and Kohler, 2013; Whitney et al., 2013; Toraman et al., 2014; Cao et al., 2017; Wiest et al., 2019; Cheng et al., 2020; Kamaci and Altunkaynak, 2020; Österle et al., 2020), with rare records in the Proterozoic (Rizzotto et al., 2019; Tiddy et al., 2020) and older crustal segments (James and Mortensen, 1992; Hoffmann et al., 2015). Paleoproterozoic, and mainly Archean terranes, commonly show dome-and-keel structures characterized by vertical tectonics (Van Kranendonk et al., 2004; 2007; Harris et al., 2012; Lin and Beakhouse, 2013; Thebaud and Rey, 2013; Gerya, 2014; Bédard, 2018; Zulauf et al., 2019), as in the Quadrilátero Ferrífero (QF – Iron Quadrangle) and Carajás areas in Brazil (Marshak et al., 1997; Cutts et al., 2019; Costa et al., 2020), in Mount Edgar and Yalgoo domes in Australia (Sandiford et al., 2004; François et al., 2014; Clos et al., 2019; Roberts and Tikoff, 2021), and in the Barberton greenstone belt in South Africa (Lana et al., 2010). On the other hand, the formation and exhumation of MCC from the lower crust is considered a result of horizontal tectonics intrinsically attributed to extensional regimes, often during post-orogenic stages (Scheffer et al.,2016; Searle and Lamont, 2020) such as those registered in the Aegean (Searle and Lamont, 2022) and Cordilleran orogens (Lister and Davies, 1989; Stevens et al., 2017). Its formation reflects particular rheological conditions, such as those associated with Moho's depth and temperature, heat concentration and the bulk of conditioned partial melting (Whitney et al., 2013; Platt et al., 2015; Cooper et al., 2017; Brun et al., 2018). MCCs occur in either continental or oceanic lithosphere (i.e., Oceanic Core Complexes – OCC), exhuming deep crustal or mantle rocks, respectively (Hayman et al., 2011; Whitney et al., 2013; Lagabrielle et al., 2015; Brun et al., 2018). MCCs normally host gneiss domes (Eskola, 1949; Allen and Chamberlain, 1989; Norlander et al., 2002), a structure related to the exhumation of high-grade metamorphic rocks from the mid-lower continental crust. Indeed, it is frequently difficult to individualize MCCs from gneiss domes associated with dome-and-keel structures, because they share regional

structural patterns and geological mechanisms of formation, diapirism being one of the most common (Teyssier and Whitney, 2003; Burg et al., 2004; Gerya et al., 2004; Whitney et al., 2004a; Blenkinsop, 2011; Platt et al., 2015). Both MCC and gneiss domes contain migmatites formed under at least high amphibolite metamorphic facies, rarely under granulite ones (Gerya et al., 2004; Barbosa et al., 2004; Blenkinsop, 2011; Chardon et al., 2011; Klepeis et al., 2016; Liu and Wei, 2018). Beyond this, gneiss dome formation combines several geological processes (Yin, 2004), generating a regional puzzle of individual terranes with their own evolutional history (Soula, 1982; Duncan, 1984; Guo et al., 2008; Denèle et al., 2009; Chardon et al., 2011; Kruckenberg and Whitney, 2011; Spalla et al., 2011; Baldim and Oliveira, 2016; Billerot et al., 2017; Walczak et al., 2017; Zhang et al., 2017).

Aeromagnetometry survey has been proved as a powerful tool to reveal regional compartmentation (Riedel et al., 2013; Mieth and Jokat, 2014a; Rajaram and Anand 2014; Xiong et al., 2016; Golynsky et al., 2018), geologic-structural features, and its interpretation (Aitken and Betts, 2009; Tominaga and Sager, 2010; Blanco-Montenegro et al., 2011; Jordan et al., 2013; Anudu et al., 2014; Gernigon et al., 2015; Block et al., 2016; Hartmann et al., 2016; Oladunjoye et al., 2016; Eldosouky et al., 2017; Kayode et al., 2017; Chopin et al., 2019). Indeed, it provides the recognition of major structures (Dossing et al., 2010; Dufréchou, 2017; Maacha et al., 2017; Catalan et al., 2018; Domingos et al., 2020; Tiddy et al., 2020), bounding individual geologic unit boundaries (Mieth and Jokat, 2014b; Oladunjoye et al., 2016; Kumar et al., 2018; Launay et al., 2018), blocks of rock associations (Aitken et al., 2014; Araujo et al., 2019;), and superficial features hidden by forest (Rosa et al., 2014; Rosa et al., 2016; Scandolara et al., 2017; Costa et al., 2020), ice (Goodge and Finn, 2010; Jordan et al., 2013;), or sedimentary basin covering (Betts et al., 2003; Murthy and Babu, 2006; Ogunmola et al., 2016; Minelli et al., 2018). Aerogammaspectrometry also contributes to regional geological mapping, its main uses being (i) detailing regional elements previously recognized by aeromagnetometry, and (ii) mapping magmatic plutons and sedimentary basins boundaries (Hartmann et al., 2016; Maacha et al., 2017; Araújo et al., 2019; Costa et al., 2020; Domingos et al., 2020).

In this paper, we use regional geological-structural data, petrography, and a high-resolution aerogeophysical survey to reinterpret the geological-tectonic framework, processes of formation, and the regional significance of the LAC in Southern Brazil. Data integration includes the available literature and the latest

advances on metamorphic petrology, supercontinents cycle and geodynamic processes active during the Siderian–Rhyacian evolution of this crustal segment.

2. Geological Setting

The LAC (Kaul, 1980) in Southern Brazil (Fig. 1) acted as a foreland landmass for the development of the Neoproterozoic Brasiliano – Pan African orogeny during the Western Gondwana assembly (Basei et al., 1998; 2009; Heilbron, 2008; Brito Neves, 2011; Passarelli et al., 2018; Bruno et al., 2018). It is composed by the Santa Catarina Granulite Complex (Hartmann et al., 1979; Fig. 2A), which shows an evolutional history from Neoarchean to Orosirian (Basei et al., 1998; 2009; Hartmann et al., 2000; Heller et al., 2021) through the generation of TTG (2.68 and 2.5 Ga), BIF and sedimentary protoliths, by two high-grade granulite metamorphic events (2.35 and 2.18 Ga), and ending with amphibolite facies retrograde metamorphism at ca. 2.0 Ga. Other geological units within the cratonic area are Neoproterozoic, correlated with the Brasiliano cycle, including granitoids of the Serra do Mar Suite and the Campo Alegre, Guaratubinha and Corupá sedimentary basins. The LAC is surrounded by four geotectonic units and partially covered by the Paleozoic Paraná Basin. Three of them were generated during the Neoproterozoic orogeny, namely the Northern Dom Feliciano Belt, the Southern Ribeira Belt and the Paranaguá Block. The fourth geotectonic unit surrounding the LAC is the Curitiba Microplate, part of the Southern Ribeira Belt, which contains Archean-Paleoproterozoic remnants strongly migmatized during the Brasiliano – Pan African orogeny (Basei et al., 2009).

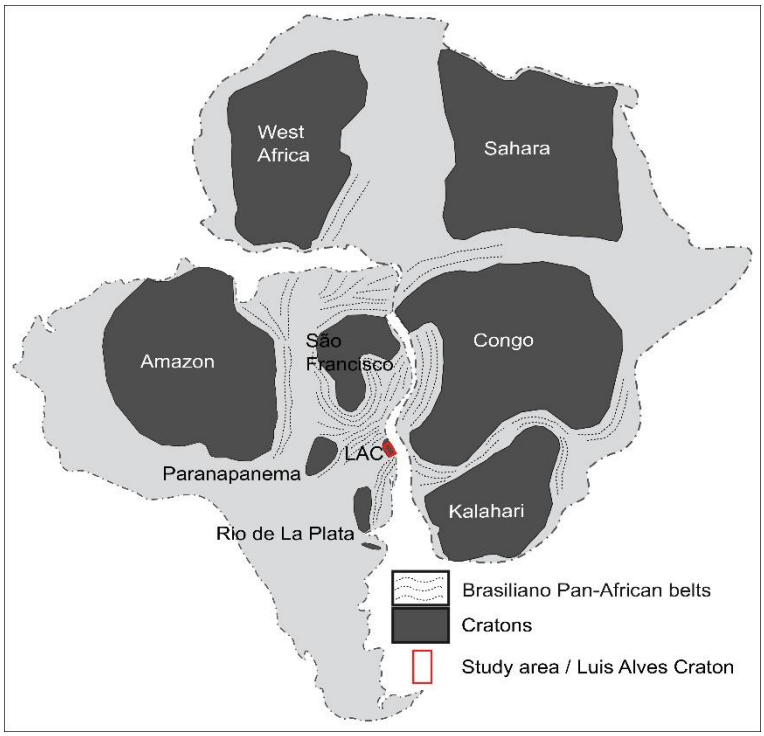

Figure 1. Schematic map of the Western Gondwana showing the study area (modified from Heilbron et al., 2004; Passarelli et al., 2018; De Toni et al., 2020).

The Dom Feliciano Belt (Basei, 1985; Hueck et al., 2018; De Toni et al., 2020) extends from South Brazil to Uruguay and surrounds the LAC in its Northern sector. It is constituted by the Brusque Metamorphic Complex (Philipp et al., 2004; Campos et al., 2012), the Florianópolis Batholith (Bitencourt and Nardi, 2000; Florisbal et al., 2012) and the Itajaí Basin (Guadagnin et al., 2010; Basei et al., 2011). The Itajaí-Perimbó (IPSZ) and Major Gercino (MGSZ) shear zones are the main regional structures limiting internal segments of the Dom Feliciano Belt. Between the IPSZ and MGSZ, metasedimentary successions of the Brusque Metamorphic Complex occur, and to its South, the Florianópolis Batholith crops out. The Southern Ribeira Belt (Heilbron, 2008; Basei et al., 2009; Passarelli et al., 2011; 2018) to the North of the LAC is represented by the Apiaí Complex (metavolcano-sedimentary sequences and calc-alkaline granitoids) and the Curitiba Microplate (gneisses and migmatites), bonded along the Lancinha shear zone (LSZ). The contact between those units and the LAC is represented by the Piên shear zone (PSZ) where the Piên Suite (Machiavelli et al., 1993; Harara, 2001) was emplaced. Finally, the Paranaguá Block (Cury, 2009) consists of metasedimentary rocks and granitoids at the Eastern LAC boundary along the Rio Palmital shear zone (RPSZ).

3. Methods

3.1. Geology and petrography

Three projects of geological mapping carried out by the Geological Survey of Brazil (SGB – CPRM) in the last decade (Iglesias et al., 2011; Betiollo et al., 2018; Iglesias et al., 2021) raised a robust geological dataset (1:250,000 and 1:50,000 scales) used in this contribution. The dataset consists of more than 1,000 described outcrops and the production of ca. 500 thin sections, which were all integrated and re-evaluated here to refine the regional understanding of the Santa Catarina Granulite Complex and the LAC (Fig. 2A). Regional geological and structural data obtained during fieldwork identified the main lithotypes and conditioning structures along the LAC. Structural data (i.e., mostly foliations and gneissic banding) obtained in the field were also used here to validate the regional aerogeophysical lineaments (Fig. 3).

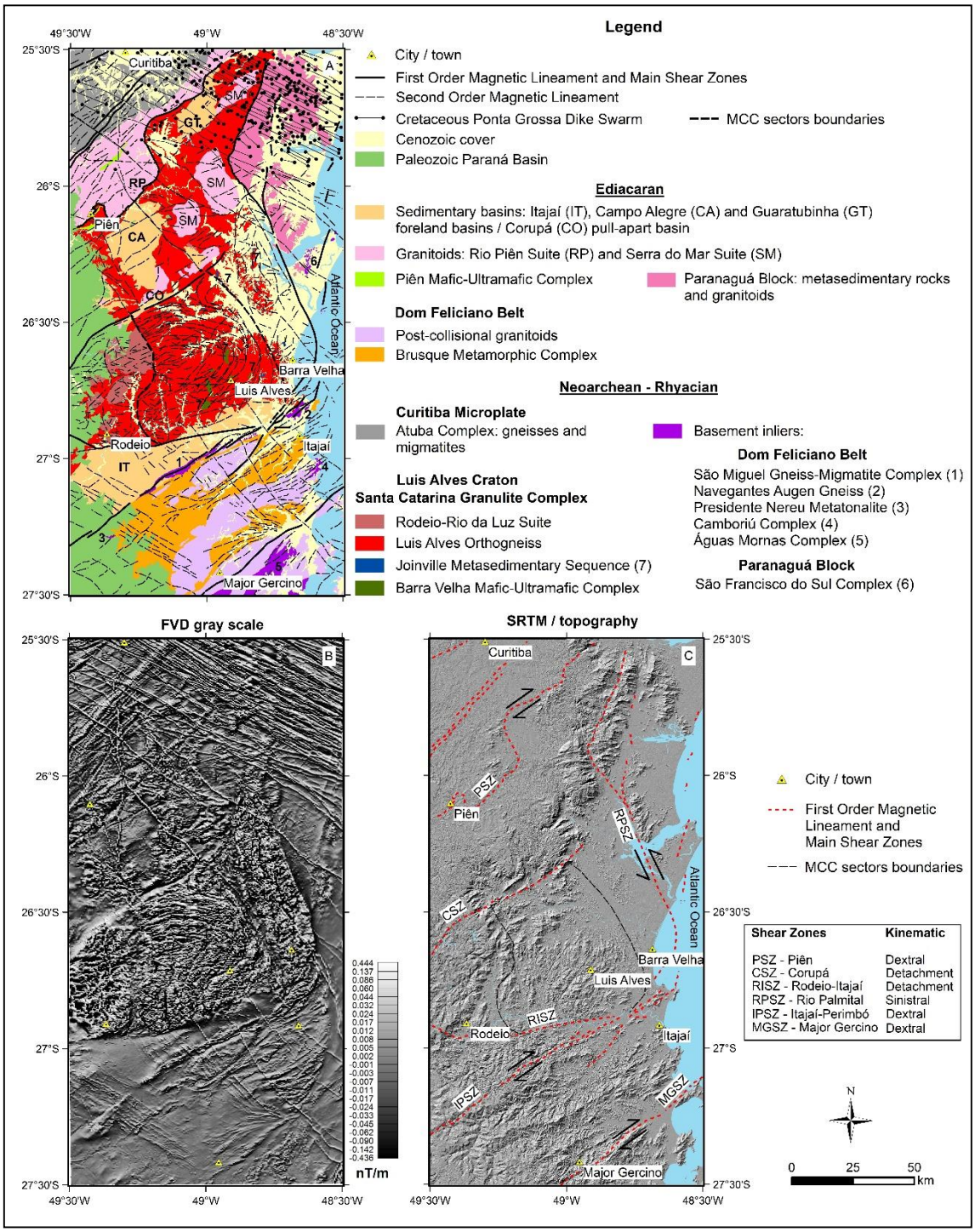

Figure 2. Geological map, aerogeophysical and satellite sensor images. A) Simplified geological map of the study area and adjacent tectonic blocks (modified from Iglesias et al., 2011; Betiollo et al., 2018; Bruno et al., 2018; Passarelli et al., 2018). B) First Vertical Derivative (FVD) image in grayscale which highlights the MCC drop-shaped structure in the central portion, and the first- and second-order magnetic lineaments, revealing regional structures and different magnetic terrains. The main shear zones coincide with first-order magnetic lineaments. C) SRTM topography image showing that the MCC is not a surface feature and does not have a correspondence in the

topography. First-order magnetic lineaments and the main shear zones limiting the MCC area are also shown for reference.

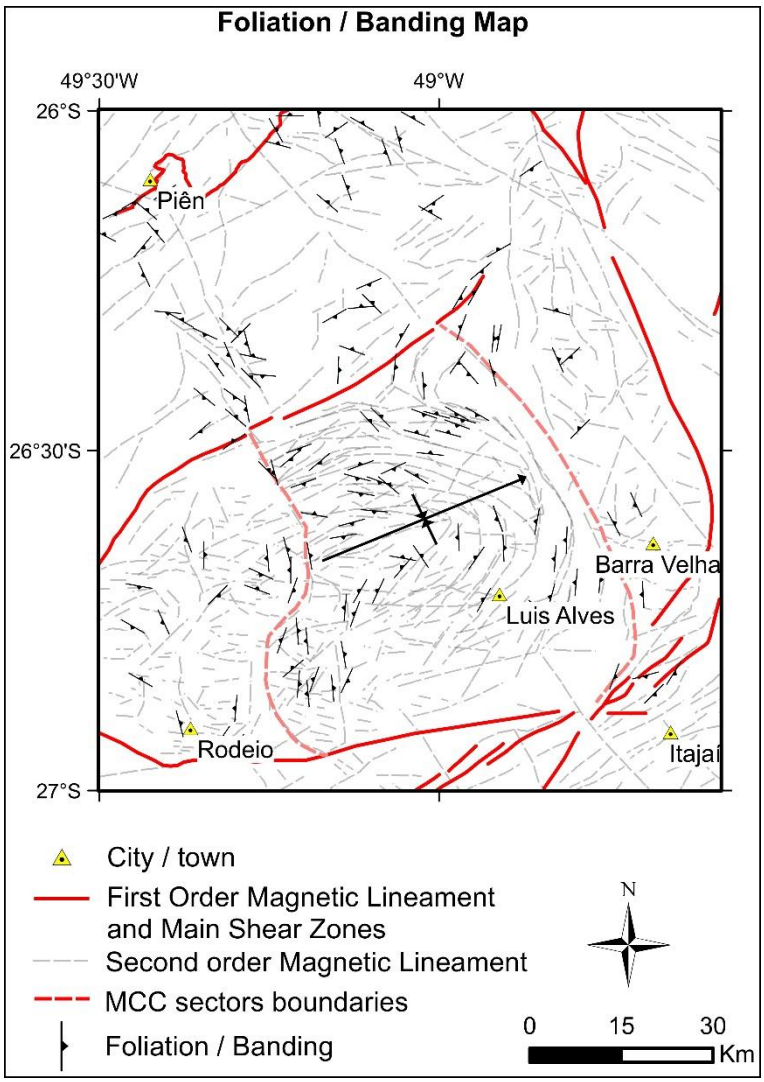

Figure 3. Map of foliation and banding attitudes, revealing a regional non-cylindrical, steeply plunging, upright synform fold in the central MCC area.

3.2. Aerogeophysics

The airborne geophysical survey (CPRM, 2011) used in this contribution covered more than 140,000 km² of high-resolution aeromagnetic and aerogammaspectrometric lines over the Paraná-Santa Catarina shield. Profile flight lines at an elevation of 100 m were oriented N-S with 500 m spacing, and E-W tie lines were spaced 10,000 m. Data were acquired and processed by Lasa Prospecções S.A. (Rio de Janeiro), using Oasis Montaj software routines, which include parallax correction, international geomagnetic reference field removal, diurnal correction, and leveling, among others. More information about the aerogeophysical survey, data

processing and the aerogeophysical database is available on the SGB – CPRM website (https://rigeo.cprm.gov.br/handle/doc/11241).

Aeromagnetometric maps were selected to evaluate and interpret regional structures in the study area (e.g., Nabighian et al., 2005; Hinze et al., 2013). The first vertical derivative (in both gray and RGB color) and the Analytic Signal Amplitude (ASA) were used to map the geometry and internal structures of geological bodies and geotectonic units, and to identify deep magnetic structures (e.g., Reeves, 2005). Gamma-ray data composed of K (%), eU (ppm) and eTh (ppm) channels, were represented in total gamma counting and ternary maps (e.g., IAEA, 2003). Radiometric data was used to map the borders of bodies and internal properties of the geotectonic units, reflecting the lithotypes diversity. Finally, magnetic and gamma-ray spectrometric data recognized by aerogeophysical analyses were investigated in the field to enhance the confidence of our interpretations.

4. Results

4.1 Geology

The LAC is mainly composed of the Santa Catarina Granulite Complex, which is divided in this paper into four units (Fig. 2A), all metamorphosed under granulite facies, as follows: (1) Barra Velha Mafic-Ultramafic Complex; (2) Joinville Metasedimentary Sequence; (3) Luis Alves Orthogneiss, and; (4) Rodeio-Rio da Luz Suite. The remaining units within the LAC geotectonic block are the Neoproterozoic units (not discussed in this paper) such as the Serra do Mar Suite, sedimentary rocks of the Campo Alegre, Guaratubinha and Corupá Basins (Fig. 2A), and the Itajaí Basin that partially covers the South-Southeastern LAC boundary.

4.1.1 Barra Velha Mafic-Ultramafic Complex

This unit crops out as sparse continuous outcrops and blocks along with the Santa Catarina Granulite Complex, mostly nearby the Luis Alves town (Fig. 2A) and towards the East. The best expositions occur along the coastline and quarries nearby the Barra Velha town.

The Barra Velha Mafic-Ultramafic Complex is composed of black to light gray plagioclase-bearing pyroxenites and (leuco-) gabbronorites. Usual macroscopic features are a prominent foliation or a millimeter-thick gneissic banding (marked by plagioclase). Rocks are mostly fine- to medium-grained, inequigranular with polygonal granoblastic texture, including scarce larger (4-5 mm) subhedral to euhedral prismatic

grains interpreted as remnants of pyroxene (locally kinked) or plagioclase. The essential mineralogy comprises Ca-Mg-Fe ortho- (enstatite and ferrosilite) and clinopyroxene (diopside, with augite/pigeonite lamellae), plagioclase, hornblende (locally as up to 5 cm porphyroblasts), biotite, and rare hercinite. Accessory minerals are pyrite, chalcopyrite, magnetite, apatite, zircon and quartz. Secondary mineralogy (retrometamorphic or hydrothermal) consists of actinolite, chlorite, epidote, and garnet (up to 5-10%).

4.1.2. Joinville Metasedimentary Sequence

This unit comprises quartzites, banded iron formations (BIF) and paragneisses. These lithotypes are found in association or not in scarce outcrops (quarries or road cuts) and blocks, along aligned ridges, or at hill peaks. The spatial association with metamafic-ultramafic rocks of the Barra Velha Mafic-Ultramafic Complex is commonly observed (Fig. 2A). Quartzite and BIF have millimeter-sized foliation and/or banding, whilst paragneisses show centimeter-size banding or isotropic granoblastic texture.

Quartzites are light yellow with a prominent millimeter-sized foliation. They are locally interlayered with meter-thick greenish layers. Quartzites mostly consist of quartz, with minor amounts of green mica, and opaque minerals. They are fine- to medium-grained, with polygonal granoblastic texture and interlobate fabric. Green mica (fuchsite?) crystals are subhedral, fine-grained and frequently show wavy extinction.

Banded iron formations also show a prominent millimeter-sized banding and foliation, and were classified in terms of facies (cf. James, 1954), described hereafter from the most to the least abundant, as follows. Silicate facies are gray to reddish and may be confused with mafic rocks in the field due to their high pyroxene contents, which reflect granulite facies metamorphism. It mostly crops out as isolated blocks, with variable proportions of ferrosilite (with pigeonite and augite lamellae), spessartine and almandine garnet, intergranular magnetite, and rare olivine (also marking granulite facies) and pyrrhotite. Silicate minerals may exceed magnetite contents, the latter not been constantly found within these facies. Oxide facies are light yellow to orange and consist of quartz and magnetite. It mostly shows a well-marked, millimeter-thick banding, alternating quartz and magnetite, and locally massive magnetite (up to 98%) layers. Both silicate and oxide facies show polygonal granoblastic texture, with straight and interlobbed grain boundaries.

Paragneisses are rare, cropping out only locally. They are gray to light gray, fine- to medium-grained holocrystalline rocks with a centimeter-thick banding. Mafic bands are composed of orthopyroxene, biotite, garnet, hercinite and cordierite, whereas felsic bands are quartz-feldspathic with sillimanite. The textures are granoblastic, lepidoblastic (biotite), and nematoblastic (pyroxene and sillimanite).

4.1.3. Luis Alves Orthogneiss

Among the LAC units, the Luis Alves Orthogneiss has the largest, continuous exposition area (Fig. 2A). It is worth noting that this feature represents the difficulty in individualizing the local predominance of other rock types at the 1:250,000 scale. Dense vegetation, large soil profiles, structural complexity, and random intercalation between lithotypes are additional obstacles to the detailed characterization of this unit.

Rocks crop out along the coastline nearby Barra Velha town and its countryside towards the West as blocks, flagstones, boulders, and continuous quarry expositions. They are usually medium-grained, gray to light gray, and vary from isotropic (polygonal granoblastic) to foliated (marked by quartz, and mafic minerals stretching). A millimeter- to metric-thick gneissic banding is observed, where individual mafic and felsic bands may be locally folded or stretched, forming isolated lenses or boudins. Mafic portions tend to be finer-grained, with plagioclase, pyroxene (locally as phenocryst remnants), hornblende, and minor amounts of biotite. They locally show pyroxenite composition. The interlayered felsic portions have tonalite, granodiorite, and quartz-diorite compositions. They are medium- to coarse-grained, with subhedral and euhedral quartz and plagioclase (as phenocryst remnants) predominance over pyroxene, hornblende, and biotite (<20% of mafic minerals). Garnet crystals (locally as porphyroblasts) are a common accessory mineral in both mafic and felsic portions.

4.1.4. Rodeio-Rio da Luz Suite

This unit consists of orthopyroxene-bearing metagranites that crop out mostly at the Southwestern LAC (Fig. 2A), with minor occurrences in its central zone where they are intrusive in the Luis Alves Orthogneisses. Outcrops are sparse with an unclear relationship with most of their hosts due to diffuse contacts. Close to inferred contacts the orthogneisses country rocks show increasing alkali-feldspar amounts, and metagranites reveal increasing mafic minerals, which suggest some kind of interaction between lithotypes.

They are gray to reddish rocks with monzogranitic and syenogranitic compositions. Mineralogy consists of euhedral to oval-shape alkali-feldspar phenocrysts immersed in a fine- to medium-grained matrix with quartz, alkali-feldspar, plagioclase, hornblende, biotite, and orthopyroxene relicts. Accessory allanite is diagnostic of this suite. Protomylonites to mylonites frequently cross-cut the Rodeio-Rio da Luz Suite.

4.2 Structural Geology

Three major, regional shear zones bound the LAC (Fig. 2). In its north-northwest limit, the Piên shear zone (PSZ) with dextral kinematics (Passarelli et al. 2018; Bruno et al. 2018) marks the contact between the LAC and the Atuba Complex, a Curitiba Microplate unit within the Southern Ribeira Belt. The contact between the LAC and the southern Dom Feliciano Belt is proposed in this paper to be along the Rodeio-Itajaí shear zone (RISZ), which is largely covered by the Itajaí Basin. To the east, the contact between the LAC and the Paranaguá Block is represented by the Rio Palmital shear zone (RPSZ) of sinistral kinematics (Cury, 2009). The LAC is covered by the Paraná Basin to the West. Another important structure that cross-cuts the LAC is the Corupá shear zone (CSZ), with normal kinematics, and the development of the Corupá pull-apart basin.

The main structures observed at the LAC are foliations and the gneissic banding observed in the Joinville Metasedimentary Sequence and the Luis Alves Orthogneiss, respectively (Fig. 3). These structures have variable strikes, dipping from 90° to 40° with the predominance of high to subvertical dips. Within the LAC area, different structural patterns occur from place to place, but from a regional perspective, they reflect mega synformals, antiformals, and vertical folds.

From the CSZ to Southeast towards Luis Alves town, E-W foliation strikes shift gradually to NW-SE, N-S, and NE-SW, configuring a non-cylindrical, steeply plunging, upright synform fold of kilometer-scale and hinge towards East. This feature records a regional pattern revealing a curvilinear structure in the Southern LAC portion. In other locations such as close to the CSZ, foliations tend to be parallel with the NE-SW shear zone. To the West and surrounding the Campo Alegre Basin, NW-SE foliations predominate over the subordinated E-W ones.

4.3. Aerogeophysical Data

4.3.1. Aeromagnetometry

The main data used to recognize and interpret the aeromagnetic features of the study area are the First Vertical Derivative in grayscale (FVDg) (Fig. 2), in RGB (FVDc) and up to 2km continuation (FVD 2km), and the Analytic Signal Amplitude (ASA) (Fig. 4). Different features observed in each of those maps allowed the production of a single integrated interpretation map (Fig. 4D).

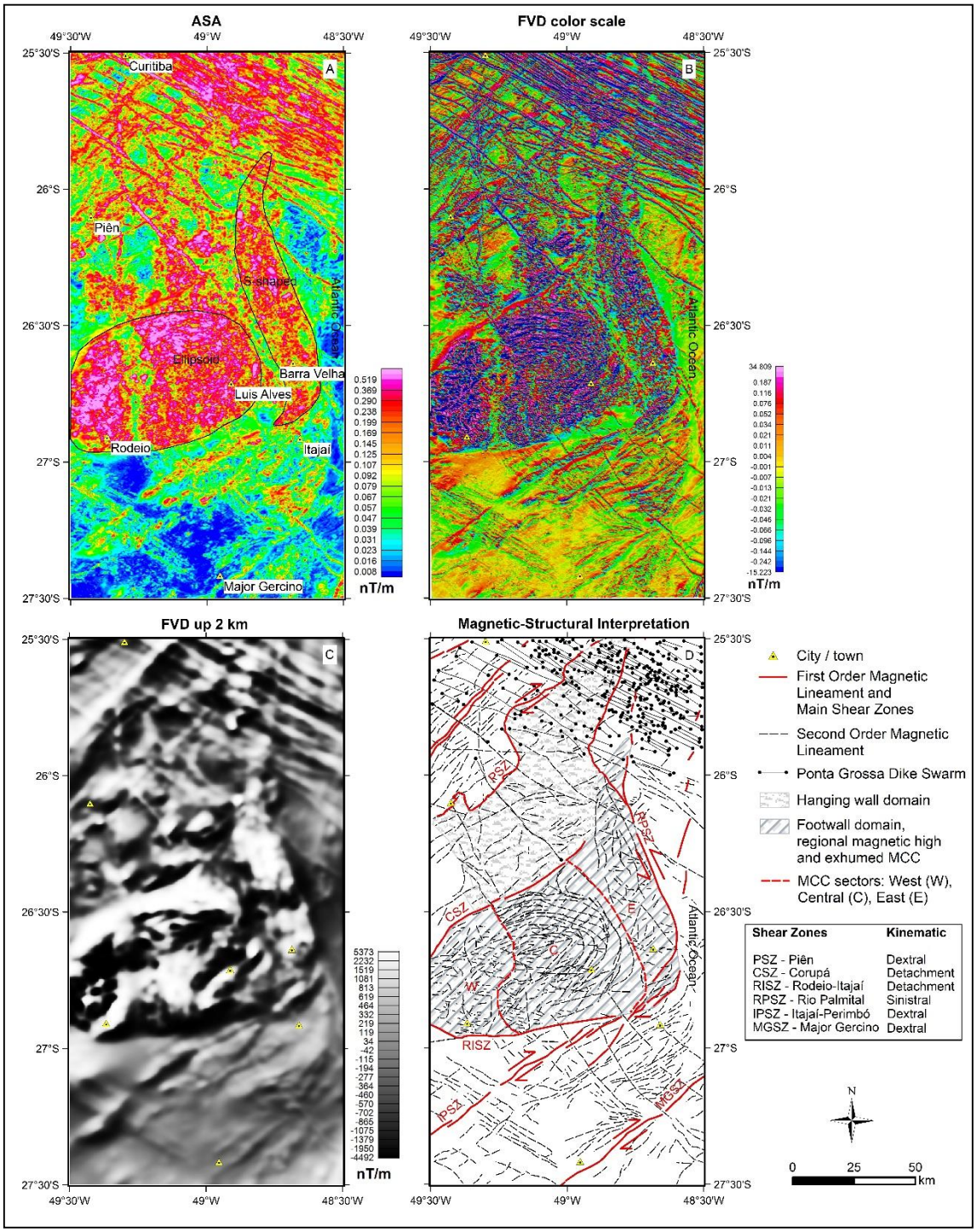

Figure 4. Aeromagnetometry maps. A) Analytical Signal Amplitude (ASA) which highlights the external limits and shape of the MCC. Both ellipsoidal and S-shaped

features observed in the MCC area are shown for reference (see text for details). B) FVD color scale evidencing external limits and shape, and internal MCC structures. First- and second-order magnetic lineaments show regional structuration and internal structures associated with individual tectonic blocks and within the MCC area. C) FVD grayscale up 2 km highlighting deeper structures associated with first-order magnetic lineaments, and the MCC drop-shaped structure in the center of the image. D) Magnetic-structural interpretation which allowed the individualization of two distinct portions within the LAC area, namely the northern and southern domains, which are interpreted as hanging wall and footwall, respectively. The MCC can be subdivided into three sectors based on its internal structure marked by the second-order magnetic lineaments. The first-order magnetic lineaments relate to deeper crustal structures which limit the MCC and the tectonic blocks.

In the central zone of the study area, the FVDg (Fig. 2B) highlights a prominent drop-shaped structure limited by first-order magnetic lineaments, besides other curvilinear, second-order magnetic lineaments in its core. The Northern half of the study area (Fig. 2B) shows variable magnetometric responses due to different rock associations and structures, such as (i) high magnetic, NW-SE linear structures corresponding to the Cretaceous Ponta Grossa Dike Swarm (PGDS; Renne et al., 1996; Marangoni and Mantovani, 2013), which are abundant to Northeast and occur in lesser amounts crosscutting the Atuba Complex and Rio Piên Suite to Northwest; and (ii) mixed magnetic responses associated with Neoproterozoic igneous rocks and sedimentary basins, respectively intruding and covering the LAC, beyond the PGDS. To the South of the drop-shaped structure, where the Dom Feliciano Belt (Hartmann et al., 2016) rocks predominate, a homogeneous, medium-intensity magnetic area highlights both NW and NE structures. Within this area, the best-marked structure is represented by the NE-SW Itajaí-Perimbó shear zone (IPSZ), with high magnetic contrast associated with a first-order magnetic lineament, followed by the Major Gercino shear zone (MGSZ). Other structures consist of shorter second-order magnetic lineaments and may correspond to ductile shear zones and dikes.

The ASA (Fig. 4A) also highlights a drop-shaped regional magnetic high in the central zone of the study area, marking its external boundaries and inner magnetic contrasts (e.g., Nabighian et al., 2005; Hinze et al., 2013). The ASA evidence two sections within this general structure, separated by a medium-intensity magnetic area. To the East, an S-shaped high-magnetic area of 90 km of extension along an N-S axis

is observed, whereas to the West, an ellipsoid-shaped area of 70 x 55 km with high-magnetic intensity occurs. These two sections are separated by a medium-intensity magnetic area, largely corresponding to Cenozoic cover, and in minor amounts to the LAC boundaries. The NW-SE Ponta Grossa Dike Swarm is highlighted again by the ASA in the extreme Northeast of the study area. In the Northern region, subordinated NE-SW lineaments, and scarce N-S ones also occur. In this same region, the low- and medium-intensity magnetic areas correspond to Neoproterozoic granitic intrusions and sedimentary basins. Along the Dom Feliciano Belt, in the Southern part of the study area, a homogeneous, low-intensity magnetic region is well-marked. Medium- and high-intensity magnetic responses are locally correlated with shear zones and Paleoproterozoic rock associations. The Paraná Basin cover at the Western and Southwestern LAC zones seems to have little influence on the magnetic response, with the basement rocks being the main sources for high-intensity magnetic signals.

The spatial connection between magnetic and geological features such as dikes, shear zones, foliations or faults are well identified in the FVDc map (Fig. 4B). The regional drop-shaped structure is marked by a magnetic high with prominent second-order, curvilinear magnetic lineaments at its core, whereas in its Eastern and Western zones lineaments are shorter and straighter. Both the ellipsoid- and the S-shaped sections are also clearly identified. A spatial connection between the Southernmost S-shaped section and the IPSZ is evidenced by an aligned, homogeneously positive magnetic signal, which is probably caused by the occurrence of Paleoproterozoic rocks along the IPSZ. To the South of the drop-shaped structure within the Dom Feliciano Belt area, the IPSZ represents a first-order magnetic lineament, accompanied by second-order ones with both NE- and NW-trends. The latter locally represents anastomosed to straight shear zones.

The FVD 2km map (Fig. 4C) evidences deeper crustal structures within the LAC, including the main drop-shaped structure and first-order magnetic lineaments limiting it. They are represented by the RISZ to the South, the RPSZ to the East, and the CSZ to the North. Another prominent first-order magnetic lineament to the Northwest of the study area has a NE-SW strike and is parallel to the PSZ. In the Dom Feliciano Belt area, the main first-order magnetic features are represented by the IPSZ, and the MGSZ that, however, shows weaker magnetic contrast in the FVD 2km map.

The magnetic-structural interpretation (Fig. 4D) comprises the compilation of the main recognized magnetic features, as well as the representation of their geological significance.

4.3.2. Aerogammaspectrometry

The aerogammaspectrometry data is shown through the Total Gamma Counting (TGC; Fig. 5A) and the Gamma Ternary (GT; Fig. 5B) maps. At a first glance, the study area shows an important gammaspectrometric boundary, represented by the contact between the LAC and the Dom Feliciano Belt along the RISZ. The Southern area has a high TGC (Fig. 5A) with a predominant whitish area (Fig. 5B) within the DFB and the Itajaí Basin. This feature is attributed to high amounts of all the three elements (K, U and Th) in these rocks. The center-North of the study area also shows high TGC, but with more red (K), blue (U) or green (Th) colors, indicating the local predominance of the corresponding elements. At the Northern LAC, small portions of the Rio Piên Suite and the Paranaguá Block are also enriched in K-U-Th, recording a whitish color. The Atuba Complex and the remaining areas of the Paranaguá Block have medium- to high- TGC, mostly influenced by U, and Th in lesser amounts.

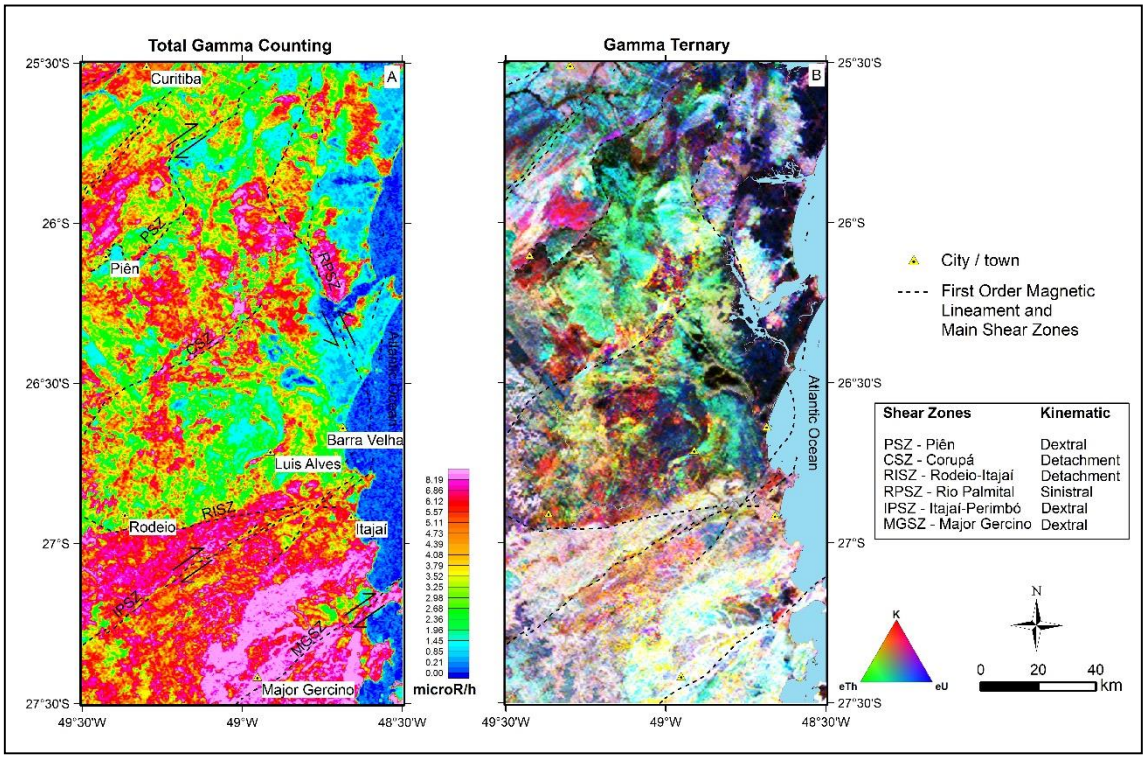

Figure 5. Aerogammaspectrometry maps. A) Total gamma counting (TGC) map showing poor- and rich-gamma elements areas. The Dom Feliciano Belt is highlighted by its high-gamma elements in the south. B) Gamma ternary (GT) map showing the variable predominance of each element (K, U, Th) in different areas. Whitish and black colors correspond to areas enriched- and depleted- in all three elements, respectively.

The central zone of TGC and GT maps (Fig. 5A and 5B) where the LAC rocks crop out is predominantly characterized by medium- to low- TGC, with different zones enriched in Th followed by minor amounts of K. Locally dark zones represent very low TGC. The main gammaspectrometric signatures that stand out are: (i) in the central LAC, to the North-Northwest of the Luis Alves town and the South of the CSZ, a rounded, dark area with very low TGC is well marked over an area of ca. 400 km^2. This zone is surrounded by a green area, whose geometry is delimited by both low- and high-Th areas; (ii) to the North of the CSZ, green Th-rich areas show high TGC corresponding to Neoproterozoic Basins and the Serra do Mar Suite; (iii) high-K signals mark, from the Rodeio town, a NE-trend of the Rodeio-Rio da Luz Suite, the Luis Alves Orthogneiss, the Serra do Mar Suite and the Paranaguá Block and; (iv) the Southern LAC zone is enriched in K-U-Th, but more influenced by K (whitish to red) to the West, and Th to the East (green), U always showing low gammaspectrometric signals.

5. Discussion

The LAC area, mostly represented by the Santa Catarina Granulite Complex, is characterized by the pervasive occurrence of granoblastic textures and, in variable amounts, of orthopyroxene and other minerals that mark the granulite metamorphic facies in most rock types. Even hornblende- or biotite-bearing rocks show orthopyroxene crystals relics, showing high-temperature conditions, followed by a cooling geothermal path (retrometamorphic) compatible with the lower crust environment. BIF with ferrosilite, garnet and olivine, also point to high-grade granulite metamorphism (Klein, 2005). There is a heterogeneous spatial distribution of different granulitic rock associations within the LAC, which are controlled by regional structures. For example, the opx-bearing Rodeio-Rio da Luz Suite is concentrated in the Southwestern LAC, marking an asymmetric distribution between high-grade metamorphic and Rhyacian metaigneous rocks. Neoproterozoic sedimentary Basins and granitoids of the Serra do Mar Suite occur only to the North of the CSZ, individualizing two geologic domains to its Northern and Southern areas. The Southern domain, represented by the drop-shaped regional magnetic high, includes different granulite units that were subjected to a common event associated with magnetite crystallization through a tectonic process not registered in the Northern domain. The Southern area concentrates BIFs and the Rodeio-Rio da Luz Suite with no occurrence of Neoproterozoic rocks. Along the CSZ the Corupá Basin crops out highlighting the

importance of this structure as an internal geological boundary. In the same way, the Itajaí Basin partially covers only the Southern LAC boundary.

Attitudes of foliation and gneissic banding in granulites are variable, but to the South of the CSZ (south-central LAC), its distribution configures a regional plunging syncline with a subvertical hinge towards the East (Fig. 3). The corresponding fold limbs show high dips towards the inner zone, displaying the most remarkable LAC structure and is comparable to regional structures formed via diapirism. In this sense, aeromagnetic data reveal a singular regional structure recorded in the continental crust, even with the partial Paraná Basin coverage to the West and without direct positive correspondence in the topography (Fig. 2B and 2C). It matches a drop-shaped, regional magnetic high, limited by first-order magnetic lineaments, which limit second-order magnetic ones that correspond with Archean-Paleoproterozoic rocks of the Santa Catarina Granulite Complex.

Integrating aeromagnetic and regional structural data (Fig. 4D), first-order magnetic lineaments largely coincide with major shear zones. The RISZ limiting the LAC and the Dom Feliciano Belt is not evidenced on the surface, is only revealed by aeromagnetometry. On the other hand, the PSZ is evidenced on the surface and does not show magnetic signals deep enough to be considered a first-order magnetic lineament. The NE-SW first-order magnetic lineament in the Atuba Complex (parallel to the PSZ), probably configures the subsurface contact between the LAC and the Curitiba Microplate covered by the Rio Piên Suite (Fig. 2A). The CSZ, previously named Corupá Lineament (Kaul, 1980), is defined here as a first-order magnetic lineament associated with the Corupá pull-apart Basin. In the aeromagnetometric maps, the CSZ proved to be an important regional structure, limiting the drop-shaped regional magnetic high to the North, as well as two magnetic domains at the Northern and Southern LAC areas. The IPSZ and the RPSZ correspond to well-marked magnetic lineaments interpreted as first-order, while the MGSZ is less pervasive. The PGDS and NW-SE second-order magnetic lineaments predominate in North-Northeast areas external to the LAC, and in the Curitiba Microplate to Northwest, NE-SW second-order magnetic lineaments predominate. In the Dom Feliciano Belt to the South, NE-SW and NW-SE second-order magnetic lineaments between 3 to 18 km-long have wavy shapes, probably representing ductile structures (shear zones). Other NW-SE lineaments of almost 50 km-long are scarce and probably represent dikes.

Besides reflecting the surficial geology, the aerogammaspectrometry also corresponds with aeromagnetic properties. Both a regional fold and a curvilinear

magnetic structure to the South of the CSZ marked by second-order magnetic lineaments coincide with very low gamma total counting, with Th predominance. The internal divisions of the drop-shaped regional magnetic high also have a correspondence in the distribution of the gamma elements, enriched in the three elements in the West, more K in the central-West, and influenced by Th in the central-East portion.

5.1 The exhumed Metamorphic Core Complex (MCC)

Based on geological-aerogeophysical data, the most prominent feature of the study area is the drop-shaped structure in the Southern LAC domain, limited by first-order magnetic lineaments. The recognition of this structure yields the individualization of two geological areas limited by the CSZ, considered as hanging wall and footwall zones in its Northern and Southern domains, respectively.

The hanging wall is limited by the PSZ (North), the CSZ (South), and the RPSZ (Northeast), characterizing areas of variable magnetic signals. Low- to medium-magnetism corresponds to Neoproterozoic intrusions, sedimentary basins and locally to granulites, whereas high-magnetic areas always represent granulites. Most high-magnetic lineaments correspond to the PGDS, and second-order magnetic lineaments to minor shear zones and faults.

The footwall is limited by the CSZ (North), the RISZ (South), and the RPSZ (East). It has a total dimension of 90 km (E-W) x 100 km (N-S), being the ellipsoidal portion restricted to an area of ca. 70 x 55 km. Unfortunately, both the extension of the aerogeophysical survey and the Paraná Basin cover precludes visualizing the closure of the ellipsoid structure to the West between the CSZ and the RISZ. The footwall marks a regional magnetic high in the study area and represents the drop-shaped structure interpreted here as an exhumed Metamorphic Core Complex (MCC), which suggests that CSZ, RISZ and RPSZ worked as paleo-detachment zones. Indeed, available geochronological data obtained on the LAC points to two-stage granulite metamorphism at 2.35 and 2.18 Ga, and a retrometamorphic, amphibolite facies event at 2.0 Ga (Hartmann et al., 2000; Basei et al., 1998; 2009; Heller et al., 2021). The latter would correspond to an extensional period responsible for the MCC exhumation during the Rhyacian-Orosirian transition. Further tectonic events, all compressive, occurred only during the Neoproterozoic Brasiliano-Pan-African Orogeny and may have reactivated Paleoproterozoic structures under lower metamorphic grade (e.g. Jelinek et al., 2021). Among the geophysical characteristics of the MCC area is the

pervasive high magnetic signal on the FVDg, FVDc, ASA and FVD 2km maps (Figs. 2B and 4) comprising all lithotypes within the inner LAC (tonalites, granodiorites, mafic-ultramafic rocks, quartzites, BIF, and granites).

The MCC proposed here can be subdivided into three sectors, namely Western, Central and Eastern (Fig. 4D). The arrangements of internal second-order magnetic lineaments, allied with the general internal magnetic signals and the geological record been the main subdivision criteria. The Western and Central sectors comprise the high magnetic ellipsoid, while the Eastern sector corresponds to the S-shaped high-magnetic area (Figs. 2 and 4).

The Western sector has a predominance of E-W, second-order, 2 to 5 km-long magnetic lineaments (including scarce N-S and NE-SW lineaments of up to 20 km-long) which coincide with high gamma contents. The Central sector is well characterized by the curvilinear second-order magnetic lineaments (40 to 60 km-long) that coincide with foliations of metamorphic rocks along a regional fold that refer to diapiric structures (Figs. 3 and 4). The very low gamma contents, mostly marked by Th is characteristic for this sector (Fig. 5). The Eastern sector has second-order magnetic lineaments up to 40 km-long with general NW-N-NE strikes, with subordinated E-W ones. Much of this sector is covered by recent sediments and partially limited by the Atlantic Ocean, influencing the gamma response, but where rocks crop out Th has shown to be an important individualizing element. Granulitic orthogneisses predominate in all the MCC sectors, with a random distribution of other lithotypes, such as observed for the Rodeio-Rio da Luz Suite (Western sector), and quartzites, BIF, paragneisses and metamafic-ultramafic rocks (Central and Eastern sectors).

Another feature that points to an MCC structure are the development of sedimentary basins (Corupá and Itajaí) at the Southern LAC domain borders, which matches spatially the location of first-order magnetic lineaments and shear zones (CSZ and RISZ), been interpreted as paleo-detachment basins.

5.2 Metamorphic Core Complex formation and comparisons with alternative models

Processes associated with Metamorphic Core Complex (MCC) formation are largely known in the Phanerozoic (Whitney et al., 2013), with few records in the Proterozoic or older crustal segments (James and Mortensen, 1992; Hoffmann et al., 2015; Rizzotto et al., 2019; Tiddy et al., 2020). Archean terranes commonly show dome-and-keel structures as in the Quadrilátero Ferrífero and Carajás areas in Brazil

(Marshak et al., 1997; Cutts et al., 2019; Costa et al., 2020), and Mount Edgar in the Pilbara Craton, Australia (Sandiford et al., 2004; François et al., 2014; Roberts and Tikoff, 2021), among others. Diapirism is a process largely documented in high-grade rocks of all ages during the exhumation of gneissic domes (Whitney et al. 2004a), being associated with processes developed during the formation of both MCC and dome-and-keel structures (Vanderhaeghe, 2004; Roberts and Tikoff, 2021). In this sense, the LAC preserves the characteristics of all the aforementioned processes. Its inner structures, particularly regional folds and associated high-angle dip foliations and banding, coincide with curvilinear second-order magnetic lineaments, a feature found in MCCs and also in diapirs (Whitney et al., 2004b; Burg et al., 2004). Dome-and-keel structures also form by diapirism (Cutts et al., 2019; Costa et al., 2020; Roberts and Tikoff, 2021), and are commonly surrounded by shear zones along keels, a geometry similar to that found in MCC.

The drop-shaped and ellipsoidal Southern LAC domain geometry, limited by regional structures such as the CSZ, RISZ and RPSZ shear zones is a key characteristic of MCC (Burg et al., 2004; Whitney et al., 2013; Platt et al., 2015; Brun et al., 2018). The asymmetric distribution of geological units in the LAC footwall also points to MCC processes. Rhyacian metaigneous rocks concentrate in the Western LAC sector, whereas BIF, quartzites and metamafic-ultramafic rocks interlayered with orthogneisses occur mainly in the Central and Eastern LAC sectors, which would correspond to the MCC boundary. Tiddy et al. (2020) used aeromagnetometric data to identify and characterize an MCC in the Gawler Craton (Australia), which has similar geometry and magnetic magnitude in comparison with those found in the LAC. On the other hand, comparatively, there is an inverse aeromagnetic response between the LAC footwall and the dome-and-keel structure recorded in the QF area (Quadrilátero Ferrífero 2050, https://qfe2050.ufop.br). In this sense, the LAC shows a high aeromagnetic signal for the ellipsoidal footwall (Southern domain) with ortho- and paragneisses, metamafic-ultramafic rocks and BIF. Moreover, orthogneiss domes of the QF are ellipsoidal with low aeromagnetic signal, whereas high magnetic responses are restricted to linear areas with BIF along keels.

It is worth noting that the LAC does not fully meet the requirements to be strictly classified as an MCC or a dome-and-keel structure. However, geological, structural and aerogeophysical data converge towards the interpretation that the LAC rather approximates the evolution of an MCC with associated diapirism. The predominance of granulite rocks is a singular feature of the LAC, since most MCC and diapiric gneissic

domes worldwide show migmatites and amphibolite facies rocks. Indeed, a key element for the characterization of such complexes is identifying detachment low-angle shear zones. However, the Paleoproterozoic MCC proposed here has only partial preservation of its main structures, and the model would benefit from detailed fieldwork focusing on structural geology along the CSZ and the RISZ. The location of sedimentary basins (Corupá and Itajaí) on top of the shear zones is similar to detachment Basins found within MCC areas, and dome-and-keel structures only preserve metaigneous rocks in domes, with metasupracrustal successions concentrating along keels bordering domes.

5.3 Tectonic implications

Studies developed in the LAC during the last decades focused mostly on petrological (Hartmann et al., 1979; Kaul, 1980; Figueiredo et al., 1997; Mantovani et al., 1987; Fornari, 1998) and geochronological data (Basei et al., 1998; 2009; Hartmann et al., 2000; Heller et al., 2021), and its role for the Neoproterozoic Gondwana Supercontinent assembly (Basei et al., 2009; Passarelli et al., 2018). As a consequence, little is known about processes and tectonic settings that took place during and after granulite formation, the Proterozoic geodynamics, and how these rocks were exhumed yet in the Rhyacian (Hartmann et al., 2000; Basei et al., 1998; 2009; Heller et al., 2021).

The LAC is considered a fragment of a mid- to large-scale granulitic terrane (Harley, 1992) including Archean-Paleoproterozoic rocks within the worldwide supercratons puzzle (Bleeker, 2003). It registers geological processes active on ancient crustal segments that are considered important sources to understand the primordial Earth's evolution. Thus, the predominance of granulitic rocks in the LAC brings us a window of process from the lower crust that happened under the Proterozoic plate tectonics rate regime, characterized by high- to ultra-high T/P geothermal gradients (Stuwe, 2007; Brown, 2009; 2014; Kelsey and Hand, 2015).

Geothermobarometric studies carried out in the LAC show average metamorphic temperatures of 800 °C and pressures between 0.5-0.7 GPa (Girardi and Ulbrich, 1978; Hartmann, 1988; Fornari, 1998). These P-T conditions suggest that granulite metamorphism occurred under a geothermal field of high T/P with thermobaric ratios between 750 – 1500 °C/GPa. These conditions are characteristic of G-UHTM (Granulite-Ultrahigh Temperature Metamorphism) metamorphic belts (Brown, 2014; Brown and Johnson, 2019), that develop in large hot orogens (Fig. 6)

since the Archean Eon (Chardon et al., 2009; Jamieson and Beaumont, 2013; Harley, 2016; Perchuk et al., 2018; Brown and Johnson, 2019; Dziggel et al., 2019), and which in turn is correlated with the supercratons and supercontinents amalgamation cycles (Brown, 2007a). Contrastingly, the formation and exhumation of MCC from the lower crust are intrinsically attributed to extensional regimes (Whitney et al. 2013; Platt et al. 2015; Brun et al. 2018), often during post-orogenic stages such as those registered in the Aegean Sea and the Cordilleran Orogen (e.g., Lister and Davies, 1989; Jolivet et al., 2004; Cao et al., 2013; Searle and Lamont, 2022; among others).

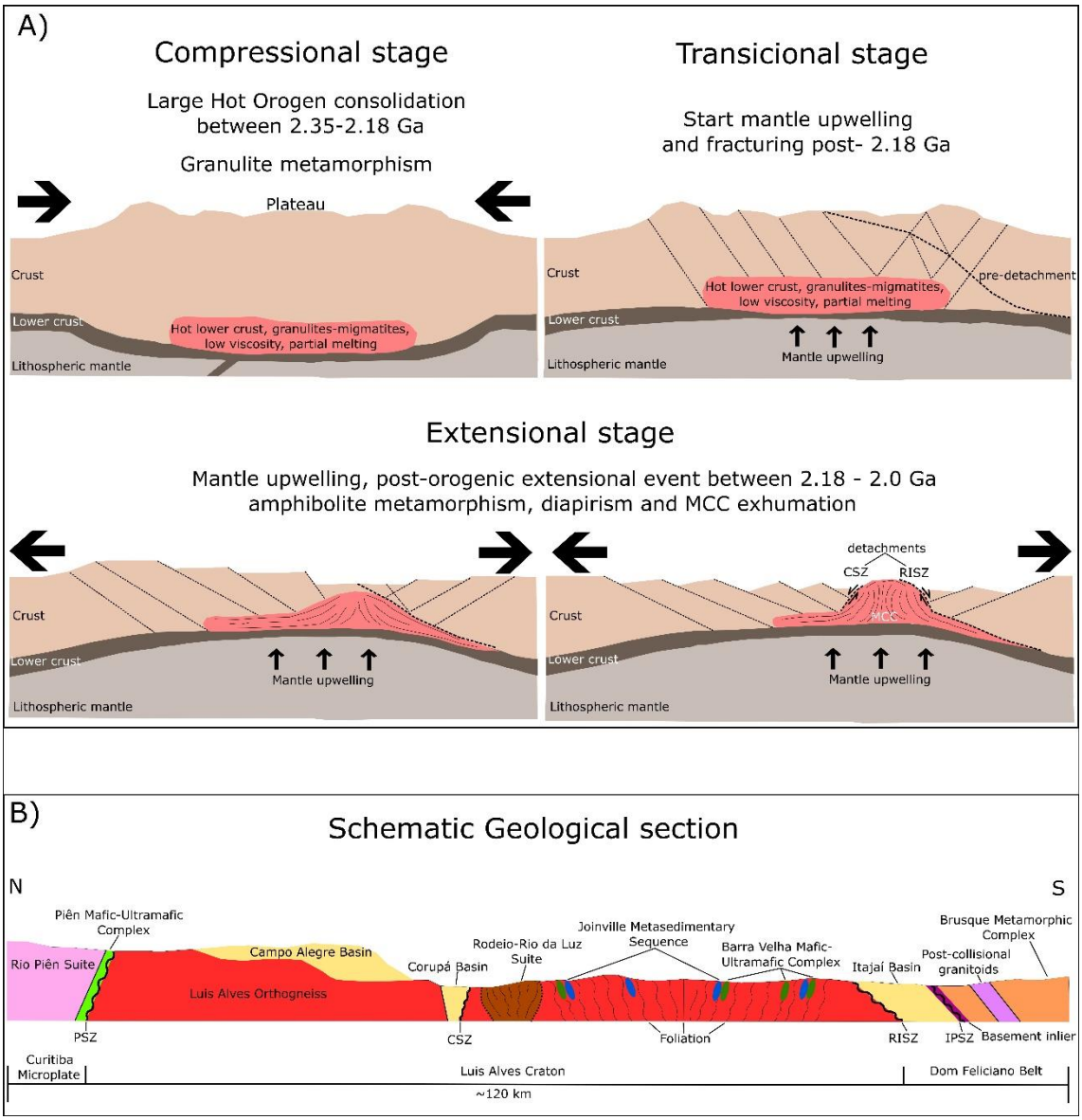

Figure 6. Evolution model and final compartmentalization of the Luis Alves Craton. A) Schematic model for the LAC evolution, including the formation of the MCC during the Paleoproterozoic (modified from Chardon et al., 2009; Jamieson and Beaumont, 2013;

Whitney et al., 2013; Brun et al., 2018. B) Schematic geological section showing the present compartmentation of different rock units and blocks within the LAC area.

Granulite metamorphism between 2.4 and 2.2 Ga is scarce in the literature (Harley, 1992; Brown, 2007b; 2014; Brown and Johnson, 2019). In general, their worldwide record is slightly younger or older both in comparison with geochronological data obtained in rocks from the LAC and ages determined for supercraton (Vaalbara, Superior or Sclavia) and supercontinent (Columbia) amalgamations. Indeed, ages obtained for the LAC granulite metamorphism (Basei et al., 1998, 2009; Hartmann et al., 2000; Heller et al., 2021) do not match these amalgamation periods, suggesting it may have a tectonic history oblivious to the main Paleoproterozoic collisional events. The peak of granulite metamorphism occurred by the end of the Siderian and the middle Rhyacian, contrasting with granulitic events which formed supercratons and the Columbia supercontinent during the Neoarchean and the Orosirian, respectively. Such transitional periods are placed between cycles 1 and 2 of the Times' Cycles of the Earth proposed by Brown and Johnson (2019).

Previous geochronological data such as U-Pb in titanite (Heller et al. 2021) and K-Ar in amphibole and biotite (Siga Jr., 1995; Basei et al., 2009; Passarelli et al., 2018) point out that during the amalgamation of Columbia by the end of the Orosirian, the LAC area stabilized as an MCC that was exhumed since the Rhyacian under a post-orogenic extensional setting (Fig. 6). This granulite lithospheric segment, fully observed only with the support of aeromagnetometric data, cannot be Neoproterozoic in age. Indeed, the record of Neoproterozoic pervasive mineral assemblages would be necessary to support this assumption, but all geochronological data from the LAC point to Paleoproterozoic to Archean ages (Basei et al., 1998, 2009; Hartmann et al., 2000; Heller et al., 2021). Thus, if we consider that the LAC was not part of Columbia, their orogenic and later extensional events may represent the amalgamation and fragmentation of an older continental segment. An alternative interpretation is that the LAC records one of the first continental collages of Columbia, and when the supercontinent blocks reached their peak convergence the LAC was under a post-orogenic extensional process.

6. Conclusions

The integration of aerogeophysical and regional geological data obtained in the Luis Alves Craton (LAC) shows us a convergence of features that allowed us to conclude the following:

(i) the Corupá shear zone (CSZ) is a geological and magnetic feature that divides the LAC into two domains, Northern and Southern, that show their own geological, magnetic and gamma-ray spectrometry characteristics;

(ii) the Southern LAC domain is a regional drop-shaped magnetic high limited by first-order magnetic lineaments, where foliations and gneissic banding of a regional fold in its Central sector coincide with curvilinear second-order magnetic lineaments and with gammaspectrometric contrasts. The attitude of regional structures in these granulite rocks refers to the intermediate depth of diapirs, exposed after erosion of their shallow rock records;

(iii) the Southern LAC domain includes opx-bearing metagranitoids, several granulite geological units and lithotypes with an asymmetric distribution that were subjected to a common event of intense crystallization of magnetite in a tectonic process not registered in the Northern domain;

(iv) the Corupá and Itajaí sedimentary basins, at the Southern domain borders, covering the first-order magnetic lineaments (CSZ and RISZ shear zones) are interpreted as paleo-detachment basins;

(v) there is no correspondence of the regional drop-shaped magnetic high with a positive topography, showing that this is a continental lithospheric, magnetic structure including rocks from the lower crust, and not a geomorphologic result of an exogenous or surficial crustal process;

(vi) the Southern LAC domain represents a partially preserved Siderian-Rhyacian Metamorphic Core Complex (MCC), limited by first-order magnetic lineaments corresponding to shear zones such as the RISZ, CSZ and RPSZ;

(vii) the MCC boundary structures (CSZ, RISZ and RPSZ) were active during the exhumation of granulitic rocks in the Rhyacian-Orosirian transition, working as detachment zones;

(viii) the Southern LAC area proposed here as an MCC can be subdivided into three sectors, Eastern, Central and Western, each with their own geological, magnetic and gamma characteristics. The Central sector has structural characteristics of diapirism;

(ix) the occurrence of a granulite facies MCC has tectonics implications for the Siderian-Rhyacian geodynamic evolution since it is uncommon in the literature. The LAC is characterized as a G-UHTM metamorphic belt with thermobaric ratios between

750 – 1500 °C/GPa, which imply in the development of a large hot orogen followed by a post-orogenic extension and exhumation;

(x) the LAC may have had an oblivious tectonic history to the main Paleoproterozoic collisional events, and may represent the amalgamation and fragmentation of an older continental segment. Contrastingly it may represent one of the first collisional events of the Columbia supercontinent and was already exhuming by the end of the Rhyacian while the remaining Columbia blocks were still colliding until the end of the Orosirian.

Acknowledgments

Leandro M. Betiollo thanks the Geological Survey of Brazil (SGB – CPRM) for providing the data and supporting the development of his Ph.D. thesis, and Andréa Sander, Andréia Gross, Paloma Rocha, and Rodrigo Cruz from the SGB – CPRM staff for their support during fieldwork, petrographic descriptions, figure elaborations and geological debates. Everton M. Bongiolo is grateful to Conselho Nacional de Desenvolvimento Científico e Tecnológico (CNPq) for his Productivity on Research grant (# 311106/2020-0).

References

Aitken, A.R.A., Betts, P.G., 2009. Constraints on the Proterozoic supercontinent cycle from the structural evolution of the south-central Musgrave Province, central Australia. Precambrian Res., 168, 284-300. https://doi.org/10.1016/j.precamres.2008.10.006

Aitken, A.R.A., Young, D.A., Ferraccioli, F., Betts, P.G., Greenbaum, J.S., Richter, T.G., Roberts, J.L., Blankenship, D.D., Siegert, M.J., 2014. The subglacial geology of Wilkes Land, East Antarctica. Geophys. Res. Lett., 41, 2390-2400. https://doi.org/10.1002/2014GL059405

Allen, T., Chamberlain, C.P., 1989. Thermal consequences of mantled gneiss dome emplacement. Earth-Planet. Sci. Lett., 93, 392-404. https://doi.org/10.1016/0012-821X(89)90038-1.

Anudu, G.K., Stephenson, R.A., Macdonald, D.I.M., 2014. Using high-resolution aeromagnetic data to recognize and map intra-sedimentary volcanic rocks and geological structures across the Cretaceous middle Benue Trough, Nigeria. J. Afr. Earth Sci., 99, 625-636. http://dx.doi.org/10.1016/j.jafrearsci.2014.02.017.

Araújo, A.J.D., Bongiolo, E.M., Ávila, C.A., 2019. The southern São Francisco Craton puzzle: Insights from aerogeophysical and geological data. J. South Am. Earth. Sci., 94, 102203. https://doi.org/10.1016/j.jsames.2019.05.019

Ashwal, L.D., Morgan, P., Hoisch, T.D., 1992. Tectonics and heat sources for granulite metamorphism of supracrustal-bearing terranes. Precambrian Res., v. 55, p. 525-538. https://doi.org/10.1016/0301-9268(92)90043-N

Baldim, M.E., and Oliveira, E.P., 2016. Anatomy of the Alto Alegre gneiss dome, São Francisco Craton, Brazil: A geological record of transpression along a Paleoproterozoic arc-continent collision zone. Precambrian Res., v. 286, p. 250-268. http://dx.doi.org/10.1016/j.precamres.2016.10.004

Barbosa, J., Nicollet, C., Leite, C., Kienast, J. R., Fuck, R. A., and Macedo, E. P., 2006. Hercynite–quartz-bearing granulites from Brejões Dome area, Jequié Block, Bahia, Brazil: Influence of charnockite intrusion on granulite facies metamorphism. Lithos, 92, 537-556. https://doi.org/10.1016/j.lithos.2006.03.064

Basei, M.A.S., 1985. O Cinturão Dom Feliciano em Santa Catarina. PhD Thesis. Universidade de São Paulo.

Basei, M.A.S.; MacReath, L.; Siga Júnior, O., 1998. The Santa Catarina Granulite Complex of Southern Brazil: a review. Gondwana Res., 1, 3-4, 383-391. https://doi.org/10.1016/S1342-937X(05)70854-6

Basei, M.A.S., Nutman, A., Siga Júnior, O., Passarelli, C.R., and Drukas, C.O., 2009. The evolution and tectonic setting of the Luis Alves Microplate of Southeastern Brazil: an exotic terrane during the assembly of Western Gondwana. *In*: Gaucher, C., Sial, A.N., Halverson, G.P., and Frimmel, H.E. (Eds): Neoproterozoic-Cambrian Tectonics, Global Change and Evolution: a focus on southwestern Gondwana. Developments in Precambrian Geol., 16, Elsevier, pp. 273-291. https://doi.org/10.1016/S0166-2635(09)01620-X

Basei, M.A.S., Drukas, C.O., Nutman, A.P., Wemmer, K., Dunyi, L., Santos, P.R., Passarelli, C.R., Campos Neto, M.C., Siga Jr O., Osako, L., 2011. The Itajaí foreland basin: A tectono-sedimentary record of the Ediacaran period, Southern Brazil. Int. J. Earth Sci., 100, 543-569. https://www.doi.org/10.1007/s00531-010-0604-4.

Bédard, J.H., 2018. Stagnant lids and mantle overturns: implications for Archaean tectonics, magmagenesis, crustal growth, mantle evolution, and the start of plate tectonics. Geosci. Front., 9, 19-49. http://dx.doi.org/10.1016/j.gsf.2017.01.005

Betiollo, L.M., Iglesias, C.M.F., Rocha, P.G., 2018. Integração geológica-geofísica e recursos minerais do Cráton Luis Alves: mapa de integração geológica-geofísica. Porto Alegre: CPRM, 1:250.000, http://rigeo.cprm.gov.br/jspui/handle/doc/16802 (May 2022).

Betts, P.G., Valenta, R.K., Finlay, J., 2003. Evolution of the Mount Woods Inlier, northern Gawler Craton, Southern Australia: an integrated structural and aeromagnetic analysis. Tectonophysics, 366, 83-111, https://doi.org/10.1016/S0040-1951(03)00062-3

Billerot, A., Duchene, S., Vanderhaeghe, O., and Sigoyer, J., 2017. Gneiss domes of the Danba Metamorphic Complex, Songpan Ganze, eastern Tibet. J. of Asian Earth Sci., 140, 48-74. http://dx.doi.org/10.1016/j.jseaes.2017.03.006

Bitencourt, M.F., Nardi, L.V.S., 2000. Tectonic setting and sources of magmatism related to the Southern Brazilian Shear Belt. Rev. Bras. Geociênc., 30-1, 186-189.

Blanco Montenegro, I., Nicolosi, I., Pignatelli, A., García, A., Chiappini, M., 2011. New evidence about the structure and growth of ocean island volcanoes from aeromagnetic data: The case of Tenerife, Canary Islands. J. Geophys. Res., 116, B03102, https://doi.org/10.1029/2010JB007646

Bleeker, W., 2003. The late Archean record: a puzzle in ca. 35 pieces. Lithos, 71, 99-134. https://doi.org/10.1016/j.lithos.2003.07.003

Blenkinsop, T.G., 2011. Archean magmatic granulites, diapirism, and Proterozoic reworking in the Northern Marginal Zone of the Limpopo Belt. *In* van Reenen, D.D., Kramers, J.D., McCourt, S., Perchuk, L.L., eds., Origin and Evolution of Precambrian High-Grade Gneiss Terranes, with Special Emphasis on the Limpopo Complex of Southern Africa, Geol. Soc. Am. Memoir 207, p. 245–267, https://doi.org/10.1130/2011.1207(13)

Block, S., Jessell, M., Aillères, L., Baratoux, L., Bruguier, O., Zeh, A., Bosch, D., Caby, R., Mensah, E., 2016. Lower crust exhumation during Paleoproterozoic (Eburnean) orogeny, NW Ghana, West African Craton: interplay of coeval contractional deformation and extensional gravitational collapse. Precambrian Res. 274, 82–109. http://dx.doi.org/10.1016/j.precamres.2015.10.014

Bohlen, S.R. 1991. On the formation of granulites. J. Metamorph. Geol., 9, 223-229. https://doi.org/10.1111/j.1525-1314.1991.tb00518.x

Bradley, D.C., 2011. Secular trends in the geologic record and the supercontinent cycle. Earth-Sci. Rev., 108, 16-33. https://doi.org/10.1016/j.earscirev.2011.05.003

Brito Neves, B.B., 2011. The Paleoproterozoic in the South-American continent: Diversity in the geologic time. J. South Am. Earth. Sci., 32, 270-286. https://doi.org/10.1016/j.jsames.2011.02.004

Brown, M., 2007a. Metamorphism, plate tectonics, and the supercontinent cycle. Earth Sci. Front., 14, 1-18. https://doi.org/10.1016/S1872-5791(07)60001-3

Brown, M., 2007b. Metamorphic conditions in orogenic belts: a record of secular change. Int. Geol. Rev. 49, 193-234. http://dx.doi.org/10.2747/0020-6814.49.3.193

Brown, M., 2009. Metamorphic patterns in orogenic systems and the geological record. *In*: Cawood, P.A., and Kröner, A. (Eds.), Accretionary Orogens in Space and Time, Geol. Soc. of London, Special Publications, 318, 37-74. https://doi.org/10.1144/SP318.2

Brown, M., 2014. The contribution of metamorphic petrology to understanding lithosphere evolution and geodynamics. Geosci. Front., 5, 553-569. http://dx.doi.org/10.1016/j.gsf.2014.02.005

Brown, M., Johnson, T., 2019. Time's arrow, time's cycle: Granulite metamorphism and geodynamics. Miner. Mag., 83, 323–338, https://doi.org/10.1180/mgm.2019.19.

Brun, J.P., Sokoutis, D., Tirel, C., Gueydan, F., Driessche, J.V.D., Beslier, M.O., 2018. Crustal versus mantle core complexes. Tectonophysics, 746, 22-45. http://dx.doi.org/10.1016/j.tecto.2017.09.017

Bruno, H., Almeida, J., Heilbron, M., Salomão, M., Cury, L., 2018. Architecture of major Precambrian tectonic boundaries in the northern part of the Dom Feliciano Orogen, southern Brazil: Implications for the West Gondwana amalgamation. J. South Am. Earth. Sci., 86, 301-317, https://doi.org/10.1016/j.jsames.2018.06.018.

Burg, J.P., Kaus, B.J.P., Podladchikov, Y.Y., 2004. Dome structures in collision orogens: Mechanical investigation of the gravity/compression interplay. *In* Whitney, D. L., Teyssier, C. and Siddoway, C. S., eds., Gneiss domes in orogeny, The Geol. Society of Am., Special Paper, v. 380, p. 47-66. https://doi.org/10.1130/0-8137-2380-9.47

Campos, R.S., Philipp, R.P., Massonne, H.J., Chemale, F., Theye, T., 2012. Petrology and isotope geology of mafic to ultramafic metavolcanic rocks of the Brusque Metamorphic complex, southern Brazil. Int. Geol. Rev., 54-6, 686-713. https://doi.org/10.1080/00206814.2011.569393

Cao, S., Neubauer, F., Bernroider, M., Liu, J., 2013. The lateral boundary of a metamorphic core complex: The Moutsounas shear zone on Naxos, Cyclades, Greece. J. Struct. Geol., 54, 103-128. https://doi.org/10.1016/j.jsg.2013.07.002

Cao, S., Neubauer, F., Bernroider, M., Genser, J., Liu, J., Friedl, G., 2017. Low-grade retrogression of a high-temperature Metamorphic core complex: Naxos, Cyclades, Greece. GSA Bulletin, 129, 93-117. https://doi.org/10.1130/B31502.1

Catalán, J.R.M., Ayarza, P., Lobato, F.A., Villalaín, J.J., Oreja, M.D., Paramio, M.M., Gómez, S.R., 2018. Magnetic anomalies in extensional detachments: The Xistral Tectonic Window of the Lugo Dome (NW Spain). Tectonics, 37, 4261-4284. https://doi.org/10.1029/2017TC004887

Chardon, D., Gapais, D., Cagnard, F., 2009. Flow of ultra-hot orogens: a view from the Precambrian, clues for the Phanerozoic. Tectonophysics, 477, 105-118. https://doi.org/10.1016/j.tecto.2009.03.008

Chardon, D., Jayananda, M., Peucat, J.J., 2011. Lateral constrictional flow of hot orogenic crust: Insights from the Neoarchean of south India, geological and geophysical implications for orogenic plateau. Geochem. Geophys. Geosyst., 12, Q02005, https://doi.org/10.1029/2010GC003398

Cheng, L., Zhang, C., Yang, X., 2020. Petrogenesis of deformed tourmaline leucogranite in the Gurla Mandhata metamorphic core complex, Southwestern Tibet. Lithos, 364-355, 105533. https://doi.org/10.1016/j.lithos.2020.105533

Chopin, F., Korja, A., Nikkilä, K., Hölttä, P., Korja, T., Abdel Zaher, M., et al., 2020. The Vaasa migmatitic complex (Svecofennian orogen, Finland): Buildup of a LP/HT dome during Nuna assembly. Tecton., 39, e2019TC005583, https://doi.org/10.1029/2019TC005583.

Clos, F., Weinberg, R.F., Zibra, I., Fenwick, M.J., 2019. Archean diapirism recorded by vertical sheath folds in the core of the Yalgoo Dome, Yilgarn Craton. Precambrian Res., 320, 391-402. https://doi.org/10.1016/j.precamres.2018.11.010

Cooper, F.J., Platt, J.P., Behr, W.M., 2017. Rheological transitions in the middle crust: insights from Cordilleran metamorphic core complexes. Solid Earth, 8, 199-215. https://doi.org/10.5194/se-8-199-2017

Costa, F.G., Santos, P.A., Serafim, I.C.C.O., Costa, I.S.L., Roopnarain, S., 2020. From Mesoarchean drips to modern–style tectonics in the Carajás Province, Amazonian Craton. J. South Am. Sci., 104, 102817. https://doi.org/10.1016/j.jsames.2020.102817

CPRM, 2011. Projeto Aerogeofísico Paraná-Santa Catarina. Serviço Geológico do Brasil, https://rigeo.cprm.gov.br/handle/doc/11241 (May 2022).

Cury, L.F., 2009. Geologia do Terreno Paranaguá. Tese (Doutorado) - Programa de Pós-Graduação em Geoquímica e Geotectônica, Universidade de São Paulo, São Paulo,187 p.

Cutts, K., Lana, C., Alkmin, F., Farina, F., Moreira, H., Coelho, V., 2019. Metamorphism and exhumation of basement gneiss domes in the Quadrilátero Ferrífero: Two stage dome-and-keel evolution?. Geosci. Front., 10, 1765-1787. https://doi.org/10.1016/j.gsf.2019.02.009

Daoudene, Y., Ruffet, G., Cocherie, A., Ledru, P., Gapais, D., 2013. Timing of exhumation of the Ereendavaa metamorphic core complex (north-eastern Mongolia) – U-Pb and $^{40}Ar/^{39}Ar$ constraints. J. Asian Earth Sci., 62, 98-116. http://dx.doi.org/10.1016%2Fj.jseaes.2011.04.009

De Toni, G.B., Bitencourt, M.F., Konopásek, J., Martini, A., Andrade, P.H.S., Florisbal, L.M., Campos, R.S., 2020. Transpressive strain partitioning between the Major Gercino Shear Zone and the Tijucas Fold Belt, Dom Feliciano Belt, Santa Catarina, southern Brazil. J. Struct. Geol., 136, 104058, https://doi.org/10.1016/j.jsg.2020.104058.

Denèle, Y., Olivier, P., Gleizes, G., and Barbey, P., 2009. Decoupling between the middle and upper crust during transpression-related lateral flow: Variscan evolution of the Aston gneiss dome (Pyrenees, France). Tectonophysics, v. 477 (3–4), p. 244-261. https://doi.org/10.1016/j.tecto.2009.04.033

Dharmapriya, P.L., Malaviarachchi, S.P.K., Kriegsman, L.M., Galli, A., Sajeev, K., Zhang, C., 2017. New constraints on the P-T path of HT/UHT metapelites from the Highland complex of Sri Lanka. Geosci. Front. 8, 1405–1430. https://doi.org/10.1016/j.gsf.2016.12.005

Domingos, N.R.R., Medeiros, W.E., Oliveira, R.G., 2020. Geophysical evidence for doming during the Pan-African/Brasiliano orogeny in the Seridó belt, Borborema Province, Brazil. Precambrian Res., 350, 105870. https://doi.org/10.1016/j.precamres.2020.105870

Dossing, A., Stemmerik, L., Dahl-Jenesen, T., Schlindwein, V., 2010. Segmentation of the eastern North Greenland oblique-shear margin: Regional plate tectonic implications. Earth-Planet. Sci. Lett., 292, 239-253. https://doi.org/10.1016/j.epsl.2009.12.036

Dufréchou, G., 2017. Aeromagnetic signature of an exhumed double dome system in the SW Grenville Province (Canada). Terra Nova, v. 29, p. 363–371. https://doi.org/10.1111/ter.12296

Duncan, I.J., 1984. Structural Evolution of the Thor-Odin Gneiss Dome. Tectonophysics, 101, 87-130. https://doi.org/10.1016/0040-1951(84)90044-1

Dziggel, A., Diener, J.F.A., Kokfelt, T.F., Kolb, J., Scherstén, A., 2019. Thermal structure and evolution of an Archean large hot orogen: insights from the Tasiusarsuaq terrane, SW Greenland. Precambrian Res., 335, 105499. https://doi.org/10.1016/j.precamres.2019.105499

Eldosouky, A.M., Abdelkareem, M., Elkhateeb, S.O., 2017. Integration of remote sensing and aeromagnetic data for mapping structural features and hydrothermal alteration zones in Wadi Allaqi area, South Eastern Desert of Egypt. J. Afr. Earth Sci., 130, 28-37. https://doi.org/10.1016/j.jafrearsci.2017.03.006

Endo, T., Tsunogae, T., Santosh, M., Shaji, E., 2012. Phase equilibrium modeling of incipient charnockite formation in NCKFMASHTO and MnNCKFMASHTO systems: A case study from Rajapalaiyam, Madurai Block, southern India. Geosci. Front., 3(6), 801-811. https://doi.org/10.1016/j.gsf.2012.05.005

Eskola, P.E., 1949. The problem of mantled gneiss domes. Geol. Soc. London, Quarterly J., 104, 461-476.

Figueiredo, M.C.H., Mcreath, I., Basei, M.A.S., Mantovani, M.S.M., 1997. Geochemistry of part of the Santa Catarina Granulitic Complex, southern Brazil: a model of differentiation from high alumina basalt. Rev. Bras. Geociênc., 27, 33-40. DOI:10.25249/0375-7536.19973340

Florisbal, L.M., Janasi, V.A., Bitencourt, M.F., Heaman, L.M., 2012. Space–time relation of post-collisional granitic magmatism in Santa Catarina, southern Brazil: U–Pb LAMC-ICP-MS zircon geochronology of coeval mafic-felsic magmatism related to the Major Gercino Shear Zone. Precambrian Res., 216, 132–15. https://doi.org/10.1016/j.precamres.2012.06.015

Fornari, A., 1998. Geologia e metalogênese da porção meridional do Cráton Luis Alves-SC. Tese (Doutorado) - Instituto de Geociências da Universidade de Campinas, Campinas, 136 pp.

François, C., Philippot, P., Rey, P., Rubatto, D., 2014. Burial and exhumation during Archean sagduction in the East Pilbara Granite-Greenstone Terrane. Earth Planet. Sci. Lett., 396, 235-251. http://dx.doi.org/10.1016/j.epsl.2014.04.025

Franek, J., Schulmann, K., Lexa, O., Tomek, C., Edel, J.B., 2011. Model of syn-convergent extrusion of orogenic lower crust in the core of the Variscan belt: implications for exhumation of high-pressure rocks in large hot orogens. J. Metamorph. Geol., 29, 53-78. https://doi.org/10.1111/j.1525-1314.2010.00903.x

Gernigon, L., Blischke, A., Nasuti, A., Sand, M., 2015. Conjugate volcanic rifted margins, seafloor spreading, and microcontinent: Insights from new high-resolution aeromagnetic surveys in the Norway Basin. Tecton., 34, 907–933, https://doi.org/10.1002/2014TC003717

Gerya, T.V., Perchuk, L.L., Maresch, W.V., and Willner, A.P., 2004. Inherent gravitational instability of hot continental crust: Implications for doming and diapirism in granulite facies terrains. *In* Whitney, D.L., Teyssier, C., and Siddoway, C.S., eds., Gneiss domes in orogeny: The Geol. Society of Am., Special Paper, v. 380, p. 97-116. https://doi.org/10.1130/0-8137-2380-9.97

Gerya, T.V., Meilick, F.I., 2011. Geodynamic regimes of subduction under an active margin: effects of rheological weakening by fluids and melts. J. Metamorph. Geol., v. 29, p. 7-31. https://doi.org/10.1111/j.1525-1314.2010.00904.x

Gerya, T.V., 2014. Precambrian geodynamics: Concepts and models. Gondwana Res., 25, 442-463. https://doi.org/10.1016/j.gr.2012.11.008

Girardi, V.A.V., Ulbrich, H.H.G.J., 1978. A sapphirine-orthopyroxene-spinel occurrence in the Piên Area, Paraná, Southern Brazil. Rev. Bras. Geociênc., 8, 284-293.

Girelli, T.J., Chemale Jr., F., Lavina, E.L.C., Laux, J.H., Bongiolo, E.M., Lana, C., 2018. Granulite accretion to Rio de la Plata Craton, based on zircon U-Pb-Hf isotopes: Tectonic implications for Columbia Supercontinent reconstruction. Gondwana Res., v. 56, p. 105-118, https://doi.org/10.1016/j.gr.2017.12.010.

Golynsky, A. V., Ferraccioli, F., Hong, J. K., Golynsky, D. A., von Frese, R. R. B., Young, D. A., et al., 2018. New magnetic anomaly map of the Antarctic. Geophys. Res. Lett., 45, 6437–6449. https://doi.org/10.1029/2018GL078153.

Goodge, J.W., Finn, C.A., 2010. Glimpses of East Antarctica: Aeromagnetic and satellite magnetic view from the central Transantarctic Mountains of East Antarctica. J. Geophys. Res., 115, B09103, https://doi.org/10.1029/2009JB006890

Grujic, D., Warren, C.J. and Wooden, J.L., 2011. Rapid synconvergent exhumation of Miocene-aged lower orogenic crust in the eastern Himalaya. Lithosphere, 3-5, 346-366. https://doi.org/10.1130/L154.1

Guadagnin, F., Chemale Jr, F., Dussin, I.A., Jelinek, A.R., dos Santos, M.N., Borba, M.L., Justino, D., Bertotti, A.L., Alessandretti, L., 2010. Depositional age and provenance of the Itajaí Basin, Santa Catarina State, Brazil: Implications for SW Gondwana correlation. Precambrian Res., 180, 3-4, 156-182. https://doi.org/10.1016/j.precamres.2010.04.002.

Guo, L., Zhang, J., and Zhang, B., 2008. Structures, kinematics, thermochronology and tectonic evolution of the Ramba gneiss dome in the northern Himalaya. Prog. Nat. Sci., 18-7, 851-860. https://doi.org/10.1016/j.pnsc.2008.01.016

Harley, S.L., 1989. The origins of granulites: a metamorphic perspective. Geol. Mag., 126, 215–247. https://doi.org/10.1017/S0016756800022330

Harley, S.L., 1992. Proterozoic Granulite Terranes. *In* Condie, K.C., ed., Proterozoic Crustal Evolution, Elsevier, v. 10, p. 301-359. https://doi.org/10.1016/S0166-2635(08)70122-1

Harley, S.L., 2016. A matter of time: The importance of the duration of UHT metamorphism. J. Miner. Petrol. Sci., 111, 50-72. https://doi.org/10.2465/jmps.160128

Harara, O.M.M., 2001. Mapeamento e investigação petrológica e geocronológica dos litotipos da região do Alto Rio Negro (PR-SC): um exemplo de sucessivas e distintas atividades magmáticas durante o Neoproterozoico III. Tese (Doutorado) - Programa de Pós-Graduação em Geoquímica e Geotectônica. Universidade de São Paulo, São Paulo, 206 pp.

Harris, L.B., Godin, L., Yakymchuk, C., 2012. Regional shortening followed by channel flow induced collapse: A new mechanism for “dome and keel” geometries in Neoarchean granite-greenstone terrains. Precambrian Res., 212-213, 139-154. https://doi.org/10.1016/j.precamres.2012.04.022

Hartmann, L.A., Silva, L.C., Orlandi F°, V., 1979. O Complexo Granulítico de Santa Catarina: descrição e implicações genéticas. Acta Geológica Leopoldensia, São Leopoldo, 6, 93-112.

Hartmann, L.A., 1988. Geoquímica de terras raras e geotermobaromelria de granulitos de Dom Pedrito e Luis Alves, no extremo sul do Brasil. Geochim. Brasil., 2, 1-14.

Hartmann, L.A., Santos, J.O.S., McNaughton, N.J., Vasconcellos, M.A.Z., Silva, L.C. da, 2000. Ion microprobe (SHRIMP) dates complex granulite from Santa Catarina, southern Brazil. An. Acad. Bras. Ciênc., 72-4, 559-572. https://doi.org/10.1590/S0001-37652000000400007

Hartmann, L.A., Savian, J.F., and Lopes, W.R., 2016. Airborne geophysical characterization of geotectonic relationships in the southern Ribeira Belt, Luis Alves Craton, and northern Dom Feliciano Belt, Brazilian Shield. Int. Geol. Rev., v. 58(4), p. 471-488. https://doi.org/10.1080/00206814.2015.1089424

Hayman, N.W., Grindlay, N.R., Perfit, M.R., Mann, P., Leroy, S., de Lépinay, B.M., 2011. Oceanic core complex development at the ultraslow spreading Mid Cayman Spreading Center. Geochem. Geophys. Geosyst., 12, Q0AG02. https://doi.org/10.1029/2010GC003240

Heilbron, M., Valeriano, C.M., Tassinari, C.C.G., Almeida, J., Tupinambá, M., Siga Jr., O., Trouw, R., 2008. Correlation of Neoproterozoic terranes between the Ribeira Belt, SE Brazil and its African counterpart: comparative tectonic evolution and open questions. *In* Pankhurst, R.J., Trouw, R.A.J., Brito Neves, B.B., De Wit, M.J., (eds) West Gondwana: Pre-Cenozoic Correlations Across the South Atlantic Region. Geological Society, London, Special Publications, 294, 211–237. https://doi.org/10.1144/SP294.12

Heller, B.M., Hueck, M., Passarelli, C.R., Basei, M.A.S., 2021. Zircon U-Pb geochronology and Hf isotopes of the Luís Alves Terrane: Archean to Paleoproterozoic evolution and Neoproterozoic overprint. J. South Am. Earth. Sci., 106, 103008, https://doi.org/10.1016/j.jsames.2020.103008.

Hinze, W., Von Frese, R., Saad, A., 2013. Gravity and Magnetic Exploration: Principles, Practices, and Applications. Cambridge: Cambridge University Press. https://doi.org/10.1017/CBO9780511843129

Hoffmann, A., Kröner, A., Xie, H., Hegner, E., Belyanin, G., Kramers, J., Bolhar, R., Slabunov, A., Reinhardt, J., Horváth, P., 2015. The Nhlangano gneiss dome in south-west Swaziland – A record of crustal destabilization of the eastern Kaapvaal craton in the Neoarchaean. Precambrian Res., 258, 109-132. https://doi.org/10.1016/j.precamres.2014.12.008

Holland, T.J.B. & Powell, R., 1985. An internally consistent thermodynamic dataset with uncertainties and correlations: 2. Data and results. J. Metamorph. Geol., 3, 343-370. https://doi.org/10.1111/j.1525-1314.1985.tb00325.x

Hueck, M., Basei, M.A.S., Wemmer, K., Oriolo, S., Heidelbach, F., Siegesmund, S., 2019. Evolution of the Major Gercino Shear Zone in the Dom Feliciano Belt, South Brazil, and implications for the assembly of southwestern Gondwana. Inter. J. Earth Sci., 108, 403-425, https://doi.org/10.1007/s00531-018-1660-4.

IAEA, INTERNATIONAL ATOMIC ENERGY AGENCY, 2003. Guidelines for Radioelement Mapping Using Gamma Ray Spectrometry Data, IAEA-TECDOC-1363, IAEA, Vienna.

Iglesias, C.M.F., Zerfass, H., Silva, M.A.S., Klein, C., 2011. Geologia e recursos minerais da Folha Joinville - SH. 22−Z−B, 1:250.000, Estado de Santa Catarina. Porto Alegre: CPRM, http://rigeo.cprm.gov.br/jspui/handle/doc/17685 (May 2022).

Iglesias, C.M.F., Klein, C., Rocha, P.G., Betiollo, L.M., Provenzano, C.A.S., Lopes, W.R., Horn, B.L.D., Rezende, G.G., 2021. Mapeamento geológico e hidrogeológico do município de Joinville, SC: produto 6, mapeamento geológico, estrutural e de recursos minerais, Estado de Santa Catarina. Porto Alegre: CPRM, https://rigeo.cprm.gov.br/handle/doc/22453 (May 2022).

James, H.L., 1954. Sedimentary Facies of Iron-Formation. Econ. Geol., 49-3, 235-293. https://doi.org/10.2113/gsecongeo.49.3.235

James, D.T., Mortensen, J.K., 1992. An Archean metamorphic core complex in the southern Slave Province: basement-cover structural relations between the Sleepy Dragon Complex and the Yellowknife Supergroup. Can. J. Earth Sci., 29, 2133-2145. https://doi.org/10.1139/e92-169

Jamieson, R.A., Beaumont, C., 2011. Coeval thrusting and extension during lower crustal ductile flow – implications for exhumation of high-grade metamorphic rocks. J. Metamorph. Geol., 29, 33-51. https://doi.org/10.1111/j.1525-1314.2010.00908.x

Jamieson, R.A., Beaumont, C., 2013. On the origin of orogens. Bull. Geol. Soc. Am., 125, 1671–1702. https://doi.org/10.1130/B30855.1

Jelinek, A.R., Machado, J.P.S.L., Santos, E.A., 2021. Evolução termocronológica do Cinturão Dom Feliciano: implicações na geodinâmica da margem continental sul do Brasil. *In* Jelinek, A.R., Sommer, C.A., eds, Contribuições à geologia do Rio Grande do Sul e Santa Catarina, Sociedade Brasileira de Geologia, Porto Alegre, Publicação Especial Núcleo RS/SC, 185-202.

Jolivet, L., Famin, V., Mehl, C., Parra, T., Aubourg, C., Hébert, R., Philippot, P., 2004. Strain localization during crustal-scale boudinage to form extensional metamorphic domes in the Aegean Sea. *In* Whitney, D. L., Teyssier, C., Siddoway, C. S., eds., Gneiss domes in orogeny, The Geol. Society of Am., Special Paper, v. 380, p. 185-210. https://doi.org/10.1130/0-8137-2380-9.185

Jordan, T.A., Ferraccioli, F., Ross, N., Corr, H.F.J., Leat, P.T., Bingham, R.G., Rippin, D.M., Brocq, A., Siegert, M.J., 2013. Inland extent of the Weddell Sea Rift imaged

by new aerogeophysical data. Tectonophysics, 585, 137-160. https://doi.org/10.1016/j.tecto.2012.09.010

Kamaci, O., Altunkaynak, S., 2020. The role of accreted continental crust in the formation of granites within the Alpine style continental collision zone: Geochemical and geochronological constrains from leucogranites in the Çataldağ Metamorphic Core Complex (NW Turkey). Lithos, 354-355, 105347. https://doi.org/10.1016/j.lithos.2019.105347

Kaul, P.F.T., 1980. O Cráton de Luis Alves. In: Congresso Brasileiro De Geologia, 31, Balneário Camboriú, Anais, SBG, v. 5, p. 2677-2683.

Kayode, J.S., Nawawi, M.N.M., Abdullah, K.B., Khalil, A.E., 2017. Integrating aeromagnetic and Landsat™ 8 data into subsurface structural mapping of Precambrian basement complex. J. Afr. Earth Sci., 125, 202-213. https://doi.org/10.1016/j.jafrearsci.2016.11.010

Kelsey, D.E., Powell, R., 2011. Progress in linking accessory mineral growth and breakdown to major mineral evolution in metamorphic rocks: a thermodynamic approach in the Na_2O-CaO-K_2O-FeO-MgO-Al_2O_3-SiO_2-H_2O-TiO_2-ZrO_2 system. J. Metamorph. Geol., 29, 151-166. https://doi.org/10.1111/j.1525-1314.2010.00910.x

Kelsey, D.E., Hand, M., 2015. On ultrahigh temperature crustal metamorphism: Phase equilibria, trace element thermometry, bulk composition, heat sources, timescales and tectonic settings. Geosci. Front., 6, 311-356. https://doi.org/10.1016/j.gsf.2014.09.006

Klein, C., 2005. Some Precambrian banded iron-formations (BIFs) from around the world: Their age, geologic setting, mineralogy, metamorphism, geochemistry, and origin. Am. Miner., 90, 1473-1499. https://doi.org/10.2138/am.2005.1871

Klepeis, K.A., Schwartz, J., Stowell, H., Tulloch, A., 2016. Gneiss domes, vertical and horizontal mass transfer, and the initiation of extension in the hot lower-crustal root of a continental arc, Fiordland, New Zealand. Lithosphere, 8-2, 116-140. https://doi.org/10.1130/L490.1

Kohn, M.J., 2014. Himalayan Metamorphism and its Tectonic Implications. Annu. Rev. Earth Planet. Sci., 42, 381-419. https://doi.org/10.1146/annurev-earth-060313-055005

Kramers, J.D., McCourt, S., Roering, C., Smit, C.A., van Reenen, D.D., 2011. Tectonic models for the Limpopo Complex: Mutual compatibilities and constraints. *In* van Reenen, D.D., Kramers, J.D., McCourt, S., and Perchuk, L.L., eds, Origin and

Evolution of Precambrian High-Grade Gneiss Terranes, with Special Emphasis on the Limpopo Complex of Southern Africa, The Geol. Society of Am., p. 311-324. https://doi.org/10.1130/2011.1207(16)

Kumar, K.S., Srinivas, K.N.S.S.S., Kumar, V.P. Prasad, P.P., Seshunarayana, T., 2018. Magnetic Mapping of Banded Iron Formation of Sandur Schist Belt, Dharwar Craton, India. J. Geol. Soc. India, 91, 174-180. https://doi.org/10.1007/s12594-018-0831-z

Lana, C., Tohver, E., Cawood, P., 2010. Quantifying rates of dome-and-keel formation in the Barberton granitoid-greenstone belt, South Africa. Precambrian Res., 177, 199-211. https://doi.org/10.1016/j.precamres.2009.12.001

Lagabrielle, Y., Brovarone, A.V., Ildefonse, B., 2015. Fossil oceanic core complexes recognized in the blueschist metaophiolites of Western Alps and Corsica. Earth-Sci. Rev., 141, 1-26. https://doi.org/10.1016/j.earscirev.2014.11.004

Launay, N., Quesnel, Y., Rochette, P., Demory, F., 2018. Iron Formations as the Source of the West African Magnetic Crustal Anomaly. Front. Earth Sci., 6, 32. https://doi.org/10.3389/feart.2018.00032

Lexa, O., Schulmann, K., Janousek, V. Stipska, P., Guy, A., Racek, M., 2011. Heat sources and trigger mechanisms of exhumation of HP granulites in Variscan orogenic root. J. Metamorph. Geol., 29, 79-102. https://doi.org/10.1111/j.1525-1314.2010.00906.x

Lin, S., Beakhouse, G.P., 2013. Synchronous vertical and horizontal tectonism at late stages of Archean cratonization and genesis of Hemlo gold deposit, Superior craton, Ontario, Canada. Geol., 41-3, 359-362. https://doi.org/10.1130/G33887.1

Lister, G.S., Davis, G.A., 1989. The origin of metamorphic core complexes and detachment faults formed during Tertiary continental extension in the northern Colorado river region, U.S.A.. J. Struct. Geol., 11, 65-94. https://doi.org/10.1016/0191-8141(89)90036-9

Liu, T., Wei, C., 2018. Metamorphic evolution of Archean ultrahigh-temperature mafic granulites from the western margin of Qian'an gneiss dome, eastern Hebei Province, North China Craton: insights into the Archean tectonic regime. Precambrian Res., 318, 170-187. https://doi.org/10.1016/j.precamres.2018.10.007

Maacha, L., Jaffal, M., Jarni, A., Kchikach, A., Mouguina, E.M., Zouhair, M., Ennaciri, A., Saddiqi, O., 2017. A contribution of airborne magnetic, gamma ray spectrometric data in

understanding the structure of the Central Jebilet Hercynian massif and implications for mining. J. Afr. Earth Sci., 134, 389-403. https://doi.org/10.1016/j.jafrearsci.2017.07.012

Machiavelli, A., Basei, M.A.S., Siga Jr., O., 1993. Suíte Granítica Rio Piên: Um Arco Magmático do Proterozoico Superior na Microplaca Curitiba. Geochim. Bras., 7-2, 11-29.

Mantovani, M.S.M.; Hawkesworth, C.J.; Basei, M.A.S., 1987. Nd and Sr isotope studies bearing on the crustal evolution of southeastern Brazil. Rev. Bras. Geociênc., 17-3, 263-268.

Marangoni, Y.R., Mantovani, M.S.M., 2013. Geophysical signatures of the alkaline intrusions bordering the Paraná Basin. J. South Am. Earth Sci., 41, 83-98. https://doi.org/10.1016/j.jsames.2012.08.004

Marshak, S., Tinkham, D., Alkmin, F., Brueckner, H., Bornhorst, T., 1997. Dome-and-keel provinces formed during Paleoproterozoic orogenic collapse-core complexes, diapirs, or neither?: Examples from the Quadrilátero Ferrífero and the Penokean orogen. Geol., 25-5, 415-418. https://doi.org/10.1130/0091-7613(1997)025<0415:DAKPFD>2.3.CO;2

Meert, J.G., and Santosh, M., 2017. The Columbia supercontinent revisited. Gondwana Res., 50, 67–83, https://doi.org/10.1016/j.gr.2017.04.011.

Mieth, M., Jokat, W., 2014a. New aeromagnetic view of the geological fabric of southern Dronning Maud Land and Coats Land, East Antarctica. Gondwana Res., 25, 358-367. https://doi.org/10.1016/j.gr.2013.04.003

Mieth, M., Jokat, W., 2014b. Banded iron formation (?) at Grunehogna Craton, East Antarctica-Constraints from aeromagnetic data. Precambrian Res., 250, 143-150. https://doi.org/10.1016/j.precamres.2014.06.001

Minelli, L., Speranza, F., Nicolosi, I., D'Ajello Caracciolo, F., Carluccio, R., Chiappini, S., Messina, A., & Chiappini, M., 2018. Aeromagnetic investigation of the central Apennine Seismogenic Zone (Italy): From basins to faults. Tecton., 37, 1435-1453. https://doi.org/10.1002/2017TC004953.

Murthy, I.V.R., Babu, S.B., 2006. Structure of Charnockitic basement in a part of the Krishna–Godavari basin, Andhra Pradesh. J. Earth Syst. Sci., 115-4, 387-393. https://doi.org/10.1007/BF02702867

Nabighian, M.N., Grauch, V.J.S., Hansen, R.O., LaFehr, T.R., Li, Y., Peirce, J.W., Ruder, M.E., 2005. The historical development of the magnetic method in exploration. Geophysics, 70, 33-61. http://dx.doi.org/10.1190/1.2133784

Norlander, B.H., Whitney, D.L., Teyssier, C., Vanderhaeghe, O., 2002. Partial melting and decompression of the Thor-Odin dome, Shuswap metamorphic core complex, Canadian Cordillera. Lithos, 61, 103-125. https://doi.org/10.1016/S0024-4937(02)00075-0

O'Brien, P., 2006. Type-locality granulites: high-pressure rocks formed at eclogite-facies conditions. Miner. and Petrol., 86, 161-175. https://doi.org/10.1007/s00710-005-0108-2

Ogunmola, J.K., Ayolabi, E.A., Olobaniyi, S.B., 2016. Structural-depth analysis of the Yola Arm of the Upper Benue Trough of Nigeria using high resolution aeromagnetic data. J. Afr. Earth Sci., 124, 32-43. https://doi.org/10.1016/j.jafrearsci.2016.09.008

Oladunjoye, M.A., Olayinka, A.I., Alaba, M., Adabanija, M.A., 2016. Interpretation of high resolution aeromagnetic data for lineaments study and occurrence of Banded Iron Formation in Ogbomoso area, Southwestern Nigeria. J. Afr. Earth Sci., 114, 43-53. https://doi.org/10.1016/j.jafrearsci.2015.10.015

Österle, J.E., Little, T.A., Seward, D., Stockli, D.F., Gamble, J., 2020. The petrology, geochronology and tectono-magmatic setting of igneous rocks in the Suckling-Dayman metamorphic core complex, Papua New Guinea. Gondwana Res., 83, 390-414. https://doi.org/10.1016/j.gr.2020.01.014

Passarelli, C.R., Basei, M.A.S., Wemmer, K., Siga Jr., O., Oyhantçabal, P., 2011. Major shear zones of southern Brazil and Uruguay: escape tectonics in the eastern border of Rio de La plata and Paranapanema cratons during the Western Gondwana amalgamation. Int. J. Earth Sci. (Geol Rundsch), 100, 391-414, https://doi.org/10.1007/s00531-010-0594-2

Passarelli, C.R., Basei, M.A.S., Siga Jr., O., and Harara, O.M.M., 2018. The Luis Alves and Curitiba Terranes: Continental Fragments in the Adamastor Ocean. *In* Siegesmund, S., Basei, M.A.S., Oyhantçabal, P., Oriolo, S., eds., Geol. of Southwest Gondwana, Regional Geol. Rev., p. 189-215. https://doi.org/10.1007/978-3-319-68920-3_8

Perchuk, A.L., Safonov, O.G., Smit, C.A., van Reenen, D.D., Zakharov, V.S., Gerya, T.V., 2018. Precambrian ultra-hot orogenic factory: making and reworking of continental crust. Tectonophysics, 746, 572-586. http://dx.doi.org/10.1016/j.tecto.2016.11.041

Philipp, R.P., Mallmann, G., Bitencourt, M.F., Souza, E.R., Liz, J.D., Wild, F., Arend, S., Oliveira, A.S., Duarte, L.C., Rivera, C.B., Prado, M., 2004. Caracterização

Litológica e Evolução Metamórfica da Porção Leste do Complexo Metamórfico Brusque, Santa Catarina. Rev. Bras. Geociênc., 34 (1), 21–34.

Platt, J.P., Behr, W.M., Cooper, F.J., 2015. Metamorphic core complexes: windows into the mechanics and rheology of the crust. J. Geol. Soc., 172, 9-27. https://doi.org/10.1144/jgs2014-036

Powell, R. & Holland, T.J.B., 1985. An internally consistent thermodynamic dataset with uncertainties and correlations. 1. Methods and a worked example. J. Metamorph. Geol., 3, 327-342. https://doi.org/10.1111/j.1525-1314.1985.tb00324.x

Powell, R. & Holland, T.J.B., 1988. An internally consistent thermodynamic dataset with uncertainties and correlations. 3. Applications to geobarometry, worked examples and a computer program. J. Metamorph. Geol., 6, 173-204. https://doi.org/10.1111/j.1525-1314.1988.tb00415.x

Quadrilátero Ferrífero 2050, 2020. Centro de Estudos Avançados Quadrilátero Ferrífero, UFOP - Univ. Fed. Ouro Preto, https://qfe2050.ufop.br (May 2022).

Rajaram, M., and Anand, S.P., 2014. Aeromagnetic signatures of Precambrian shield and suture zones of Peninsular India. Geosci. Front., 5-1, 3-15. http://dx.doi.org/10.1016/j.gsf.2013.06.005

Reeves, C., 2005. Aeromagnetic Surveys: Principles, Practice and Interpretation. Earth- works, Washington DC, 155 p.

Renne, P.R., Deckart, K., Ernesto, M., Féraud, G., Piccirillo, E.M., 1996. Age of the Ponta Grossa dike swarm (Brazil), and implications to Paraná flood volcanism, Earth and Planet. Sci. Lett., 144, 1-2, 199-211, https://doi.org/10.1016/0012-821X(96)00155-0

Riedel, S., Jacobs, J., Jokat, W., 2013. Interpretation of new regional aeromagnetic data over Dronning Maud Land (East Antarctica). Tectonophysics, 585, 161-171. http://dx.doi.org/10.1016/j.tecto.2012.10.011

Rizzotto, G.J., Alves, C.L., Rios, F.S., Barros, M.A.S., 2019. The Nova Monte Verde Metamorphic core complex: Tectonic implications for the southern Amazonian craton. J. South Am. Earth Sci., 91, 154-172. https://doi.org/10.1016/j.jsames.2019.01.003

Roberts, N.M., Tikoff, B., 2021. Internal structure of the Paleoarchean Mt Edgar dome, Pilbara Craton, Western Australia. Precambrian Res., 358, 106163. https://doi.org/10.1016/j.precamres.2021.106163

Rosa, J.W.C., Rosa, J.W.C., Fuck, R.A., 2014. Geophysical structures and tectonic evolution of the southern Guyana shield, Brazil. J. South Am. Earth Sci., 52, 57-71. http://dx.doi.org/10.1016/j.jsames.2014.02.006

Rosa, J.W.C., Rosa, J.W.C., Fuck, R.A., 2016. The structure of the Amazonian craton: Available geophysical evidence. J. South Am. Earth Sci., 70, 162-173. http://dx.doi.org/10.1016/j.jsames.2016.05.006

Sajeev, K., Windley, B.F., Hegner, E., Komiya, T., 2013. High-temperature, high-pressure granulites (retrogressed eclogites) in the central region of the Lewisian, NW Scotland: Crustal-scale subduction in the Neoarchean. Gondwana Res., v. 23, p. 526-538. https://doi.org/10.1016/j.gr.2012.05.002

Sandiford, M., Van Kranendonk, M.J., Bodorkos, S., 2004. Conductive incubation and the origin of dome-and-keel structure in Archean granite-greenstone terrains: A model based on the eastern Pilbara Craton, Western Australia. Tecton., 23, TC1009. https://doi.org/10.1029/2002TC001452

Scandolara, J.E., Correa, R.T., Fuck, R.A., Souza, V.S., Rodrigues, J.B., Ribeiro, P.S.E., Frasca, A.A.S., Saboia, A.M., Lacerda Filho, J.V., 2017. Paleo-Mesoproterozoic arc-accretion along the southwestern margin of the Amazonian craton: The Juruena accretionary orogen and possible implications for Columbia supercontinent. J. South Am. Earth Sci., 73, 223-247. http://dx.doi.org/10.1016/j.jsames.2016.12.005

Scheffer, C., Vanderhaeghe, O., Lanari, P., Tarantola, A., Ponthus, L., Photiades, A., France, L., 2016. Syn- to post-orogenic exhumation of metamorphic nappes: Structure and thermobarometry of the western Attic-Cycladic metamorphic complex (Lavrion, Greece). J. Geodyn., 96, 174-193. http://dx.doi.org/10.1016/j.jog.2015.08.005

Searle, M.P., Lamont, T.N., 2020. Compressional metamorphic core complexes, low-angle normal faults and extensional fabrics in compressional tectonic settings. Geol. Mag., 157, 101-118. https://doi.org/10.1017/S0016756819000207

Searle, M.P., Lamont, T.N., 2022. Compressional origin of the Aegean Orogeny, Greece. Geosci. Front., 13, 101049. https://doi.org/10.1016/j.gsf.2020.07.008

Soula, J.C., 1982. Characteristics and mode of emplacement of gneiss domes and plutonic domes in central-eastern Pyrenees. J. Struct. Geol., 4-3, 313-342. https://doi.org/10.1016/0191-8141(82)90017-7

Spalla, M.I., Zanoni, D., Williams, P.F., Gosso, G., 2011. Deciphering cryptic P-T-d-t histories in the western Thor-Odin dome, Monashee Mountains, Canadian

Cordillera: A key to unravelling pre-Cordilleran tectonic signatures. J. Struct. Geol., 33, 399-421. https://doi.org/10.1016/j.jsg.2010.11.014

Stevens, L.M., Bebdick, R., Baldwin, J.A., 2017. Synconvergent exhumation of metamorphic core complexes in the northern North American Cordillera. Geol., 45-6, 495-498. https://doi.org/10.1130/G38802.1

Stüwe, K., 2007. Geodynamics of the Lithosphere. Springer, Berlin, 493 p.

Taylor, J., Stevens, G., Armstrong, R., Kisters, A.F.M., 2010. Granulite facies anatexis in the Ancient Gneiss Complex, Swaziland, at 2.73 Ga: Mid-crustal metamorphic evidence for mantle heating of the Kaapvaal craton during Ventersdorp magmatism. Precambrian Res., 177, 88-102. https://doi.org/10.1016/j.precamres.2009.11.005

Teyssier, C., Whitney, D.L., 2002. Gneiss domes and orogeny. Geol., 30-12, 1139-1142. https://doi.org/10.1130/0091-7613(2002)030<1139:GDAO>2.0.CO;2

Thébaud, N., Rey, P.F., 2013. Archean gravity-driven tectonics on hot and flooded continents: Controls on long-lived mineralized hydrothermal systems away from continental margins. Precambrian Res., 229, 93-104. https://doi.org/10.1016/j.precamres.2012.03.001

Tichomirowa, M., Köhler, R., 2013. Discrimination of protolithic versus metamorphic zircon ages in eclogites: Constraints from the Erzgebirge metamorphic core complex (Germany). Lithos, 177, 436-450. http://dx.doi.org/10.1016/j.lithos.2013.07.013

Tiddy, C.J., Betts, P.G., Neumann, M.R., Murphy, F.C., Stewart, J., Giles, D., Sawyer, M., Freeman, H., Jourdan, F., 2020. Interpretation of a ca. 1600-1580 Ma metamorphic core complex in the northern Gawler Craton, Australia. Gondwana Res., 85, 263-290. https://doi.org/10.1016/j.gr.2020.04.008

Tominaga, M., Sager, W.W., 2010. Origin of the smooth zone in early Cretaceous North Atlantic magnetic anomalies. Geophys. Res. Lett., 37, L01304, https://doi.org/10.1029/2009GL040984

Toraman, E., Teyssier, C., Whitney, D.L., Fayon, A.K., Thomson, S.N., Reiners, P.W., 2014. Low-temperature thermochronologic record of Eocene migmatite dome emplacement and late Cenozoic landscape development, Shuswap core complex, British Columbia. Tecton., 33, 1616–1635, https://doi.org/10.1002/2013TC003442

Touret, J.L.R., Santosh, M., Huizenga, J.M., 2016. High-temperature granulites and supercontinents. Geosci. Front., 7, 101-113. http://dx.doi.org/10.1016/j.gsf.2015.09.001

Van Kranendonk, M.J., Collins, W.J., Hickman, A., Pawley, M.J., 2004. Critical tests of vertical vs. horizontal tectonic models for the Archean East Pilbara Granite-Greenstone Terrane, Pilbara Craton, Western Australia. Precambrian Res., 131, 173-211. https://doi.org/10.1016/j.precamres.2003.12.015

Van Kranendonk, M.J., Smithies, R.H., Hickman, A.H., Champion, D.C., 2007. Review: secular tectonic evolution of Archean continental crust: interplay between horizontal and vertical process in the formation of the Pilbara Craton, Australia. Terra Nova, 19, 1-38. https://doi.org/10.1111/j.1365-3121.2006.00723.x

Vanderhaeghe, O., 2004. Structural development of the Naxos migmatite dome. *In* Whitney, D.L., Teyssier, C., Siddoway, C.S., eds., Gneiss domes in orogeny, The Geol. Society of Am., Special Paper, v. 380, p. 211-227. https://doi.org/10.1130/0-8137-2380-9.211

Vansutre, S., Hari, K.R., 2010. Granulite belts of central India with special reference to the Bhopalpatnam Granulite Belt: significance in crustal evolution and implications for Columbia supercontinent. J. of Asian Earth Sci., 39, 794-803. https://doi.org/10.1016/j.jseaes.2010.06.004

Verdel, C., Wernicke, B.P., Ramezani, J., Hassanzadeh, J., Renne, P.R., Spell, T.L., 2007. Geology and thermochronology of Tertiary Cordilleran-style metamorphic core complexes in the Saghand region of central Iran. GSA Bulletin, 119, 961-977. https://doi.org/10.1130/B26102.1

Walczak, K., Anczkiewicz, R., Szczepanski, J., Rubatto, D., Kosler, J., 2017. Combined garnet and zircon geochronology of the ultra-high temperature metamorphism: Constraints on the rise of the Orlica-Śnieżnik Dome, NE Bohemian Massif, SW Poland. Lithos, 292-293, 388-400. https://doi.org/10.1016/j.lithos.2017.09.013

Wang, T., Guo, L., Zheng, Y., Donskaya, T., Gladkochub, D., Zeng, L., Li, J., Wang, Y., Mazukabzov, A., 2012. Timing and processes of late Mesozoic mid-lower-crustal extension in continental NE Asia and implications for the tectonic setting of the destruction of the North China Craton: Mainly constrained by zircon U–Pb ages from metamorphic core complexes. Lithos, 154, 315-345. http://dx.doi.org/10.1016/j.lithos.2012.07.020

White, R.W., Powell, R., 2011. On the interpretation of retrograde reaction textures in granulite facies rocks. J. Metamorph. Geol., 29, 131-149. https://doi.org/10.1111/j.1525-1314.2010.00905.x

Whitney, D.L., Teyssier, C., Siddoway, C.S., eds., 2004a. Gneiss domes in orogeny. The Geol. Society of Am., Special Paper, v. 380, 393 pp. https://doi.org/10.1130/SPE380

Whitney, D.L., Teyssier, C., Vanderhaeghe, O., 2004b. Gneiss domes and crustal flow. *In* Whitney, D.L., Teyssier, C., Siddoway, C.S., eds., Gneiss domes in orogeny, The Geol. Society of Am., Special Paper, v. 380, p. 15-34. https://doi.org/10.1130/0-8137-2380-9.15

Whitney, D.L., Teyssier, C., Rey, P., Buck, W.R., 2013. Continental and oceanic core complexes. GSA Bulletin, 125, 273-298. https://doi.org/10.1130/B30754.1

Wiest, J.D., Osmundsen, P.T., Jacobs, J., Fossen, H., 2019. Deep Crustal Flow Within Postorogenic Metamorphic Core Complexes: Insights from the Southern Western Gneiss Region of Norway. Tecton., 38, 4267–4289, https://doi.org/10.1029/2019TC005708

Xiong, S.Q., Tong, J., Ding, Y.Y., Li, Z.K., 2016. Aeromagnetic data and geological structure of continental China: A review. Appl. Geophys., 13-2, 227-237. http://doi.org/10.1007/s11770-016-0552-2

Yin, A., 2004. Gneiss domes and gneiss dome systems. *In* Whitney, D.L., Teyssier, C., Siddoway, C.S., eds., Gneiss domes in orogeny, The Geol. Society of Am., Special Paper, v. 380, p. 1-14. https://doi.org/10.1130/0-8137-2380-9.1

Zhang, B., Chai, Z., Yin, C.Y., Huang, W.T., Wang, Y., Zhang, J.J., Wang, X.X., Cao, K., 2017. Intra-continental transpression and gneiss doming in an obliquely convergent regime in SE Asia. J. Struct. Geol., 97, 48-70. http://dx.doi.org/10.1016/j.jsg.2017.02.010

Zhang, Z.M., Ding, H.X., Palin, R.M., Dong, X., Tian, Z.L., Kang, D.Y., Jiang, Y.Y., Qin, S.K., Li, W.T., 2022. On the origin of high-pressure mafic granulite in the Eastern Himalayan Syntaxis: Implications for the tectonic evolution of the Himalayan orogen. Gondwana Res., 104, 4-22. https://doi.org/10.1016/j.gr.2021.05.011

Zhao, G., Sun, M., Wilde, S.A., and Li, S., 2004. A Paleo-Mesoproterozoic supercontinent: assembly, growth and breakup. Earth-Sci. Rev., 67, 91–123. https://doi.org/10.1016/j.earscirev.2004.02.003

Zulauf, G., Zulauf, J., Thiessen, A., Hattingen, E., 2019. Formation of dome-in-dome structures: Results from experimental studies and comparison with natural examples. J. Struct. Geol., 118, 324-339. https://doi.org/10.1016/j.jsg.2018.11.008

Artigo 2

Gmail

Leandro Betiollo <le.vermelho@gmail.com>

GEXPLO-D-22-00534 - Confirming your submission to Journal of Geochemical Exploration

1 mensagem

Journal of Geochemical Exploration <em@editorialmanager.com> 23 de dezembro de 2022 às 01:03
Responder a: Journal of Geochemical Exploration <support@elsevier.com>
Para: Leandro Menezes Betiollo <le.vermelho@gmail.com>

ELSEVIER

This is an automated message.

Geochemistry of granulite facies BIFs from the Luis Alves Craton (southern Brazil): implications for Archean-Paleoproterozoic depositional and tectonic settings

Dear Sr Betiollo,

We have received the above referenced manuscript you submitted to Journal of Geochemical Exploration. It has been assigned the following manuscript number: GEXPLO-D-22-00534.

To track the status of your manuscript, please log in as an author at https://www.editorialmanager.com/gexplo/, and navigate to the "Submissions Being Processed" folder.

Thank you for submitting your work to this journal.

Kind regards,
Journal of Geochemical Exploration

More information and support

You will find information relevant for you as an author on Elsevier's Author Hub: https://www.elsevier.com/authors

FAQ: How can I reset a forgotten password?
https://service.elsevier.com/app/answers/detail/a_id/28452/supporthub/publishing/kw/editorial+manager/

For further assistance, please visit our customer service site: https://service.elsevier.com/app/home/supporthub/publishing/. Here you can search for solutions on a range of topics, find answers to frequently asked questions, and learn more about Editorial Manager via interactive tutorials. You can also talk 24/7 to our customer support team by phone and 24/7 by live chat and email.

This journal uses the Elsevier Article Transfer Service. This means that if an editor feels your manuscript is more suitable for an alternative journal, then you might be asked to consider transferring the manuscript to such a journal. The recommendation might be provided by a Journal Editor, a dedicated Scientific Managing Editor, a tool assisted recommendation, or a combination. For more details see the journal guide for authors.

#AU_GEXPLO#

To ensure this email reaches the intended recipient, please do not delete the above code

ELSEVIER

RELX™

Geochemistry of granulite facies BIFs from the Luis Alves Craton (southern Brazil): implications for Archean-Paleoproterozoic depositional and tectonic settings

Leandro Menezes Betiollo[1,2*], Everton Marques Bongiolo[2]

[1]*Gerência de Geologia e Recursos Minerais, Serviço Geológico do Brasil (CPRM), Rua Banco da Província 105, 90840-030, Porto Alegre, Rio Grande do Sul, Brazil*

[2]*Instituto de Geociências, Universidade Federal do Rio Grande do Sul, Avenida Bento Gonçalves 9500, 91500-000, Porto Alegre, Rio Grande do Sul, Brazil*

**corresponding author: leandro.betiollo@sgb.gov.br*

Abstract

Banded Iron Formations (BIF) developed strongly during the Neoarchean – Paleoproterozoic Eras linked with global environmental processes such as the Great Oxidation Event (GOE) and changes in geodynamics, sea level, geobiology, hydrothermal systems, and sediment deposition conditions. BIF development and distribution worldwide is also related with supercontinent cycles, being a powerful tool to understand the evolution of plate tectonics. In this paper we used field-based geological-structural data, petrography, X-ray diffraction, and lithogeochemical analyses to perform the first characterization of Banded Iron Formations at the Luis Alves Craton (LAC), Southern Brazil. The LAC BIF are classified as oxide and silicate facies, both with granoblastic texture. Oxide facies consists of quartz and magnetite. Besides these minerals, silicate facies contains olivine and ferrosilite, evidencing high-grade granulite metamorphism. Based on major elements oxide facies has a hydrothermal signature, with low content of Al_2O_3 and TiO_2, whereas silicate facies register a continental sediment contribution been more enriched in these elements, beyond MgO, MnO and CaO. Trace-elements also exposed that main source for both silicate and oxide facies, which is seawater with major influence of low-T hydrothermal sources, besides continental sedimentation sources. The true negative Ce/Ce* anomaly, representing oxidizing waters, which also may represent a shallow water

column depth. The depositional environment is inferred as a shallow, restricted basin. Oxide facies represents sedimentation closer to hydrothermal vents and with weak influence from continental clastic sedimentation, while silicate facies represent sedimentation closer to an adjoining continental landmass. Oxide facies has more Algoma-like characteristics, such as higher Fe and Eu contents, Sm/Yb and Eu/Sm typical of higher hydrothermal fluid inputs, and low siliciclastic contibution. On the other hand, silicate facies resembles Superior-type BIF, with higher siliciclastic contribution, negative Ce/Ce* anomalies and Eu/Eu* < 1.8. In summary, we propose the LAC BIF are representative of a transitional environment from Algoma- to Superior-type. The first depositions of the LAC BIFs may have developed within an Algoma-like environment during the Neoarchean. The waning tectonic and volcanic activity during the Siderian shifted to a platformal environment, with shallower waters that may induce the deposition of carbonates typical of Superior-type deposits. The depositional basin may have close by the Rhyacian, when a Large Hot Orogen formed, and those sediments were then pushed down to the lower crust and underwent granulite facies metamorphism.

Keywords: BIF, granulite, geochemistry.

1. Introduction

Banded Iron Formations (BIF) is a type of rocks present on all continents that developed strongly in Neoarchean – Paleoproterozoic Era and are linked with environmental conditions intrinsic such as the Great Oxidation Event (GOE), linking geobiology, hydrothermal systems, sea level changes and sediment deposition, and particular tectonic setting for its full development (Trendall, 2002; Bekker et al., 2010; Konhauser et al., 2017). The combination of tectonic and environmental conditions creates basins with sedimentary and physical-chemical systems that reflect the main mineralogy and observed in different BIF facies (James, 1954). On a broader perspective, BIF development and distribution is also related with the supercontinent cycle, being an additional tool to understand the evolution of plate tectonics (Bekker et al., 2010).

James (1954) was the first to define four BIF facies based on its chemical precipitate mineralogy, namely oxide, silicate, carbonate and sulphide facies. However, the sulphide facies was originally considered as a pyritic carbonaceous shale

and not a chemical sediment, and thus it is no longer considered as a BIF facies (Bekker et al., 2010). All facies show quartz, and additionally magnetite and/or hematite (oxide facies), siderite and/or ankerite (carbonate facies), and cummingtonite, grunerite, garnet, pyroxene and fayalite (silicate facies) depending on the metamorphic grade (Klein, 2005; Bekker et al., 2010; Lan et al., 2019).

Gross (1980, 1983) was the first author to characterize and interpret depositional and tectonic environments for BIF genesis, including the distribution of different facies within those environments. The author also coined the widely known nomenclature of the main recognized BIF deposits: the Algoma- and Superior-types. Algoma-type deposits are usually Archean in age, distributed along small areas and thin, associated with volcanic rocks and graywackes in greenstone belts. Superior-type are Paleoproterozoic larger and thicker deposits, associated with continental shelves and interbedded with sandstones, carbonates and shales.

BIF are rocks that normally contain more than 15% of Fe, with micro- to macro-banding formed by intercalation of iron-bearing minerals (mostly magnetite and/or hematite) and quartz. Its original mineralogy in the time of deposition is inferred to be a Fe-silicate gels of greenalite-type composition, an initial Fe-oxyhydroxide, amorphous Fe-oxides, ferrihydrite [$Fe(OH)_3$] and hydromagnetite [$Fe_3(OH)_8$] (Klein, 2005; Bekker et al., 2010; Konhauser et al., 2017; Aftabi et al., 2021). These precipitated gels are then transformed by diagenesis and metamorphism into the minerals currently recognized in rocks, such as magnetite and hematite.

The main BIF deposits, such as Carajás in Brazil (Justo et al., 2020; Klein and Ladeira 2002; Tavares et al., 2018), Hamersley in West Australia (Haugaard et al., 2016; Trendall et al., 2004; Warchola et al., 2018), Transvaal in South Africa (Bau and Dulski 1996; Franchi and Mapeo 2019; Pickard, 2003; Smith and Beukes, 2016), and Quadrilátero Ferrífero in Brazil (Araújo and Lobato, 2019; Spier et al., 2007; Soares et al., 2017), underwent metamorphism of at most amphibolite facies. BIF occurrences that have underwent granulite metamorphism are rare and have only few exposures around the world, such as in West Greenland (Friend et al., 2008; Nutman et al., 2002; Papineau et al., 2010), Voronezh Crystaline Massif (Fonarev et al., 2006), Southern Granulite Terrain (Dutta et al., 2022; Reddy and Sashidhar, 1989; Yellappa et al., 2016), Dharwar Craton (Mukhopadhyay, 2020), Kaapvaal Craton (Horváth et al., 2014), North China Craton (Han et al., 2014; Lan et al., 2014; 2019; Li et al., 2019; Zheng et al., 2017), Yangtze Craton (Cen et al., 2012), Congo Craton (Ganno et al.,

2017; Moudioh et al., 2020; Teutsong et al., 2017), and now in the Luis Alves Craton in Southern Brazil, focus of the present contribution. With the original BIF sedimentary basins dismantled and deformed, mineralogy and texture change strongly. Thus, the recognition of BIF context within granulite terranes, with the exception of the banded oxide facies, can be extremelly difficult (Klein, 2005).

The Luis Alves Craton (LAC) (Kaul, 1979; 1980) is a small piece in the worldwide puzzle composed of *ca.* 35 exposed Archean-Paleoproterozoic crusts (Bleeker, 2003), being considered as an important nucleous of well-documented Siderian crustal growth period in South America (Brito Neves, 2011). Its main unit is the Santa Catarina Granulite Complex (Hartmann, 1979), which is composed by metamafic-ultramafic rocks, TTG gneisses, metagranites, quartzites and BIF, all metamorphosed in granulite facies though a complex structural arrangement and with presence of ferrosilite (exception to quartzite) marking high-grade metamorphism (Basei, 1998; Betiollo et al., 2018; Passarelli et al., 2018).

In the LAC, Fornari (1998) considered massive oxide facies BIF composed by 100% of magnetite (i.e., magnetitites) as formed in a magmatic context within a layered stratiform complex associated with ultramafic rocks. However, field relationships with the host rocks, as well as the discovery of silicate BIF facies close to these massive magnetite rocks led us to interpret them as of chemical-sedimentary origin. It is important to mention that according to previous studies (Angerer et al., 2013; Duuring et al., 2020; Egglseder et al., 2016; Morrisey et al., 2016; Stanton, 2006; Zheng et al., 2017), the formation of high-grade iron-ore deposits is correlated with hydrothermalism, deformation, metamorphism, and processes of segregation and mineral concentration. It worth noting that the only works developed in the LAC BIF were those of Barbosa (1940) and Fornari (1998). According to Barbosa (1940), there is an estimated reserve of 2 million tons of iron-ore in the LAC BIF exposures, however with high P contents, pointing to low quality ore and unsuitability for economic use and exporting.

The presence of granulite BIFs in the LAC gives us the scientific opportunity to understand the (i) ancient geologic basin of the craton, (ii) the tectonic setting before and during granulite metamorphism, and (iii) how it evolved. Using new field data, associated with petrography and the geochemistry of major, traces and REE+Y (REY) elements we unravel these characteristics of the LAC BIF. We also contribute to the

general understanding of the rare exposures of granulite facies BIF with orthopyroxene, garnet and olivine.

2. Regional Geology

The Luis Alves Craton (LAC, Kaul, 1979; 1980) is a small fragment of Archean-Paleoproterozoic crust in southern Brazil (Fig. 1). It is surrounded by geotectonic units assembled during the Neoproterozoic Brasiliano – Pan African orogeny for the formation of Western Gondwana (Basei et al., 1998; 2009; Heilbron, 2008; Brito Neves, 2011; Passarelli et al., 2018; Bruno et al., 2018). The LAC is surrounded by the Northern Dom Feliciano Belt, the Curitiba Microplate (part of the Southern Ribeira Belt) and the Paranaguá Block, and partially covered by the Paleozoic Paraná Basin in its western portion.

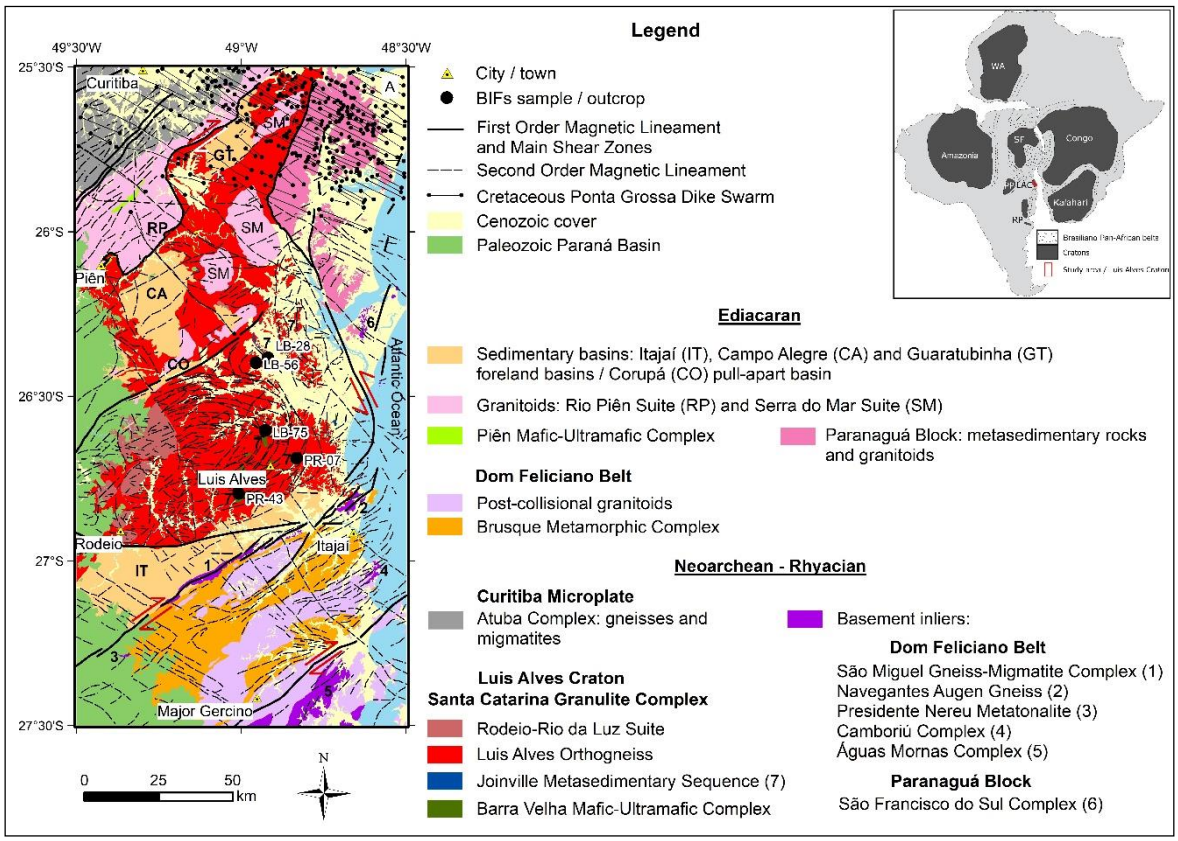

Figure 1. Simplified geological map of the study area and adjacent tectonic blocks (modified from Iglesias et al., 2011; Betiollo et al., 2018; Bruno et al., 2018; Passarelli et al., 2018). Box inset schematic map of the Western Gondwana showing the study area (modified from Heilbron et al., 2004; Passarelli et al., 2018; De Toni et al., 2020).

The Northern Dom Feliciano Belt is constituted by the Brusque Metamorphic Complex (Philipp et al., 2004; Campos et al., 2012), the Itajaí Basin (Guadagnin et al., 2010; Basei et al., 2011) and the Florianópolis Batholith (Bitencourt and Nardi, 2000; Florisbal et al., 2012). The southern LAC is in contact with volcano-sedimentary rocks of the Itajaí Basin, that partially cover a hidden geophysical contact (cf. Betiollo et al., submitted), and the low- to medium-grade metavolcano-sedimentary rocks of the Brusque Metamorphic Complex along the Itajaí-Perimbó shear zone (IPSZ). The contact with the Curitiba Microplate is represented by the Piên shear zone (PSZ). The Curitiba Microplate consists of gneisses and migmatites of the Atuba Complex, part of the Southern Ribeira Belt (Heilbron, 2008; Basei et al., 2009; Passarelli et al., 2011; 2018). To the east, the LAC make contact along the Rio Palmital shear zone (RPSZ) with metasedimentary rocks and granitoids of the Paranaguá Block (Cury, 2009).

2.1. Luis Alves Craton Geology

The LAC geotectonic block is composed (Fig. 1) by Archean-Paleoproterozoic units (Basei et al., 1998; 2009; Hartmann et al., 2000; Passarelli et al., 2018; Heller et al., 2021) of the Santa Catarina Granulite Complex (SCGC; Hartmann et al., 1979), Neoproterozoic sedimentary rocks of the Campo Alegre, Guaratubinha and Corupá basins (Basei et al., 1998; Citroni et al., 2001), and Neoproterozoic granitoids of the Serra do Mar Suite (Kaul, 1984; Gualda and Vlach, 2007).

The SCGC can be divided into four units: (1) Barra Velha Mafic-Ultramafic Complex, (2) Joinville Metasedimentary Sequence, (3) Luis Alves Orthogneiss, and (4) Rodeio-Rio da Luz Suite (Fig. 1).

The Barra Velha Mafic-Ultramafic Complex is composed of plagioclase-bearing pyroxenites and (leuco-) gabbronorites with massive, foliated or millimeter-thick gneissic banding structures. It is fine- to medium-grained, inequigranular with polygonal granoblastic texture, with subhedral to euhedral prismatic grains. It is composed by ortho- (enstatite and ferrosilite) and clinopyroxene (diopside), plagioclase, hornblende, biotite and rare hercinite. Accessory minerals are magnetite, apatite, pyrite, chalcopyrite, quartz and zircon. Actinolite, chlorite, epidote and garnet are retrometamorphic or hydrothermal minerals.

The Joinville Metasedimentary Sequence comprises quartzites, banded iron formations (BIF) and paragneisses. Rocks are medium-grained with polygonal granoblastic texture and foliated with millimeter- to centimeter-sized banding. Quartzites consist of quartz, few amounts of green mica and opaque minerals. Banded iron formations can be divided into oxide and silicate facies (see section 4). Paragneisses show compositional banding, with mafic bands composed of orthopyroxene, biotite, garnet, hercinite and cordierite, whereas felsic bands are quartz-feldspathic with sillimanite.

The Luis Alves Orthogneiss is medium-grained polygonal granoblastic, massive to foliated or banded. Banded rocks show mafic band composed by plagioclase, pyroxene, hornblende and biotite, locally with pyroxenite composition. Felsic bands have tonalite, granodiorite and quartz-diorite compositions with hornblende and biotite. Garnet may locally occur as accessory mineral.

Rodeio-Rio da Luz Suite are orthopyroxene-bearing metagranites predominant at the southwestern LAC area. Rocks show monzogranitic and syenogranitic compositions with euhedral to oval-shape alkali-feldspar phenocrysts, as well as hornblende and biotite. Acessorry allanite is characteristic of this unit.

3. Methods

3.1. Field geology and petrography

The identification and characterization of banded iron-formations (BIF) in the Luis Alves Craton (LAC) result from regional geological mapping at the 1:250,000 scale carried out by the Geological Survey of Brazil (Betiollo et al., 2018). Only five BIF outcrops (Fig. 1) were identified over a >5,000 km^2 area, from where eight samples were collected. Two additional samples were obtained from a drill core (location LB-56) provided by Geosistema Geologia e Sondagens Ltda (Curitiba – Brazil) that performed a mineral exploration program in the LAC. Thin sections were produced from all samples (n=10) in order to obtain textural relationships and mineralogy by optical petrography. Additional techniques such as X-ray diffraction (XRD) and Scanning Electron Microscopy (SEM) were also used for mineral identification and characterization (see below).

3.2. Geochemical analyzes

Ten banded iron-formation samples obtained from both surface expositions and drill core were reduced to <200-mesh grain size in an agate disc mill after crushing. Analyzes were performed at SGS GEOSOL Laboratories by lithium metaborate fusion and reading by ICP-AES for major elements and ICP-MS for REE, and multi-acid digestion and reading by ICP-MS for other trace elements. Detailed analytical procedures are available at https://www.sgsgeosol.com.br/.

In the analytical results of REE, the Y was added according to the methodology of Bau and Dulski (1996), configuring a REY pattern (REE+Y) with the Y inserted between the Dy and the Ho in accordance with the ionic radius. The REY data were normalized to PAAS (Post-Archean Australian Shale; Taylor and Mclennan, 1985) and the anomalies of Ce*, Eu* and others, also normalized to PAAS and identified by "sn" (shale-normalized), calculated according to Bau and Dulski (1996) and Bolhar et al. (2004).

3.3. X-ray diffraction (XRD)

The XRD analyzes were carried out using an X'PERT PRO MPD X-ray Diffractometer (PW 3040/60) from PANalytical at the Geological Survey of Brazil in the city of Manaus. The equipment has a PW3050/60 goniometer (Theta/Theta) and a Cu anode and ceramic X-ray tube (Kα1 1.5406 Å) model PW3373/00, long fine focus, 2200 W and 60 kv, using a RTMS type, Pixcel/1D detector. Data acquisition was performed with the X'Pert Data Collector software, version 2.1a, and the data processing was performed with the X'Pert HighScore software, version 3.0d, also from PANalytical. The following analysis conditions were used: Voltage (kV): 40; Current (mA): 40; Scan range (° 2θ): 5-70; Step size (° 2θ): 0.02; Scan mode: Continuous; Counting time (s): 50; Divergence slit: Slit Fixed 1/2°; Mask Fixed 10 mm; Anti-scatter slit Name: 5.7 mm. The identification of minerals was made by comparing the diffraction diagram obtained with patterns (sheets) from the ICDD-PDF (International Center for Diffraction Data – Powder Diffraction File) database.

4. Luis Alves Craton banded iron-formations

4.1 Geology

Banded iron-formation outcrops (Fig. 2A and 2B) are scarce, occurring as disperse, up to 2m blocks (location LB-75), and along small inactive quarries (locations PR-07 and PR-43; Fig. 2A). Location LB-28 is the only site with good exposition (Fig. 2B) which allows structural measures (Fig. 2C). In general BIF show medium- to intense chemical weathering, characteristic for the subtropical climate of southern Brazil. Thus, up to 40m-thick soil profiles are found in the study area, locally precluding the observation of rock unit extensions, their field relations, and structural parameters. Two drill core samples are the soundest rocks (Fig. 2D and 2E) to perform further analyses.

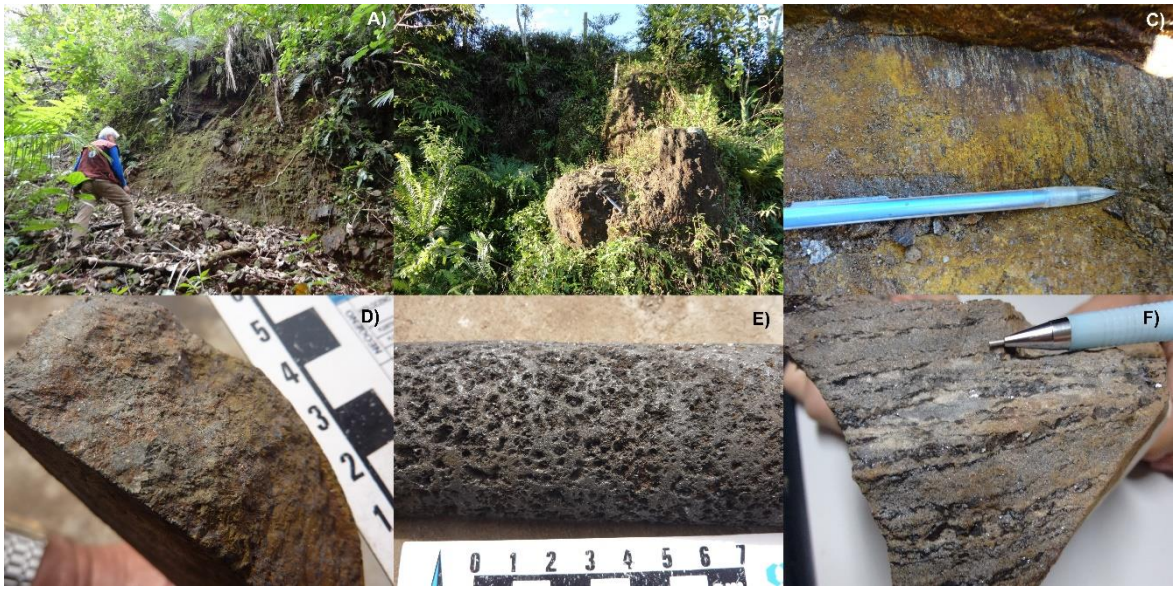

Figure 2. Outcrops and macroscopic texture of LAC BIF. A) small ancient quarry (PR07A); B) and C) location LB-28 with an *in situ* outcrop where structural data was collected. D) drill core sample (LB-56D) of silicate facies BIF with a massive structure and no alteration. E) LB-56C, drill core sample of oxide facies BIF with cavities indicating weathering. F) LB-56A with bands of quartz and magnetite.

The LAC banded iron-formations vary from gray, reddish, light yellow or orange in color (Fig. 2C and 2F), that only locally show millimeter-sized banding and foliation (Fig. 2C). The banding consists of an intercalation of magnetite and quartz layers interpreted as the original bedding (S_0) which is parallel to the main tectonic foliation (S_1). Foliation dips are medium angle (41° to 65°) with random dip directions ranging E to S and SSW, indicating a regional folding.

4.2. Petrography

The LAC BIFs can be classified (Table 1) according James (1954) into oxide facies (samples LB-28A, LB-28B, LB-56B and LB-56C) and silicate facies (samples LB-56D, LB-75A, PR-07A, PR-07B, PR-43A and PR-43B). There is a predominance of medium- to very fine-grained rocks in all BIF facies, with polygonal granoblastic texture, some with subhedral magnetite and pyroxene crystals. Oxide facies has both well-developed banding (Fig. 3A and 3B) and massive structure, while silicate facies have an incipient to massive structure.

Table 1: facies and petrography classification, and geochemical compositions of LAC BIFs.

Sample		LB 28A	LB 28B	LB 56B	LB 56C	LB 56D	LB 75A	PR 07A	PR 07B	PR 43A	PR 43B
BIF facies		Oxide facies				Silicate facies					
Petrographic classification		Magnetite - Quartz BIF	Magnetite - Quartz BIF	Magnetite BIF	pyrrhotite-magnetite BIF	pyrrhotite-olivine-magnetite BIF	ferrosilite-quartz BIF	ferrosilite-spessartine BIF	Magnetite -Quartz BIF bearing opx	Ankerite-Magnetite - Ferrosilite Quartz BIF	Almandine - Magnetite-Ferrosilite Quartz BIF
SiO_2	%	37,18	48,48	0,55	2,87	28,18	59,13	44,15	66,47	35,55	54,76
TiO_2	%	0,05	0,02	0,03	0,05	0,22	1,20	0,11	0,09	0,05	0,03
Al_2O_3	%	0,28	0,08	0,78	1,27	1,27	0,73	4,98	0,51	2,70	3,51
$Fe_2O_3^T$	%	58,13	46,48	95,50	92,40	56,49	21,41	28,30	28,38	49,26	31,84
MnO	%	0,02	0,02	2,06	0,85	2,22	0,65	10,00	0,08	5,99	4,71
MgO	%	0,02	0,10	1,05	2,31	8,03	12,59	8,66	0,10	3,50	1,89
CaO	%	<0,01	0,02	<0,01	0,04	0,20	0,47	2,81	0,08	0,57	0,52
Na_2O	%	<0,01	<0,01	<0,01	<0,01	<0,01	0,02	0,04	<0,01	0,01	<0,01
K_2O	%	<0,01	<0,01	0,02	<0,01	<0,01	<0,01	0,01	<0,01	<0,01	<0,01
P_2O_5	%	<0,01	<0,01	<0,01	<0,01	0,09	<0,01	0,05	0,03	0,06	<0,01
Ba	ppm	12,00	10,00	215,00	11,00	9,00	6,00	29,00	19,00	7,00	8,00
Co	ppm	14,10	2,70	7,90	15,60	44,10	102,80	12,40	6,10	7,20	3,40
Cu	ppm	41,70	4,90	95,90	8,10	515,50	799,50	5,30	2,60	53,70	4,10
Hf	ppm	0,08	0,19	0,26	1,09	0,70	69,25	0,75	0,16	0,44	0,48
Mo	ppm	0,59	1,50	35,38	214,38	402,18	1,76	7,93	0,99	5,47	3,88
Nb	ppm	0,90	1,10	0,60	15,10	8,80	9,70	0,60	1,80	2,80	2,40
Ni	ppm	22,00	<0.5	<0.5	<0.5	56,00	106,40	8,00	4,40	<0.5	<0.5
Rb	ppm	0,40	1,30	2,00	1,10	1,50	0,50	3,20	1,40	0,90	0,50
S	%	<0.01	<0.01	0,03	0,37	3,03	1,16	<0.01	<0.01	<0.01	<0.01
Sc	ppm	2,80	<0.5	6,20	27,70	15,10	44,50	20,20	1,80	4,70	2,70
Ta	ppm	0,19	0,24	0,10	9,89	1,28	0,45	0,10	0,07	0,40	0,57
Th	ppm	0,20	0,90	0,10	1,60	1,10	15,60	2,80	1,10	3,60	5,60
U	ppm	0,20	0,10	0,80	1,10	1,20	11,50	0,90	0,30	0,80	4,50
V	ppm	111,00	27,00	12,00	23,00	30,00	56,00	28,00	18,00	12,00	5,00
Zr	ppm	18,00	14,40	30,60	43,90	35,00	2032,30	31,70	12,60	26,50	20,60
La	ppm	1,90	0,05	0,05	0,40	3,50	12,50	4,90	5,40	11,60	6,00
Ce	ppm	2,97	0,03	15,55	0,65	5,85	19,28	9,92	8,86	18,70	9,53
Pr	ppm	1,15	0,40	0,60	0,15	0,78	2,29	1,22	1,28	2,37	1,28
Nd	ppm	4,50	1,70	2,00	0,50	3,00	7,40	5,80	4,80	8,30	4,40
Sm	ppm	1,10	0,40	0,40	0,05	0,60	1,10	2,70	0,90	1,70	1,20
Eu	ppm	0,38	0,22	0,11	0,03	0,08	0,05	0,66	0,23	0,27	0,15
Gd	ppm	1,17	0,49	0,40	0,10	0,64	1,10	5,03	0,74	2,06	1,63
Tb	ppm	0,30	0,12	0,12	0,03	0,09	0,16	1,13	0,13	0,42	0,35
Dy	ppm	1,31	0,47	0,59	0,11	0,51	1,27	7,47	0,62	3,03	2,42
Y	ppm	7,00	4,00	3,30	0,40	5,20	10,70	61,60	4,20	30,40	22,80
Ho	ppm	0,27	0,11	0,13	0,03	0,11	0,38	1,64	0,11	0,74	0,48
Er	ppm	0,85	0,31	0,50	0,07	0,40	1,74	5,09	0,34	2,69	1,34
Tm	ppm	0,13	0,05	0,08	0,03	0,07	0,38	0,74	0,03	0,47	0,19
Yb	ppm	1,10	0,30	1,00	0,05	0,80	3,70	5,70	0,30	3,80	1,20
Lu	ppm	0,16	0,06	0,16	0,02	0,17	0,80	0,87	0,05	0,62	0,15
∑REE	ppm	17,29	4,71	21,69	2,20	16,60	52,15	52,87	23,79	56,77	30,32
∑REEY	ppm	24,29	8,71	24,99	2,60	21,80	62,85	114,47	27,99	87,17	53,12
Y/Ho		25,93	36,36	25,38	16,00	47,27	28,16	37,56	38,18	41,08	47,50
Fe/Ti		1356,33	2711,27	3713,80	2155,95	299,56	20,81	300,14	367,88	1149,37	1238,19
Al/Al+Mn+Fe		0,00	0,00	0,01	0,01	0,02	0,02	0,09	0,01	0,04	0,07
Eu/Sm		0,35	0,55	0,28	0,50	0,13	0,05	0,24	0,26	0,16	1,00
Sm/Yb		1,00	1,33	0,40	1,00	0,75	0,30	0,47	3,00	0,45	0,47

Co/Zn	0,07	0,02	0,07	0,09	0,23	0,52	0,06	0,23	0,03	0,02
Th/U	1,00	9,00	0,13	1,45	0,92	1,36	3,11	3,67	4,50	1,24
La/Th	9,50	0,06	0,50	0,25	3,18	0,80	1,75	4,91	3,22	1,07
k/Rb	0,01	0,00	0,01	0,02	0,00	0,01	0,01	0,00	0,02	0,01
Eu/Eu*	1,35	2,04	1,02	1,38	0,67	0,23	0,75	1,30	0,65	0,47
Ce/Ce*	0,41	0,01	5,64	0,59	0,82	0,83	0,94	0,78	0,82	0,79
Pr/Pr*	1,53	1,80	0,53	1,48	1,09	1,13	0,93	1,15	1,12	1,16
Pr/Yb*	0,33	0,43	0,19	0,96	0,31	0,20	0,07	1,36	0,20	0,34
Y/Y*	0,94	1,40	0,95	0,61	1,75	1,21	1,40	1,28	1,61	1,69
La/La*	0,40	0,04	0,02	0,49	1,04	0,96	1,77	0,93	0,96	0,90
Sm/Yb*	0,51	0,68	0,20	0,51	0,38	0,15	0,24	1,52	0,23	0,51

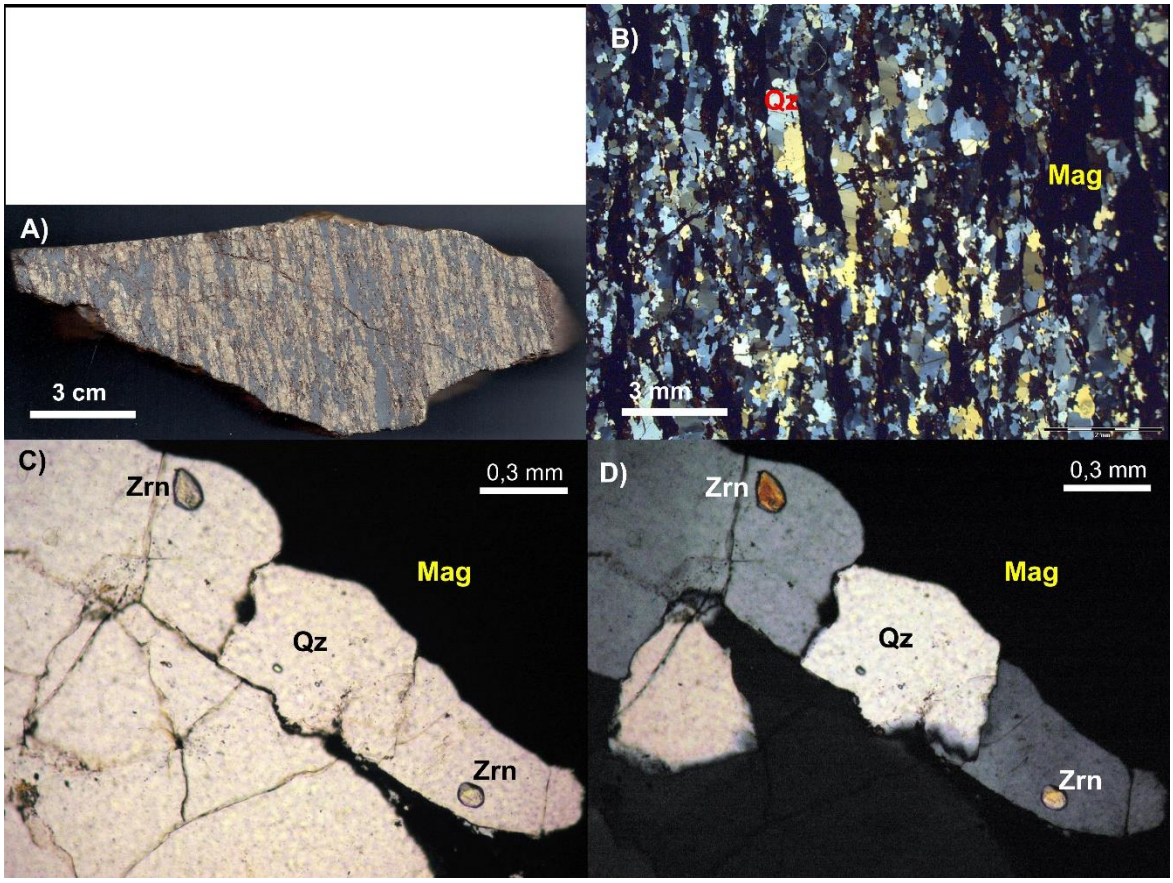

Figure 3. Oxide facies BIF, sample LB-28A, A) macroscopic aspect of magnetite – quartz BIF with well-marked foliation. B) XPL thin section photo showing foliation of quartz and magnetite intercalation and polygonal granoblastic texture with interlobed edges and recrystallized grains. C) same as B using PPL. D) XPL, LB-28A thin section photo of oxide facies BIF with rounded zircon (Zrn) grains.

Oxide facies (Table 1) is medium- to very fine-grained, with millimeter banding developed by the alternation of quartz and magnetite, which are their main mineralogical constituents, coupled with minor amounts of very fine-grained (up to 0,15 mm), rounded zircon crystals (Fig. 3C and 3D). Locally quartz is absent, and magnetite monomineralic rock (sample LB-56B; Fig. 2E) shows massive texture. All rocks have

polygonal granoblastic texture with interlobed edges and recrystallized grains (Fig. 3B, 3C and 3D).

Other than quartz and magnetite, silicate facies (Table 1) shows orthopyroxene, garnet and olivine (Fig. 4), besides ankerite and pyrrhotite, and Mo-sulfide (molybdenite?). The most common mineralogical feature of this facies is the presence of ferrosilite, with the exception of sample PR-07B. Likewise, quartz is a rock-forming mineral in silicate facies with the exception of sample PR-07A (Table 1), and magnetite is absent in samples LB-75A and PR-07A. Ferrosilite (Fig. 4A, 4B and 4C) grains are 2 mm in average, reaching up to 3 cm (location PR-07A, see below). Crystals are polygonal to subhedral, and locally show sigmoidal shape indicating deformation. Orthopyroxene are slightly saussuritized close to crosscutting quartz veins, associated with very fine-grained biotite along fracture planes. Opaque mineral exsolutions along cleavage form a fishbone texture. Quartz occurs as up to 1 mm interstitial grains, some recrystallized, with anhedral and polygonal shapes (Fig 4C). Magnetite (Fig. 4C and 4D) grow in rock interstices or is massive. Subhedral to anhedral crystals (up to 5 mm) form aggregates or bands, and in some cases surrounding and encompassing pyroxene and olivine. Garnet (Fig. 4A, 4B and 4C) is an uncommon mineral in BIF. Spessartine and almandine are observed in only two silicate facies samples. The almandine (Fig 4B) occurs in a BIF (PR-43B) composed by magnetite, quartz and ferrosilite, while spessartine (Fig. 4A and 4B) occurs in a rock (PR-07A) composed only by coarse-grained (up to 3 cm), ferrosilite, and spessartine (50% modal each). Olivine (Fig. 4D) is globular (up to 1 mm) with mesh texture and lamellae of alteration and deformation, as well as with altered edges; its alteration products are serpentine, talc and tremolite. Zircon is an accessory mineral, except in location LB-75A where it occurs in large amounts (0.5% of the rock). Crystals are subhedral (up to 0.1 mm) with internal zoning, and locally occur as inclusions in pyroxene crystals.

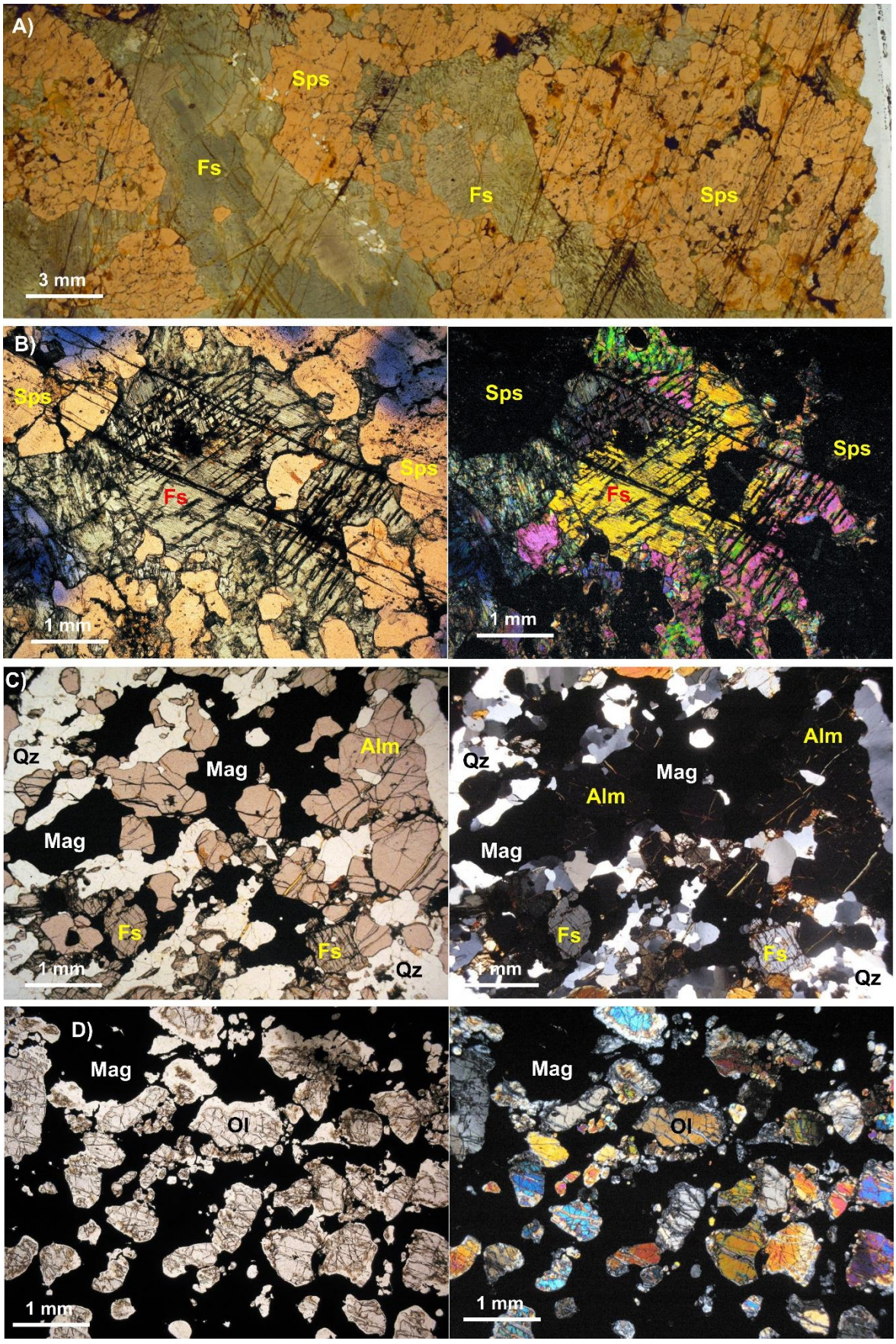

Figure 4. Silicate facies BIF. PR-07A, A) macroscopic aspect and B) thin section (PPL and XPL) of coarse-grained silicate facies BIF composed by ferrosilite (Fs) and

spessartine (Sps) garnet. C) PR-43B thin section (PPL and XPL) of silicate facies BIF with subhedral orthopyroxene ferrosilite (Px), almandine garnet (Grt) and quartz (Qtz) with anhedral and polygonal shapes. D) LB-56D thin section (PPL and XPL) of silicate facies BIF with olivine (Ol) surrounded by magnetite.

5. Geochemistry

The rocks investigated here are chemically classified as banded-iron formations (cf. James, 1954; Klein, 2005) due to either their Fe (15 to 66 wt.%) or $Fe_2O_3^T$ (21.41 to 95.5 wt.%) contents, with relatively lower and higher iron associated with silicate and oxide facies, respectively (Table 1). Particular geochemical characteristics of major, trace and REE elements are described below for each BIF facies identified in the LAC.

5.1. Oxide facies

Four samples (LB-28A, LB-28B, LB-56B and LB-56C) have high $Fe_2O_3^T$ values (46 to 95 wt.%), followed by SiO_2 (0.55 to 48 wt.%), both elements representing 94 to 96% of the oxide facies composition. Major elements concentration ranges are (Fig. 5A): Al_2O_3 (0.08-1.27 wt.%), MgO (0.02-2.31 wt.%), MnO (0.02-2.06 wt.%), and TiO_2 (0.02-0.05 wt.%). Cr_2O_3, CaO, Na_2O, K_2O and P_2O_5 have most values below or close to the detection limit (< 0.01 wt.%; Table 1).

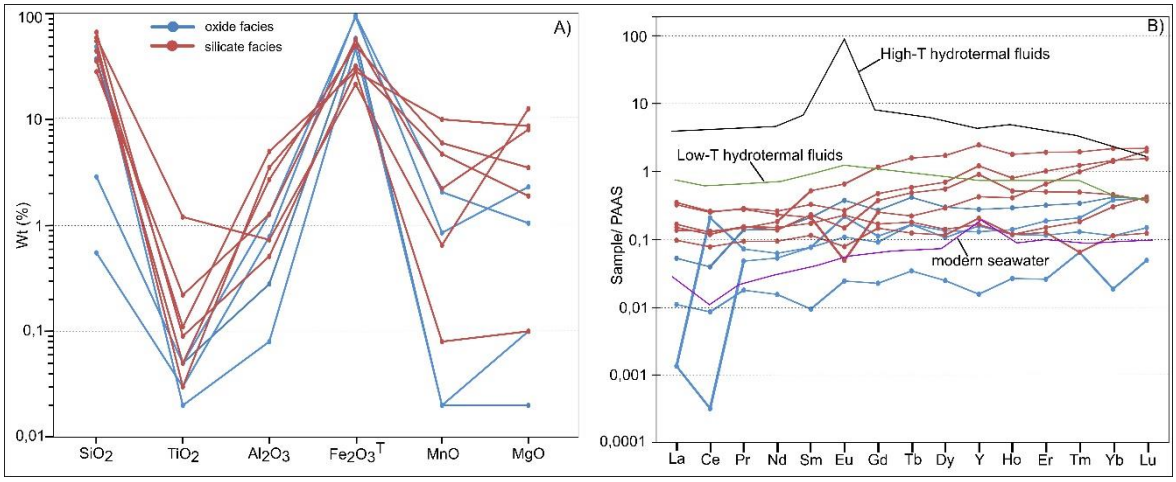

Figure 5. Chemical elements distribution in LAC BIF. A) major elements. B) PAAS-normalized REY including curves corresponding to high-T hydrothermal fluids, low-T hydrothermal fluids, and modern seawater.

Among trace elements have positive anomalous values in some samples (Table 1), and the presence of Ba (215 ppm), Cu (95 ppm), Mo (214 ppm), Nb (15 ppm), Sc (27 ppm), Ta (9 ppm) and V (111 ppm) is highlighted. Low amounts of S (0.37 wt. %) reflect the occurrence of pyrrhotite.

REY elements are depleted in comparison with normalized PAAS (Fig. 5B), with ∑REY between 2.6 and 24.9 ppm. Samples are enriched in HREE in comparison with LREE (Pr/Yb* = 0.19-0.95) and MREE (Sm/Yb* = 0.20-0.67). Based on the geochemical patterns on spidergrams, oxide facies shows slightly positive La, Eu and Tb anomalies. Sample LB-56B has very strong positive Ce anomaly, whereas the remaining elements show slight to strong negative anomalies. The Y shows slightly negative anomalies in most samples, except sample LB-56C where it is slightly positive. In general, the signature of oxide facies is flat-parallel, showing a mixing pattern between seawater and low-T hidrotermal fluids influence (Fig. 5B).

Calculated PAAS-normalized REE anomalies are (Table 1): (i) negative La/La* (0.01-0.48); (ii) positive Eu/Eu* (1.02-2.04); (iii) negative Ce/Ce* (0.01-0.59, except for sample LB-56B); and (iv) slightly negative to positive Y/Y* (0.60-1.40). The Y/Ho vary from subchondritic to superchondritic, showing values between 16 and 36 (Table 1). The true anomalies of Ce in the diagram Pr/Pr* vs. Ce/Ce* (Fig. 6) plot in the field of true negative Ce anomaly, except for the sample LB-56B that has a strong positive Ce/Ce* anomaly of 5.64.

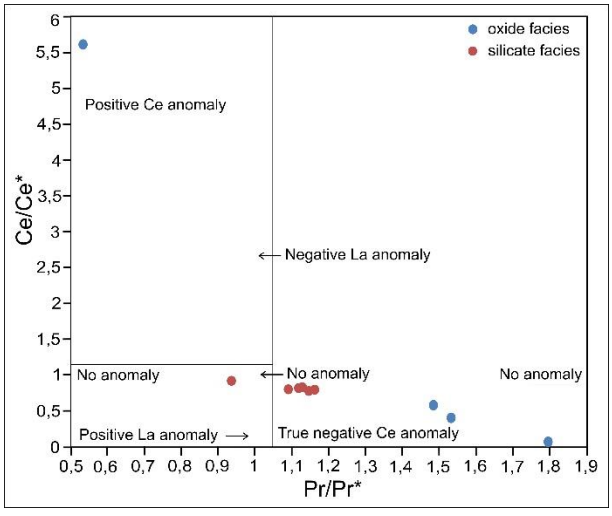

Figure 6. Pr/Pr* x Ce/Ce* diagram used to identify true negative Ce anomaly.

5.2. Silicate Facies

Silcate facies (n=6, Table 1) shows $Fe_2O_3^T$ values from 21 to 56 wt.%, followed by SiO_2 between 28 and 66 wt.%. These two major elements represent 72 to 94 wt.% of the total geochemical composition of samples.

As for the oxide facies, the major elements concentration is highly variable (Fig. 5A), as follows: Al_2O_3 (0.73-4.98 wt.%), MgO (0.1-12.59 wt.%), MnO (0.08-10 wt.%), TiO_2 (0.03-1.2 wt.%), and CaO (0.08-2.81 wt.%). The remaining elements contents are below the detection limit (< 0.01%) or slightly above (Table 1), such as P_2O_5 (0.03-0.09 wt.%) and Na_2O (0.01-0.04 wt.%).

Silicate facies has more significant positive trace elements values (Table 1) than oxide facies, such as prominent Co (102 ppm), Cu (799 ppm), Hf (69 ppm), Mo (402 ppm), Nb (9.7 ppm), Ni (106 ppm), S (3%), Sc (44 ppm), Th (15 ppm), V (56 ppm) and Zr (2032 ppm). The highly anomalous Zr value of sample LB-75A is allowed by the extremely high zircon contents, a very uncommon feature to BIFs.

REY elements of silicate facies normalized to PAAS are slightly depleted (Fig. 5B), except for sample PR-07A which is slightly enriched in both MREE (Sm/Yb* = 0.24) and HREE (Pr/Yb* = 0.06), whereas samples PR-43A (Pr/Yb* = 0.19) and LB-75A (Pr/Yb* = 0.19) are enriched in HREE. The ∑REY is a little higher than for the oxide facies, ranging between 21.8-114.47 ppm. The geochemical patterns on the spidergram (Fig. 5B), silicate facies shows slight positive La and Y anomalies, Ce shows slight negative anomaly, and Eu shows slight to strong negative anomalies in four samples (LB-56D, LB-75A, PR-43A and PR-43B), whilst samples PR-07A and PR-07B show slight positive Eu. The general signature pattern of silicate facies is parallel and flat, with a slight enrichment in HREE in some samples, and as observed for the oxide facies, indicating a mixing pattern between seawater and low-T hydrothermal fluid influence. The strong negative Eu anomaly in two samples (LB-75A and PR-43B) may indicate its mobility during metamorphism (Lan et al., 2019).

The calculate anomalies (Table 1) normalized to PAAS are: (i) slightly negative to positive La/La* (0.89-1.77); (ii) negative to slightly positive Eu/Eu* (0.22-1.29); (iii) slightly negative Ce/Ce* (0.77-0.93); and (iv) positive Y/Y* (1.2-1.75). The Y/Ho vary from chondritic to superchondritic, showing values between 28 and 47. The true anomalies of Ce in the diagram Pr/Pr* vs. Ce/Ce* (Fig. 6), plot in the field of true negative anomaly, except for sample LB-07A that has neither Ce nor La anomalies.

6. Discussion

6.1. Metamorphic or post-depositional hydrothermal fluids effects

The studied BIF underwent granulite facies metamorphism, as evidenced by its high-temperature mineral assemblage, such as ferrosilite and olivine (Fig. 4). Thus it is expected changes in original rock geochemistry, mostly for major and trace elements driven by partial melting processes (Morrisey et al., 2016). However, field and petrographic features like veins, migmatitic structures or secondary minerals that clearly point for those high-temperature processes were not observed. Low-temperature secondary mineralogy is only observed along fracture planes.

The K/Rb, Th/U and La/Th are parameters that estimate the influence of high-grade metamorphism based on the mobility of such elements (Rudnick et al., 1985; Fernandes et al., 1987; Bauernhofer et al., 2009; Ganno et al., 2017; Lan et al., 2019). Figure 7A shows that the LAC BIFs are both K- and Rb-poor, plotting outside the compositional fields proposed by Rudnick et al. (1985). Samples plotting to the left of the main trend (MT) represent depletion in Rb, especially along the granulite trend (GT) field. If we graphically continued the fields, the LAC BIF samples would still plot to the right of the MT, symbolizing that there was no Rb-loss. In Figure 7B most of the samples plot in the field where there is no loss of U or Th, except for sample LB-28B (oxide facies) that shows Th/U = 9.

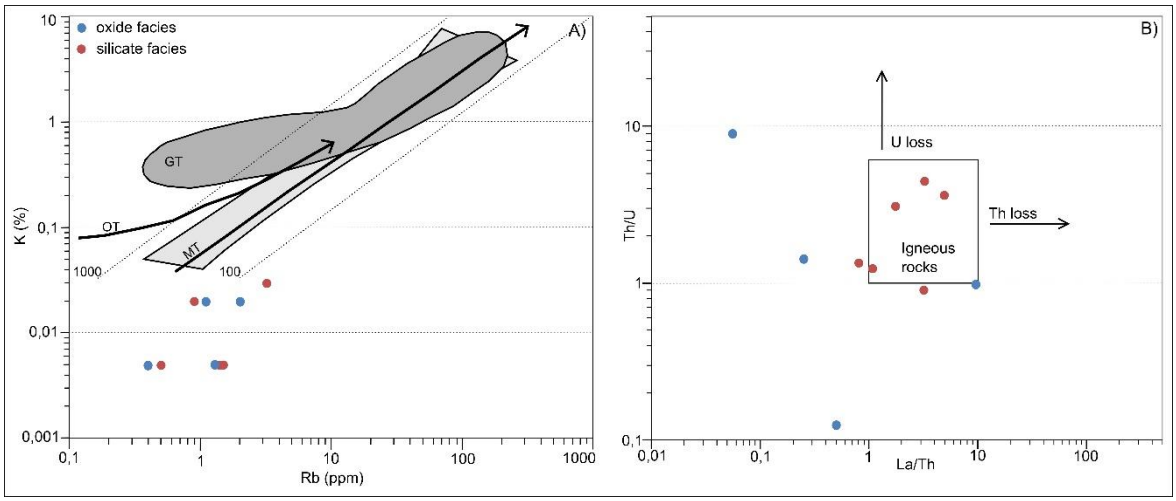

Figure 7. Diagrams used to identify the influence of metamorphism on the studied BIF samples. A) Rb x K to identify the influence of metamorphism in the loss of Rb. GT:

granulite trend; OT: orogenic trend; MT: main trend. B) La/Th x Th/U to identify Th and U loss by metamorphism.

The signature pattern of REY elements normalized to PAAS (Fig. 5B) denotes at least a slight influence of high-grade metamorphism that enable elemental mobility. Ce anomalies observed in two oxide facies samples, one strong positive (sample LB-56B) and another strong negative (sample LB-28B), deviating from the general pattern, are indicative of post-depositional alteration. Eu negative anomalies in silicate facies are also an indicative of post-depositional mobility (cf. Lan et al., 2019), since the standard curves of low-T and high-T hydrothermal fluids influence show moderate to strong Eu positive anomaly, respectively, which is not typically observed under influence of seawater (Fig. 5B).

Considering all the geochemical evidence, we interpret that granulite facies metamorphism did not modified considerably the original geochemical patterns of BIF. Indeed, we interpret that geochemical signature patterns observed on spidergrams rather demonstrate variations in the main BIF endmember sources, which are hydrothermal and seawater fluids (see below).

6.2. Sources of BIF and its detrital inputs

BIFs are recognized as chemical sediments formed in the marine environment under variable influence of hydrothermal vents and continental debris inputs, depending on the distance between their forming basin and the continent (Planavsky et al., 2010). Geochemical data is the better way to identify and to characterize those sources and influences (Boström, 1970; Bau and Dulski, 1996; Bolhar et al., 2004; Alexander et al., 2008), as well as paleoredox conditions of seawater, which may fluctuate in response to different water depths (Planavsky et al., 2010).

The Al_2O_3 x SiO_2 (Wounder et al., 1988) individualize different source fields (Fig. 8A). Higher Al_2O_3 contents coincides with increasing influence of continental debris, as well as larger amounts of oceanic, hemipelagic clay minerals that contain low SiO_2 in comparison with hydrothermal vents. The LAC BIFs mostly plot in the field of hydrothermal vents, except for two oxide facies samples (LB-56B and LB-56C)

associated with deep-sea sediments influence, and one silicate facies (PR-07A) that shows continental clastic influence.

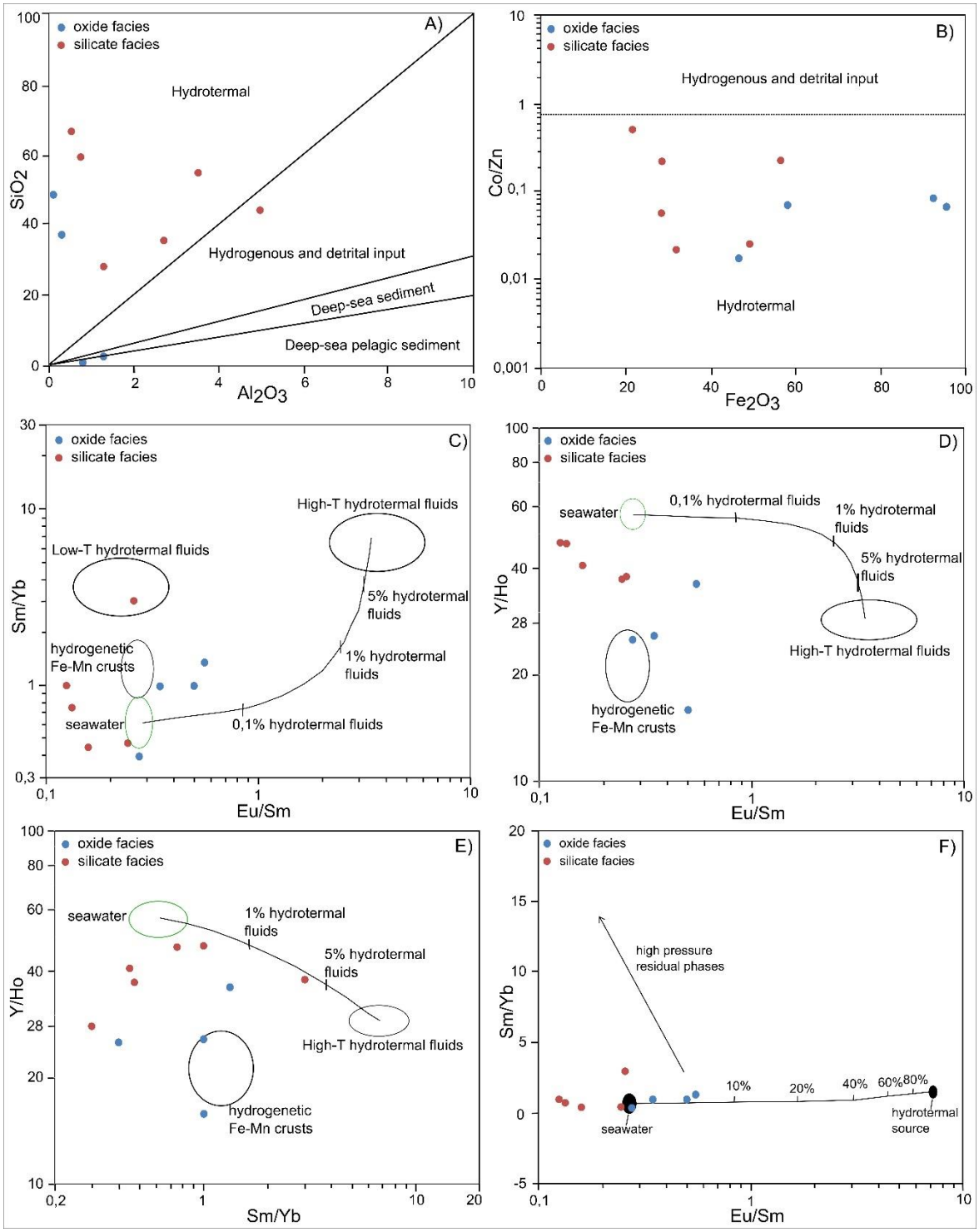

Figure 8. Diagrams to show the sources of LAC BIFs. A) Al_2O_3 x SiO_2 illustrates the origin of primary chemical precipitates (after Wonder et al., 1988). B) Fe_2O_3 x Co/Zn discrimination diagram separating exhalative hydrothermal from the hydrogenous-detrital input field to LAC BIFs (Toth, 1980). C) to E) Elemental ratio diagrams showing a conservative mixing line between high-temperature hydrothermal fluids and seawater

(Alexander et al., 2008). F) Eu/Sm x Sm/Yb plot used to assess the potential influence of high-T hydrothermal fluids on the BIF chemistry (Gourcerol et al., 2016).

The $Fe_2O_3^T$ x Co/Zn diagram (Toth, 1980; Fig. 8B) shows the total iron amounts but also demonstrates the hydrothermal influence of zinc or of continental-sourced cobalt. All BIF samples plot in the hydrothermal field, demonstrating poor influence of continental input.

We used a set of three elemental ratio diagrams with calculated conservative mixing line between seawater and hydrothermal fluids (Alexander et al., 2008) to correlate HREE depletion (Sm/Yb), Eu enrichment (Eu/Sm), and influence of continental sources (Y/Ho). Using the Eu/Sm vs. Sm/Yb diagram (Fig. 8C) oxide facies samples show the highest Eu amounts, approaching 0.1% contribution of hydrothermal fluids, close to the compositional field of seawater and hydrogenetic Fe-Mn crusts influence. The silicate facies samples demonstrate composition close to the seawater and hydrogenetic Fe-Mn crusts, without contribution of hydrothermal fluids, including one sample with high HREE depletion (PR-07B) plotting in the low-T hydrothermal field. In the Eu/Sm vs. Y/Ho diagram (Fig. 8D) samples from different facies plot in different fields. Again, the oxide facies samples approach the hydrothermal contribution field and the hydrogenetic Fe-Mn crusts. The lowest Y/Ho indices, controversially indicate slightly higher continental contribution, what is expected from the silicate facies. Silicate facies samples approximate the composition of seawater and demonstrate a positive trend with respect to Eu enrichment and Ho, representing low influence of hydrothermal fluids. The Sm/Yb vs. Y/Ho diagram (Fig. 8E) correlates the depletion in HREE with the continental contribution. The oxide facies samples again demonstrate higher contribution from hydrothermal vents (close to 1%) and plot close to the hydrogenetic Fe-Mn crusts. The silicate facies samples have the lowest hydrothermal contributions and plot close to seawater composition, with the exception of sample (PR-07B) with up to 5% hydrothermal contribution, corroborating its Sm/Yb vs. Eu/Sm signature (Fig. 8C). A similar plot proposed by Gourcerol et al. (2016) also correlates Eu enrichment with HREE depletion, demonstrating that both silicate and oxide facies plot in distinct fields (Fig. 8F). Using this diagram all samples plot close to seawater composition, but with oxide facies showing higher hydrothermal contribution close to 3%.

Boström (1970) proposed a binary mixing curve to identify the terrigenous contribution in BIFs based on the direct correlation of Ti and Al enrichments with continental sediments contribution (Fig. 9A). Using these parameters, the LAC BIFs plot very close to the hydrothermal field, especially the oxide facies. Silicate facies samples show the higher contribution of continental sediments (up to 20%). The influence of continental debris on LAC BIFs is also evidenced by the strong positive correlation between Al_2O_3 and the sum of Y+Nb+Zr in both facies (Fig. 9B). Sample LB-75A with anomalous Zr content (2000 ppm) was excluded from this plot for statistical purposes. The very low concentrations of K and Rb (Table 1; Fig. 7A) suggests that continental sediment sources may not be felsic or granitic in nature, having probably more basic compositions such as those from island arc environments.

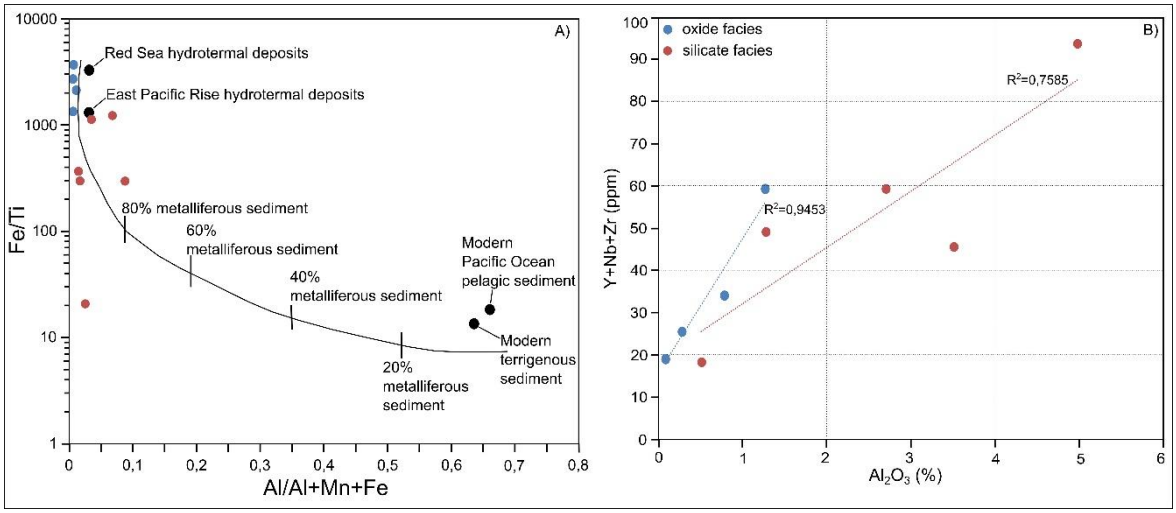

Figure 9. Diagrams to show the detrital influence in LAC BIFs. A) Al/(Al + Fe + Mn) x Fe/Ti plot to assess the detrital contamination in LAC BIF samples (Boström, 1970). B) Al_2O_3 x Y+Nb+Zr (detrital trace elements) to show correlation of continental sediment contribution (Ganno et al., 2017).

In order to identify negative Ce anomalies correlated with seawater paleoredox conditions, and taking aside the La influence, Bau and Dulski (1996) proposed the Pr/Pr* x Ce/Ce* diagram. LAC BIF samples plot predominantly in the field of true negative Ce anomaly, except for one silicate facies (PR-07A) that has no anomaly and an oxide facies (LB-56B) sample that has a strong positive Ce anomaly (Fig. 6). This

indicates that most samples were under oxidizing conditions of seawater (similar to current seawater) at the time of their deposition.

6.3. Depositional settings

The seawater-hydrothermal system contribution to the formation of BIF is unquestionable in the scientific community, as reviewed by Aftabi et al. (2019). To assemble the depositional environment of the LAC BIF, several factors have to be taken into account, starting with field relations, petrographic features, and geochemical REY evidences.

Silicate facies composed of ferrosilite, spessartine, almandine and olivine in the LAC BIF are strong indications of continental sediments contribution for their formation. This contribution is also evidenced by Al_2O_3, TiO_2 and MgO enrichment in those samples. Their high MnO contents, which even led to spessartine crystallization, are correlated with hydrothermal vents, as well as $Fe_2O_3^T$ and SiO_2. The field association of these BIF with paragneisses (i.e., rich in aluminosilicates) is also an evidence that points to an environment of formation not far from the continent. Additional clue to identify the depositional environment is the occurrence of ankerite (sample PR-43A), indicating shallow basins close to the continental shelf.

The geochemical data exposed in previous sections show that the main source for both silicate and oxide facies BIF formation is seawater (Fig 5B), with major influence of low-T hydrothermal sources (Fig. 8), followed by less important contribution of continental sedimentation (Fig. 9A). La and Eu anomalies vary between silicate and oxide facies, the more negative the La/La* and more positive the Eu/Eu* anomalies, the greater the influence of hydrothermal fluids. The predominant Ce anomaly is the true negative Ce/Ce* anomaly, representing oxidizing waters, which also may represent a shallow water column depth (Fig 6). However, in the spidergram of REY normalized to PAAS (Fig. 5B), positive anomalies of Ce and Eu present in the oxide facies may also be correlated with water depth, where deep portions characteristically present these geochemical anomalies (Planavsky et al., 2010).

Taking into account the geochemical characteristics show above of each facies, we suggest that different facies were deposited (i) in different portions of the same basin, or (ii) at different evolutionary times of the basin. In this sense, the oxide facies

may represent sedimentation closer to hydrothermal vents and with weak influence from continental clastic sedimentation, while silicate facies would represent a contrasting zone closer to the continent with weak hydrothermal contribution. The negative Ce/Ce* anomaly points to oxidizing, shallow basin environments for both facies. In summary, the depositional environment of the LAC BIF is inferred as a shallow, restricted basin, able to be influenced by both hydrothermal vents and continental sediments.

6.4. Tectonic settings and evolution

There are many variables that can be sued to individualize Algoma, Superior, Rapitan and Ediacaran BIF types. Among them we can quote age, the different degrees of continental sediments contribution, proximity to hydrothermal vents, basin architecture, and depth for chemical and clastic sediments deposition, among others. Taking as a reference the survey carried out by Aftabi et al. (2021), in which the authors geochemically compare worldwide BIF types, we looked for similarities to classify the LAC BIF samples.

Starting with the LAC sediments deposition referred to be Neoarchean to Siderian in age, followed by Rhyacian granulite metamorphism, our samples are restricted to two types of BIF, namely Algoma- and Superior-type. The $Fe_2O_3^T$ and SiO_2 concentrations of LAC BIFs are very similar to Algoma-type, where $Fe_2O_3^T$ concentrations are higher than 20% and can reach almost 100%. In the case of the study area, it must be considered that the granulite metamorphism may have influenced the high-grade ore concentrations, as observed in other areas worldwide (Morrisey et al., 2016). With the exception of two samples of the oxide facies that have more than 90% of $Fe_2O_3^T$, the other samples have between 20-60 wt.% of $Fe_2O_3^T$ and 30-65 wt.% of SiO_2, resembling concentrations of the Superior-type.

The relation between SiO_2 and Al_2O_3 in the LAC BIF (Fig. 8A) is also more similar to Algoma-type (which can have both low SiO_2 and Al_2O_3 concentrations) especially when taking into account the oxide facies. The samples of silicate facies have higher Al_2O_3 (up to 4 wt.%), being slightly similar to Superior-type deposits, but even more similar to the Rapitan- and Ediacaran-types, which commonly have higher Al_2O_3 contents, but the latter two deposit types were discarded due to their age.

Therefore, these anomalous Al_2O_3 concentrations for our Archean-Paleoproterozoic BIF may be correlated with geochemical changes driven by granulite metamorphism.

In the $Fe_2O_3^T$ vs. Co/Zn (Fig. 8B) the behavior of the LAC BIF samples is very similar to the Algoma-type, where all Co/Zn ratios are <1. In the Al_2O_3 vs. Eu/Eu* relation, our samples do not fit very well neither with the Algoma- nor Superior-types, showing several negative Eu/Eu* anomalies, mostly observed in silicate facies. The Al_2O_3 content, as mentioned above, also does not fit very well in the two oldest deposit types, being more similar to Ediacaran-type BIF.

In the Sm/Yb vs. Y/Ho diagram (Fig. 8E) the LAC BIFs are similar to both Algoma- and Superior-type, with Sm/Yb of at most 3, and most of samples show Y/Ho above 28, corresponding to chondritic to superchondritic. However, some samples from the oxide facies show Y/Ho between 16 and 28. The lower Y/Ho is uncommon even for Rapitan or Ediacaran BIF, which may also be a feature induced by granulite metamorphism. Regarding the continental sedimentary contribution (Fig. 9), the LAC BIF are very similar to the Superior type, with higher clastic contribution than Algoma type, and the Fe/Ti with slightly lower values. The Ce/Ce* anomaly of the LAC BIF are predominantly negative (Fig. 6) in both facies, which is similar to Superior type deposits, while in Algoma types the La anomaly or absence of anomalies is common. The geochemical signature of REYs (Fig. 5B) is more similar to Superior-type BIF, with moderate Eu and more pronounced Y anomalies. Similarities with Algoma-type BIF is mostly associated with PAAS-normalized LREE contents.

Superior-type BIF comprises the largest known Fe ore reserves worldwide, while Algoma-type deposits are usually much smaller, which reflects directly the extent of their associated depositional basins. The LAC BIF are scarcely distributed in the LAC area which itself consist of a small-scale geotectonic block. Taking this into account, the LAC BIF are more similar to the Algoma-type. But the presence of ankerite in one of the samples of LAC BIFs silicate facies reminds us of the platform environment, characteristic of the Superior type deposit, which in a way is corroborated by the negative anomalies of Ce/Ce* that characterize shallow and oxygenated waters.

As shown, the LAC BIF do not have a direct and clear association with only one of the deposit types, depending on the analyzed facies, they may have more characteristics of the Algoma or Superior type. The association of rocks in the field with the LAC BIFs is with aluminous paragneisses, quartzites and meta-pyroxenites. With

the action of the granulite metamorphism, the reconstitution of the protolith rocks, their stratigraphy, horizontal and vertical distribution becomes very difficult to characterize the depositional basin, and the protoliths could be either from the Algoma or Superior environment. The oxide facies has more Algoma-like characteristics, higher Fe concentrations, more enriched in Eu, lower clastic contribution, Sm/Yb and Eu/Sm ratios of higher hydrothermal contribution. On the other hand, the silicate facies shows more similarities with the Superior type, with greater clastic contribution, ankerite presence, negative Ce/Ce* anomalies and Eu/Eu* < 1,8 (Tamehe et al., 2018).

The ambiguity of this information leads us to believe that the LAC BIFs are representative of a transitional environment from Algoma to Superior type. As the deposition of rocks in the basin dates back to the Siderian and Neoarchean with granulite metamorphism in the Rhyacian, this period in the history of the Earth and the deposition of BIFs lies right in the transition between the two types of deposit (Aftabi et al., 2021; Klein, 2005).

Considering the evolutionary history based on geochronological data, which identified zircon nuclei with ages of 2.7 - 2.5 Ga, in the Neoarchean there were probably the first depositions of BIF in an Algoma-like environment. This environment reduced tectonic and volcanic activity in the transition to the Siderian, evolving to a platform environment, with shallower waters and which even led to the deposition of carbonates, forming the Superior type deposits. This basin was closed until the Rhyacian, a Large Hot Orogen formed (Betiollo et al., submitted), and these sediments were pushed down to the lower crust and underwent granulite metamorphism.

7. Conclusions

Analyzing the data set it was possible to conclude that:

- LAC BIFs are divided in two facies based on its mineralogy: oxide and silicate facies. Quartz and magnetite prevails in oxide facies, while in silicate facies also contains ferrosilite, garnet and olivine;

- These rocks reached the highest granulite metamorphic grade, confirmed by ferrosilite and olivine in silicate facies;

- Based on major elements and petrographic evidences, oxide facies has a hydrothermal signature, with low content of Al_2O_3 and TiO_2, whereas silicate facies

register a continental sediment contribution, been enriched in those elements, beyond MgO, MnO and CaO;

- K and Rb concentrations, as well as Th/U and La/Th lead us to infer that granulite facies metamorphism did not modified considerably the original geochemical patterns of LAC BIF;

- The geochemical data exposed that the main source for both silicate and oxide facies BIF is seawater with major influence of low-T hydrothermal sources, followed by less important contribution of continental sedimentation;

- The true negative Ce/Ce* anomaly represents oxidizing, shallow waters. Thus, the depositional environment of the LAC BIF is inferred as a shallow, restricted basin, able to be influenced by both hydrothermal vents and continental sediments;

- Oxide facies represents sedimentation closer to hydrothermal vents and with weak influence from continental clastic sedimentation, while silicate facies would represents a contrasting zone closer to the continent with its influence;

- Oxide facies has more Algoma-like characteristics, higher Fe and Eu contents, low siliciclastic contribution, and Sm/Yb and Eu/Sm of higher hydrothermal contribution. On the other hand, the silicate facies resembles Superior-type BIF, with higher siliciclastic contribution, negative Ce/Ce* anomalies and Eu/Eu* < 1.8;

- LAC BIFs do not have a direct and clear association with only one of the deposit types. Depending on the analyzed facies, they may have more characteristics of the Algoma- or Superior-type. This ambiguity of information leads us to infer that the LAC BIFs are representative of a transitional environment from Algoma- to Superior-type;

- During the Neoarchean occur the first depositions of the LAC BIFs in an Algoma-like environment. This environment reduced the tectonic and volcanic activity in the transition to the Siderian, evolving to a platform environment, with shallower waters and which even led to the deposition of carbonates, typical of Superior type deposits. This basin was closed until the Rhyacian, a Large Hot Orogen formed, and these sediments were pushed down to the lower crust and underwent granulite metamorphism.

Acknowledgments

Leandro M. Betiollo thanks the Geological Survey of Brazil (SGB – CPRM) for providing the data and supporting the development of his Ph.D. thesis, and Andréa Sander and Andréia Gross from the SGB – CPRM staff for their support during fieldwork, petrographic descriptions, figure elaborations and geological debates. Everton M. Bongiolo is grateful to Conselho Nacional de Desenvolvimento Científico e Tecnológico (CNPq) for his Productivity on Research grant (# 311106/2020-0).

References

Aftabi, A., Atapour, H., Mohseni, S., Babaki, A., 2021. Geochemical discrimination among different types of banded iron formations (BIFs): A comparative review. Ore Geology Reviews, 136, 104244. https://doi.org/10.1016/j.oregeorev.2021.104244

Alexander, B.W., Bau, M., Andersson, P., Dulski, P., 2008. Continentally-derived solutes in shallow Archean seawater: Rare earth element and Nd isotope evidence in iron formation from the 2.9 Ga Pongola Supergroup, South Africa. Geochimica et Cosmochimica Acta, 72, 378–394. doi:10.1016/j.gca.2007.10.028

Angerer, T., Hagemann, S.G., Danyushevsky, L., 2013. High-grade iron ore at Windarling, Yilgarn Craton: a product of syn-orogenic deformation, hypogene hydrothermal alteration and supergene modification in an Archean BIF-basalt lithostratigraphy. Miner Deposita, 48, 697–728. DOI 10.1007/s00126-012-0450-3

Araújo, J.C.S., Lobato, L.M., 2019. Depositional model for banded iron formation host to gold in the Archean Rio das Velhas greenstone belt, Brazil, based on geochemistry and LA-ICP-MS magnetite analyses. Journal of South American Earth Sciences, 94, 102205. https://doi.org/10.1016/j.jsames.2019.05.021

Basei, M.A.S.; MacReath, L.; Siga Júnior, O., 1998. The Santa Catarina Granulite Complex of Southern Brazil: a review. Gondwana Res., 1, 3-4, 383-391. https://doi.org/10.1016/S1342-937X(05)70854-6

Basei, M.A.S., Nutman, A., Siga Júnior, O., Passarelli, C.R., and Drukas, C.O., 2009. The evolution and tectonic setting of the Luis Alves Microplate of Southeastern Brazil: an exotic terrane during the assembly of Western Gondwana. *In*: Gaucher, C., Sial, A.N., Halverson, G.P., and Frimmel, H.E. (Eds): Neoproterozoic-Cambrian Tectonics, Global Change and Evolution: a focus on southwestern Gondwana.

Developments in Precambrian Geol., 16, Elsevier, pp. 273-291. https://doi.org/10.1016/S0166-2635(09)01620-X

Basei, M.A.S., Drukas, C.O., Nutman, A.P., Wemmer, K., Dunyi, L., Santos, P.R., Passarelli, C.R., Campos Neto, M.C., Siga Jr O., Osako, L., 2011. The Itajaí foreland basin: A tectono-sedimentary record of the Ediacaran period, Southern Brazil. Int. J. Earth Sci., 100, 543-569. https://www.doi.org/10.1007/s00531-010-0604-4.

Bau, M., Dulski, P., 1996. Distribution of yttrium and rare-earth elements in the Penge and Kuruman iron-formations, Transvaal Supergroup, South Africa. Precambrian Research, 79, 37-55.

Bauernhofer, A.H., Hauzenberger, C.A., Wallbrecher, E., Muhongo, S., Hoinkes, G., Mogessie, A., Opiyo-Akech, N., Tenczer, V., 2009. Geochemistry of basement rocks from SE Kenya and NE Tanzania: indications for rifting and early Pan-African subduction. Int J Earth Sci (Geol Rundsch), 98, 1809–1834. DOI 10.1007/s00531-008-0345-9.

Bekker, A., Slack, J.F., Planavsky, N., Krapež, B., Hofmann A., Konhauser K.O., Rouxel, O. J., 2010. Iron Formation: The Sedimentary Product of a Complex Interplay among Mantle, Tectonic, Oceanic, and Biospheric Processes. Economic Geology, 105, 467–508.

Betiollo, L.M., Iglesias, C.M.F., Rocha, P.G., 2018. Integração geológica-geofísica e recursos minerais do Cráton Luis Alves: mapa de integração geológica-geofísica. Porto Alegre: CPRM, 1:250.000, http://rigeo.cprm.gov.br/jspui/handle/doc/16802 (April 2022)

Bitencourt, M.F., Nardi, L.V.S., 2000. Tectonic setting and sources of magmatism related to the Southern Brazilian Shear Belt. Rev. Bras. Geociênc., 30-1, 186-189.

Bleeker, W., 2003. The late Archean record: a puzzle in ca. 35 pieces. Lithos, 71, 99-134. https://doi.org/10.1016/j.lithos.2003.07.003

Bolhar, R., Kamber, B.S., Moorbath, S., Fedo, C.M., Whitehouse, M.J., 2004. Characterisation of early Archaean chemical sediments by trace element signatures. Earth and Planetary Science Letters, 222, 43– 60. doi:10.1016/j.epsl.2004.02.016

Boström, K., 1970. Submarine volcanism as a source for iron. Earth and Plantetary Science Letters, 9, 348-354.

Brito Neves, B.B., 2011. The Paleoproterozoic in the South-American continent: Diversity in the geologic time. J. South Am. Earth. Sci., 32, 270-286. https://doi.org/10.1016/j.jsames.2011.02.004

Bruno, H., Almeida, J., Heilbron, M., Salomão, M., Cury, L., 2018. Architecture of major Precambrian tectonic boundaries in the northern part of the Dom Feliciano Orogen, southern Brazil: Implications for the West Gondwana amalgamation. J. South Am. Earth. Sci., 86, 301-317, https://doi.org/10.1016/j.jsames.2018.06.018.

Campos, R.S., Philipp, R.P., Massonne, H.J., Chemale, F., Theye, T., 2012. Petrology and isotope geology of mafic to ultramafic metavolcanic rocks of the Brusque Metamorphic complex, southern Brazil. Int. Geol. Rev., 54-6, 686-713. https://doi.org/10.1080/00206814.2011.569393

Cen, Y., Peng, S., Kusky, T.M., Jiang, X., Wang, L., 2012. Granulite facies metamorphic age and tectonic implications of BIFs from the Kongling Group in the northern Huangling anticline. Journal of Earth Science, 23 (5), 648–658. DOI: 10.1007/s12583-012-0286-x

Cury, L.F., 2009. Geologia do Terreno Paranaguá. Tese (Doutorado) - Programa de Pós-Graduação em Geoquímica e Geotectônica, Universidade de São Paulo, São Paulo,187 p.

Dutta, D., Misra, S., Karmakar, S., 2022. Deformation mechanisms and characteristics of the meta-BIFs from an early Proterozoic shear system of the Southern Granulite Terrane (SGT), India. Journal of Structural Geology, 156, 104534. https://doi.org/10.1016/j.jsg.2022.104534

Duuring, P., ThomasAngerer, T., Hagemann, S.G., Banks, D.A., 2020. Iron deposits hosted by banded iron-formations in the Yilgarn Craton: Products of sequential iron enrichment by magmatic, marine and meteoric fluids. Ore Geology Reviews, 116, 103251. https://doi.org/10.1016/j.oregeorev.2019.103251

Egglseder, M.S., Cruden, A.R., Tomkins, A.G., Wilson, C.J.L., 2016. Deformation-induced silica redistribution in banded iron formation, Hamersley Province, Australia. Lithos, 266–267, 87–97. https://doi.org/10.1016/j.lithos.2016.09.033

Fernandes, J.F., Iyer, S.S., Imakuma, K., 1987. Geochemical studies in the proterozoic metamorphic terrane of the Guaxupé Massif, Minas Gerais, Brazil. A discussion on large ion lithophile element fractionation during highgrade metamorphism. Precambrian Research, 36, 65-79.

Florisbal, L.M., Janasi, V.A., Bitencourt, M.F., Heaman, L.M., 2012. Space–time relation of post-collisional granitic magmatism in Santa Catarina, southern Brazil: U–Pb LAMC-ICP-MS zircon geochronology of coeval mafic-felsic magmatism related to the Major Gercino Shear Zone. Precambrian Res., 216, 132–15. https://doi.org/10.1016/j.precamres.2012.06.015

Fonarev, V.I., Pilugin, S.M., Savko, K.A., Novikova, M.A., 2006. Exsolution textures of orthopyroxene and clinopyroxene in high-grade BIF of the Voronezh Crystalline Massif: evidence of ultrahigh-temperature metamorphism. J. metamorphic Geol., 24, 135–151. doi:10.1111/j.1525-1314.2006.00630.x

Fornari, A., 1998. Geologia e metalogênese da porção meridional do Cráton Luis Alves-SC. Tese (Doutorado) - Instituto de Geociências da Universidade de Campinas, Campinas, 136 pp.

Franchi, F., Mapeo, L.B.M., 2019. Evolution of an Archaean intracratonic basin: A review of the Transvaal Supergroup lithostratigraphy in Botswana. Earth-Science Reviews, 191, 273–290. https://doi.org/10.1016/j.earscirev.2019.02.007

Friend, C.R.L., Nutman, A. P., Bennett, V.C., Norman, M. D., 2008. Seawater-like trace element signatures (REE + Y) of Eoarchaean chemical sedimentary rocks from southern West Greenland, and their corruption during high-grade metamorphism. Contrib Mineral Petrol, 155, 229–246. DOI 10.1007/s00410-007-0239-z

Ganno, S., Tanko, E. L. N., Nono, G. D. K., Soh, A. D., Moudioh, C., Ngnotué, T., Nzenti, J. P., 2017. A mixed seawater and hydrothermal origin of superior-type banded iron formation (BIF)-hosted Kouambo iron deposit, Palaeoproterozoic Nyong series, Southwestern Cameroon: Constraints from petrography and geochemistry. Ore Geology Reviews, 80, 860–875. https://doi.org/10.1016/j.oregeorev.2016.08.021

Gourcerol, B., Thurston, P.C., Kontak, D.J., Côté-Mantha, O., Biczok, J., 2016. Depositional setting of Algoma-type banded iron formation. Precambrian Research, 281, 47–79. https://doi.org/10.1016/j.precamres.2016.04.019

Gross, G. A., 1980. A classification of iron formations based on depositional environments. Canadian Mineralogist, 18, 215-222.

Gross, G. A., 1983. Tectonic systems and the deposition of iron-formation. Precambrian Research, 20, 171-187.

Guadagnin, F., Chemale Jr, F., Dussin, I.A., Jelinek, A.R., dos Santos, M.N., Borba, M.L., Justino, D., Bertotti, A.L., Alessandretti, L., 2010. Depositional age and provenance of the Itajaí Basin, Santa Catarina State, Brazil: Implications for SW Gondwana correlation. Precambrian Res., 180, 3-4, 156-182. https://doi.org/10.1016/j.precamres.2010.04.002.

Han, C., Xiao, W., Su, B., Chen, Z., Zhang, X., Ao, S., Zhang, J., Zhang, Z., Wan, B., Song, D., Wang, Z., 2014. Neoarchean Algoma-type banded iron formations from Eastern Hebei, North China Craton: SHRIMP U-Pb age, origin and tectonic setting. Precambrian Research, 251, 212–231. https://doi.org/10.1016/j.precamres.2014.06.019

Hartmann, L.A., Silva, L.C., Orlandi F°, V., 1979. O Complexo Granulítico de Santa Catarina: descrição e implicações genéticas. Acta Geológica Leopoldensia, São Leopoldo, 6, 93-112.

Hartmann, L.A., Santos, J.O.S., McNaughton, N.J., Vasconcellos, M.A.Z., Silva, L.C. da, 2000. Ion microprobe (SHRIMP) dates complex granulite from Santa Catarina, southern Brazil. An. Acad. Bras. Ciênc., 72-4, 559-572. https://doi.org/10.1590/S0001-37652000000400007

Haugaard, R., Pecoits, E., Lalonde, S., Rouxel, O., Konhauser, K., 2016. The Joffre banded iron formation, Hamersley Group, Western Australia: Assessing the palaeoenvironment through detailed petrology and chemostratigraphy. Precambrian Research, 273, 12–37. https://doi.org/10.1016/j.precamres.2015.10.024

Heilbron, M., Valeriano, C.M., Tassinari, C.C.G., Almeida, J., Tupinambá, M., Siga Jr., O., Trouw, R., 2008. Correlation of Neoproterozoic terranes between the Ribeira Belt, SE Brazil and its African counterpart: comparative tectonic evolution and open questions. *In* Pankhurst, R.J., Trouw, R.A.J., Brito Neves, B.B., De Wit, M.J., (eds) West Gondwana: Pre-Cenozoic Correlations Across the South Atlantic

Region. Geological Society, London, Special Publications, 294, 211–237. https://doi.org/10.1144/SP294.12

Heller, B.M., Hueck, M., Passarelli, C.R., Basei, M.A.S., 2021. Zircon U-Pb geochronology and Hf isotopes of the Luís Alves Terrane: Archean to Paleoproterozoic evolution and Neoproterozoic overprint. J. South Am. Earth. Sci., 106, 103008, https://doi.org/10.1016/j.jsames.2020.103008.

Horváth, P., Reinhardt, J., Hofmann, A., 2014. High-grade metamorphism of ironstones in the Mesoarchaean of southwest Swaziland. Miner Petrol, 108, 589–605. DOI 10.1007/s00710-013-0307-1

James, H.L., 1954. Sedimentary Facies of Iron-Formation. Econ. Geol., 49-3, 235-293. https://doi.org/10.2113/gsecongeo.49.3.235

Justo, A. P., Dantas, E. L., Bau, M., Freitas-Silva, F. H., Santos, R. V., Schorscher, J. H. D., 2020. Paleobasinal to band-scale REE + Y distribution in iron formations from Carajás, Amazon Craton, Brazil. Ore Geology Reviews, 127, 103750. https://doi.org/10.1016/j.oregeorev.2020.103750

Kaul, P.F.T., 1980. O Cráton de Luis Alves. In: Congresso Brasileiro De Geologia, 31, Balneário Camboriú, Anais, SBG, v. 5, p. 2677-2683.

Klein, C., Ladeira, E.A., 2002. Petrography and geochemistry of the least altered banded iron-formation of the Archean Carajás Formation, Northern Brazil. Economic Geology, 97, 643–651.

Klein, C., 2005. Some Precambrian banded iron-formations (BIFs) from around the world: Their age, geologic setting, mineralogy, metamorphism, geochemistry, and origin. Am. Miner., 90, 1473-1499. https://doi.org/10.2138/am.2005.1871

Konhauser, K.O., Planavsky, N.J., Hardisty, D.S., Robbins, L.J., Warchola, T.J., Haugaard, R., Lalonde, S.V., Partin, C.A., Oonk, P.B.H., Tsikos, H., Lyons, T.W., Bekker, A., Johnson, C.M., 2017. Iron formations: A global record of Neoarchaean to Palaeoproterozoic environmental history. Earth-Science Reviews, 172, 140–177. http://dx.doi.org/10.1016/j.earscirev.2017.06.012

Lan, C., Zhao T., Zhang, L., Wang, C., 2014. The Origin of Granulite Facies Metamorphic Iron Formations in Wuyang, Henan Province, Southern of North China Craton. Acta Geologica Sinica (English Edition), 88 (2), 88-89.

Lan, C., Long, X., Zhao, T., Zhai, M., 2019. In-site mineral geochemistry and whole-rock Fe isotopes of the quartzmagnetite-pyroxene rocks in the Wuyang area, North China Craton: Constraints on the genesis of the pyroxene-rich BIF. Precambrian Research, 333, 105445. https://doi.org/10.1016/j.precamres.2019.105445

Li, H-Z, Liang, J., Yang, F., Zhai, M-G, Zhang, L-C., Voudouris, P.Ch., Yang, Z-J., Zhou, Y-Z., He, J-G., Spry, P.G., 2019. The mineralogy, mineral chemistry, and origin of the Wuyang banded iron formations, North China Craton. Precambrian Research, 328, 111–127. https://doi.org/10.1016/j.precamres.2019.03.011

Morrissey, L.J., Hand, M., Lane, K., Kelsey, D.E., Dutch, R.A., 2016. Upgrading iron-ore deposits by melt loss during granulite facies metamorphism. Ore Geology Reviews, 74, 101–121. https://doi.org/10.1016/j.oregeorev.2015.11.012

Moudioh, C., Tamehe, L.S., Ganno, S., Tankwa, M.N., Soares, M.B., Ghosh, R., Kankeu, B., Nzenti, J.P., 2020. Tectonic setting of the Bipindi greenstone belt, northwest Congo craton, Cameroon: Implications on BIF deposition. https://doi.org/10.1016/j.jafrearsci.2020.103971

Mukhopadhyay, J., 2020. Archean banded iron formations of India. Earth-Science Reviews, 201, 102927. https://doi.org/10.1016/j.earscirev.2019.102927

Nutman, A.P., McGregor, V.R., Shiraishi, K., Friend, C.R.L., Bennett, V.C., Kinny, P.D., 2002. ≥ 3850 Ma BIF and mafic inclusions in the early Archaean Itsaq Gneiss Complex around Akilia, southern West Greenland? The difficulties of precise dating of zircon-free protoliths in migmatites. Precambrian Research, 117, 185-224.

Papineau, D., Gregorio, B.T., Cody, G.D., Fries, M.D., Mojzsis, S.J., Steele, A., Stroud, R.M., Fogel, M.L., 2010. Ancient graphite in the Eoarchean quartz–pyroxene rocks from Akilia in southern West Greenland I: Petrographic and spectroscopic characterization. Geochimica et Cosmochimica Acta, 74, 5862–5883. https://doi.org/10.1016/j.gca.2010.05.025

Passarelli, C.R., Basei, M.A.S., Wemmer, K., Siga Jr., O., Oyhantçabal, P., 2011. Major shear zones of southern Brazil and Uruguay: escape tectonics in the eastern border of Rio de La plata and Paranapanema cratons during the Western Gondwana amalgamation. Int. J. Earth Sci. (Geol Rundsch), 100, 391-414, https://doi.org/10.1007/s00531-010-0594-2

Passarelli, C.R., Basei, M.A.S., Siga Jr., O., and Harara, O.M.M., 2018. The Luis Alves and Curitiba Terranes: Continental Fragments in the Adamastor Ocean. *In* Siegesmund, S., Basei, M.A.S., Oyhantçabal, P., Oriolo, S., eds., Geol. of Southwest Gondwana, Regional Geol. Rev., p. 189-215. https://doi.org/10.1007/978-3-319-68920-3_8

Philipp, R.P., Mallmann, G., Bitencourt, M.F., Souza, E.R., Liz, J.D., Wild, F., Arend, S., Oliveira, A.S., Duarte, L.C., Rivera, C.B., Prado, M., 2004. Caracterização Litológica e Evolução Metamórfica da Porção Leste do Complexo Metamórfico Brusque, Santa Catarina. Rev. Bras. Geociênc., 34 (1), 21–34.

Pickard, A.L., 2003. SHRIMP U–Pb zircon ages for the Palaeoproterozoic Kuruman Iron Formation, Northern Cape Province, South Africa: evidence for simultaneous BIF deposition on Kaapvaal and Pilbara Cratons. Precambrian Research, 125, 275–315. doi:10.1016/S0301-9268(03)00113-X

Planavsky, N., Bekker, A., Rouxel, O.J., Kamber, B., Hofmann, A., Knudsen, A., Lyons, T.W., 2010. Rare Earth Element and yttrium compositions of Archean and Paleoproterozoic Fe formations revisited: New perspectives on the significance and mechanisms of deposition. Geochimica et Cosmochimica Acta, 74, 6387–6405. doi:10.1016/j.gca.2010.07.021

Reddy, N.S., Sashidhar, A.N., 1989. Mineralogy and chemistry of handed iron formations (BIF) of Tiruvannamalai area, Tamil Nadu. Proc. Indian Acad. Sci. (Earth Planet. Sci.), 98 (2), 167-172.

Rudnick, R.L., McLennan, S.M., Taylor, S.R., 1985. Large ion lithophile elements in rocks from high-pressure granulite facies terrains. Geochimica et Cosmochimica Acta, 49, 1645-1655.

Smith, A.J.B., Beuker, N., 2016. Palaeoproterozoic banded iron formationhosted high-grade hematite iron ore deposits of the Transvaal Supergroup, South Africa. Episodes, 39 (2), 269-284. DOI: 10.18814/epiiugs/2016/v39i2/95778

Soares, M.B., Neto, A.V.C., Zeh, A., Cabral, A.R., Pereira, L.F., Prado, M.G.B., Almeida, A.M., Manduca, L.G., Silva, P.H.M., Mabub, R.O.A., Schlichta, T.M.,2017. Geology of the Pitangui greenstone belt, Minas Gerais, Brazil: Stratigraphy, geochronology and BIF geochemistry. Precambrian Research, 291, 17–41. https://doi.org/10.1016/j.precamres.2017.01.008

Spier, C.A., Oliveira, S.M.B., Sial, A.N., Rios, F.J., 2007. Geochemistry and genesis of the banded iron formations of the Cauê Formation, Quadrilátero Ferrífero, Minas Gerais, Brazil. Precambrian Research, 152, 170–206. https://doi.org/10.1016/j.precamres.2006.10.003

Stanton, R.L., 2006. On limits to distances of movement of matter during regional metamorphism: an investigation of nine samples from high-grade metamorphic terranes. The Canadian Mineralogist, 44, 985-1024.

Tamehe, L.S., Tankwa, M.N., Chongtao, W., Ganno, S., Ngnotue, T., Nono, G.D.K., Simon, S.J., Zhang, J., Nzenti, J.P., 2018. Geology and geochemical constrains on the origin and depositional setting of the Kpwa–Atog Boga banded iron formations (BIFs), northwestern Congo craton, southern Cameroon. Ore Geology Reviews, 95, 620–638. https://doi.org/10.1016/j.oregeorev.2018.03.017

Tavares, F. M., Trouw, R. A. J., Silva, C. M. G., Justo, A. P., Oliveira, J. K. M., 2018. The multistage tectonic evolution of the northeastern Carajás Province, Amazonian Craton, Brazil: Revealing complex structural patterns. Journal of South American Earth Sciences, 88, 238–252. https://doi.org/10.1016/j.jsames.2018.08.024

Teutsong, T., Bontognali, T.R.R., Ndjigui, P-D., Vrijmoed, J.C., Teagle, D., Cooper, M., Vance, D., 2017. Petrography and geochemistry of the Mesoarchean Bikoula banded iron formation in the Ntem complex (Congo craton), Southern Cameroon: Implications for its origin. Ore Geology Reviews, 80, 267–288. https://doi.org/10.1016/j.oregeorev.2016.07.003

Trendall, A.F., 2002. The significance of iron-formation in the Precambrian stratigraphic record. Spec. Publs int. Ass. Sediment., 33, 33-66.

Trendall, A.F., Compston, W., Nelson, D. R., De Laeter, J. R., Bennett, V. C., 2004. SHRIMP zircon ages constraining the depositional chronology of the Hamersley Group, Western Australia. Australian Journal of Earth Sciences, 51,621–644.

Warchola, T., Lalonde, S.V. Pecoits, E., Gunten, K., Robbins, L. J., Alessi, D.S., Philippot, P., Konhauser, K.O., 2018. Petrology and geochemistry of the Boolgeeda Iron Formation, Hamersley Basin, Western Australia. Precambrian Research, 316, 155–173. https://doi.org/10.1016/j.precamres.2018.07.015

Yellappa, T., Chetty, T.R.K., Santosh, M., 2016. Precambrian iron formations from the Cauvery Suture Zone, Southern India: Implications for sub-marine hydrothermal origin in Neoarchean and Neoproterozoic convergent margin settings. Ore Geology Reviews, 72, 1177–1196 https://doi.org/10.1016/j.oregeorev.2015.05.002

Zheng, Y., Han, X., Gao, X., Geng, X., Chen, X., Liu, J., 2017. Enrichment of iron ores by folding in the BIF-hosted deposit: A case study from the Archean Qian'an iron deposit, North China Craton. Geological Journal, 53, 617–628. https://doi.org/10.1002/gj.2916

Artigo 3

Gmail

Leandro Betiollo <le.vermelho@gmail.com>

Brazilian Journal of Geology - Manuscript ID BJGEO-2022-0098

1 mensagem

Tatiana Alonso <onbehalfof@manuscriptcentral.com> 23 de dezembro de 2022 às 19:39
Responder a: secretaria@zeppelini.com.br
Para: le.vermelho@gmail.com
Cc: le.vermelho@gmail.com, bongiolo@ufrgs.br, andreia.gross@sgb.gov.br, cristianebrivera@gmail.com

23-Dec-2022

Dear Dr. BETIOLLO:

Your manuscript entitled "Geochemistry of orthogranulites and opx-bearing metagranites from the Luis Alves Craton (southern Brazil): island arc and a large hot orogen in the Neoarchean - Rhyacian" has been received by the Editorial Office of the Brazilian Journal of Geology.

Please note that this message is not a confirmation of submission, which will only be given once your manuscript is considered to be within the scope and of interest to the journal.

Your manuscript ID is BJGEO-2022-0098.

Please mention the above manuscript ID in all future correspondence or when calling the office for questions. If there are any changes in your street address or e-mail address, please log in to ScholarOne Manuscripts at https://mc04.manuscriptcentral.com/bjgeo-scielo and edit your user information as appropriate.

You can also view the status of your manuscript at any time by checking your Author Center after logging in to https://mc04.manuscriptcentral.com/bjgeo-scielo.

Thank you for submitting your manuscript to the Brazilian Journal of Geology.

Sincerely,
Brazilian Journal of Geology Editorial Office

Geochemistry of orthogranulites and opx-bearing metagranites from the Luis Alves Craton (southern Brazil): island arc and a large hot orogen in the Neoarchean - Rhyacian

Leandro Menezes Betiollo[1,2*], Everton Marques Bongiolo[2], Andréia O. M. Gross[1], Cristiane Butori Rivera[2]

[1]Gerência de Geologia e Recursos Minerais, Serviço Geológico do Brasil (SGB ï CPRM), Rua Banco da Província 105, 90840-030, Porto Alegre, Rio Grande do Sul, Brazil
[2]Programa de Pós-graduação em Geociências, Universidade Federal do Rio Grande do Sul, Avenida Bento Gonçalves 9500, 91500-000, Porto Alegre, Rio Grande do Sul, Brazil
**corresponding author: leandro.betiollo@sgb.gov.br*

Abstract

The Luis Alves Craton is considered a fragment of a mid- to large-scale granulitic terrane including Archean-Paleoproterozoic. In this contribution, we use regional geological-structural mapping, petrography and lithogeochemical data to determine the geological-tectonic framework, processes of formation and exhumation, and the regional significance of the LAC in the light of metamorphic petrology, supercontinent cycles, and Paleoproterozoic geodynamic processes. The lithogeochemical study showed that granulite rocks are dioritic, granodiorite, granitic and gabbroic composition. Opx-bearing granites show a highly enriched pattern in the REE. Felsic granulites and opx-granites REE geochemical signatures are similar to signatures of calc-alkaline magmas, the Na-K-Ca cationic diagram also show this. All lithotypes showed affinity with orogenic environments, highlighting an island arc setting for their genesis. Subduction in such island arc generated partial melting and bimodal magmatism, both mafic and felsic granulites being products of partial melting of an Archean oceanic crust. When subduction ceased, with the total consumption of oceanic crust and the adjacent basin closed, a Large Hot Orogen was established forming an orogenic plateau. The orogenic plateau supported the P-T conditions for the granulite metamorphism and the partial melting of the felsic granulites triggered the generation of the Rodeio-Rio da Luz Suite granites.

Keywords: granulite, geochemistry, supercontinent cycle.

1. Introduction

Granulite terranes have their origin and geological meaning studied since Weiss (1803; O'Brien, 2006). In the last four decades, granulite geological modeling took advantage of robust thermodynamic datasets (Holland and Powell, 1985; Powell and Holland, 1985; 1988), and advances in analytical techniques. Metamorphic events under up to 1200 °C and 6 GPa (or up to 200 km crustal depth) were determined, and these extreme metamorphic petrological fields were built in association with new geodynamic views (Brown, 2007a,b; 2014; Stuwe, 2007; Brown and Johnson, 2019). Granulite terrane generation was mainly related to volcanic and continental arc environments with extra heat sources (Harley 1989, 1992; Bohlen 1991; Ashwal et al., 1992; Gerya and Meilick, 2011; Kramers et al., 2011; Lexa et al., 2011; Sajeev et al., 2013), and their present understanding involve: (i) the formation, evolution and consolidation of large hot orogens (Chardon et al., 2009; Franek et al., 2011; Jamieson and Beaumont, 2013; Kohn, 2014; Harley, 2016; Perchuk et al., 2018; Brown and Johnson, 2019; Dziggel et al., 2019), (ii) supercontinent amalgamation (Bleeker, 2003; Zhao et al., 2004; Brown, 2007a; Vansutre and Hari, 2010; Bradley 2011; Touret et al.. 2016), and (iii) Earth time's cycles (Brown and Johnson, 2019). However, even with the prominent scientific advances, exhumation, P-T-t paths, deformational patterns, microstructural processes, and the regional structuration of these lower crust terranes, are still subjects of increasing investigations (Harley, 1989, 1992; Barbosa et al., 2006; Taylor et al., 2010; Jamieson and Beaumont, 2011; Kelsey and Powell, 2011; Spalla et al., 2011; White and Powell, 2011; Endo et al., 2012; Block et al., 2016; Dharmapriya et al., 2017; Girelli et al., 2018; Zhang et al., 2021).

In this paper, we use regional geological-structural data, petrography, and a lithogeochemical data to reinterpret the geological-tectonic framework, processes of formation, and the regional significance of the LAC in Southern Brazil. Data integration includes the available literature and the latest advances on metamorphic petrology, supercontinents cycle and geodynamic processes.

2. Regional Geology

The Luis Alves Craton (LAC) (Kaul, 1980) is a small fragment of Archean-Paleoproterozoic crust in southern Brazil (Fig. 1) surrounded by geotectonic units assembled during the Neoproterozoic Brasiliano – Pan African orogeny which led to the amalgamation of Western Gondwana (Basei et al., 1998; 2009; Heilbron, 2008; Brito Neves, 2011; Passarelli et al., 2018; Bruno et al., 2018). Thus, the LAC acted as one of the foreland landmasses that structured the formation of the surrounding Neoproterozoic orogens, such as the Northern Dom Feliciano Belt, the Curitiba Microplate (part of Southern Ribeira Belt) and the Paranaguá Block.

The LAC geotectonic block (Fig. 1) is composed by the Santa Catarina Granulite Complex (SCGC) (Hartmann et al., 1979), an Archean-Paleoproterozoic unit (Basei et al., 1998; 2009; Hartmann et al., 2000; Passarelli et al., 2018; Heller et al., 2021) divided into four units: (1) Barra Velha Ultramafic Complex, (2) Joinville Metasedimentary Sequence, (3) Luis Alves Orthogneiss, and (4) Rodeio-Rio da Luz Suite (Fig. 1). In this contribution, we focused on the Luis Alves Orthogneiss and the Rodeio-Rio da Luz Suite. Neoproterozoic units within the LAC area consists of sedimentary basins of Campo Alegre, Guaratubinha and Corupá (Basei et al., 1998; Citroni et al., 2001) cover, and granitoids of the Serra do Mar Suite (Kaul, 1984; Gualda and Vlach, 2007), which represent an extensional, late-collisional stage of the Brasiliano – Pan African orogeny.

The Northern Dom Feliciano Belt is constituted by the Brusque Metamorphic Complex (Philipp et al., 2004; Campos et al., 2012), the Itajaí Basin (Guadagnin et al., 2010; Basei et al., 2011) and the Florianópolis Batholith (Bitencourt and Nardi, 2000; Florisbal et al., 2012). The units in contact with the southern LAC are the volcano-sedimentary rocks of the Itajaí Basin, and the low- to medium-grade metavolcano-sedimentary rocks of the Brusque Metamorphic Complex along the Itajaí-Perimbó shear zone (IPSZ). The northwestern LAC area is bounded to the Curitiba Microplate (gneisses and migmatites of the Atuba Complex), of the Southern Ribeira Belt (Heilbron, 2008; Basei et al., 2009; Passarelli et al., 2011; 2018) by the Piên shear zone (PSZ). To the east, the Rio Palmital shear zone (RPSZ) limits the LAC and the Paranaguá Block (Cury, 2009), a geotectonic unit with metasedimentary rocks and granitoids.

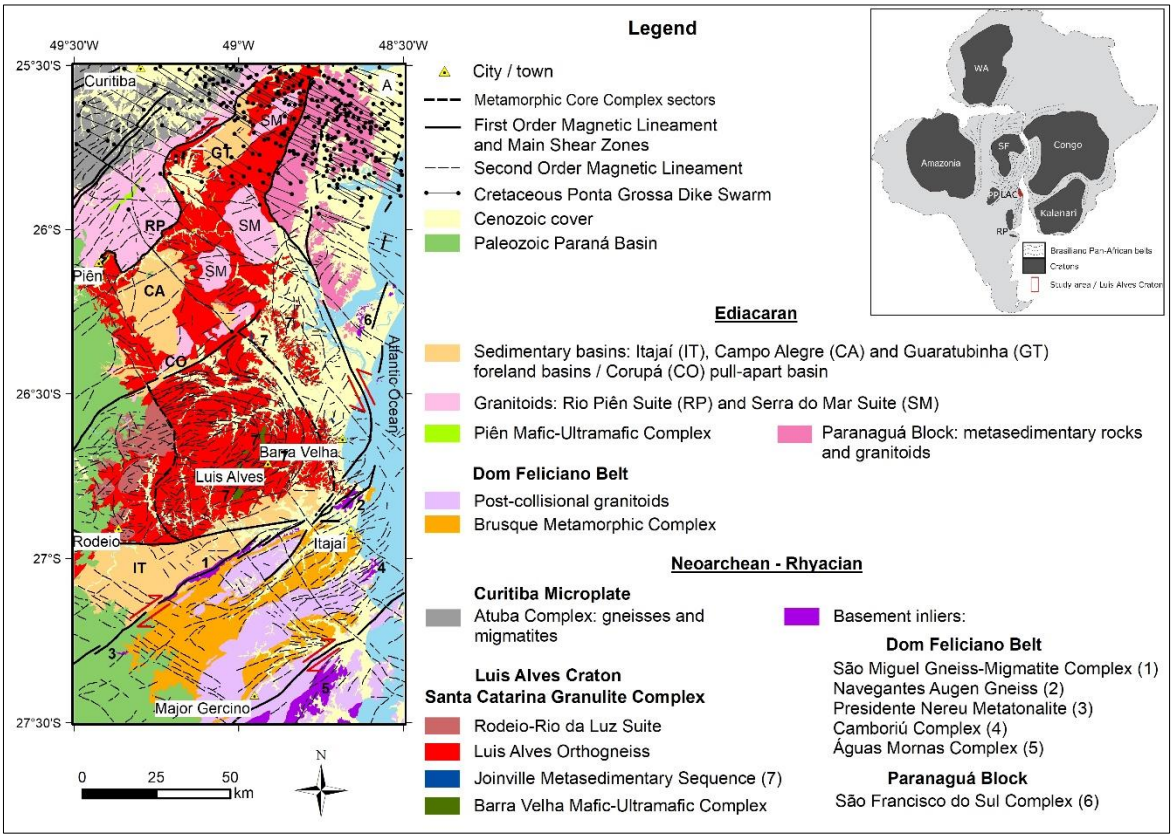

Figure 1: Geological map of study area. Box in the upper right corner showing the position of the LAC during the Brasiliano orogen and Western Gondwana assembly.

3. Methods

3.1. Field geology and petrography

Three projects of geological mapping carried out by the Geological Survey of Brazil (SGB – CPRM) in the last decade (Iglesias et al., 2011; Betiollo et al., 2018; Iglesias et al., 2021) raised a robust geological dataset (1:250,000 and 1:50,000 scales) used in this contribution. The dataset consists of more than 1,000 described outcrops and the production of ca. 500 thin sections, which were all integrated and re-evaluated here to refine the regional understanding of the Santa Catarina Granulite Complex (SCGC) and the entire LAC (Fig. 1). From those, 61 thin sections relate with the Luis Alves Orthogneiss, and 17 with the Rodeio-Rio da Luz Suite, focus of this paper. Regional geological and structural data obtained during fieldwork identified the main lithotypes and conditioning structures along the LAC.

3.2. Geochemical analyzes

Eighty samples obtained from surface expositions of the Luis Alves othogneiss (n= 63) and the Rodeio-Rio da Luz opx-bearing metagranites (n= 17) were reduced to <200-mesh grain size in an agate disc mill after crushing. Analyzes were performed at SGS GEOSOL Laboratories by lithium metaborate fusion and reading by ICP-AES for major elements and ICP-MS for REE, and multi-acid digestion and reading by ICP-MS for other trace elements. Detailed analytical procedures are available at https://www.sgsgeosol.com.br/.

4. Results

4.1. Fieldwork and petrography

Three lithotypes were identified in the SCGC: mafic and felsic granulites of the Luis Alves Orthogneiss, and opx-bearing metagranites of the Rodeio-Rio da Luz Suite.

4.1.1. Luis Alves Orthogneiss

Among the LAC units, the Luis Alves Orthogneiss has the largest, continuous exposition area. Rocks crop out along the coastline nearby Barra Velha town and its countryside towards the West as blocks, flagstones, boulders, and continuous quarry expositions. Consists of medium-grained, polygonal granoblastic, massive to foliated and banded rocks intercalating mafic and felsic bands. Mafic bands are composed by plagioclase, pyroxene, hornblende and biotite with (leuco) gabbroic compositions, whereas felsic ones has tonalite, granodiorite and quartz-diorite compositions with hornblende and biotite. Garnet occur locally as an accessory mineral (Fig. 2).

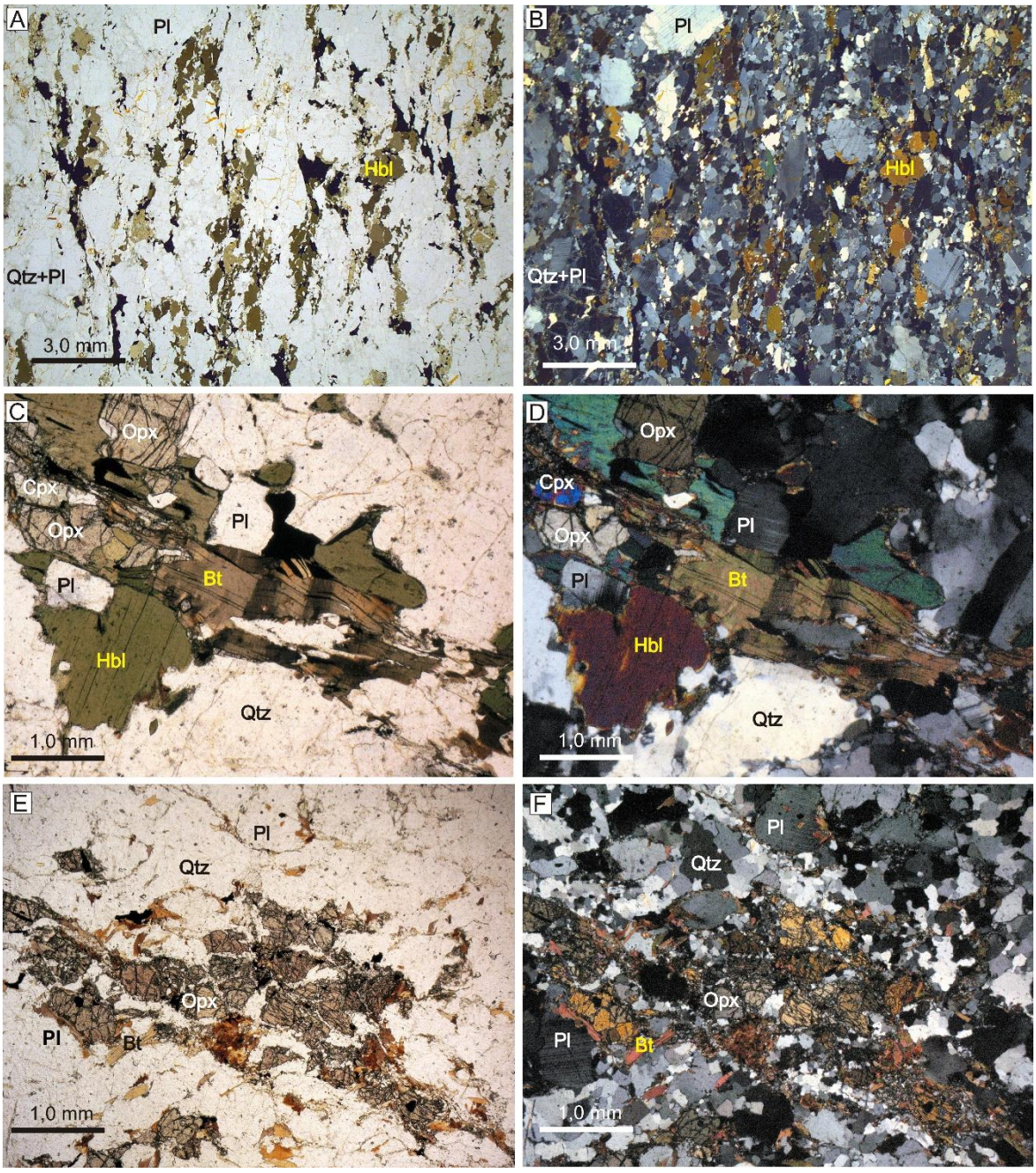

Figure 2: Thin sections of felsic granulite from Luis Alves Orthogneiss. Pl: plagioclase, Hbl: hornblende, Qtz: quartz, Opx: orthopyroxene, Cpx: clinopyroxene, Bt: biotite.

4.1.2. Rodeio-Rio da Luz Suite

This unit consists of orthopyroxene-bearing metagranites that crop out mostly at the Southwestern LAC (Fig. 1), with minor occurrences in its central zone where they are intrusive in the Luis Alves Orthogneisses. Outcrops are sparse with an unclear relationship with most of their hosts due to diffuse contacts. Close to inferred contacts the orthogneisses country rocks show increasing alkali-feldspar amounts, and

metagranites reveal increasing mafic minerals, which suggest some kind of interaction between lithotypes.

They are gray to reddish rocks with monzogranitic and syenogranitic compositions. Mineralogy consists of euhedral to oval-shape alkali-feldspar phenocrysts immersed in a fine- to medium-grained matrix with quartz, alkali-feldspar, plagioclase, hornblende, biotite, and orthopyroxene relicts. Accessory allanite is diagnostic of this suite. Protomylonites to mylonites frequently cross-cut the Rodeio-Rio da Luz Suite (Fig. 3).

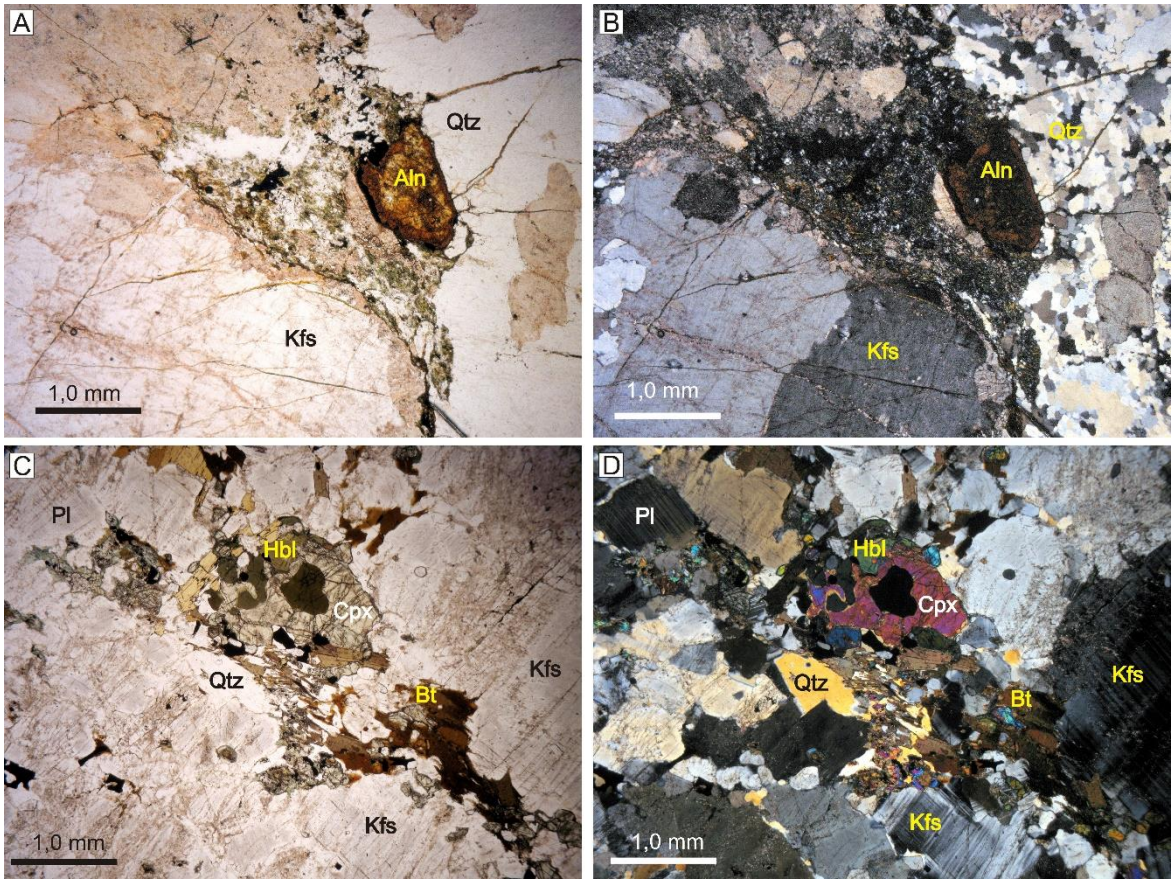

Figure 3: Thin sections of Rodeio-Rio da Luz metagranites. Qtz: quartz, Cpx: clinopyroxene, Bt: biotite, Aln: allanite, Kfs: alkali-feldspar.

4.2. Lithogeochemistry

A first step for geochemical evaluation was analyzing the influence of the metamorphic imprint on these rocks via K, Rb, Th/U and La/Th mobility parameters (Rudnick et al., 1985; Fernandes et al., 1987). In the Rb *vs*. K diagram, samples cluster along the granulitic trend, showing loss of Rb (Fig. 4a). In the La/Th x Th/U diagram

(Fig. 4b), most of the samples showed Th and U loss, few samples plotting in the field of no-element loss igneous rocks. With these informations, we used low-mobility elements such as REE for geochemical evaluations, and be cautious with interpretations based on anomalous major and trace elements contents.

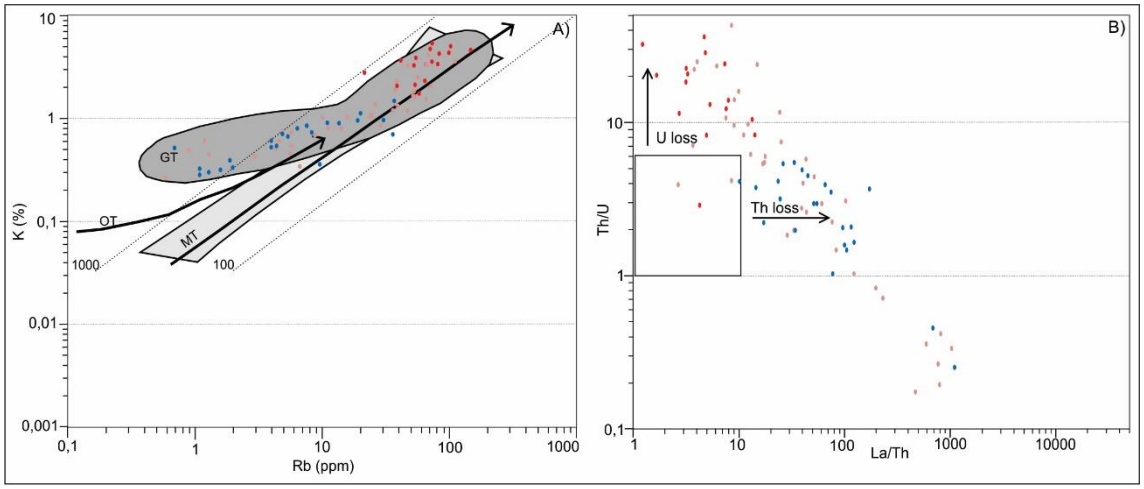

Figure 4: binary diagrams to show the metamorphic influence on these rocks. Blue triangles: mafic granulites; purple squares: felsic granulites; red balls: opx-bearing granites.

4.2.1. Geochemistry classification and signatures

The felsic granulites mostly show diorite to granodiorite geochemical compositions, some plotting in the granite and gabbro fields (Figs. 5a and 5b). Mafic granulites are geochemically compatible with gabbro, monzogabro and gabbro-diorite. The rocks of the Rodeio-Rio da Luz Suite are geochemically classified as granites, with some samples of tonalite, granodiorite and quartz-monzonite composition.

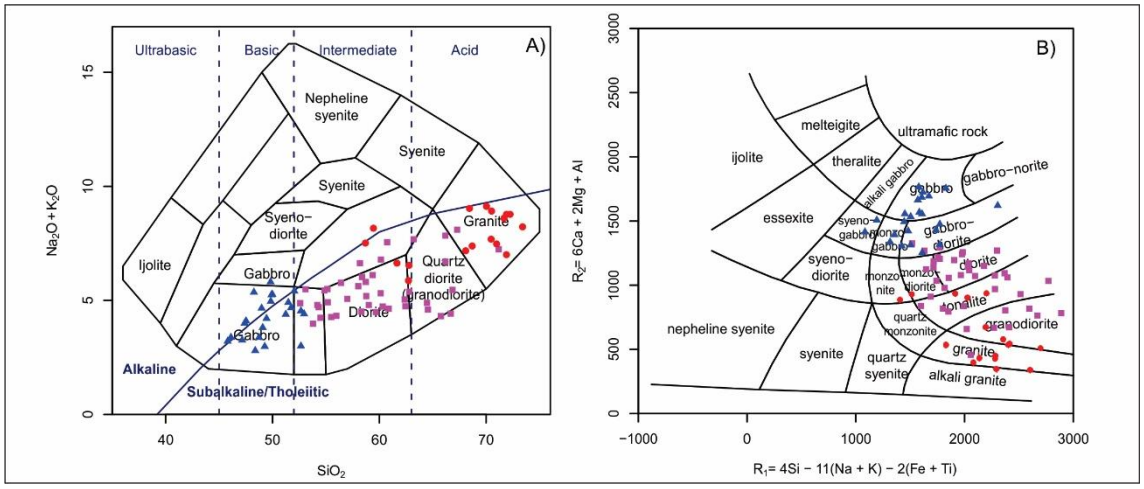

Figure 5: diagrams to geochemistry classification. A) TAS by Cox et al., (1979). B) R1R2 by De la Roche et al., (1980). Blue triangles: mafic granulites; purple squares: felsic granulites; red balls: opx-bearing granites.

In the AFM diagram (Fig. 6a) samples cluster along the calc-alkaline trend, with few samples in the tholeiitic field. According to the alkalinity index of Shand (1943) these rocks are mostly metaluminous, with few peraluminous samples (Fig. 6b). In the Harker diagrams (Fig. 7) samples show negative trends with most of the major elements with increasing silica. Exceptions are the positive correlation for K_2O, and the random pattern for Na_2O.

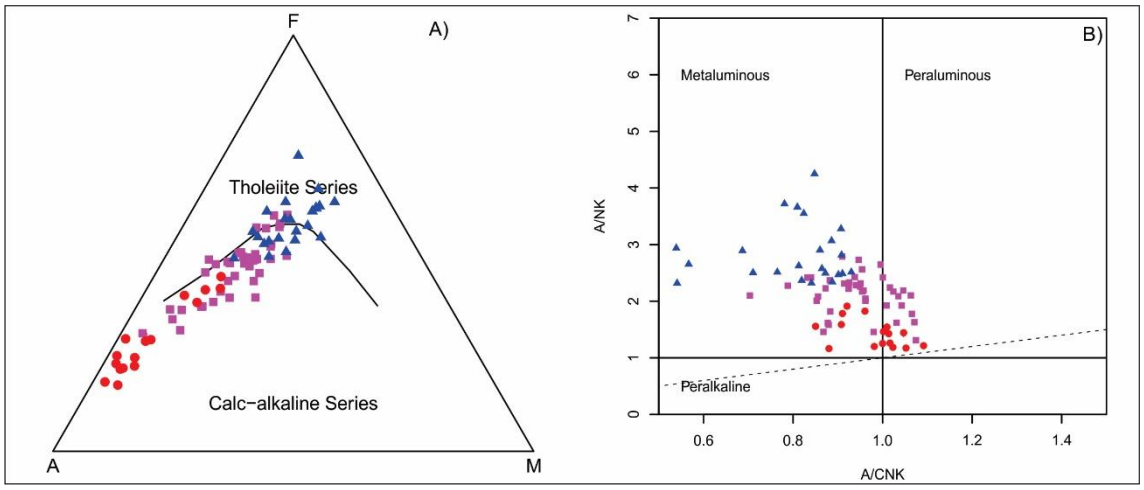

Figure 6: diagrams to geochemistry classification. A) AFM by Irvine and Baragar, (1971). B) alkaline index by Shand (1943). Blue triangles: mafic granulites; purple squares: felsic granulites; red balls: opx-bearing granites.

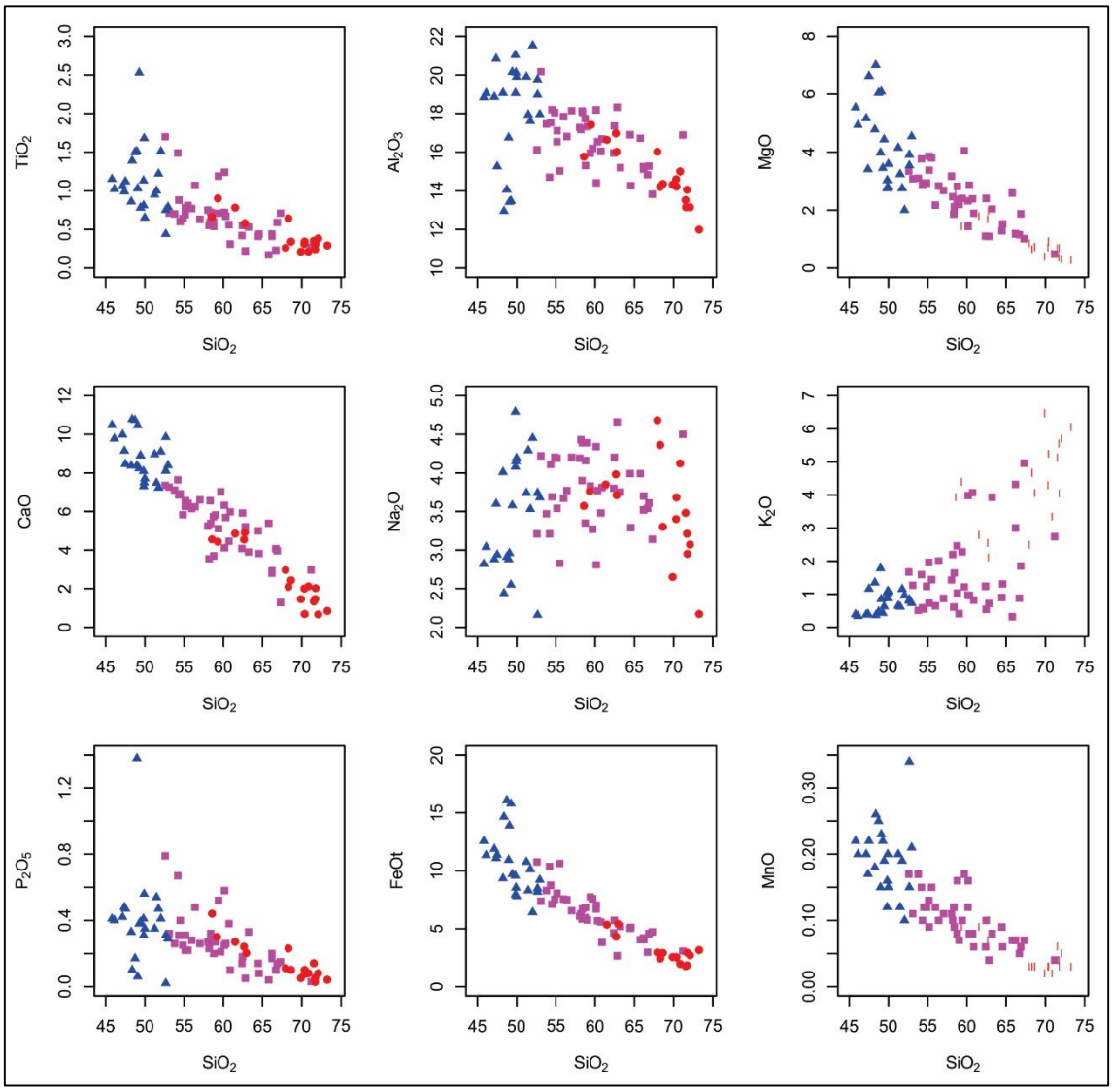

Figure 7: Harker diagrams. Blue triangles: mafic granulites; purple squares: felsic granulites; red balls: opx-bearing granites.

In the primitive mantle-normalized multielement diagram for trace elements (Fig 8a) mafic granulites have a strong negative Ti anomaly in some samples, and moderate negative Th and Ta anomalies, whereas with moderate positive Ba anomaly. In the chondrite-normalized diagram for REE (Fig 8b) the same rocks show slight enrichment in REE, with enriched MORB-like pattern (E-MORB) and moderate negative Eu anomaly. Trace elements normalized to the primitive mantle for felsic granulites (Fig 9a) behave very similarly to mafic granulites. Some samples have a strong negative Ti anomaly, with moderate negative Th anomaly, and moderate positive Ba and La anomalies. In the chondrite-normalized diagram for REE (Fig. 9b) the felsic granulites have a REE-enriched pattern, most samples having moderate

negative Eu anomaly, some positive. The opx-bearing metagranites normalized to the primitive mantle (Fig.10a) show uniform anomalies in their sample set. They show positive anomalies for Ba and Th, and negative ones for Nb, Ta, P and Ti, which by comparison, is a similar behavior observed in felsic granulites. In the chondrite-normalized REE (Fig. 10b) the opx-bearing metagranites show a highly enriched REE pattern with moderate negative Eu anomalies in most samples. Again the felsic granulites and opx-bearing metagranites show very similar patterns, with their REE geochemical signatures similar to those of calc-alkaline rocks, as well as of orthoderived granulites, charnokites, and slight TTG-like tendency (Moyen and Martin, 2012; Kumar et al., 2016).

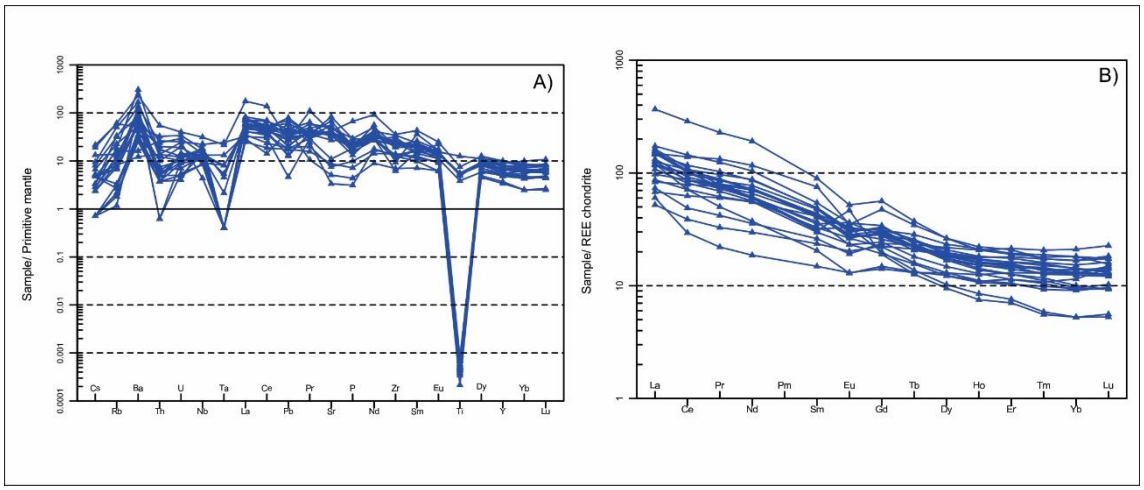

Figure 8: multielement spidergram to mafic granulites. A) trace elements primitive mantle normalized (McDonough and Sun, 1995). B) REE chondrite normalized (Boynton, 1984).

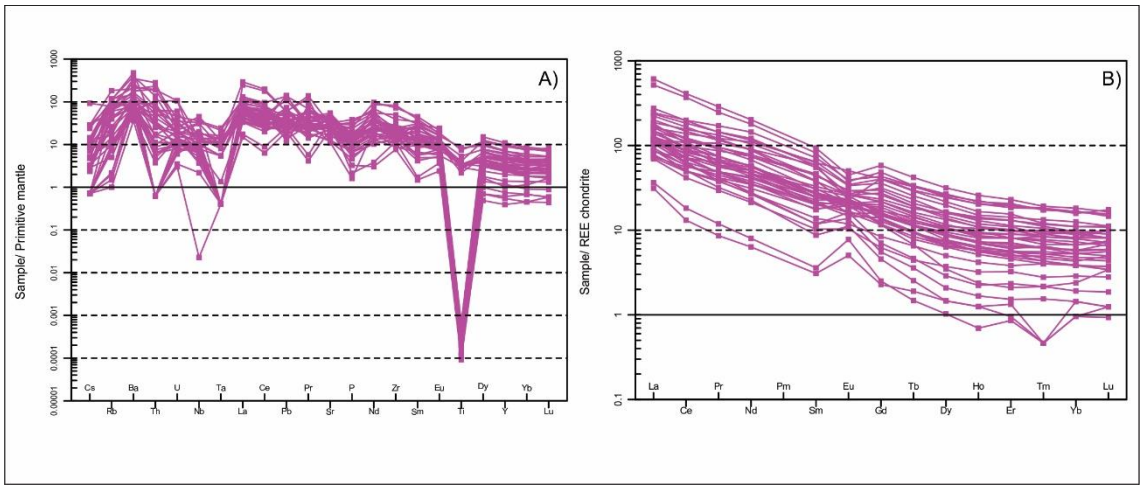

Figure 9: multielement spidergram to felsic granulites. A) trace elements primitive mantle normalized (McDonough and Sun, 1995). B) REE chondrite normalized (Boynton, 1984).

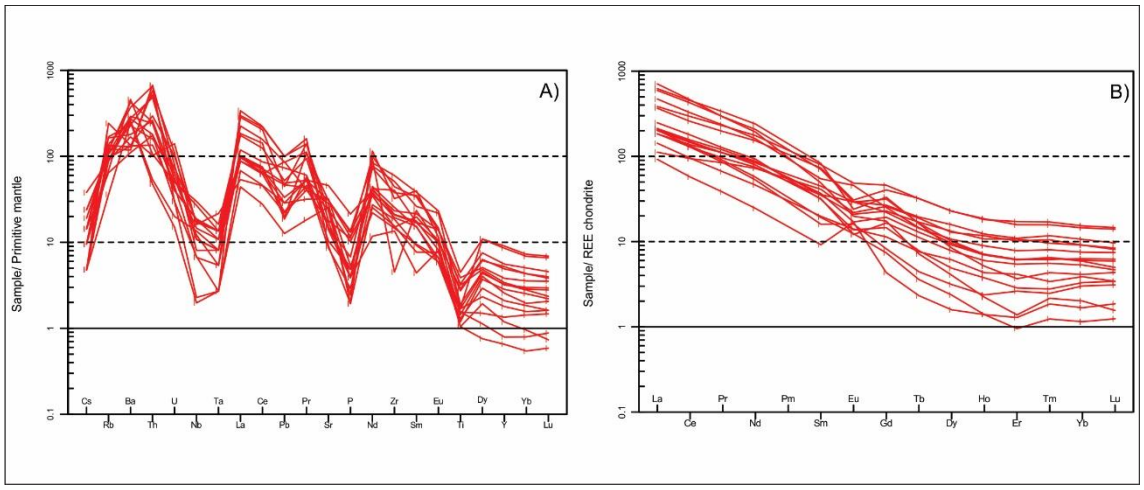

Figure 10: multielement spidergram to opx-bearing granites. A) trace elements primitive mantle normalized (McDonough and Sun, 1995). B) REE chondrite normalized (Boynton, 1984).

The felsic granulites and opx-bearing metagranites were plotted together in two ternary diagrams, the An-Ab-Or normative compositions diagram (O'Connor, 1965), and the Na-K-Ca cationic diagram (Figs. 11a and 11b). In the An-Ab-Or diagram of normative compositions (Fig. 11a) it is demonstrated that the compositions of these rocks are tonalitic to granitic, without trondhjemitic compositions. And in the Na-K-Ca cationic diagram (Fig. 11b) these rocks also showed their calc-alkaline character, without evidence of trondhjemitic or sodic trend.

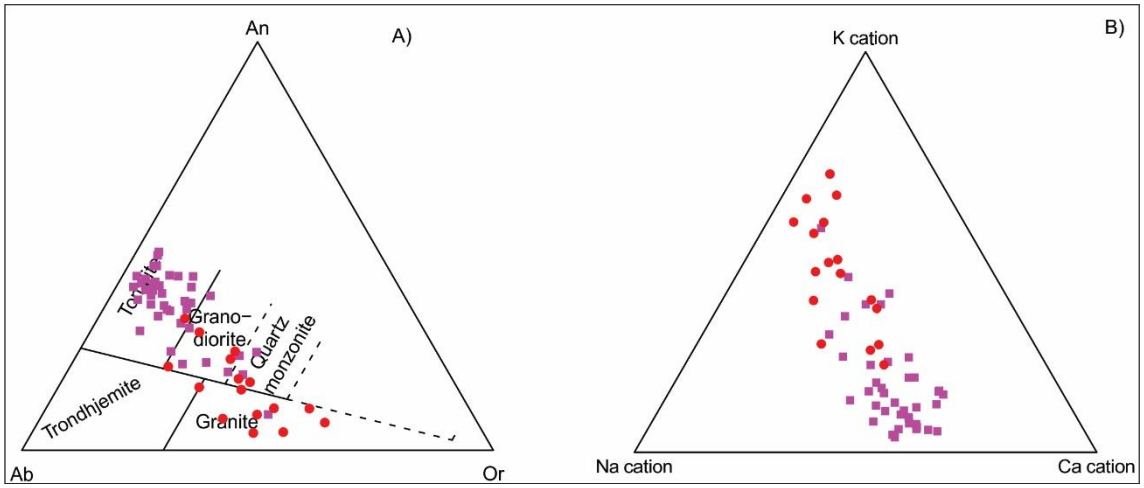

Figure 11: ternay plots to identify calc-alkaline trend. A) An-Ab-Or normative compositions diagram (O'Connor, 1965). B) Na-K-Ca cationic diagram, enrichment in K is calc-alkaline trend. Purple squares: felsic granulites; red balls: opx-bearing granites.

4.2.2. Geotectonic Interpretation

For tectonic interpretation we used the ternary diagrams MgO-FeOt-Al2O3 (Pearce et al., 1977) and Zr/Nb/Y (Meschede, 1986), and discriminant functions diagrams (DF1 x DF2; Agrawal (2008)) for mafic granulites. These rocks show orogenic affinity (Fig. 12a), corresponding with volcanic arc basalts (Fig. 12b, group C). In addition, mafic granulites show good affinity (Fig. 13) with ocean island basalts (OIB) and continental rift basalts (CRB) environments, and little affinity with MORB, and island arc basalts (IAB).

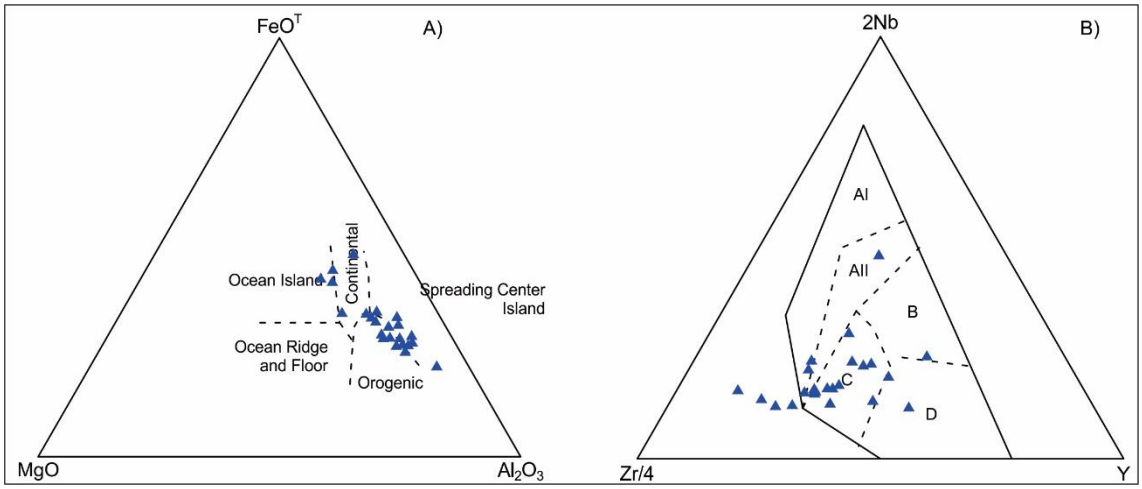

Figure 12: ternary plots to tectonic mafic rocks tectonic interpretation. A) MgO-FeOt-Al2O3 (Pearce et al., 1977). B) Zr/Nb/Y (Meschede, 1986).

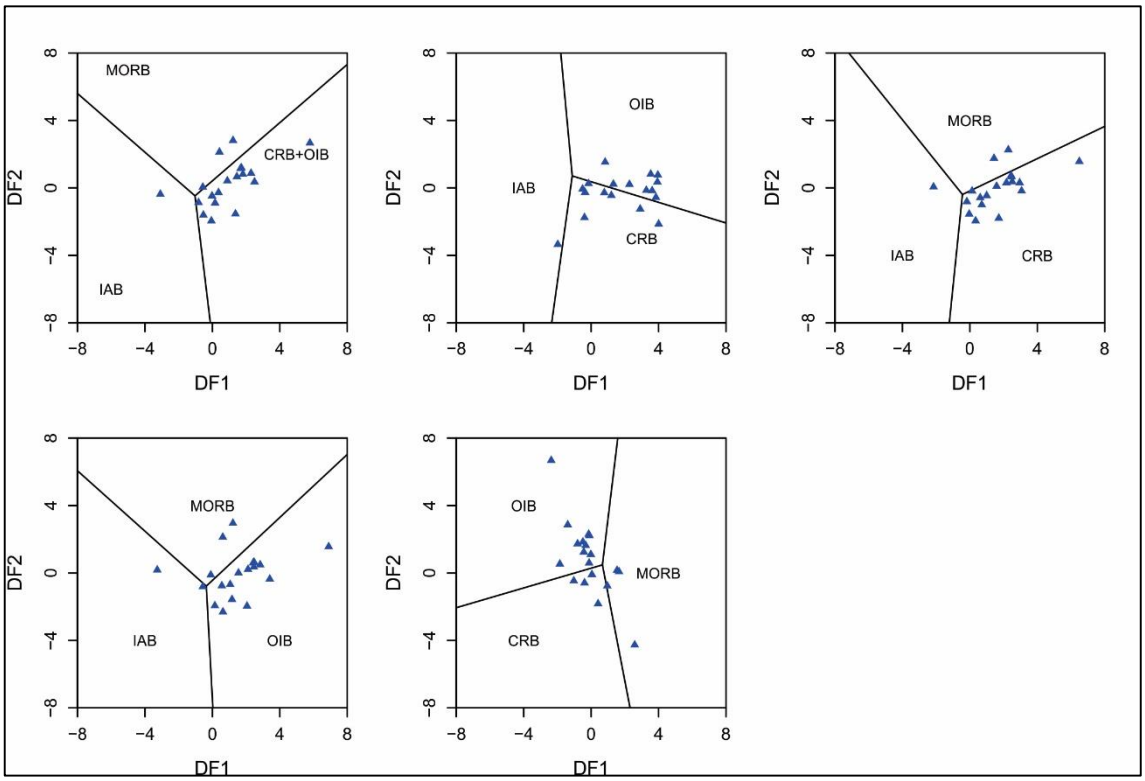

Figure 13: discriminant functions diagrams DF1 x DF2 to mafic rocks tectonic interpretation, Agrawal (2008).

Felsic granulites and opx-bearing metagranites are compatible with volcanic arc rocks (Figs. 14 and 15). Using the MALI index of Frost et al. (2008), most felsic granulites and opx-bearing metagranite samples are more calc-alkalic, however ranging through the entire geochemical spectrum from calcic to alkali-calcic (Fig. 16a) with magnesium affinity (Fig. 16b). In the Batchelor's R1-R2 diagram (Fig. 17a) these rocks plot dominantly in the fields of pre-collisional to syn-collisional environments. To test the possibility of these rocks being Archean island arcs the Ybn x (La/Yb)n diagram (Fig. 17B) was constructed, confirming that possibility. In the ternary diagram of Cabanis (1989) granulites and metagranites group in a trend towards acid, LREE-enriched, orogenic rocks (Fig. 18a). In order to verify the source protoliths of felsic granulites and opx-bearing metagranites, we used the Laurent diagram (2014; Fig. 18b). Felsic granulites show affinity with both of low- and high-K mafic rock sources. The opx-bearing metagranites, on the other hand, showed affinity with alkalis and plot in the metasediment melting field, representing a reworking continental crust source.

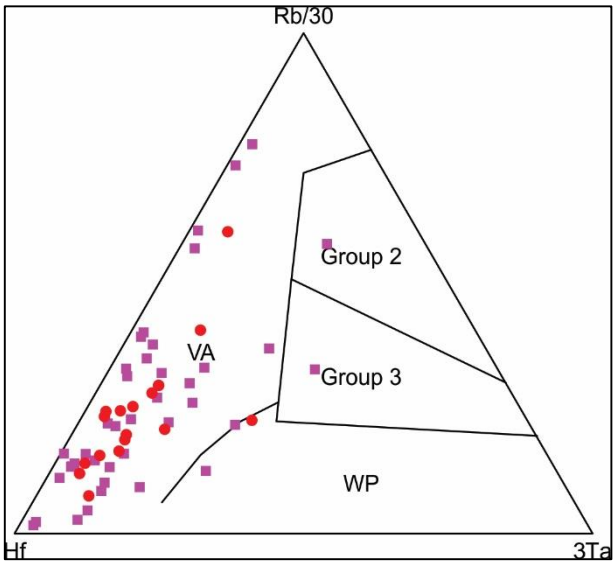

Figure 14: ternary plots to granitoids tectonic interpretation (Harris et al.,1986). Purple squares: felsic granulites; red balls: opx-bearing granites.

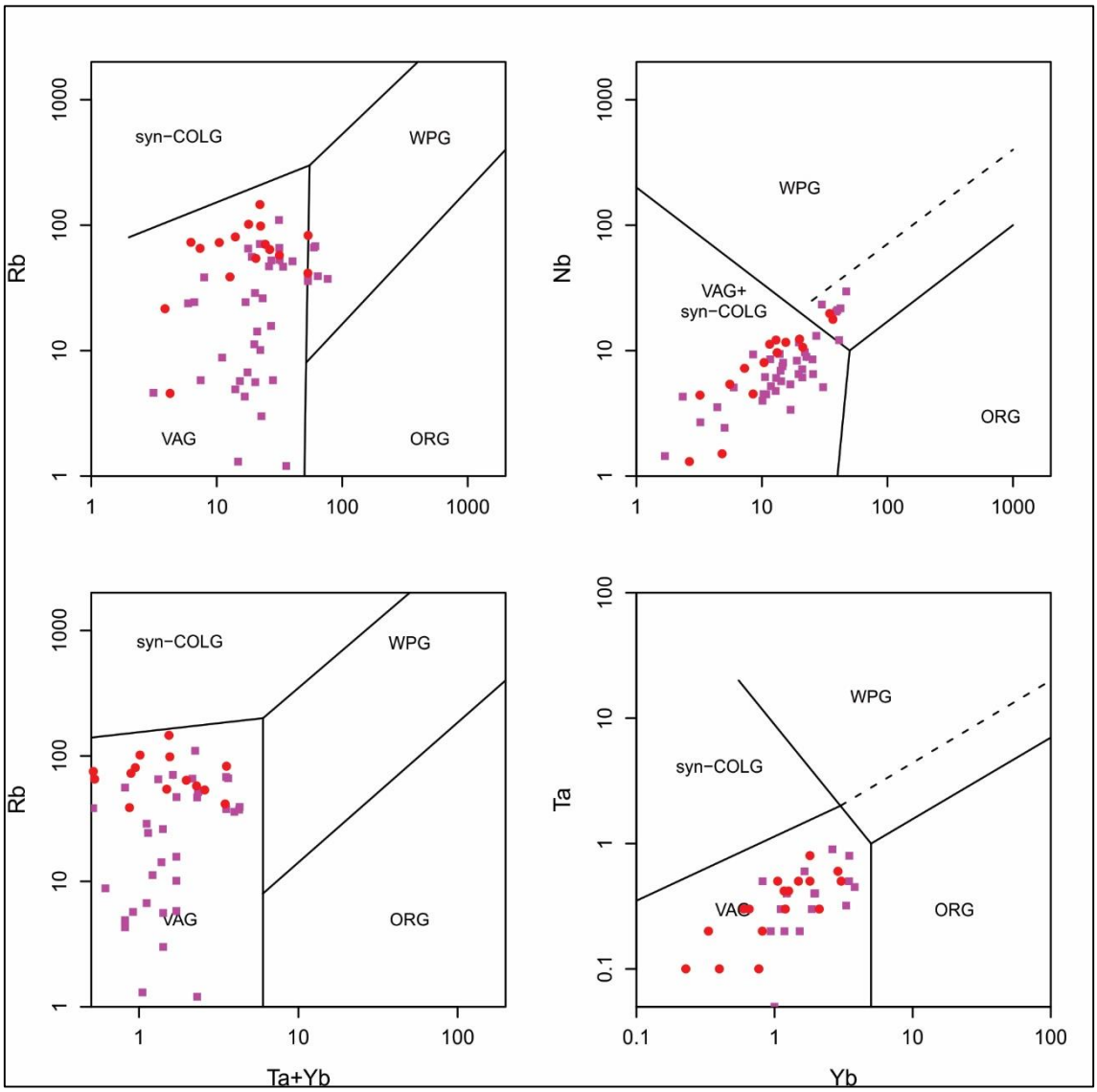

Figure 15: granitoids tectonic discrimination diagrams (Pearce et al., 1984). Purple squares: felsic granulites; red balls: opx-bearing granites.

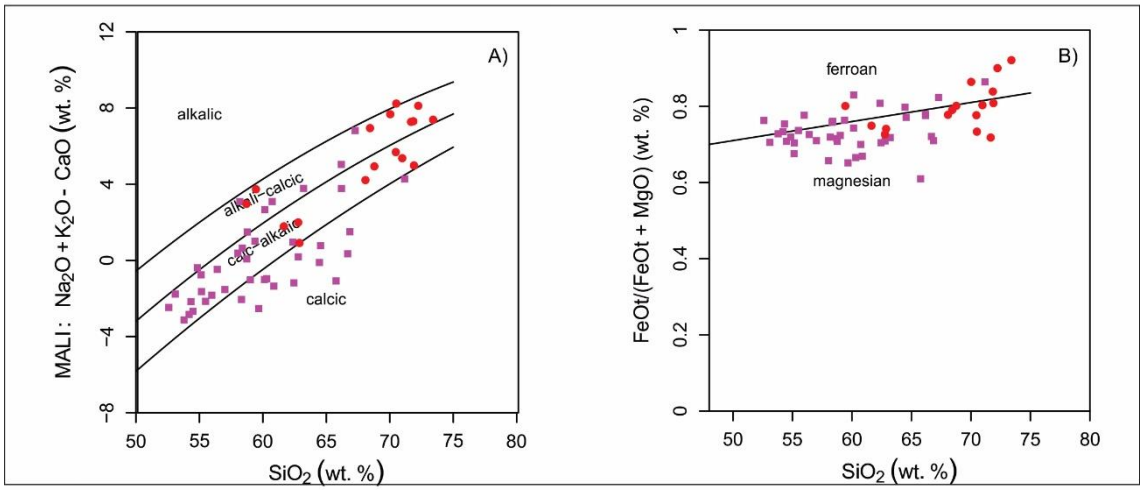

Figure 16: granitoids tectonic discrimination diagrams (Frost and Frost, 2008). Purple squares: felsic granulites; red balls: opx-bearing granites.

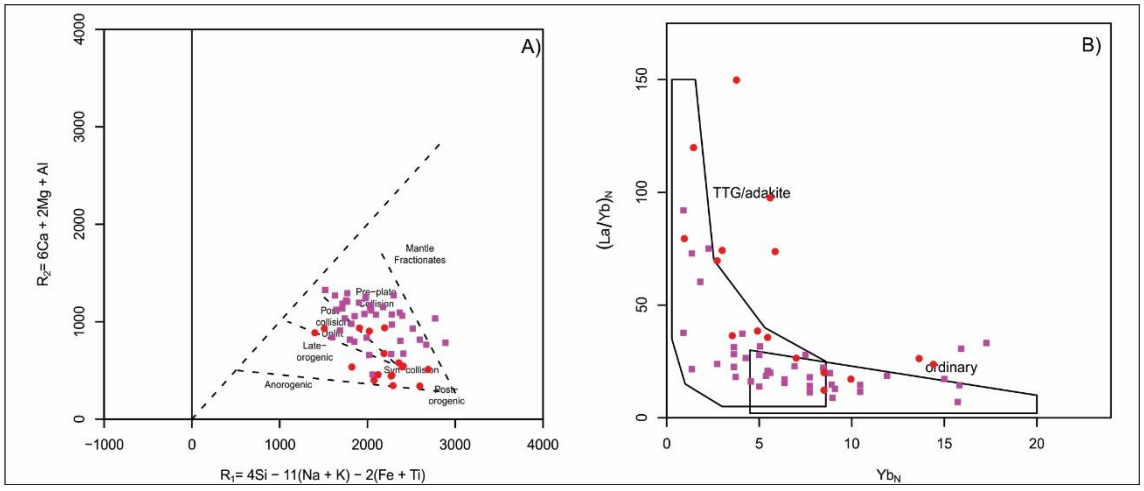

Figure 17: plots to granitoids tectonic interpretation. A) R1-R2 (Batchelor and Bowden, 1985). B) Ybn x (La/Yb)n diagram (Martin, 1986). Purple squares: felsic granulites; red balls: opx-bearing granites.

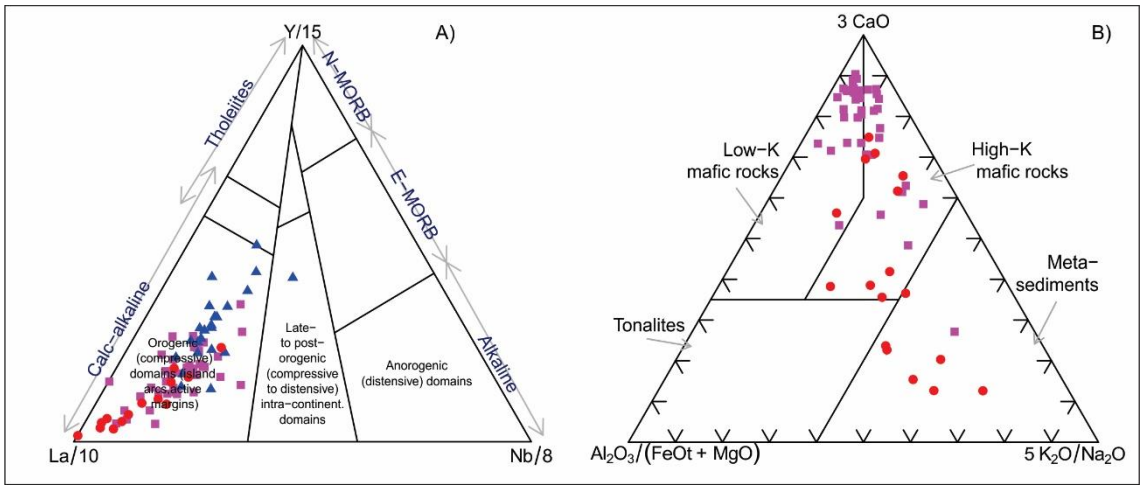

Figure 18: ternary plots to tectonic and source interpretation. A) tectonic diagram, Cabanis (1989). B) source diagram Laurent (2014). Blue triangles: mafic granulites; purple squares: felsic granulites; red balls: opx-bearing granites.

5. Discussion

5.1. Luis Alves Orthogneiss: mafic and felsic orthogranulites

Mafic and felsic granulites crops out in different ways and have complex relationships, where the felsic one predominates volumetrically within the SCGC and the LAC (Fig. 1).

Mafic granulites occur as metric-width bands within the felsic granulite and as rare isolated metric bodies. Previously, mafic granulites were grouped with metapyroxenites within a mafic-ultramafic unit (Iglesias, 2011, Betiollo, 2018). However, field relationships and geochemical behavior point to a genetic affinity with their felsic counterparts rather than with ultramafic rocks. This assumption is supported by a set of geochemical diagrams (Figs. 5, 6, 7, 8a and 8b) where both granulite types show superposing patterns or trends, suggesting a genetic correlation such as fractional crystallization. Regarding the geotectonic interpretation, mafic granulites showed constant affinity with basic rocks generated in an orogenic environment. Most of the diagrams demonstrated correlation with an island arc environment (Fig. 12), a characteristic also demonstrated by their calc-alkaline trend (Fig. 18a), pointing to subduction settings that may evolve to collisional/orogenic scenarios. By the diagrams of Agrawal (2008) with discriminant function (Fig. 13), the mafic granulites showed more affinity with environments of oceanic islands and rift (or backarc basins), which

in the LAC regional context is also plausible since there are associations with BIF (Betiollo et al., submitted).

The felsic granulites show even stronger affinity with granites formed in volcanic arc environments (Figs. 14 and 15). Taking into account the Neoarchean-Paleoproterozoic age of these rocks, the affinity of felsic granulites with Archean island arc environment is demonstrated (Fig. 17b). The calc-alkaline affinity of the subduction environment is also indicated by the calc-alkaline trend (Figs. 11a and 11b). The fact that these rocks are classified as magnesian and calcic with calc-alkalic affinity (Figs. 16) reinforces the link with Archean subduction environments. Further corroborating these interpretations, the studied granulites have collisional environment affinity (Figs. 17 and 18). We also interpret that felsic granulites are products of partial melting of mafic rocks (Figs.18b), which converges with the island arc model with subduction of oceanic crust.

5.2. Opx-bearing metagranites from Rodeio-Rio da Luz Suite

The opx-bearing metagranites of the Rodeio-Rio da Luz Suite have an intrinsic field relationship with the felsic granulites. They occur in the southwest of the area and contacts between units are not normally observed. The few contacts observed were diffuse, showing a certain physical interaction between those rocks. They also showed a very similar geochemical behavior regarding major, trace and REE elements, in addition to most of samples trending in several diagrams. Indeed, both lithotypes behave as representative of the most evolved magmatic series terms (Figs. 5, 6, 7, 10, 11, 17 and 18).

Primitive mantle-normalized trace element signature (Figs. 10a) of opx-bearing metagranites is quite similar to felsic granulites in concentrations and patterns. On the other hand, REE normalized to chondrite (Figs. 10b) are highly enriched in LREE, corroborating more evolved rock patterns. The geotectonic interpretation for both units (Figs. 15, 16, 17 and 18) is quite similar towards orogenic, volcanic arc or island arc environments typically containing SiO_2- and REE-rich terms. They show magnesian affinity (Fig.16a) demonstrating the origin of their protolith, which evolved from melting of mafic rocks from the oceanic crust in island arc setting with calc-alkaline to alkali-calcic signature (Fig. 16b). The sources for the original granites are much probably continental crust melting (Fig. 18b) since they are alkalis-enriched and plot in the

metasediment melting field, while felsic granulites may have originated from basic rock melting.

5.3. Neoarchean – Rhyacian tectonic settings and evolution

This dataset leads us to interpret the following scenario for the genesis of mafic and felsic granulites and opx-bearing metagranites. We propose an island arc was established in the Neoarchean, with an adjacent sedimentary basin with siliciclastic and chemical sedimentation, evidenced by rocks of the Joinville Metasedimentary Sequence (Betiollo et al., submitted). The protoliths of mafic and felsic orthogranulites may have mostly generated during the subduction period, including participation of oceanic crust melting. After this island arc scenario with bimodal magmatism, adjacent sedimentary basin may have closed, and the original igneus rocks experienced subduction and ultimately granulite-facies metamorphism. Currently, there is a consensus in the fields of metamorphic petrology and geotectonic that the conditions for granulite metamorphism in medium-large terrains such as the LAC have great correspondence with the formation of orogenic plateaus and supercontinent amalgamation (Brown, 2007; Brown and Johnson, 2019 ; Chardon et al., 2009; Harley, 1992; Jamieson and Beaumont, 2013). Along with granulite metamorphism, partial melting of felsic granulites, perhaps with influence of metasedimentary rocks (Fig. 18b), the original opx-bearing granites of the Rodeio-Rio da Luz Suite may have emplaced in the crust.

In summary, our data points that the LAC represents a record of a Large Hot Orogen settled in this area during the Siderian-Rhyacian. This orogen culminated in the formation of a plateau that provided the P-T conditions for the generation of granulites in the middle-lower crust. The exhumation of these rocks occurred in an extensional event after the collapse of this orogen and the plateau, with the formation of a Metamorphic Core Complex (Betiollo et al., submitted), where metamafic-ultramafic, metafelsic, and metasedimentary siliciclastic rocks, BIFs and metagranites are currently exposed, in a complex structural framework that build the current LAC granulite terrain in Southern Brazil.

6. Conclusions

Gathering information from the field, petrography, and lithogeochemistry, we conclude that:

- the mafic and felsic granulites of the Luis Alves Orthogneiss demonstrate affinities in the field and in the lithogeochemical results;

- likewise, the opx-bearing metagranites of the Rodeio-Rio da Luz Suite have lithogeochemical signatures and patterns coincident with those of the felsic granulites;

- all lithotypes showed affinity with orogenic environments, highlighting an island arc setting for their genesis;

- subduction in such island arc generated partial melting and bimodal magmatism, both mafic and felsic granulites being products of partial melting of an Archean oceanic crust;

- when subduction ceased, with the total consumption of oceanic crust and the adjacent basin closed, a Large Hot Orogen was established forming an orogenic plateau;

- the orogenic plateau supported the P-T conditions for the granulite metamorphism and the partial melting of the felsic granulites triggered the generation of the Rodeio-Rio da Luz Suite granites;

- with the collapse of the Large Hot Orogen and the plateau, the exhumation of the studied rocks occurred in an extensional event during the Rhyacian, within a Metamorphic Core Complex context.

Acknowledgments

Leandro M. Betiollo thanks the Geological Survey of Brazil (SGB – CPRM) for providing the data and supporting the development of his Ph.D. thesis, and to the SGB – CPRM staff for their support during fieldwork, petrographic descriptions, figure elaborations and geological debates. Everton M. Bongiolo is grateful to Conselho Nacional de Desenvolvimento Científico e Tecnológico (CNPq) for his Productivity on Research grant (# 311106/2020-0).

References

Agrawal S, Guevara M, Verma S., 2008. Tectonic discrimination of basic and ultrabasic volcanic rocks through log-transformed ratios of immobile trace elements. Int Geol Review 50: 1057-1079. doi: 10.2747/00206814.50.12.1057

Barker, F., 1979. Trondhjemite; definition, environment and hypotheses of origin. In _____. (Ed.), Trondhjemites, dacites and related rocks. Amsterdam: Elsevier, p. 1-12. (Developments in Petrology, v. 6)

Basei, M.A.S.; MacReath, L.; Siga Júnior, O., 1998. The Santa Catarina Granulite Complex of Southern Brazil: a review. Gondwana Res., 1, 3-4, 383-391. https://doi.org/10.1016/S1342-937X(05)70854-6

Basei, M.A.S., Nutman, A., Siga Júnior, O., Passarelli, C.R., and Drukas, C.O., 2009. The evolution and tectonic setting of the Luis Alves Microplate of Southeastern Brazil: an exotic terrane during the assembly of Western Gondwana. *In*: Gaucher, C., Sial, A.N., Halverson, G.P., and Frimmel, H.E. (Eds): Neoproterozoic-Cambrian Tectonics, Global Change and Evolution: a focus on southwestern Gondwana. Developments in Precambrian Geol., 16, Elsevier, pp. 273-291. https://doi.org/10.1016/S0166-2635(09)01620-X

Basei, M.A.S., Drukas, C.O., Nutman, A.P., Wemmer, K., Dunyi, L., Santos, P.R., Passarelli, C.R., Campos Neto, M.C., Siga Jr O., Osako, L., 2011. The Itajaí foreland basin: A tectono-sedimentary record of the Ediacaran period, Southern Brazil. Int. J. Earth Sci., 100, 543-569. https://www.doi.org/10.1007/s00531-010-0604-4.

Batchelor, R. A., Bowden, P., 1985. Petrogenetic interpretation of granitic rock series using multicationic parameters. Chemical Geology, v.48, p.43-55.

Betiollo, L.M., Iglesias, C.M.F., Rocha, P.G., 2018. Integração geológica-geofísica e recursos minerais do Cráton Luis Alves: mapa de integração geológica-geofísica. Porto Alegre: CPRM, 1:250.000, http://rigeo.cprm.gov.br/jspui/handle/doc/16802 (April 2022).

Bitencourt, M.F., Nardi, L.V.S., 2000. Tectonic setting and sources of magmatism related to the Southern Brazilian Shear Belt. Rev. Bras. Geociênc., 30-1, 186-189.

Brito Neves, B.B., 2011. The Paleoproterozoic in the South-American continent: Diversity in the geologic time. J. South Am. Earth. Sci., 32, 270-286. https://doi.org/10.1016/j.jsames.2011.02.004

Boynton, W. V., 1984. Cosmochemistry of the rare earth elements: meteorite studies. In: HENDERSON, P. (Ed.) Rare Earth Element Geochemistry. Amsterdam: Elsevier, p.63-114.

Brown, M., 2007a. Metamorphism, plate tectonics, and the supercontinent cycle. Earth Sci. Front., 14, 1-18. https://doi.org/10.1016/S1872-5791(07)60001-3

Brown, M., 2007b. Metamorphic conditions in orogenic belts: a record of secular change. Int. Geol. Rev. 49, 193-234. http://dx.doi.org/10.2747/0020-6814.49.3.193

Brown, M., Johnson, T., 2019. Time's arrow, time's cycle: Granulite metamorphism and geodynamics. Miner. Mag., 83, 323–338, https://doi.org/10.1180/mgm.2019.19.

Bruno, H., Almeida, J., Heilbron, M., Salomão, M., Cury, L., 2018. Architecture of major Precambrian tectonic boundaries in the northern part of the Dom Feliciano Orogen, southern Brazil: Implications for the West Gondwana amalgamation. J. South Am. Earth. Sci., 86, 301-317, https://doi.org/10.1016/j.jsames.2018.06.018.

Cabanis, B., Lecolle, M., 1989. Le diagramme La/10-Y/15-Nb/8: un outil pour la discrimination des séries volcaniques et la mise en évidence des processus de mélange et/ou de contamination crustale. CR Acad Sci IIA 309: 2023-2029.

Campos, R.S., Philipp, R.P., Massonne, H.J., Chemale, F., Theye, T., 2012. Petrology and isotope geology of mafic to ultramafic metavolcanic rocks of the Brusque Metamorphic complex, southern Brazil. Int. Geol. Rev., 54-6, 686-713. https://doi.org/10.1080/00206814.2011.569393

Chardon, D., Gapais, D., Cagnard, F., 2009. Flow of ultra-hot orogens: a view from the Precambrian, clues for the Phanerozoic. Tectonophysics, 477, 105-118. https://doi.org/10.1016/j.tecto.2009.03.008

Citroni, S. B. et al., 2001. Volcanism and Stratigraphy of the Neoproterozoic Campo Alegre Basin, SC, Brazil. Anais da Academia Brasileira de Ciências, v.73, n.4, p.581-597.

Cox, K.G., Bell, J. D., Pankhurst, R. J., 1979. The Interpretation of Igneous Rocks. Allen and Unwin, London, 450 p.

Cury, L.F., 2009. Geologia do Terreno Paranaguá. Tese (Doutorado) - Programa de Pós-Graduação em Geoquímica e Geotectônica, Universidade de São Paulo, São Paulo,187 p.

De La Roche, H.; Leterrier, J.; Grandclaud, P. & Marchal, M. 1980. A classification of volcanic and plutonic rocks using R1-R2 diagrams and major elements analysis - its relationships with current nomenclature. Chemical Geology. 29:183-210.

Fernandes, J.F., Iyer, S.S., Imakuma, K., 1987. Geochemical studies in the proterozoic metamorphic terrane of the Guaxupé Massif, Minas Gerais, Brazil. A discussion

on large ion lithophile element fractionation during highgrade metamorphism. Precambrian Research, 36, 65-79.

Florisbal, L.M., Janasi, V.A., Bitencourt, M.F., Heaman, L.M., 2012. Space–time relation of post-collisional granitic magmatism in Santa Catarina, southern Brazil: U–Pb LAMC-ICP-MS zircon geochronology of coeval mafic-felsic magmatism related to the Major Gercino Shear Zone. Precambrian Res., 216, 132–15. https://doi.org/10.1016/j.precamres.2012.06.015

Frost B.R., Frost, C.D., 2008. A geochemical classification for feldspathic igneous rocks. J Petrol 49:1955-1969. doi: 10.1093/petrology/egn054

Guadagnin, F., Chemale Jr, F., Dussin, I.A., Jelinek, A.R., dos Santos, M.N., Borba, M.L., Justino, D., Bertotti, A.L., Alessandretti, L., 2010. Depositional age and provenance of the Itajaí Basin, Santa Catarina State, Brazil: Implications for SW Gondwana correlation. Precambrian Res., 180, 3-4, 156-182. https://doi.org/10.1016/j.precamres.2010.04.002.

Gualda, G. A. R.; Vlach, S. R. F., 2007. The Serra da Graciosa A-type Granites and Syenites, southern Brazil: part 1, regional setting and geological characterization. Anais da Academia Brasileira de Ciências, v. 79, n. 3, p.405-430.

Harley, S.L., 1992. Proterozoic Granulite Terranes. *In* Condie, K.C., ed., Proterozoic Crustal Evolution, Elsevier, v. 10, p. 301-359. https://doi.org/10.1016/S0166-2635(08)70122-1

Harris, N. B. W.; Pearce, J. A.; Tindle, A. G., 1986. Geochemical characteristics of collision-zone magma-tism. In: COWARD, M. P.; RIES, A. C. (Ed.) Collision Tectonics. London: Geological Society London, p.67-81. (Geological Society London Special Publication, 19).

Hartmann, L.A., Silva, L.C., Orlandi F°, V., 1979. O Complexo Granulítico de Santa Catarina: descrição e implicações genéticas. Acta Geológica Leopoldensia, São Leopoldo, 6, 93-112.

Hartmann, L.A., Santos, J.O.S., McNaughton, N.J., Vasconcellos, M.A.Z., Silva, L.C. da, 2000. Ion microprobe (SHRIMP) dates complex granulite from Santa Catarina, southern Brazil. An. Acad. Bras. Ciênc., 72-4, 559-572. https://doi.org/10.1590/S0001-37652000000400007

Heilbron, M., Valeriano, C.M., Tassinari, C.C.G., Almeida, J., Tupinambá, M., Siga Jr., O., Trouw, R., 2008. Correlation of Neoproterozoic terranes between the Ribeira Belt, SE Brazil and its African counterpart: comparative tectonic evolution and open questions. *In* Pankhurst, R.J., Trouw, R.A.J., Brito Neves, B.B., De Wit, M.J.,

(eds) West Gondwana: Pre-Cenozoic Correlations Across the South Atlantic Region. Geological Society, London, Special Publications, 294, 211–237. https://doi.org/10.1144/SP294.12

Heller, B.M., Hueck, M., Passarelli, C.R., Basei, M.A.S., 2021. Zircon U-Pb geochronology and Hf isotopes of the Luís Alves Terrane: Archean to Paleoproterozoic evolution and Neoproterozoic overprint. J. South Am. Earth. Sci., 106, 103008, https://doi.org/10.1016/j.jsames.2020.103008.

Iglesias, C.M.F., Zerfass, H., Silva, M.A.S., Klein, C., 2011. Geologia e recursos minerais da Folha Joinville - SH. 22−Z−B, 1:250.000, Estado de Santa Catarina. Porto Alegre: CPRM, http://rigeo.cprm.gov.br/jspui/handle/doc/17685 (April 2022).

Irvine, T. M.; Baragar, W. R., 1971. A guide to the chemical classification of common volcanic rocks. Ca-nadian Journal of Earth Sciences, v.8, p. 523-548.

Jamieson, R.A., Beaumont, C., 2013. On the origin of orogens. Bull. Geol. Soc. Am., 125, 1671–1702. https://doi.org/10.1130/B30855.1

Kaul, P.F.T., 1980. O Cráton de Luis Alves. In: Congresso Brasileiro De Geologia, 31, Balneário Camboriú, Anais, SBG, v. 5, p. 2677-2683.

Kaul, P. F. T., 1984. Significado dos granitos anorogênicos da Suíte Intrusiva Serra do Mar na evolução da crosta do sul-sudeste do Brasil, no âmbito das Folhas SG-22 - Curitiba e SG-23 - Iguape. In: CONGRESSO BRASILEIRO DE GEOLOGIA, 33., 1984, Rio de Janeiro. Anais... Rio de Janeiro: SBG, v.6, p.2815-2825.

Kumar, G.R.R., Sreejith, C., 2016. Petrology and geochemistry of charnockites (felsic ortho-granulites) from the Kerala Khondalite Belt, Southern India: Evidence for intra-crustal melting, magmatic differentiation and episodic crustal growth. Lithos, 262, 334–354. https://doi.org/10.1016/j.lithos.2016.07.009

Laurent, O., Martin, H., Moyen, J.F., Doucelance, R., 2014. The diversity and evolution of late-Archean granitoids: evidence for the onset of 'modern-style' plate tectonics between 3.0 and 2.5 Ga. Lithos. 205:208-235 doi: 10.1016/j.lithos.2014.06.012

Martin, H., 1986. Effect of steeper Archean geothermal gradient on geochemistry of subduction-zone magmas. Geology 14: 753-756 doi: 10.1130/00917613(1986)14<753:EOSAGG>2.0.CO;2

Martin, L., Suguio, K., 1986. Excursion Route along the Coastal Plains of the States of Paraná and Santa Catarina. In: INTERNATIONAL SYMPOSIUM ON SEA LEVEL CHANGES AND QUATERNARY SHORELINES, São Paulo. Special Publication… São Paulo: s.n. 124 p.

McDonough, W.; Sun, S. S., 1995. The composition of the Earth. Chemical Geology, v.120, p.223-253.

Meschede, M., 1986. A method of discriminating between different types of mid-ocean ridge basalts and continental tholeiites with the Nb-Zr-Y diagram. Chemical Geology, v.56, p.207-218.

Moyen, J.-F., Martin, H., 2012. Forty Years of TTG Research. Lithos, 148, 312-336. https://doi.org/10.1016/j.lithos.2012.06.010

O'Connor, J. T., 1965. A classification for quartz-rich igneous rocks based on feldspar ratios. US Geological Survey, Professional Papers, v. 525- B, p.79-84.

Passarelli, C.R., Basei, M.A.S., Wemmer, K., Siga Jr., O., Oyhantçabal, P., 2011. Major shear zones of southern Brazil and Uruguay: escape tectonics in the eastern border of Rio de La plata and Paranapanema cratons during the Western Gondwana amalgamation. Int. J. Earth Sci. (Geol Rundsch), 100, 391-414, https://doi.org/10.1007/s00531-010-0594-2

Passarelli, C.R., Basei, M.A.S., Siga Jr., O., and Harara, O.M.M., 2018. The Luis Alves and Curitiba Terranes: Continental Fragments in the Adamastor Ocean. *In* Siegesmund, S., Basei, M.A.S., Oyhantçabal, P., Oriolo, S., eds., Geol. of Southwest Gondwana, Regional Geol. Rev., p. 189-215. https://doi.org/10.1007/978-3-319-68920-3_8

Pearce, T. H.; Gorman, B. E.; Birkett, T. C., 1977. The relationship between major element geochemistry and tectonic environment of basic and intermediate volcanic rocks. Earth Planetary Science Letters, v.36, p.121-132.

Pearce, J.A., Harris, N.W., Tindle, A.G., 1984. Trace element discrimination diagrams for the tectonic interpretation of granitic rocks. J Petrology 25: 956-983. doi: 10.1093/petrology/25.4.956.

Philipp, R.P., Mallmann, G., Bitencourt, M.F., Souza, E.R., Liz, J.D., Wild, F., Arend, S., Oliveira, A.S., Duarte, L.C., Rivera, C.B., Prado, M., 2004. Caracterização Litológica e Evolução Metamórfica da Porção Leste do Complexo Metamórfico Brusque, Santa Catarina. Rev. Bras. Geociênc., 34 (1), 21–34.

Rudnick, R.L., McLennan, S.M., Taylor, S.R., 1985. Large ion lithophile elements in rocks from high-pressure granulite facies terrains. Geochimica et Cosmochimica Acta, 49, 1645-1655.

Shand, S. J., 1943. The Eruptive Rocks. 2.ed. New York: John Wiley. 444 p.

6. Resultados, interpretações e discussão

O desenvolvimento desta Tese ficou alicerçada em três pilares principais, excetuando-se a aquisição de dados, que são (i) a integração e reinterpretação de dados disponíveis no banco de dados do Serviço Geológico do Brasil, (ii) a interpretação do levantamento aerogeofísico regional, e (iii) a geoquímica de rocha total das amostras para investigação petrológica.

Na integração e reinterpretação de dados disponíveis no banco de dados do Serviço Geológico do Brasil, em conjunto com o disponível na literatura e o mapeamento geológico efetuado por este autor, com papel fundamental da interpretação geoquímica, as unidades geológicas pertencentes ao Complexo Granulítico de Santa Catarina (CGSC), parte fundamental do Cráton Luis Alves (CLA), foram atualizadas e redefinidas em quatro unidades, que são (i) Complexo Ultramáfico Barra Velha, (ii) Ortognaisses Luis Alves, (iii) Sequência Metassedimentar Joinville e (iv) Suíte Rodeio-Rio da Luz.

Os litotipos presentes no CGSC dividem-se basicamente em metapiroxenitos, granulitos máficos, granulitos félsicos, granulitos pelíticos, rochas metassedimentares, formações ferríferas e metagranitoides. Os metapiroxenitos pertencem ao Complexo Ultramáfico Barra Velha, os granulitos máficos e félsicos pertencem à unidade Ortognaisses Luis Alves, os granulitos pelíticos, metassedimentares siliciclásticas e formações ferríferas estão agrupados na unidade Sequência Metassedimentar Joinville, por fim os metagranitos na unidade Suíte Rodeio-Rio da Luz.

O Complexo Ultramáfico Barra Velha anteriormente era considerado um complexo máfico-ultramáfico, onde os granulitos máficos e metapiroxenitos eram agrupados e considerados cogenéticos (Figueiredo *et al*., 1997). No entanto, dado o volume de amostras coletadas, pelas relações de campo e dados de litogeoquímica, essa cogeneticidade não se confirma, tendo inclusive os granulitos máficos mais familiaridade geoquímica com os granulitos félsicos. Outra mudança com relação ao disposto na bibliografia, é a ocorrência de magnetititos associados a metapiroxenitos, e que segundo Fornari (1998) seria interpretada como uma associação de rochas cumuláticas de um complexo estratiforme tipo Bushveld. No entanto esses magnetititos são aqui interpretados como meta-*BIFs* de fácies óxido com estrutura maciça, pois ocorrem no campo sempre associados com outros meta-*BIFs* de fácies óxido de estrutura bandada, como também com meta-*BIFs* de fácies silicato.

A Sequência Metassedimentar Joinville é uma nova nomenclatura aqui proposta, e é onde estão agrupados os quartzitos, granulitos pelíticos, e os *BIFs*, devido à correlação espacial dessas rochas em campo. Localizadamente o quartzito tem em sua composição mineralógica mica verde, além do quartzo. Os granulitos pelíticos são caracterizados por conterem silimanita e as vezes cordierita em sua composição mineralógica. Os *BIFs*, fruto de um estudo litogeoquímico nesta Tese, foram divididos em duas fácies (cf. James, 1954), fácies óxido e fácies silicato. A fácies óxido tem amostras compostas por quartzo e magnetita, estas com estrutura bandada, como também amostras enriquecidas em magnetita e pouquíssimo quartzo, estas de estrutura maciça. A fácies silicato tem em sua composição ferrosilita, quartzo, magnetita, espessartita, almandina e rara olivina. Essa mineralogia em *BIF* comprova que estas rochas foram submetidas a metamorfismo granulítico. Além disso, a presença de *BIF* fácies silicato demonstra a influência de sedimentação continental nessa paleobacia, influência também demostrada pelos dados litogeoquímicos.

Dentre as unidades do CGSC, os Ortognaisses Luis Alves possuem a maior área de exposição. Nesta unidade estão agrupados os granulitos máficos e félsicos, que tem correlação no campo e nos resultados litogeoquímicos. Os granulitos félsicos são o litotipo predominante em volume, os granulitos máficos são subordinados e ocorrem muitas vezes como bandas nos granulitos félsicos, ou como corpos isolados ocupando áreas maiores. Os granulitos félsicos tem composições mais tonalíticas enquanto os máficos tem composições gabróicas, ocorrendo também, localizadamente, quartzo-gabros.

Outra unidade proposta nesta Tese é a Suíte Rodeio-Rio da Luz. Esta unidade consiste em metagranitos portadores de ortopiroxênios que afloram principalmente no sudoeste do CLA, com ocorrências menores em sua zona central onde são intrusivos nos Ortognaisses Luis Alves. Os afloramentos são esparsos com uma relação pouco clara com a encaixante devido a contatos difusos. Perto dos contatos, os ortognaisses mostram quantidades crescentes de feldspato alcalino, e os metagranitos revelam minerais máficos em quantidades crescentes, o que sugere algum tipo de interação entre os litotipos. São rochas com composições monzograníticas e sienograníticas. A mineralogia consiste em fenocristais de feldspato alcalino de formato euédrico a oval imersos em uma matriz de granulação fina a média com quartzo, feldspato alcalino, plagioclásio, hornblenda, biotita e ortopiroxênio. O acessório allanita é diagnóstico desta suíte.

Outro ponto forte trabalhado nesta Tese foi a utilização do levantamento aerogeofísico, que corresponde a aeromagnetometria e aerogamaespectrometria. Esse levantamento possibilitou o reconhecimento de estruturas tectônicas regionais importantes, algumas até então ocultas ao olho humano e imagens aéreas da superfície. Entre essas estruturas destaca-se uma anomalia magnética positiva de forma elipsoidal de aproximadamente 50 x 90 km que abrange grande parte da porção aflorante do CLA e é limitada por lineamentos magnéticos de 1ª ordem que correspondem em campo a zonas de cisalhamento. Internamente essa estrutura magnética também tem características próprias, que ainda coincidem com foliações, variações litológicas e das respostas aerogamaespectrométricas. A integração desses dados levou à interpretação e proposição do reconhecimento de um *metamorphic core complex ï MCC* Sideriano-Riaciano de fácies granulito no CLA.

A litogeoquímica dos ortognaisses (granulitos máficos e félsicos) em conjunto com os metagranitos da Suíte Rodeio-Rio da Luz demonstrou que estes são cogenéticos e formam um *trend* cálcio-alcalino de rochas metaluminosas a peraluminosas, com assinaturas geoquímicas de arco de ilhas. Os metapiroxenitos são um grupo à parte e tem características de crosta oceânica, sendo rochas mais magnesianas e de afinidade mantélica.

A ocorrência dos BIFs e sua caracterização geoquímica levou a interpretação paleoambiental dessa bacia, que caracteriza a presença de fontes hidrotermais oceânicas e que implica em uma proximidade com uma zona divergente para a fonte de calor, ao mesmo tempo que há contribuição de sedimentos terrígenos nessa bacia revelando também proximidade a um paleocontinente.

Após esse cenário de arco de ilhas com uma bacia adjacente, próxima a uma zona divergente e fontes hidrotermais, esses protólitos foram subductados e condicionados ao metamorfismo granulítico. Atualmente há consenso em petrologia metamórfica e geotectônica, que as condições para o metamorfismo granulítico em terrenos de médio-grande porte como o CLA, tem grande correspondência com a formação de *large hot orogens*, platôs orogênicos e colagem de supercontinentes (Brown, 2007; Brown and Johnson, 2019; Chardon *et al*., 2009; Harley, 1992; Jamieson and Beaumont, 2013).

Junto com este metamorfismo granulítico houve a fusão parcial dessas rochas, que acabaram por dar origem aos granitos da Suíte Rodeio-Rio da Luz. Esse cenário

de colagem de grandes placas tectônicas com formação de um platô orogênico com metamorfismo granulítico e fusão parcial na sua crosta inferior, foi seguido de um evento extensional. Esse evento possibilitou a ascensão de rochas dúcteis da crosta média-inferior e a formação e exumação de um MCC, que hoje compõe grande parte do CLA, no final do Riaciano. O CLA permaneceu estável até a amalgamação do Supercontinente Gondwana Oeste, onde funcionou como uma das massas de terra que deram suporte para a colagem e crescimento do Orógeno Brasiliano.

Questões ainda permanecem em aberto no CLA e estudos podem ser aprofundados. As condições P-T-t dos granulitos precisam ser feitas à luz das novas tecnologias, caracterizando o metamorfismo granulítico, sua T máxima e a trajetória, se horária ou anti-horária e qual processo de exumação final, descompressão isotermal ou resfriamento isobárico? As rochas ultramáficas precisam de um estudo litogeoquímico e petrológico para detalhar sua gênese e ambiente tectônico, se cogenéticas aos granulitos máficos ou não. Um mapeamento geológico-estrutural em escala apropriada se faz necessário afim de reconhecer e detalhar as estruturas condicionantes do MCC, sua cinemática e taxas de deformação e cisalhamento. Os processos que podem levar ao enriquecimento de magnetita nos BIFs também merecem aprofundamento para estimar o potencial mineral de Fe em terrenos granulíticos. A resposta dessas questões levará a um melhor entendimento da crosta inferior e da litosfera, sua geodinâmica e processos evolutivos.

7. Conclusões

A partir das informações do artigo "**Aerogeophysical and geological data highlights a Sideriani Rhyacian granulite Metamorphic Core Complex in the Luis Alves Craton (Southern Brazil)ò** a integração de dados aerogeofísico e geológicos regionais obtidos no Cráton Luis Alves (CLA) nos mostra uma convergência de feições que nos permitiu concluir o seguinte:

- A zona de cisalhamento de Corupá é uma feição geológica e magnética que divide a LAC em dois domínios, Norte e Sul, que apresentam características geológicas, magnéticas e de espectrometria de raios gama próprias;

- O domínio CLA Sul é um alto magnético regional de forma sigmoidal limitado por lineamentos magnéticos de primeira ordem, onde foliações e bandeamentos gnáissicos de uma dobra regional em seu setor Central coincidem com lineamentos magnéticos curvilíneos de segunda ordem e com contrastes gamaespectrométricos. A atitude das estruturas regionais nestas rochas granulíticas refere-se à profundidade intermediária de diápiros, expostos após a erosão de seus registros rochosos rasos;

- O domínio CLA Sul inclui metagranitóides portadores de opx, diversas unidades geológicas de granulitos e litotipos com distribuição assimétrica que foram submetidos a um evento comum de intensa cristalização de magnetita em um processo tectônico não registrado no domínio Norte;

- As bacias sedimentares de Corupá e Itajaí, nos limites do domínio Sul, abrangendo os lineamentos magnéticos de primeira ordem (zonas de cisalhamento CSZ e RISZ) são interpretadas como bacias de paleo-*detachment*;

- Não há correspondência do alto magnético regional elipsoidal a sigmoide com uma topografia positiva, mostrando que se trata de uma estrutura magnética litosférica continental, incluindo rochas da crosta inferior, e não um resultado geomorfológico de um processo crustal exógeno ou superficial;

- O domínio CLA Sul representa um *Metamotrphic Core Complex* Sideriano-Riaciano (MCC) parcialmente preservado, limitado por lineamentos magnéticos de primeira ordem correspondentes a zonas de cisalhamento como RISZ, CSZ e RPSZ;

- As estruturas de contorno do MCC (CSZ, RISZ e RPSZ) estiveram ativas durante a exumação de rochas granulíticas na transição Riaciano-Orosiriano, funcionando como zonas *detachment*;

- A área do CLA Sul proposta aqui como MCC pode ser subdividida em três setores, leste, centro e oeste, cada um com suas próprias características geológicas, magnéticas e gama. O setor Central tem características estruturais de diapirismo;

- A ocorrência de um MCC fácies granulito tem implicações tectônicas para a evolução geodinâmica do Sideriano-Riaciano, uma vez que é incomum na literatura. O CLA é caracterizado como um cinturão metamórfico G-UHTM com razões termobáricas entre 750 – 1500 °C/GPa, que implicam no desenvolvimento de um *Large Hot Orogen* seguido de extensão pós-orogênica e exumação;

- O LAC pode ter tido uma história tectônica alheia aos principais eventos colisionais do Paleoproterozóico, e pode representar a fusão e fragmentação de um segmento continental mais antigo. Por outro lado, pode representar um dos primeiros eventos de colisão do supercontinente Columbia e já estava sendo exumado no final do Riaciano, enquanto os blocos restantes do Columbia ainda estavam colidindo até o final do Orosiriano.

Analisando o conjunto de dados das formações ferríferas bandadas do artigo "**Geochemistry of granulite facies BIFs from the Luis Alves Craton (southern Brazil): implications for Archean-Paleoproterozoic depositional and tectonic settings**" foi possível concluir que:

- Os BIFs do CLA são divididos em duas fácies com base em sua mineralogia: fácies óxido e silicato. O quartzo e a magnetita predominam na fácies óxido, enquanto na fácies silicato também contém ferrosilita, granada e olivina;

- Estas rochas atingiram o mais alto grau metamórfico granulítico, confirmado por ferrossilita e olivina em fácies silicato;

- Com base nos principais elementos e evidências petrográficas, a fácies óxidos apresenta assinatura hidrotermal, com baixo teor de Al_2O_3 e TiO2, enquanto a fácies silicato registra uma contribuição sedimentar continental, enriquecida nesses elementos, além de MgO, MnO e CaO;

- As concentrações de K e Rb, assim como Th/U e La/Th nos levam a inferir que o metamorfismo de fácies granulito não modificou consideravelmente os padrões geoquímicos originais dos BIFs do CLA;

- Os dados geoquímicos expuseram que a principal fonte para ambas as fácies, silicato e óxido dos BIFs do CLA, é a água do mar com maior influência de fontes hidrotermais de baixa T, seguida de contribuição menos importante de sedimentação continental;

- A verdadeira anomalia negativa Ce/Ce* representa águas rasas e oxidantes. Assim, o ambiente deposicional dos BIFs do CLA é inferido como uma bacia rasa e restrita, capaz de ser influenciada tanto por fontes hidrotermais quanto por sedimentos continentais;

- A fácies óxido representaria a sedimentação mais próxima das fontes hidrotermais e com fraca influência da sedimentação clástica continental, enquanto a fácies silicato representaria uma zona contrastante mais próxima do continente com sua influência;

- A fácies óxido tem características mais semelhantes a depósitos do tipo Algoma, maiores teores de Fe e Eu, baixa contribuição siliciclástica e razões Sm/Yb e Eu/Sm de maior contribuição hidrotermal. Por outro lado, a fácies silicato assemelha-se a BIF do tipo Superior, com maior contribuição siliciclástica, anomalias Ce/Ce* negativas e Eu/Eu* < 1,8;

- Os BIFs do CLA não têm uma associação direta e clara com apenas um dos tipos de depósito. Dependendo das fácies analisadas, podem apresentar mais características do tipo Algoma ou Superior. Essa ambigüidade de informações nos leva a inferir que os BIFs do CLA são representativos de um ambiente de transição do tipo Algoma para o tipo Superior;

- Durante o Neoarqueano ocorrem as primeiras deposições dos BIFs do CLA em um ambiente tipo Algoma. Este ambiente reduziu a atividade tectônica e vulcânica na transição para o Sideriano, evoluindo para um ambiente de plataforma, com águas mais rasas e que inclusive levou à deposição de carbonatos, típicos de depósitos do tipo Superior. Esta bacia foi fechada até o Riaciano, com a formação do *Large Hot Orogen*, e esses sedimentos foram subductados para a crosta inferior onde sofreram metamorfismo granulítico.

Reunindo informações de campo, petrografia, litogeoquímica e aerogeofísica no artigo “**Geochemistry of orthogranulites and opx-bearing metagranites from**

the Luis Alves Craton (southern Brazil): island arc and a large hot orogen in the Neoarchean ï Rhyacian", concluímos que:

- Os granulitos máficos e félsicos dos Ortognaisses Luis Alves demonstram afinidades no campo e nos resultados litogeoquímicos.

- Da mesma forma, os granitos à ortopiroxênio da Suíte Rodeio-Rio da Luz apresentam assinaturas e padrões litogeoquímicos que se alinham e se complementam com os dados dos granulitos félsicos.

- Todos os litotipos apresentaram afinidade com ambientes de geração orogênica, destacando-se o cenário tectônico de arco de ilhas.

- A subducção neste cenário tectônico de arco de ilhas gerou fusão parcial e magmatismo bimodal, e os granulitos máficos e félsicos são produtos da fusão parcial da crosta oceânica Arqueana.

- Quando a subducção cessou com o consumo total da crosta oceânica e a bacia adjacente se fechou, um *Large Hot Orogen* foi estabelecido formando um platô orogênico.

- Este platô orogênico deu suporte para as condições P-T para o metamorfismo granulítico e a fusão parcial dos granulitos félsicos que deram origem aos granitos da Suíte Rodeio-Rio da Luz.

- Com o colapso deste *Large Hot Orogen* e do platô, ocorreu a exumação dessas rochas em um evento extensional no Riaciano com a formação de um *Metamorphic Core Complex*.

8. Referências Bibliográficas

Aftabi, A., Atapour, H., Mohseni, S., Babaki, A., 2021. Geochemical discrimination among different types of banded iron formations (BIFs): A comparative review. Ore Geology Reviews, 136, 104244. https://doi.org/10.1016/j.oregeorev.2021.104244

Aitken, A.R.A., Betts, P.G., 2009. Constraints on the Proterozoic supercontinent cycle from the structural evolution of the south-central Musgrave Province, central Australia. Precambrian Res., 168, 284-300. https://doi.org/10.1016/j.precamres.2008.10.006

Aitken, A.R.A., Young, D.A., Ferraccioli, F., Betts, P.G., Greenbaum, J.S., Richter, T.G., Roberts, J.L., Blankenship, D.D., Siegert, M.J., 2014. The subglacial geology of Wilkes Land, East Antarctica. Geophys. Res. Lett., 41, 2390-2400. https://doi.org/10.1002/2014GL059405

Allen, T., Chamberlain, C.P., 1989. Thermal consequences of mantled gneiss dome emplacement. Earth-Planet. Sci. Lett., 93, 392-404. https://doi.org/10.1016/0012-821X(89)90038-1.

Angerer, T., Hagemann, S.G., Danyushevsky, L., 2013. High-grade iron ore at Windarling, Yilgarn Craton: a product of syn-orogenic deformation, hypogene hydrothermal alteration and supergene modification in an Archean BIF-basalt lithostratigraphy. Miner Deposita, 48, 697–728. DOI 10.1007/s00126-012-0450-3

Anudu, G.K., Stephenson, R.A., Macdonald, D.I.M., 2014. Using high-resolution aeromagnetic data to recognize and map intra-sedimentary volcanic rocks and geological structures across the Cretaceous middle Benue Trough, Nigeria. J. Afr. Earth Sci., 99, 625-636. http://dx.doi.org/10.1016/j.jafrearsci.2014.02.017.

Araújo, A.J.D., Bongiolo, E.M., Ávila, C.A., 2019. The southern São Francisco Craton puzzle: Insights from aerogeophysical and geological data. J. South Am. Earth. Sci., 94, 102203. https://doi.org/10.1016/j.jsames.2019.05.019

Araújo, J.C.S., Lobato, L.M., 2019. Depositional model for banded iron formation host to gold in the Archean Rio das Velhas greenstone belt, Brazil, based on geochemistry and LA-ICP-MS magnetite analyses. Journal of South American Earth Sciences, 94, 102205. https://doi.org/10.1016/j.jsames.2019.05.021

Ashwal, L.D., Morgan, P., Hoisch, T.D., 1992. Tectonics and heat sources for granulite metamorphism of supracrustal-bearing terranes. Precambrian Res., v. 55, p. 525-538. https://doi.org/10.1016/0301-9268(92)90043-N

Baldim, M.E., and Oliveira, E.P., 2016. Anatomy of the Alto Alegre gneiss dome, São Francisco Craton, Brazil: A geological record of transpression along a Paleoproterozoic arc-continent collision zone. Precambrian Res., v. 286, p. 250-268. http://dx.doi.org/10.1016/j.precamres.2016.10.004

Barbosa, O. Reservas de minério de ferro em Santa Catarina. Mineração e Metalurgia, São Paulo, v. 5, n. 25, p.21-24. 1940.

Barbosa, J., Martin, H., Peucat, J-J., 2004. Palaeoproterozoic dome-forming structures related to granulite-facies metamorphism, Jequié block, Bahia, Brazil: petrogenetic approaches. Precambrian Research, 135, 105–131. doi:10.1016/j.precamres.2004.08.002

Barbosa, J., Nicollet, C., Leite, C., Kienast, J. R., Fuck, R. A., and Macedo, E. P., 2006. Hercynite–quartz-bearing granulites from Brejões Dome area, Jequié Block, Bahia, Brazil: Influence of charnockite intrusion on granulite facies metamorphism. Lithos, 92, 537-556. https://doi.org/10.1016/j.lithos.2006.03.064

Basei, M.A.S.; MacReath, L.; Siga Júnior, O., 1998. The Santa Catarina Granulite Complex of Southern Brazil: a review. Gondwana Res., 1, 3-4, 383-391. https://doi.org/10.1016/S1342-937X(05)70854-6

Basei, M.A.S., Nutman, A., Siga Júnior, O., Passarelli, C.R., and Drukas, C.O., 2009. The evolution and tectonic setting of the Luis Alves Microplate of Southeastern Brazil: an exotic terrane during the assembly of Western Gondwana. *In*: Gaucher, C., Sial, A.N., Halverson, G.P., and Frimmel, H.E. (Eds): Neoproterozoic-Cambrian Tectonics, Global Change and Evolution: a focus on southwestern Gondwana. Developments in Precambrian Geol., 16, Elsevier, pp. 273-291. https://doi.org/10.1016/S0166-2635(09)01620-X

Bau, M., Dulski, P., 1996. Distribution of yttrium and rare-earth elements in the Penge and Kuruman iron-formations, Transvaal Supergroup, South Africa. Precambrian Research, 79, 37-55.

Bédard, J.H., 2018. Stagnant lids and mantle overturns: implications for Archaean tectonics, magmagenesis, crustal growth, mantle evolution, and the start of plate tectonics. Geosci. Front., 9, 19-49. http://dx.doi.org/10.1016/j.gsf.2017.01.005

Bekker, A., Slack, J.F., Planavsky, N., Krapež, B., Hofmann A., Konhauser K.O., Rouxel, O. J., 2010. Iron Formation: The Sedimentary Product of a Complex Interplay among Mantle, Tectonic, Oceanic, and Biospheric Processes. Economic Geology, 105, 467–508.

Betiollo, L.M., Iglesias, C.M.F., Rocha, P.G., 2018. Integração geológica-geofísica e recursos minerais do Cráton Luis Alves: mapa de integração geológica-geofísica. Porto Alegre: CPRM, 1:250.000, http://rigeo.cprm.gov.br/jspui/handle/doc/16802 (April 2022).

Betts, P.G., Valenta, R.K., Finlay, J., 2003. Evolution of the Mount Woods Inlier, northern Gawler Craton, Southern Australia: an integrated structural and aeromagnetic analysis. Tectonophysics, 366, 83-111, https://doi.org/10.1016/S0040-1951(03)00062-3

Billerot, A., Duchene, S., Vanderhaeghe, O., and Sigoyer, J., 2017. Gneiss domes of the Danba Metamorphic Complex, Songpan Ganze, eastern Tibet. J. of Asian Earth Sci., 140, 48-74. http://dx.doi.org/10.1016/j.jseaes.2017.03.006

Blanco Montenegro, I., Nicolosi, I., Pignatelli, A., García, A., Chiappini, M., 2011. New evidence about the structure and growth of ocean island volcanoes from aeromagnetic

data: The case of Tenerife, Canary Islands. J. Geophys. Res., 116, B03102, https://doi.org/10.1029/2010JB007646

Bleeker, W., 2003. The late Archean record: a puzzle in ca. 35 pieces. Lithos, 71, 99-134. https://doi.org/10.1016/j.lithos.2003.07.003

Blenkinsop, T.G., 2011. Archean magmatic granulites, diapirism, and Proterozoic reworking in the Northern Marginal Zone of the Limpopo Belt. *In* van Reenen, D.D., Kramers, J.D., McCourt, S., Perchuk, L.L., eds., Origin and Evolution of Precambrian High-Grade Gneiss Terranes, with Special Emphasis on the Limpopo Complex of Southern Africa, Geol. Soc. Am. Memoir 207, p. 245–267, https://doi.org/10.1130/2011.1207(13)

Block, S., Jessell, M., Aillères, L., Baratoux, L., Bruguier, O., Zeh, A., Bosch, D., Caby, R., Mensah, E., 2016. Lower crust exhumation during Paleoproterozoic (Eburnean) orogeny, NW Ghana, West African Craton: interplay of coeval contractional deformation and extensional gravitational collapse. Precambrian Res. 274, 82–109. http://dx.doi.org/10.1016/j.precamres.2015.10.014

Bohlen, S.R. 1991. On the formation of granulites. J. Metamorph. Geol**.**, 9, 223-229. https://doi.org/10.1111/j.1525-1314.1991.tb00518.x

Bolhar, R., Kamber, B.S., Moorbath, S., Fedo, C.M., Whitehouse, M.J., 2004. Characterisation of early Archaean chemical sediments by trace element signatures. Earth and Planetary Science Letters, 222, 43– 60. doi:10.1016/j.epsl.2004.02.016

Bradley, D.C., 2011. Secular trends in the geologic record and the supercontinent cycle. Earth-Sci. Rev., 108, 16-33. https://doi.org/10.1016/j.earscirev.2011.05.003

Brito Neves, B.B., 2011. The Paleoproterozoic in the South-American continent: Diversity in the geologic time. J. South Am. Earth. Sci., 32, 270-286. https://doi.org/10.1016/j.jsames.2011.02.004

Brown, M., 2007a. Metamorphism, plate tectonics, and the supercontinent cycle. Earth Sci. Front., 14, 1-18. https://doi.org/10.1016/S1872-5791(07)60001-3

Brown, M., 2007b. Metamorphic conditions in orogenic belts: a record of secular change. Int. Geol. Rev. 49, 193-234. http://dx.doi.org/10.2747/0020-6814.49.3.193

Brown, M., 2009. Metamorphic patterns in orogenic systems and the geological record. *In*: Cawood, P.A., and Kröner, A. (Eds.), Accretionary Orogens in Space and Time, Geol. Soc. of London, Special Publications, 318, 37-74. https://doi.org/10.1144/SP318.2

Brown, M., 2014. The contribution of metamorphic petrology to understanding lithosphere evolution and geodynamics. Geosci. Front., 5, 553-569. http://dx.doi.org/10.1016/j.gsf.2014.02.005

Brown, M., Johnson, T., 2019. Time's arrow, time's cycle: Granulite metamorphism and geodynamics. Miner. Mag., 83, 323–338, https://doi.org/10.1180/mgm.2019.19.

Brun, J.P., Sokoutis, D., Tirel, C., Gueydan, F., Driessche, J.V.D., Beslier, M.O., 2018. Crustal versus mantle core complexes. Tectonophysics, 746, 22-45. http://dx.doi.org/10.1016/j.tecto.2017.09.017

Bruno, H., Almeida, J., Heilbron, M., Salomão, M., Cury, L., 2018. Architecture of major Precambrian tectonic boundaries in the northern part of the Dom Feliciano Orogen, southern Brazil: Implications for the West Gondwana amalgamation. J. South Am. Earth. Sci., 86, 301-317, https://doi.org/10.1016/j.jsames.2018.06.018.

Burg, J.P., Kaus, B.J.P., Podladchikov, Y.Y., 2004. Dome structures in collision orogens: Mechanical investigation of the gravity/compression interplay. *In* Whitney, D. L., Teyssier, C. and Siddoway, C. S., eds., Gneiss domes in orogeny, The Geol. Society of Am., Special Paper, v. 380, p. 47-66. https://doi.org/10.1130/0-8137-2380-9.47

Cao, S., Neubauer, F., Bernroider, M., Genser, J., Liu, J., Friedl, G., 2017. Low-grade retrogression of a high-temperature Metamorphic core complex: Naxos, Cyclades, Greece. GSA Bulletin, 129, 93-117. https://doi.org/10.1130/B31502.1

Catalán, J.R.M., Ayarza, P., Lobato, F.A., Villalaín, J.J., Oreja, M.D., Paramio, M.M., Gómez, S.R., 2018. Magnetic anomalies in extensional detachments: The Xistral Tectonic Window of the Lugo Dome (NW Spain). Tectonics, 37, 4261-4284. https://doi.org/10.1029/2017TC004887

Cen, Y., Peng, S., Kusky, T.M., Jiang, X., Wang, L., 2012. Granulite facies metamorphic age and tectonic implications of BIFs from the Kongling Group in the northern Huangling anticline. Journal of Earth Science, 23 (5), 648–658. DOI: 10.1007/s12583-012-0286-x

Chardon, D., Gapais, D., Cagnard, F., 2009. Flow of ultra-hot orogens: a view from the Precambrian, clues for the Phanerozoic. Tectonophysics, 477, 105-118. https://doi.org/10.1016/j.tecto.2009.03.008

Chardon, D., Jayananda, M., Peucat, J. J., 2011. Lateral constrictional flow of hot orogenic crust: Insights from the Neoarchean of south India, geological and geophysical implications for orogenic plateau. Geochem. Geophys. Geosyst., 12, Q02005, https://doi.org/10.1029/2010GC003398

Cheng, L., Zhang, C., Yang, X., 2020. Petrogenesis of deformed tourmaline leucogranite in the Gurla Mandhata metamorphic core complex, Southwestern Tibet. Lithos, 364-355, 105533. https://doi.org/10.1016/j.lithos.2020.105533

Chopin, C., 2003. Ultrahigh-pressure metamorphism: tracing continental crust into the mantle. Earth and Planetary Science Letters, 212, 1-14.

Chopin, F., Korja, A., Nikkilä, K., Hölttä, P., Korja, T., Abdel Zaher, M., et al., 2020. The Vaasa migmatitic complex (Svecofennian orogen, Finland): Buildup of a LP/HT dome during Nuna assembly. Tecton., 39, e2019TC005583, https://doi.org/10.1029/2019TC005583.

Clos, F., Weinberg, R.F., Zibra, I., Fenwick, M.J., 2019. Archean diapirism recorded by vertical sheath folds in the core of the Yalgoo Dome, Yilgarn Craton. Precambrian Res., 320, 391-402. https://doi.org/10.1016/j.precamres.2018.11.010

Coney, P.J., Harms, T.A. 1984. Cordilleran metamorphic core complexes: Cenozoic extensional relics of Mesozoic compression. Geology, 12, 550-554.

Cooper, F.J., Platt, J.P., Behr, W.M., 2017. Rheological transitions in the middle crust: insights from Cordilleran metamorphic core complexes. Solid Earth, 8, 199-215. https://doi.org/10.5194/se-8-199-2017

Costa, F.G., Santos, P.A., Serafim, I.C.C.O., Costa, I.S.L., Roopnarain, S., 2020. From Mesoarchean drips to modern–style tectonics in the Carajás Province, Amazonian Craton. J. South Am. Sci., 104, 102817. https://doi.org/10.1016/j.jsames.2020.102817

Cutts, K., Lana, C., Alkmin, F., Farina, F., Moreira, H., Coelho, V., 2019. Metamorphism and exhumation of basement gneiss domes in the Quadrilátero Ferrífero: Two stage dome-and-keel evolution?. Geosci. Front., 10, 1765-1787. https://doi.org/10.1016/j.gsf.2019.02.009

Daoudene, Y., Ruffet, G., Cocherie, A., Ledru, P., Gapais, D., 2013. Timing of exhumation of the Ereendavaa metamorphic core complex (north-eastern Mongolia) – U-Pb and $^{40}Ar/^{39}Ar$ constraints. J. Asian Earth Sci., 62, 98-116. http://dx.doi.org/10.1016%2Fj.jseaes.2011.04.009

Davis, G.H., 1983. Shear-zone model for the origin of metamorphic core complexes. Geology, v. II, 342-347.

De Toni, G.B., Bitencourt, M.F., Konopásek, J., Martini, A., Andrade, P.H.S., Florisbal, L.M., Campos, R.S., 2020. Transpressive strain partitioning between the Major Gercino Shear Zone and the Tijucas Fold Belt, Dom Feliciano Belt, Santa Catarina, southern Brazil. J. Struct. Geol., 136, 104058, https://doi.org/10.1016/j.jsg.2020.104058.

Denèle, Y., Olivier, P., Gleizes, G., and Barbey, P., 2009. Decoupling between the middle and upper crust during transpression-related lateral flow: Variscan evolution of the Aston gneiss dome (Pyrenees, France). Tectonophysics, v. 477 (3–4), p. 244-261. https://doi.org/10.1016/j.tecto.2009.04.033

Dharmapriya, P.L., Malaviarachchi, S.P.K., Kriegsman, L.M., Galli, A., Sajeev, K., Zhang, C., 2017. New constraints on the P-T path of HT/UHT metapelites from the Highland complex of Sri Lanka. Geosci. Front. 8, 1405–1430. https://doi.org/10.1016/j.gsf.2016.12.005

Domingos, N.R.R., Medeiros, W.E., Oliveira, R.G., 2020. Geophysical evidence for doming during the Pan-African/Brasiliano orogeny in the Seridó belt, Borborema Province, Brazil. Precambrian Res., 350, 105870. https://doi.org/10.1016/j.precamres.2020.105870

Dostal, J., Keppie, D. J., Jutras, P., Miller, B. V., Murphy, B. J. 2006. Evidence for the granulite–granite connection: Penecontemporaneous high-grade metamorphism, granitic

magmatism and core complex development in the Liscomb Complex, Nova Scotia, Canada. Lithos, v. 86, pp. 77-90.

Dossing, A., Stemmerik, L., Dahl-Jenesen, T., Schlindwein, V., 2010. Segmentation of the eastern North Greenland oblique-shear margin: Regional plate tectonic implications. Earth-Planet. Sci. Lett., 292, 239-253. https://doi.org/10.1016/j.epsl.2009.12.036

Dufréchou, G., 2017. Aeromagnetic signature of an exhumed double dome system in the SW Grenville Province (Canada). Terra Nova, v. 29, p. 363–371. https://doi.org/10.1111/ter.12296

Duncan, I.J., 1984. Structural Evolution of the Thor-Odin Gneiss Dome. Tectonophysics, 101, 87-130. https://doi.org/10.1016/0040-1951(84)90044-1

Duuring, P., ThomasAngerer, T., Hagemann, S.G., Banks, D.A., 2020. Iron deposits hosted by banded iron-formations in the Yilgarn Craton: Products of sequential iron enrichment by magmatic, marine and meteoric fluids. Ore Geology Reviews, 116, 103251. https://doi.org/10.1016/j.oregeorev.2019.103251

Dutta, D., Misra, S., Karmakar, S., 2022. Deformation mechanisms and characteristics of the meta-BIFs from an early Proterozoic shear system of the Southern Granulite Terrane (SGT), India. Journal of Structural Geology, 156, 104534. https://doi.org/10.1016/j.jsg.2022.104534

Dziggel, A., Diener, J.F.A., Kokfelt, T.F., Kolb, J., Scherstén, A., 2019. Thermal structure and evolution of an Archean large hot orogen: insights from the Tasiusarsuaq terrane, SW Greenland. Precambrian Res., 335, 105499. https://doi.org/10.1016/j.precamres.2019.105499

Egglseder, M.S., Cruden, A.R., Tomkins, A.G., Wilson, C.J.L., 2016. Deformation-induced silica redistribution in banded iron formation, Hamersley Province, Australia. Lithos, 266–267, 87–97. https://doi.org/10.1016/j.lithos.2016.09.033

Eldosouky, A.M., Abdelkareem, M., Elkhateeb, S.O., 2017. Integration of remote sensing and aeromagnetic data for mapping structural features and hydrothermal alteration zones in Wadi Allaqi area, South Eastern Desert of Egypt. J. Afr. Earth Sci., 130, 28-37. https://doi.org/10.1016/j.jafrearsci.2017.03.006

Endo, T., Tsunogae, T., Santosh, M., Shaji, E., 2012. Phase equilibrium modeling of incipient charnockite formation in NCKFMASHTO and MnNCKFMASHTO systems: A case study from Rajapalaiyam, Madurai Block, southern India. Geosci. Front., 3(6), 801-811. https://doi.org/10.1016/j.gsf.2012.05.005

Eskola, P.E., 1949. The problem of mantled gneiss domes. Geol. Soc. London, Quarterly J., 104, 461-476.

Figueiredo, M.C.H., Mcreath, I., Basei, M.A.S., Mantovani, M.S.M., 1997. Geochemistry of part of the Santa Catarina Granulitic Complex, southern Brazil: a model of differentiation from

high alumina basalt. Rev. Bras. Geociênc., 27, 33-40. DOI:10.25249/0375-7536.19973340

Fonarev, V.I., Pilugin, S.M., Savko, K.A., Novikova, M.A., 2006. Exsolution textures of orthopyroxene and clinopyroxene in high-grade BIF of the Voronezh Crystalline Massif: evidence of ultrahigh-temperature metamorphism. J. metamorphic Geol., 24, 135–151. doi:10.1111/j.1525-1314.2006.00630.x

Fornari, A., 1998. Geologia e metalogênese da porção meridional do Cráton Luis Alves-SC. Tese (Doutorado) - Instituto de Geociências da Universidade de Campinas, Campinas, 136 pp.

Franchi, F., Mapeo, L.B.M., 2019. Evolution of an Archaean intracratonic basin: A review of the Transvaal Supergroup lithostratigraphy in Botswana. Earth-Science Reviews, 191, 273–290. https://doi.org/10.1016/j.earscirev.2019.02.007

François, C., Philippot, P., Rey, P., Rubatto, D., 2014. Burial and exhumation during Archean sagduction in the East Pilbara Granite-Greenstone Terrane. Earth Planet. Sci. Lett., 396, 235-251. http://dx.doi.org/10.1016/j.epsl.2014.04.025

Franek, J., Schulmann, K., Lexa, O., Tomek, C., Edel, J.B., 2011. Model of syn-convergent extrusion of orogenic lower crust in the core of the Variscan belt: implications for exhumation of high-pressure rocks in large hot orogens. J. Metamorph. Geol., 29, 53-78. https://doi.org/10.1111/j.1525-1314.2010.00903.x

Friend, C.R.L., Nutman, A. P., Bennett, V.C., Norman, M. D., 2008. Seawater-like trace element signatures (REE + Y) of Eoarchaean chemical sedimentary rocks from southern West Greenland, and their corruption during high-grade metamorphism. Contrib Mineral Petrol, 155, 229–246. DOI 10.1007/s00410-007-0239-z

Ganno, S., Tanko, E. L. N., Nono, G. D. K., Soh, A. D., Moudioh, C., Ngnotué, T., Nzenti, J. P., 2017. A mixed seawater and hydrothermal origin of superior-type banded iron formation (BIF)-hosted Kouambo iron deposit, Palaeoproterozoic Nyong series, Southwestern Cameroon: Constraints from petrography and geochemistry. Ore Geology Reviews, 80, 860–875. https://doi.org/10.1016/j.oregeorev.2016.08.021

Gernigon, L., Blischke, A., Nasuti, A., Sand, M., 2015. Conjugate volcanic rifted margins, seafloor spreading, and microcontinent: Insights from new high-resolution aeromagnetic surveys in the Norway Basin. Tecton., 34, 907–933, https://doi.org/10.1002/2014TC003717

Gerya, T.V., Perchuk, L.L., Maresch, W.V., and Willner, A.P., 2004. Inherent gravitational instability of hot continental crust: Implications for doming and diapirism in granulite facies terrains. *In* Whitney, D.L., Teyssier, C., and Siddoway, C.S., eds., Gneiss domes in orogeny: The Geol. Society of Am., Special Paper, v. 380, p. 97-116. https://doi.org/10.1130/0-8137-2380-9.97

Gerya, T.V., Meilick, F.I., 2011. Geodynamic regimes of subduction under an active margin: effects of rheological weakening by fluids and melts. J. Metamorph. Geol., v. 29, p. 7-31. https://doi.org/10.1111/j.1525-1314.2010.00904.x

Gerya, T.V., 2014. Precambrian geodynamics: Concepts and models. Gondwana Res., 25, 442-463. https://doi.org/10.1016/j.gr.2012.11.008

Girelli, T.J., Chemale Jr., F., Lavina, E.L.C., Laux, J.H., Bongiolo, E.M., Lana, C., 2018. Granulite accretion to Rio de la Plata Craton, based on zircon U-Pb-Hf isotopes: Tectonic implications for Columbia Supercontinent reconstruction. Gondwana Res., v. 56, p. 105-118, https://doi.org/10.1016/j.gr.2017.12.010.

Guernina, S., Sawyer, E. W. 2003. Large-scale melt-depletion in granulite terranes: an example from the Archean Ashuanipi Subprovince of Quebec. Journal of metamorphic geology, v. 21, pp. 181-201.

Golynsky, A. V., Ferraccioli, F., Hong, J. K., Golynsky, D. A., von Frese, R. R. B., Young, D. A., et al., 2018. New magnetic anomaly map of the Antarctic. Geophys. Res. Lett., 45, 6437–6449. https://doi.org/10.1029/2018GL078153.

Goodge, J.W., Finn, C.A., 2010. Glimpses of East Antarctica: Aeromagnetic and satellite magnetic view from the central Transantarctic Mountains of East Antarctica. J. Geophys. Res., 115, B09103, https://doi.org/10.1029/2009JB006890

Gross, G. A., 1980. A classification of iron formations based on depositional environments. Canadian Mineralogist, 18, 215-222.

Gross, G. A., 1983. Tectonic systems and the deposition of iron-formation. Precambrian Research, 20, 171-187.

Guo, L., Zhang, J., and Zhang, B., 2008. Structures, kinematics, thermochronology and tectonic evolution of the Ramba gneiss dome in the northern Himalaya. Prog. Nat. Sci., 18-7, 851-860. https://doi.org/10.1016/j.pnsc.2008.01.016

Han, C., Xiao, W., Su, B., Chen, Z., Zhang, X., Ao, S., Zhang, J., Zhang, Z., Wan, B., Song, D., Wang, Z., 2014. Neoarchean Algoma-type banded iron formations from Eastern Hebei, North China Craton: SHRIMP U-Pb age, origin and tectonic setting. Precambrian Research, 251, 212–231. https://doi.org/10.1016/j.precamres.2014.06.019

Harley, S.L., 1989. The origins of granulites: a metamorphic perspective. Geol. Mag., 126, 215–247. https://doi.org/10.1017/S0016756800022330

Harley, S.L., 1998. Ultrahigh temperature granulite metamorphism (1050°C, 12kbar) and decompression in garnet (Mg70)-orthopyroxene-sillimanite gneisses from the Rauer Group, East Antarctica. J. metamorphic Geol., 16, 541-562.

Harley, S.L., 1992. Proterozoic Granulite Terranes. *In* Condie, K.C., ed., Proterozoic Crustal Evolution, Elsevier, v. 10, p. 301-359. https://doi.org/10.1016/S0166-2635(08)70122-1

Harley, S.L., 2016. A matter of time: The importance of the duration of UHT metamorphism. J. Miner. Petrol. Sci., 111, 50-72. https://doi.org/10.2465/jmps.160128

Harris, L.B., Godin, L., Yakymchuk, C., 2012. Regional shortening followed by channel flow induced collapse: A new mechanism for “dome and keel” geometries in Neoarchean granite-greenstone terrains. Precambrian Res., 212-213, 139-154. https://doi.org/10.1016/j.precamres.2012.04.022

Hartmann, L.A., Silva, L.C., Orlandi F°, V., 1979. O Complexo Granulítico de Santa Catarina: descrição e implicações genéticas. Acta Geológica Leopoldensia, São Leopoldo, 6, 93-112.

Hartmann, L.A., 1988. Geoquímica de terras raras e geotermobaromelria de granulitos de Dom Pedrito e Luis Alves, no extremo sul do Brasil. Geochim. Brasil., 2, 1-14.

Hartmann, L.A., Santos, J.O.S., McNaughton, N.J., Vasconcellos, M.A.Z., Silva, L.C. da, 2000. Ion microprobe (SHRIMP) dates complex granulite from Santa Catarina, southern Brazil. An. Acad. Bras. Ciênc., 72-4, 559-572. https://doi.org/10.1590/S0001-37652000000400007

Hartmann, L.A., Savian, J.F., and Lopes, W.R., 2016. Airborne geophysical characterization of geotectonic relationships in the southern Ribeira Belt, Luis Alves Craton, and northern Dom Feliciano Belt, Brazilian Shield. Int. Geol. Rev., v. 58(4), p. 471-488. https://doi.org/10.1080/00206814.2015.1089424

Haugaard, R., Pecoits, E., Lalonde, S., Rouxel, O., Konhauser, K., 2016. The Joffre banded iron formation, Hamersley Group, Western Australia: Assessing the palaeoenvironment through detailed petrology and chemostratigraphy. Precambrian Research, 273, 12–37. https://doi.org/10.1016/j.precamres.2015.10.024

Hayman, N.W., Grindlay, N.R., Perfit, M.R., Mann, P., Leroy, S., de Lépinay, B.M., 2011. Oceanic core complex development at the ultraslow spreading Mid-Cayman Spreading Center. Geochem. Geophys. Geosyst., 12, Q0AG02. https://doi.org/10.1029/2010GC003240

Heilbron, M. et al., 2004. Província Mantiqueira. In: MANTESSO-NETO, V.; BARTORELLI, A.; CARNEIRO, C. D. R.; BRITO-NEVES, B. B. de (Org.) Geologia do continente sul-americano: evolução da obra de Fernando Flávio Marques de Almeida. São Paulo: Beca, 203-235.

Heilbron, M., Valeriano, C.M., Tassinari, C.C.G., Almeida, J., Tupinambá, M., Siga Jr., O., Trouw, R., 2008. Correlation of Neoproterozoic terranes between the Ribeira Belt, SE Brazil and its African counterpart: comparative tectonic evolution and open questions. *In* Pankhurst, R.J., Trouw, R.A.J., Brito Neves, B.B., De Wit, M.J., (eds) West Gondwana: Pre-Cenozoic Correlations Across the South Atlantic Region. Geological Society, London, Special Publications, 294, 211–237. https://doi.org/10.1144/SP294.12

Heller, B.M., Hueck, M., Passarelli, C.R., Basei, M.A.S., 2021. Zircon U-Pb geochronology and Hf isotopes of the Luís Alves Terrane: Archean to Paleoproterozoic evolution and

Neoproterozoic overprint. J. South Am. Earth. Sci., 106, 103008, https://doi.org/10.1016/j.jsames.2020.103008.

Hinze, W., Von Frese, R., Saad, A., 2013. Gravity and Magnetic Exploration: Principles, Practices, and Applications. Cambridge: Cambridge University Press. https://doi.org/10.1017/CBO9780511843129

Hoffmann, A., Kröner, A., Xie, H., Hegner, E., Belyanin, G., Kramers, J., Bolhar, R., Slabunov, A., Reinhardt, J., Horváth, P., 2015. The Nhlangano gneiss dome in south-west Swaziland – A record of crustal destabilization of the eastern Kaapvaal craton in the Neoarchaean. Precambrian Res., 258, 109-132. https://doi.org/10.1016/j.precamres.2014.12.008

Holland, T.J.B. & Powell, R., 1985. An internally consistent thermodynamic dataset with uncertainties and correlations: 2. Data and results. J. Metamorph. Geol., 3, 343-370. https://doi.org/10.1111/j.1525-1314.1985.tb00325.x

Horváth, P., Reinhardt, J., Hofmann, A., 2014. High-grade metamorphism of ironstones in the Mesoarchaean of southwest Swaziland. Miner Petrol, 108, 589–605. DOI 10.1007/s00710-013-0307-1

IAEA, INTERNATIONAL ATOMIC ENERGY AGENCY, 2003. Guidelines for Radioelement Mapping Using Gamma Ray Spectrometry Data, IAEA-TECDOC-1363, IAEA, Vienna.

Iglesias, C.M.F., Zerfass, H., Silva, M.A.S., Klein, C., 2011. Geologia e recursos minerais da Folha Joinville - SH. 22−Z−B, 1:250.000, Estado de Santa Catarina. Porto Alegre: CPRM, http://rigeo.cprm.gov.br/jspui/handle/doc/17685 (April 2022).

Iglesias, C.M.F., Klein, C., Rocha, P.G., Betiollo, L.M., Provenzano, C.A.S., Lopes, W.R., Horn, B.L.D., Rezende, G.G., 2021. Mapeamento geológico e hidrogeológico do município de Joinville, SC: produto 6, mapeamento geológico, estrutural e de recursos minerais, Estado de Santa Catarina. Porto Alegre: CPRM, https://rigeo.cprm.gov.br/handle/doc/22453 (April 2022).

James, H.L., 1954. Sedimentary Facies of Iron-Formation. Econ. Geol., 49-3, 235-293. https://doi.org/10.2113/gsecongeo.49.3.235

James, D.T., Mortensen, J.K., 1992. An Archean metamorphic core complex in the southern Slave Province: basement-cover structural relations between the Sleepy Dragon Complex and the Yellowknife Supergroup. Can. J. Earth Sci., 29, 2133-2145. https://doi.org/10.1139/e92-169

Jamieson, R.A., Beaumont, C., 2011. Coeval thrusting and extension during lower crustal ductile flow – implications for exhumation of high-grade metamorphic rocks. J. Metamorph. Geol., 29, 33-51. https://doi.org/10.1111/j.1525-1314.2010.00908.x

Jamieson, R.A., Beaumont, C., 2013. On the origin of orogens. Bull. Geol. Soc. Am., 125, 1671–1702. https://doi.org/10.1130/B30855.1

Jordan, T.A., Ferraccioli, F., Ross, N., Corr, H.F.J., Leat, P.T., Bingham, R.G., Rippin, D.M., Brocq, A., Siegert, M.J., 2013. Inland extent of the Weddell Sea Rift imaged by new

aerogeophysical data. Tectonophysics, 585, 137-160. https://doi.org/10.1016/j.tecto.2012.09.010

Justo, A. P., Dantas, E. L., Bau, M., Freitas-Silva, F. H., Santos, R. V., Schorscher, J. H. D., 2020. Paleobasinal to band-scale REE + Y distribution in iron formations from Carajás, Amazon Craton, Brazil. Ore Geology Reviews, 127, 103750. https://doi.org/10.1016/j.oregeorev.2020.103750

Kamaci, O., Altunkaynak, S., 2020. The role of accreted continental crust in the formation of granites within the Alpine style continental collision zone: Geochemical and geochronological constrains from leucogranites in the Çataldağ Metamorphic Core Complex (NW Turkey). Lithos, 354-355, 105347. https://doi.org/10.1016/j.lithos.2019.105347

Kaul, P. F. T., 1979. Pré-Cambriano e Eo-Paleozoico do Nordeste de Santa Catarina e Leste do Paraná: reavaliação de dados e correlações com a África. In: SIMPÓSIO REGIONAL DE GEOLOGIA, 2., 1979, Rio Claro. Atas... Rio Claro: SBG, v.1, p. 1-15.

Kaul, P.F.T., 1980. O Cráton de Luis Alves. In: Congresso Brasileiro De Geologia, 31, Balneário Camboriú, Anais, SBG, v. 5, p. 2677-2683.

Kaul, P. F. T.; Teixeira, W., 1982. Archean and Early Proterozoic Complexes of Santa Catarina, Paraná and São Paulo States, South-eastern Brasil: an outline of their geologic evolution. Revista Brasileira de Geociências, São Paulo, 12, (1-3),172-182.

Kayode, J.S., Nawawi, M.N.M., Abdullah, K.B., Khalil, A.E., 2017. Integrating aeromagnetic and Landsat™ 8 data into subsurface structural mapping of Precambrian basement complex. J. Afr. Earth Sci., 125, 202-213. https://doi.org/10.1016/j.jafrearsci.2016.11.010

Kelsey, D.E., Powell, R., 2011. Progress in linking accessory mineral growth and breakdown to major mineral evolution in metamorphic rocks: a thermodynamic approach in the Na_2O-CaO-K_2O-FeO-MgO-Al_2O_3-SiO_2-H_2O-TiO_2-ZrO_2 system. J. Metamorph. Geol., 29, 151-166. https://doi.org/10.1111/j.1525-1314.2010.00910.x

Klein, C., Ladeira, E.A., 2002. Petrography and geochemistry of the least altered banded iron-formation of the Archean Carajás Formation, Northern Brazil. Economic Geology, 97, 643–651.

Klein, C., 2005. Some Precambrian banded iron-formations (BIFs) from around the world: Their age, geologic setting, mineralogy, metamorphism, geochemistry, and origin. Am. Miner., 90, 1473-1499. https://doi.org/10.2138/am.2005.1871

Klepeis, K.A., Schwartz, J., Stowell, H., Tulloch, A., 2016. Gneiss domes, vertical and horizontal mass transfer, and the initiation of extension in the hot lower-crustal root of a continental arc, Fiordland, New Zealand. Lithosphere, 8-2, 116-140. https://doi.org/10.1130/L490.1

Kohn, M.J., 2014. Himalayan Metamorphism and its Tectonic Implications. Annu. Rev. Earth Planet. Sci., 42, 381-419. https://doi.org/10.1146/annurev-earth-060313-055005

Konhauser, K.O., Planavsky, N.J., Hardisty, D.S., Robbins, L.J., Warchola, T.J., Haugaard, R., Lalonde, S.V., Partin, C.A., Oonk, P.B.H., Tsikos, H., Lyons, T.W., Bekker, A., Johnson, C.M., 2017. Iron formations: A global record of Neoarchaean to Palaeoproterozoic environmental history. Earth-Science Reviews, 172, 140–177. http://dx.doi.org/10.1016/j.earscirev.2017.06.012

Kramers, J.D., McCourt, S., Roering, C., Smit, C.A., van Reenen, D.D., 2011. Tectonic models for the Limpopo Complex: Mutual compatibilities and constraints. *In* van Reenen, D.D., Kramers, J.D., McCourt, S., and Perchuk, L.L., eds, Origin and Evolution of Precambrian High-Grade Gneiss Terranes, with Special Emphasis on the Limpopo Complex of Southern Africa, The Geol. Society of Am., p. 311-324. https://doi.org/10.1130/2011.1207(16)

Kruckenberg, S.C., Whitney, D.L., 2011. Metamorphic evolution of sapphirine- and orthoamphibole-cordierite-bearing gneiss, Okanogan dome, Washington, USA. J. metamorphic Geol., 29, 425–449. doi:10.1111/j.1525-1314.2010.00926.x

Kumar, K.S., Srinivas, K.N.S.S.S., Kumar, V.P. Prasad, P.P., Seshunarayana, T., 2018. Magnetic Mapping of Banded Iron Formation of Sandur Schist Belt, Dharwar Craton, India. J. Geol. Soc. India, 91, 174-180. https://doi.org/10.1007/s12594-018-0831-z

Lan, C., Zhao T., Zhang, L., Wang, C., 2014. The Origin of Granulite Facies Metamorphic Iron Formations in Wuyang, Henan Province, Southern of North China Craton. Acta Geologica Sinica (English Edition), 88 (2), 88-89.

Lan, C., Long, X., Zhao, T., Zhai, M., 2019. In-site mineral geochemistry and whole-rock Fe isotopes of the quartzmagnetite-pyroxene rocks in the Wuyang area, North China Craton: Constraints on the genesis of the pyroxene-rich BIF. Precambrian Research, 333, 105445. https://doi.org/10.1016/j.precamres.2019.105445

Lana, C., Tohver, E., Cawood, P., 2010. Quantifying rates of dome-and-keel formation in the Barberton granitoid-greenstone belt, South Africa. Precambrian Res., 177, 199-211. https://doi.org/10.1016/j.precamres.2009.12.001

Lagabrielle, Y., Brovarone, A.V., Ildefonse, B., 2015. Fossil oceanic core complexes recognized in the blueschist metaophiolites of Western Alps and Corsica. Earth-Sci. Rev., 141, 1-26. https://doi.org/10.1016/j.earscirev.2014.11.004

Launay, N., Quesnel, Y., Rochette, P., Demory, F., 2018. Iron Formations as the Source of the West African Magnetic Crustal Anomaly. Front. Earth Sci., 6, 32. https://doi.org/10.3389/feart.2018.00032

Lexa, O., Schulmann, K., Janousek, V. Stipska, P., Guy, A., Racek, M., 2011. Heat sources and trigger mechanisms of exhumation of HP granulites in Variscan orogenic root. J. Metamorph. Geol., 29, 79-102. https://doi.org/10.1111/j.1525-1314.2010.00906.x

Li, H-Z, Liang, J., Yang, F., Zhai, M-G, Zhang, L-C., Voudouris, P.Ch., Yang, Z-J., Zhou, Y-Z., He, J-G., Spry, P.G., 2019. The mineralogy, mineral chemistry, and origin of the Wuyang

banded iron formations, North China Craton. Precambrian Research, 328, 111–127. https://doi.org/10.1016/j.precamres.2019.03.011

Lin, S., Beakhouse, G.P., 2013. Synchronous vertical and horizontal tectonism at late stages of Archean cratonization and genesis of Hemlo gold deposit, Superior craton, Ontario, Canada. Geol., 41-3, 359-362. https://doi.org/10.1130/G33887.1

Lister, G.S., Davis, G.A., 1989. The origin of metamorphic core complexes and detachment faults formed during Tertiary continental extension in the northern Colorado river region, U.S.A.. J. Struct. Geol., 11, 65-94. https://doi.org/10.1016/0191-8141(89)90036-9

Liu, T., Wei, C., 2018. Metamorphic evolution of Archean ultrahigh-temperature mafic granulites from the western margin of Qian'an gneiss dome, eastern Hebei Province, North China Craton: insights into the Archean tectonic regime. Precambrian Res., 318, 170-187. https://doi.org/10.1016/j.precamres.2018.10.007

Maacha, L., Jaffal, M., Jarni, A., Kchikach, A., Mouguina, E.M., Zouhair, M., Ennaciri, A., Saddiqi, O., 2017. A contribution of airborne magnetic, gamma ray spectrometric data in understanding the structure of the Central Jebilet Hercynian massif and implications for mining. J. Afr. Earth Sci., 134, 389-403. https://doi.org/10.1016/j.jafrearsci.2017.07.012

Mantovani, M.S.M.; Hawkesworth, C.J.; Basei, M.A.S., 1987. Nd and Sr isotope studies bearing on the crustal evolution of southeastern Brazil. Rev. Bras. Geociênc., 17-3, 263-268.

Marshak, S., Tinkham, D., Alkmin, F., Brueckner, H., Bornhorst, T., 1997. Dome-and-keel provinces formed during Paleoproterozoic orogenic collapse-core complexes, diapirs, or neither?: Examples from the Quadrilátero Ferrífero and the Penokean orogen. Geol., 25-5, 415-418. https://doi.org/10.1130/0091-7613(1997)025<0415:DAKPFD>2.3.CO;2

Miyashiro, A. 1961. Evolution of metamorphic belts. Journal of Petrology, 2, 277–311.

Mieth, M., Jokat, W., 2014a. New aeromagnetic view of the geological fabric of southern Dronning Maud Land and Coats Land, East Antarctica. Gondwana Res., 25, 358-367. https://doi.org/10.1016/j.gr.2013.04.003

Mieth, M., Jokat, W., 2014b. Banded iron formation (?) at Grunehogna Craton, East Antarctica-Constraints from aeromagnetic data. Precambrian Res., 250, 143-150. https://doi.org/10.1016/j.precamres.2014.06.001

Minelli, L., Speranza, F., Nicolosi, I., D'Ajello Caracciolo, F., Carluccio, R., Chiappini, S., Messina, A., & Chiappini, M., 2018. Aeromagnetic investigation of the central Apennine Seismogenic Zone (Italy): From basins to faults. Tecton., 37, 1435-1453. https://doi.org/10.1002/2017TC004953.

Morrissey, L.J., Hand, M., Lane, K., Kelsey, D.E., Dutch, R.A., 2016. Upgrading iron-ore deposits by melt loss during granulite facies metamorphism. Ore Geology Reviews, 74, 101–121. https://doi.org/10.1016/j.oregeorev.2015.11.012

Moudioh, C., Tamehe, L.S., Ganno, S., Tankwa, M.N., Soares, M.B., Ghosh, R., Kankeu, B., Nzenti, J.P., 2020. Tectonic setting of the Bipindi greenstone belt, northwest Congo craton, Cameroon: Implications on BIF deposition. https://doi.org/10.1016/j.jafrearsci.2020.103971

Mukhopadhyay, J., 2020. Archean banded iron formations of India. Earth-Science Reviews, 201, 102927. https://doi.org/10.1016/j.earscirev.2019.102927

Murthy, I.V.R., Babu, S.B., 2006. Structure of Charnockitic basement in a part of the Krishna–Godavari basin, Andhra Pradesh. J. Earth Syst. Sci., 115-4, 387-393. https://doi.org/10.1007/BF02702867

Nabighian, M.N., Grauch, V.J.S., Hansen, R.O., LaFehr, T.R., Li, Y., Peirce, J.W., Ruder, M.E., 2005. The historical development of the magnetic method in exploration. Geophysics, 70, 33-61. http://dx.doi.org/10.1190/1.2133784

Norlander, B.H., Whitney, D.L., Teyssier, C., Vanderhaeghe, O., 2002. Partial melting and decompression of the Thor-Odin dome, Shuswap metamorphic core complex, Canadian Cordillera. Lithos, 61, 103-125. https://doi.org/10.1016/S0024-4937(02)00075-0

Nutman, A.P., McGregor, V.R., Shiraishi, K., Friend, C.R.L., Bennett, V.C., Kinny, P.D., 2002. ≥ 3850 Ma BIF and mafic inclusions in the early Archaean Itsaq Gneiss Complex around Akilia, southern West Greenland? The difficulties of precise dating of zircon-free protoliths in migmatites. Precambrian Research, 117, 185-224.

O'Brien, P., 2006. Type-locality granulites: high-pressure rocks formed at eclogite-facies conditions. Miner. and Petrol., 86, 161-175. https://doi.org/10.1007/s00710-005-0108-2

Ogunmola, J.K., Ayolabi, E.A., Olobaniyi, S.B., 2016. Structural-depth analysis of the Yola Arm of the Upper Benue Trough of Nigeria using high resolution aeromagnetic data. J. Afr. Earth Sci., 124, 32-43. https://doi.org/10.1016/j.jafrearsci.2016.09.008

Oladunjoye, M.A., Olayinka, A.I., Alaba, M., Adabanija, M.A., 2016. Interpretation of high resolution aeromagnetic data for lineaments study and occurrence of Banded Iron Formation in Ogbomoso area, Southwestern Nigeria. J. Afr. Earth Sci., 114, 43-53. https://doi.org/10.1016/j.jafrearsci.2015.10.015

Österle, J.E., Little, T.A., Seward, D., Stockli, D.F., Gamble, J., 2020. The petrology, geochronology and tectono-magmatic setting of igneous rocks in the Suckling-Dayman metamorphic core complex, Papua New Guinea. Gondwana Res., 83, 390-414. https://doi.org/10.1016/j.gr.2020.01.014

Papineau, D., Gregorio, B.T., Cody, G.D., Fries, M.D., Mojzsis, S.J., Steele, A., Stroud, R.M., Fogel, M.L., 2010. Ancient graphite in the Eoarchean quartz–pyroxene rocks from Akilia in southern West Greenland I: Petrographic and spectroscopic characterization. Geochimica et Cosmochimica Acta, 74, 5862–5883. https://doi.org/10.1016/j.gca.2010.05.025

Passarelli, C.R., Basei, M.A.S., Siga Jr., O., and Harara, O.M.M., 2018. The Luis Alves and Curitiba Terranes: Continental Fragments in the Adamastor Ocean. *In* Siegesmund, S., Basei, M.A.S., Oyhantçabal, P., Oriolo, S., eds., Geol. of Southwest Gondwana, Regional Geol. Rev., p. 189-215. https://doi.org/10.1007/978-3-319-68920-3_8

Perchuk, A.L., Safonov, O.G., Smit, C.A., van Reenen, D.D., Zakharov, V.S., Gerya, T.V., 2018. Precambrian ultra-hot orogenic factory: making and reworking of continental crust. Tectonophysics, 746, 572-586. http://dx.doi.org/10.1016/j.tecto.2016.11.041

Pickard, A.L., 2003. SHRIMP U–Pb zircon ages for the Palaeoproterozoic Kuruman Iron Formation, Northern Cape Province, South Africa: evidence for simultaneous BIF deposition on Kaapvaal and Pilbara Cratons. Precambrian Research, 125, 275–315. doi:10.1016/S0301-9268(03)00113-X

Platt, J.P., Behr, W.M., Cooper, F.J., 2015. Metamorphic core complexes: windows into the mechanics and rheology of the crust. J. Geol. Soc., 172, 9-27. https://doi.org/10.1144/jgs2014-036

Powell, R. & Holland, T.J.B., 1985. An internally consistent thermodynamic dataset with uncertainties and correlations. 1. Methods and a worked example. J. Metamorph. Geol., 3, 327-342. https://doi.org/10.1111/j.1525-1314.1985.tb00324.x

Powell, R. & Holland, T.J.B., 1988. An internally consistent thermodynamic dataset with uncertainties and correlations. 3. Applications to geobarometry, worked examples and a computer program. J. Metamorph. Geol., 6, 173-204. https://doi.org/10.1111/j.1525-1314.1988.tb00415.x

Rajaram, M., and Anand, S.P., 2014. Aeromagnetic signatures of Precambrian shield and suture zones of Peninsular India. Geosci. Front., 5-1, 3-15. http://dx.doi.org/10.1016/j.gsf.2013.06.005

Reddy, N.S., Sashidhar, A.N., 1989. Mineralogy and chemistry of handed iron formations (BIF) of Tiruvannamalai area, Tamil Nadu. Proc. Indian Acad. Sci. (Earth Planet. Sci.), 98 (2), 167-172.

Reeves, C., 2005. Aeromagnetic Surveys: Principles, Practice and Interpretation. Earth-works, Washington DC, 155 p.

Riedel, S., Jacobs, J., Jokat, W., 2013. Interpretation of new regional aeromagnetic data over Dronning Maud Land (East Antarctica). Tectonophysics, 585, 161-171. http://dx.doi.org/10.1016/j.tecto.2012.10.011

Rizzotto, G.J., Alves, C.L., Rios, F.S., Barros, M.A.S., 2019. The Nova Monte Verde Metamorphic core complex: Tectonic implications for the southern Amazonian craton. J. South Am. Earth Sci., 91, 154-172. https://doi.org/10.1016/j.jsames.2019.01.003

Roberts, N.M., Tikoff, B., 2021. Internal structure of the Paleoarchean Mt Edgar dome, Pilbara Craton, Western Australia. Precambrian Res., 358, 106163. https://doi.org/10.1016/j.precamres.2021.106163

Rosa, J.W.C., Rosa, J.W.C., Fuck, R.A., 2014. Geophysical structures and tectonic evolution of the southern Guyana shield, Brazil. J. South Am. Earth Sci., 52, 57-71. http://dx.doi.org/10.1016/j.jsames.2014.02.006

Rosa, J.W.C., Rosa, J.W.C., Fuck, R.A., 2016. The structure of the Amazonian craton: Available geophysical evidence. J. South Am. Earth Sci., 70, 162-173. http://dx.doi.org/10.1016/j.jsames.2016.05.006

Sajeev, K., Windley, B.F., Hegner, E., Komiya, T., 2013. High-temperature, high-pressure granulites (retrogressed eclogites) in the central region of the Lewisian, NW Scotland: Crustal-scale subduction in the Neoarchean. Gondwana Res., v. 23, p. 526-538. https://doi.org/10.1016/j.gr.2012.05.002

Sandiford, M., Van Kranendonk, M.J., Bodorkos, S., 2004. Conductive incubation and the origin of dome-and-keel structure in Archean granite-greenstone terrains: A model based on the eastern Pilbara Craton, Western Australia. Tecton., 23, TC1009. https://doi.org/10.1029/2002TC001452

Scandolara, J.E., Correa, R.T., Fuck, R.A., Souza, V.S., Rodrigues, J.B., Ribeiro, P.S.E., Frasca, A.A.S., Saboia, A.M., Lacerda Filho, J.V., 2017. Paleo-Mesoproterozoic arc-accretion along the southwestern margin of the Amazonian craton: The Juruena accretionary orogen and possible implications for Columbia supercontinent. J. South Am. Earth Sci., 73, 223-247. http://dx.doi.org/10.1016/j.jsames.2016.12.005

Scheffer, C., Vanderhaeghe, O., Lanari, P., Tarantola, A., Ponthus, L., Photiades, A., France, L., 2016. Syn- to post-orogenic exhumation of metamorphic nappes: Structure and thermobarometry of the western Attic-Cycladic metamorphic complex (Lavrion, Greece). J. Geodyn., 96, 174-193. http://dx.doi.org/10.1016/j.jog.2015.08.005

Searle, M.P., Lamont, T.N., 2020. Compressional metamorphic core complexes, low-angle normal faults and extensional fabrics in compressional tectonic settings. Geol. Mag., 157, 101-118. https://doi.org/10.1017/S0016756819000207

Searle, M.P., Lamont, T.N., 2022. Compressional origin of the Aegean Orogeny, Greece. Geosci. Front., 13, 101049. https://doi.org/10.1016/j.gsf.2020.07.008

Smith, A.J.B., Beuker, N., 2016. Palaeoproterozoic banded iron formationhosted high-grade hematite iron ore deposits of the Transvaal Supergroup, South Africa. Episodes, 39 (2), 269-284. DOI: 10.18814/epiiugs/2016/v39i2/95778

Soares, M.B., Neto, A.V.C., Zeh, A., Cabral, A.R., Pereira, L.F., Prado, M.G.B., Almeida, A.M., Manduca, L.G., Silva, P.H.M., Mabub, R.O.A., Schlichta, T.M.,2017. Geology of the Pitangui greenstone belt, Minas Gerais, Brazil: Stratigraphy, geochronology and BIF geochemistry. Precambrian Research, 291, 17–41. https://doi.org/10.1016/j.precamres.2017.01.008

Soula, J.C., 1982. Characteristics and mode of emplacement of gneiss domes and plutonic domes in central-eastern Pyrenees. J. Struct. Geol., 4-3, 313-342. https://doi.org/10.1016/0191-8141(82)90017-7

Spalla, M.I., Zanoni, D., Williams, P.F., Gosso, G., 2011. Deciphering cryptic P-T-d-t histories in the western Thor-Odin dome, Monashee Mountains, Canadian Cordillera: A key to unravelling pre-Cordilleran tectonic signatures. J. Struct. Geol., 33, 399-421. https://doi.org/10.1016/j.jsg.2010.11.014

Spier, C.A., Oliveira, S.M.B., Sial, A.N., Rios, F.J., 2007. Geochemistry and genesis of the banded iron formations of the Cauê Formation, Quadrilátero Ferrífero, Minas Gerais, Brazil. Precambrian Research, 152, 170–206. https://doi.org/10.1016/j.precamres.2006.10.003

Stanton, R.L., 2006. On limits to distances of movement of matter during regional metamorphism: an investigation of nine samples from high-grade metamorphic terranes. The Canadian Mineralogist, 44, 985-1024.

Stevens, L.M., Bebdick, R., Baldwin, J.A., 2017. Synconvergent exhumation of metamorphic core complexes in the northern North American Cordillera. Geol., 45-6, 495-498. https://doi.org/10.1130/G38802.1

Stüwe, K., 2007. Geodynamics of the Lithosphere. Springer, Berlin, 493 p.

Tavares, F. M., Trouw, R. A. J., Silva, C. M. G., Justo, A. P., Oliveira, J. K. M., 2018. The multistage tectonic evolution of the northeastern Carajás Province, Amazonian Craton, Brazil: Revealing complex structural patterns. Journal of South American Earth Sciences, 88, 238–252. https://doi.org/10.1016/j.jsames.2018.08.024

Taylor, S.R. and McLennan, S.M., 1985. The Continental Crust: Its Composition and Evolution. Blackwell, Oxford, 1-312.

Taylor, J., Stevens, G., Armstrong, R., Kisters, A.F.M., 2010. Granulite facies anatexis in the Ancient Gneiss Complex, Swaziland, at 2.73 Ga: Mid-crustal metamorphic evidence for mantle heating of the Kaapvaal craton during Ventersdorp magmatism. Precambrian Res., 177, 88-102. https://doi.org/10.1016/j.precamres.2009.11.005

Teutsong, T., Bontognali, T.R.R., Ndjigui, P-D., Vrijmoed, J.C., Teagle, D., Cooper, M., Vance, D., 2017. Petrography and geochemistry of the Mesoarchean Bikoula banded iron formation in the Ntem complex (Congo craton), Southern Cameroon: Implications for its origin. Ore Geology Reviews, 80, 267–288. https://doi.org/10.1016/j.oregeorev.2016.07.003

Teyssier, C., Whitney, D.L., 2002. Gneiss domes and orogeny. Geol., 30-12, 1139-1142. https://doi.org/10.1130/0091-7613(2002)030<1139:GDAO>2.0.CO;2

Thébaud, N., Rey, P.F., 2013. Archean gravity-driven tectonics on hot and flooded continents: Controls on long-lived mineralized hydrothermal systems away from continental margins. Precambrian Res., 229, 93-104. https://doi.org/10.1016/j.precamres.2012.03.001

Tichomirowa, M., Köhler, R., 2013. Discrimination of protolithic versus metamorphic zircon ages in eclogites: Constraints from the Erzgebirge metamorphic core complex (Germany). Lithos, 177, 436-450. http://dx.doi.org/10.1016/j.lithos.2013.07.013

Tiddy, C.J., Betts, P.G., Neumann, M.R., Murphy, F.C., Stewart, J., Giles, D., Sawyer, M., Freeman, H., Jourdan, F., 2020. Interpretation of a ca. 1600-1580 Ma metamorphic core complex in the northern Gawler Craton, Australia. Gondwana Res., 85, 263-290. https://doi.org/10.1016/j.gr.2020.04.008

Tominaga, M., Sager, W.W., 2010. Origin of the smooth zone in early Cretaceous North Atlantic magnetic anomalies. Geophys. Res. Lett., 37, L01304, https://doi.org/10.1029/2009GL040984

Toraman, E., Teyssier, C., Whitney, D.L., Fayon, A.K., Thomson, S.N., Reiners, P.W., 2014. Low-temperature thermochronologic record of Eocene migmatite dome emplacement and late Cenozoic landscape development, Shuswap core complex, British Columbia. Tecton., 33, 1616–1635, https://doi.org/10.1002/2013TC003442

Touret, J.L.R., Santosh, M., Huizenga, J.M., 2016. High-temperature granulites and supercontinents. Geosci. Front., 7, 101-113. http://dx.doi.org/10.1016/j.gsf.2015.09.001

Trendall, A.F., 2002. The significance of iron-formation in the Precambrian stratigraphic record. Spec. Publs int. Ass. Sediment., 33, 33-66.

Trendall, A.F., Compston, W., Nelson, D. R., De Laeter, J. R., Bennett, V. C., 2004. SHRIMP zircon ages constraining the depositional chronology of the Hamersley Group, Western Australia. Australian Journal of Earth Sciences, 51,621–644.

Van Kranendonk, M.J., Collins, W.J., Hickman, A., Pawley, M.J., 2004. Critical tests of vertical vs. horizontal tectonic models for the Archean East Pilbara Granite-Greenstone Terrane, Pilbara Craton, Western Australia. Precambrian Res., 131, 173-211. https://doi.org/10.1016/j.precamres.2003.12.015

Van Kranendonk, M.J., Smithies, R.H., Hickman, A.H., Champion, D.C., 2007. Review: secular tectonic evolution of Archean continental crust: interplay between horizontal and vertical process in the formation of the Pilbara Craton, Australia. Terra Nova, 19, 1-38. https://doi.org/10.1111/j.1365-3121.2006.00723.x

Vansutre, S., Hari, K.R., 2010. Granulite belts of central India with special reference to the Bhopalpatnam Granulite Belt: significance in crustal evolution and implications for Columbia supercontinent. J. of Asian Earth Sci., 39, 794-803. https://doi.org/10.1016/j.jseaes.2010.06.004

Verdel, C., Wernicke, B.P., Ramezani, J., Hassanzadeh, J., Renne, P.R., Spell, T.L., 2007. Geology and thermochronology of Tertiary Cordilleran-style metamorphic core complexes in the Saghand region of central Iran. GSA Bulletin, 119, 961-977. https://doi.org/10.1130/B26102.1

Walczak, K., Anczkiewicz, R., Szczepanski, J., Rubatto, D., Kosler, J., 2017. Combined garnet and zircon geochronology of the ultra-high temperature metamorphism: Constraints on the rise of the Orlica-Śnieżnik Dome, NE Bohemian Massif, SW Poland. Lithos, 292-293, 388-400. https://doi.org/10.1016/j.lithos.2017.09.013

Wang, T., Guo, L., Zheng, Y., Donskaya, T., Gladkochub, D., Zeng, L., Li, J., Wang, Y., Mazukabzov, A., 2012. Timing and processes of late Mesozoic mid-lower-crustal extension in continental NE Asia and implications for the tectonic setting of the destruction of the North China Craton: Mainly constrained by zircon U–Pb ages from metamorphic core complexes. Lithos, 154, 315-345. http://dx.doi.org/10.1016/j.lithos.2012.07.020

Warchola, T., Lalonde, S.V. Pecoits, E., Gunten, K., Robbins, L. J., Alessi, D.S., Philippot, P., Konhauser, K.O., 2018. Petrology and geochemistry of the Boolgeeda Iron Formation, Hamersley Basin, Western Australia. Precambrian Research, 316, 155–173. https://doi.org/10.1016/j.precamres.2018.07.015

White, R. W.; Powell, R. 2002. Melt loss and the preservation of granulite facies mineral assemblages. Journal of metamorphic geology, v. 20, pp. 621-632.

White, R.W., Powell, R., 2011. On the interpretation of retrograde reaction textures in granulite facies rocks. J. Metamorph. Geol., 29, 131-149. https://doi.org/10.1111/j.1525-1314.2010.00905.x

Whitney, D.L., Teyssier, C., Siddoway, C.S., eds., 2004a. Gneiss domes in orogeny. The Geol. Society of Am., Special Paper, v. 380, 393 pp. https://doi.org/10.1130/SPE380

Whitney, D.L., Teyssier, C., Vanderhaeghe, O., 2004b. Gneiss domes and crustal flow. *In* Whitney, D.L., Teyssier, C., Siddoway, C.S., eds., Gneiss domes in orogeny, The Geol. Society of Am., Special Paper, v. 380, p. 15-34. https://doi.org/10.1130/0-8137-2380-9.15

Whitney, D.L., Teyssier, C., Rey, P., Buck, W.R., 2013. Continental and oceanic core complexes. GSA Bulletin, 125, 273-298. https://doi.org/10.1130/B30754.1

Wiest, J.D., Osmundsen, P.T., Jacobs, J., Fossen, H., 2019. Deep Crustal Flow Within Postorogenic Metamorphic Core Complexes: Insights from the Southern Western Gneiss Region of Norway. Tecton., 38, 4267–4289, https://doi.org/10.1029/2019TC005708

Winter, J. 2014. Principles of Igneous and Metamorphic Petrology. Pearson Education, 2nd. ed., pp. 737.

Xiong, S.Q., Tong, J., Ding, Y.Y., Li, Z.K., 2016. Aeromagnetic data and geological structure of continental China: A review. Appl. Geophys., 13-2, 227-237. http://doi.org/10.1007/s11770-016-0552-2

Yellappa, T., Chetty, T.R.K., Santosh, M., 2016. Precambrian iron formations from the Cauvery Suture Zone, Southern India: Implications for sub-marine hydrothermal origin in Neoarchean and Neoproterozoic convergent margin settings. Ore Geology Reviews, 72, 1177–1196 https://doi.org/10.1016/j.oregeorev.2015.05.002

Yin, A., 2004. Gneiss domes and gneiss dome systems. *In* Whitney, D.L., Teyssier, C., Siddoway, C.S., eds., Gneiss domes in orogeny, The Geol. Society of Am., Special Paper, v. 380, p. 1-14. https://doi.org/10.1130/0-8137-2380-9.1

Zhang, B., Chai, Z., Yin, C.Y., Huang, W.T., Wang, Y., Zhang, J.J., Wang, X.X., Cao, K., 2017. Intra-continental transpression and gneiss doming in an obliquely convergent regime in SE Asia. J. Struct. Geol., 97, 48-70. http://dx.doi.org/10.1016/j.jsg.2017.02.010

Zhang, Z.M., Ding, H.X., Palin, R.M., Dong, X., Tian, Z.L., Kang, D.Y., Jiang, Y.Y., Qin, S.K., Li, W.T., 2022. On the origin of high-pressure mafic granulite in the Eastern Himalayan Syntaxis: Implications for the tectonic evolution of the Himalayan orogen. Gondwana Res., 104, 4-22. https://doi.org/10.1016/j.gr.2021.05.011

Zhao, G., Sun, M., Wilde, S.A., and Li, S., 2004. A Paleo-Mesoproterozoic supercontinent: assembly, growth and breakup. Earth-Sci. Rev., 67, 91–123. https://doi.org/10.1016/j.earscirev.2004.02.003

Zheng, Y., Han, X., Gao, X., Geng, X., Chen, X., Liu, J., 2017. Enrichment of iron ores by folding in the BIF-hosted deposit: A case study from the Archean Qian'an iron deposit, North China Craton. Geological Journal, 53, 617–628. https://doi.org/10.1002/gj.2916

Zulauf, G., Zulauf, J., Thiessen, A., Hattingen, E., 2019. Formation of dome-in-dome structures: Results from experimental studies and comparison with natural examples. J. Struct. Geol., 118, 324-339. https://doi.org/10.1016/j.jsg.2018.11.008